Development of analytical techniques for probing the effects of β-haematin inhibiting compounds on the malaria parasite *Plasmodium falciparum*

Division of Clinical Pharmacology

Department of Medicine

University of Cape Town

This dissertation is presented for the degree of Doctor of Philosophy

By Makgalanoto Keletso Maepa

Supervisors:
Prof. Timothy Egan (late), Assoc. Prof. Lubbe Wiesner, Dr Kathryn Wicht, and Dr Jill Combrinck

Plagiarism declaration

Declaration

I, **Makgalanoto Keletso Maepa**, hereby declare that the work on which this dissertation/thesis is based is my original work (except where acknowledgements indicate otherwise) and that neither the whole work nor any part of it has been, is being, or is to be submitted for another degree in this or any other university.

I empower the university to reproduce for the purpose of research either the whole or any portion of the contents in any manner whatsoever.

Signature: ……

Date: ……

Abstract

Phenotypic screening for novel compounds that inhibit the growth of the malaria parasite remains one of the most effective ways to identify novel antimalarial drugs. Subsequent deconvolution of the drug target and mechanism of action (MoA) are a vital part of the drug development process. This is often a limitation since the appropriate assays can be expensive, time-consuming, or inconclusive. One of the primary MoAs of the clinically approved antimalarials against *Plasmodium falciparum* is via the inhibition of haem detoxification. Drugs with this MoA, including chloroquine and amodiaquine, exert their therapeutic effect by disrupting haemozoin formation, which leads to increased accumulation of cytotoxic haem.

Typically, the activity of potential haemozoin inhibitors is assessed using an *in vitro* detergent-mediated β-haematin inhibition assay. However, this is inadequate for identifying true whole-cell inhibitors of haemozoin since the assay is performed extracellularly. The intracellular pyridine-based assay by Combrinck *et al*. is used to determine whether prioritised β-haematin inhibitors cause significant dose-dependent increases in unsequestered haem (free haem) in the parasite. However, this assay has limitations and disadvantages in terms of its low throughput and the use of toxic reagents. In addition, this method is not readily transferable to other malaria drug discovery laboratories because of the need for specific knowledge of haem chemistry, highly specialised training, and given the labour-intensive nature of the assay. Therefore, developing improved assays that are readily accessible with increased throughput will lead to substantial progress in this area. It is also notable that the processes by which haem kills the parasite are not fully understood and hence the understanding of the effects caused by the unsequestered haem levels in the parasite needs considerable advancement.

Consequently, in this work, a novel 96-well plate HPLC-DAD cellular haem fractionation method was developed and validated for quantifying intracellular haem species in the *P. falciparum* cell. The technique has eliminated the use of toxic pyridine to complex haem for the detection of unsequestered haem. Instead, it uses non-volatile imidazole for complex formation and has also reduced parasite starting material four-fold compared with the original method. Furthermore, this 96-well plate method allows the simultaneous evaluation of four test compounds at five selected concentrations, instead of only one test compound per 24-well plate. The assay was validated against the original pyridine-based method using four known haemozoin-inhibiting drugs, including chloroquine, amodiaquine, lapatinib and lomitapide, as well as four known non-inhibiting haemozoin drugs, including mefloquine,

lumefantrine, pyrimethamine and tetrahydrocannabinol (THC). This higher throughput cellular fractionation assay will significantly increase throughput while also becoming an invaluable technique for probing haemozoin inhibition as a relevant MoA for new compounds in antimalarial drug discovery pipelines.

Following successful validation of the 96-well four-compound cellular haem assay, the method was modified to a 96-well 33-compound qualitative high-throughput haem fractionation assay. Applications of the high-throughput method are intended to provide a valuable technique to accommodate the standard high-throughput screening campaigns that focus on identifying haemozoin-inhibiting molecules. Thus, this qualitative high-throughput assay enabled the quantifying of intracellular haem species in *P. falciparum* cells for 33 compounds tested simultaneously at a single-point concentration corresponding to 2x the 50% inhibitory concentration (IC_{50}). The compounds used to validate the assay consisted of known haemozoin inhibitors, non-haemozoin inhibitors, and novel experimental compounds sourced from different drug discovery projects at the University of Cape Town. Notably, ten of the experimental compounds were from a high-throughput screening campaign to identify β-haematin inhibiting compounds, which were invaluable for proof-of-concept application. In order to further validate the single-point results for these compounds, four (one predicted to be a non-haemozoin inhibitor and three to be haemozoin inhibitors) of this set were chosen to evaluate the method's haemozoin inhibition predictive capability using a full-dose response approach. By employing the 96-well HPLC-DAD four-compound method, we demonstrated that the single-point 33-compound high-throughput haem fractionation assay could correctly classify all four experimental compounds and the known antimalarial drugs as haemozoin or non-haemozoin inhibitors. These findings are substantial, as the validated 33-compound high-throughput assay can be used in conjunction with the extracellular β-haematin method during MoA studies for newly developed or existing compounds. This is even in cases when haemozoin inhibition is not the desired drug target, as those which cause increased unsequestered haem levels can be eliminated from further progression.

After investigating a diverse series of haemozoin-inhibiting compounds using the cellular haem fractionation methods, we discovered that each compound exhibited varying levels of unsequestered haem in the parasite at their relevant IC_{50}. Surprisingly, more active compounds (lower IC_{50} values) often produced lower levels of unsequestered haem than less active ones (higher IC_{50} values). These observations imply that the common notion that haemozoin inhibitors cause an accumulation of unsequestered haem, which directly leads to parasite death, does not hold. If this were to be the case, the unsequestered haem levels

would be expected to be the same at the IC_{50} of each compound. This prompted an investigation of the toxicity and effect of unsequestered haem on the parasite. A flow cytometry assay was developed to investigate the killing speed and the stage-specific effects of the various haemozoin-inhibiting compounds. The findings show that compounds that produce lower levels of unsequestered haem tend to kill the parasites earlier in the life cycle. In contrast, those compounds that exhibit higher levels of unsequestered haem tend to kill later in the life cycle. Furthermore, it was also observed that the surviving parasite population post-compound incubation differed. Compounds releasing lower levels of unsequestered haem resulted in a less mature parasite population, while those releasing higher levels of unsequestered haem resulted in a more mature parasite population. These results suggest that the toxicity of haem is compound-specific. This leads to the hypothesis that the compounds present as haem–inhibitor complexes and that haemozoin inhibitors act as complexes exerting unique activities. This has important implications for the study and the design of future hemozoin-inhibiting antimalarial drugs, as well as for our understanding of parasite resistance mechanisms.

Publications and Conference Proceedings

Manuscripts associated with this thesis:

- Openshaw, R.; Maepa, K.; Benjamin, S. J.; Wainwright, L.; Combrinck, J. M.; Hunter, R.; Egan, T. J. A Diverse Range of Hemozoin Inhibiting Scaffolds Act on Plasmodium Falciparum as Heme Complexes. *ACS Infect. Dis.* **2021**, *7* (2), 362–376.
- De Sousa, A. C. C.; Combrinck, J. M.; Maepa, K.; Egan, T. J. THC Shows Activity Against Cultured Plasmodium Falciparum. *Bioorg. Med. Chem. Lett.* **2021**, *54*, 128442.
- De Sousa, A. C. C.; Maepa, K.; Combrinck, J. M.; Egan, T. J. Lapatinib, Nilotinib and Lomitapide Inhibit Haemozoin Formation in Malaria Parasites. *Molecules* **2020**, *25* (7), 1–15.
- De Sousa, A. C. C.; Combrinck, J. M.; Maepa, K.; Egan, T. J. Virtual Screening as a Tool to Discover New β-Haematin Inhibitors with Activity against Malaria Parasites. *Sci. Rep.* **2020**, *10* (1), 3374.

Conference presentations:

- **2022:** Malaria: Confronting Challenges from Drug Discovery to Treatment (2022 Keystone Symposia Conference) held at Beaver Run Conference Center, Breckenridge, Colorado, on April 10–13, 2022.
  Poster title: The development of a high-throughput heme quantification method for detection by HPLC-UV-Vis.
- **2022:** 27th Virtual Congress of the South African Society of Biochemistry and Molecular Biology 2022 (SASBMB 2022) – technical biochemistry session on January 25, 2022.
  Talk Title: The isolation of *Plasmodium falciparum* haem species for detection by HPLC-UV-Vis.
- **2020:** Royal Society of Chemistry/South African Chemical Institute Young Chemists' Virtual Symposium 2020 on September 30 and October 1, 2020.
  Talk Title: The isolation of *Plasmodium* falciparum haem species for detection by LC-MS/MS.
- **2019:** Malaria Research Symposium: Crossing Boundaries, held at Wallenberg Center, Stellenbosch, South Africa on September 30 and October 1, 2019.
  Poster: Probing the effects of β-haematin inhibiting scaffolds on the malaria parasite *Plasmodium falciparum*.

Acknowledgements

I would like to offer my sincerest gratitude to the following people:

- To my late supervisor Prof. Timothy John Egan, many thanks for having been an incredible and readily available mentor. Your excellent pieces of advice, enormous support, encouragement, and sharing of knowledge were very inspiring throughout the trying times, and especially during the Covid-19 pandemic. Thank you for your guidance and commitment to this project until the very end. May your soul forever rest in peace my Prof.
- To Assoc. Prof. Lubbe Wiesner, my deepest gratitude for assuming the big responsibility of supervising this project to completion. Thank you for your guidance, excellent support, and excellent supervision. I could not have asked for anything more than what you provided.
- To my co-supervisors Dr Kathryn Wicht and Dr Jill Combrinck, thank you for your enormous contribution to this project. I am very grateful for the knowledge you imparted during this study. Thank you for making yourselves available at such short notice to take on the new responsibility.
- The members of the Bioinorganic Chemistry and Pharmacokinetics research groups for their invaluable assistance and support. A special mention goes to Mr Anton Joubert for his invaluable assistance with both the LC-MS/MS and HPLC-DAD instrumentations.
- A special thanks are due to Dr Ana de Sousa for providing the virtually screened compounds and performing all the β-haematin assay work reported in this work.
- Thanks are due to the Holistic Drug Discovery and Development Centre's (H3D) malaria biology team (Dale, Sumaya and Virgil) for helping with the tissue culturing work, and Dr Liezl Gibhard for assistance with flow cytometry.
- Drs Roxanne Mohunlal and Daniel Watson proofread this thesis.
- My partner Phiwe and my friends who provided me with unwavering love, encouragement and support throughout my study.
- My parents (Suzan and Thami Mayekiso) and family are thanked for their support and for allowing me to follow my dreams and passions.

Lastly, I offer appreciation to the National Research Foundation (NRF), the National Institute of Health (NIH) (grant number R01AI143521), the Harry Crossley Foundation (through the UCT Postgraduate funding office), and the Division of Clinical Pharmacology for providing financial support.

Contents

List of Abbreviations

ACN	Acetonitrile
ACT	Artemisinin combination therapy
AL	Artemether + Lumefantrine
AQ	Amodiaquine
ASAQ	Artesunate + Amodiaquine
ATPase	Adenosine 5'-triphosphate hydrogen proton pump
tert-But (or But)	Tertiary-Butanol
CC-BY licence	Creative commons licence
CHO	Chinese hamster ovary
CM	Complete culture media
CQ	Chloroquine
CQR	Chloroquine resistant
CQS	Chloroquine sensitive
Cryo-EM	Cryogenic electron microscopy
DAD	Diode array detector
DMSO	Dimethyl sulfoxide
DNA	Deoxyribonucleic acid
DV	Digestive vacuole
Fe(II)PPIX	Ferroprotoporphyrin
Fe(III)PPIX	Ferriprotoporphyrin
FSC	Forward scatter
GTS	Global technical strategy
G6PD	Glucose-6-phosphate dehydrogenase
H^+	Hydrogen proton
Hb	Haemoglobin
HDP	Haem detoxification protein
HEPES	4-(2-hydroxyethyl)-1-piperazineethanesulfonic acid)
H_2O_2	Hydrogen peroxide
HPLC	High-performance liquid chromatography
HRP	Histidine rich protein
IC_{50}	50% inhibitory concentration
IPTp	Intermittent preventative treatment in pregnancies
iRBC	Infected red blood cell
IRS	Indoor residual spraying
ITN	Insecticide-treated mosquito nets
K13	Kelch-13 protein
LBVS	Ligand-based virtual screening
LC-MS/MS	Liquid chromatography with a tandem mass spectrometer
LDH	Lactate dehydrogenase
LOM	Lomitapide
LPT	Lapatinib
LUM	Lumefantrine
MDA	Mass drug administration
MDG	Millennium development goal
MeOH	Methanol
MMV	Medicines for malaria venture
MoA	Mechanism of action
MQ	Mefloquine
NAD	Nicotinamide adenine dinucleotide
NaF	Sodium fluoride
NBT	Nitro blue tetrazolium

NP-40	Nonidet P-40
P. falciparum	*Plasmodium falciparum*
PBS	Phosphate buffered saline
PPM	Parasite plasma membrane
PV	Parasitophorous vacuole
PVM	Parasitophorous vacuole membrane
pLDH	*Plasmodium* lactate dehydrogenase
PfCRT	*P. falciparum* choroquine resistant transporter protein
pfcrt	*P. falciparum* choroquine resistant transporter gene
P. vivax	*Plasmodium vivax*
PfEMP1	*P. falciparum* erythrocyte membrane protein 1
PfMDR1	*P. falciparum* multidrug-resistant transporter protein 1
pfmdr1	*P. falciparum* multidrug-resistant transporter 1 gene
Pgh1	P-glycoprotein homolog 1
pRBC	Parasitised red blood cell
PYR	Pyrimethamine
QC	Quality control
QCH	High concentration quality control
QCL	Low concentration quality control
QCM	Medium concentration quality control
qHTS	Quantitative high-throughput screening
QSAR	Quantitative structure-activity relationship
RBC	Red blood cell
RNA	Ribonucleic acid
SERcap	Single-exposure radical cure and prophylaxis
SBVS	Structure-based virtual screening
SDG	Sustainable development goals
TEM	Transmission electron microscopy
THC	Delta-9-tetrahydrocannabinol
TPP	Target product profile
UHC	Universal health coverage
WHO	World Health Organization

Chapter 1: Literature and Introduction

1.1. Malaria in the present day

After centuries of intervention, malaria remains one of the leading global causes of death among communicable diseases. This is despite the disease being ancient and researchers having extensive knowledge of the mosquito life cycle, and of the biology, genetics and epidemiology. Nearly half of the world's population is at risk of malaria infection, and it claims hundreds of thousands of lives each year. The high prevalence and mortality rates remain in tropical regions, specifically sub-Saharan Africa and South East Asia.[1] These are low-income and lower- to middle-income countries that already bear high poverty rates and limited equitable healthcare.[2] The lack of equitable access to healthcare in these countries necessitates their heavy reliance on the World Health Organisation's (WHO) universal health coverage (UHC) policy, which seeks to provide global equitable healthcare.

The UHC policy is set out under a system of millennium development goals (MDGs) and sustainable development goals (SDGs) of the United Nation's 2016–2030 agenda, which follows the previously lapsed agenda that ran from 2000 to 2015.[3] Specific to the previous strategy for malaria control and elimination (2000 to 2015), the aim was to substantially decrease the disease incidence with a vision to achieve a world free of malaria. Thus, in the 15 years between 2000 and 2015, the malaria incidence rate decreased by an estimated 37% globally, and the mortality rate fell by an impressive 60%.[4] This was from an estimation of over a million deaths per year in the 1980s and 1990s to approximately 438000 deaths in 2015 (Figure 1.1a), all thanks to the WHO's MDGs.[4–6] This trend in decreasing cases and mortalities remained through 2019 but showed a minor increase in 2020, most probably resulting from the effects of the COVID-19 pandemic.

According to the 2022 world malaria report, there were an estimated 247 million cases in 2021 with 619000 deaths from 85 malaria-endemic countries.[1] This significant increase in cases compared to previous years was associated with the COVID-19 pandemic, which led to disruptions in healthcare services. As a result, this hampered the MDGs and SDGs set for vision 2016 to 2030 of ultimately reducing malaria incidence by at least 90% compared to 2015. However, unsurprisingly, the burden of malaria cases and mortality rates remained higher in the WHO Africa region, which accounted for 95% and 96% of these incidents, respectively.[1] As with previous trends, the 2022 report further estimates that over 80% of these deaths occurred in children under the age of five years, so placing them at the forefront of the disease's morbidity (Figure 1.1b).[1,6] Although this was significantly lower than the 87% of deaths they accounted for in the early 2000s, it still presented as overwhelmingly high. Other

notable areas of success with the MDGs and SDGs have been the eradication of malaria transmission (reporting zero transmission cases for three consecutive years) in 14 countries between 2000 and 2021.[1]

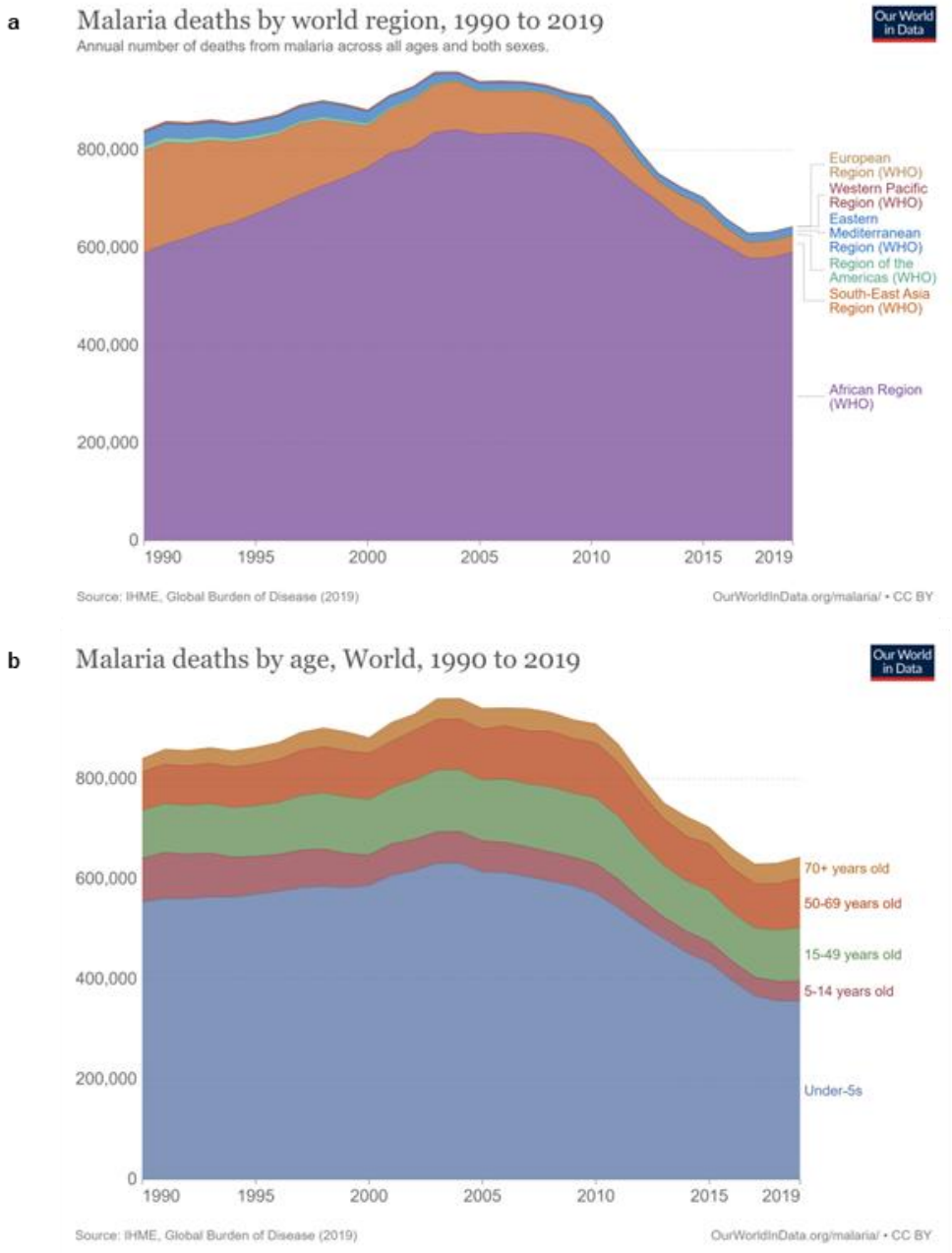

Figure 1.1: Trends of the estimated number of global malaria deaths by region from 1990 to 2019. (a) Represents the annual number of deaths from malaria across all ages and sexes by all regions classified by WHO. (b) Number of malaria deaths by age in the same period. Figures were reproduced from the *Our World in Data* website (https://ourworldindata.org/) under the permissive creative commons licence: the CC-BY licence.[6]

The attainment of these successes has been mainly because of the implementation of indoor residual spraying (IRS), the use of insecticide-treated mosquito nets (ITN), and artemisinin combination therapy (ACT), among other things.[1,4] Most recently, seasonal malarial chemoprevention has also been introduced. Unfortunately, it is notable that although IRS is effective, it poses environmental health risks and must be used with caution as per WHO-recommended guidelines.[7] The primary use of these measures is aimed at reducing the high burden of malaria, specifically in sub-Saharan Africa, since it is more cost-effective to prevent the transmissions and infections than to cure the actual disease. Moreover, severe malaria poses a danger because it can result in life-threatening complications like kidney, lung and brain damage.[8] Thus, prevention serves as a mechanism to reduce the number of potentially life-threatening conditions leading to fatalities, which can in turn have future health and economic impacts on the populations concerned. Furthermore, there is a threat of resistance to the current antimalarial drugs (ACTs), especially in malaria-endemic regions.[1] Therefore, preventing transmissions can help protect against the overuse of the current drug arsenal.

1.2. Origins of malaria

The historical origins of the malaria disease are open to debate. However, it is widely believed that malaria is one of the world's ancient diseases, dating from 3000 BC to 400 BC during the times of ancient China and ancient Egypt, and the bygone Greek era.[9,10] It is reported to have arrived in Rome or Europe after the first century AD, most probably from up the Nile River from the African rainforest.[11] Initially, the disease was believed to be seasonal fevers caused by miasmas rising from swamps; this reinforced the belief that the disease derived from spoiled air.[12,13] This was primarily because it was prevalent in mostly poor communities in marshland (always wet with characteristics of grasses) that were characterised by poor health systems. Often there were reported cases of dead victims who presented with enlarged spleens and black deposits in other body organs.[11] These black deposits are now known to have been the haemozoin crystal, a by-product of haemoglobin digestion.

The search for the cause of these fevers led to a breakthrough when Antony van Leeuwenhoek discovered bacteria in 1676.[14] This further intensified when Louis Pasteur and Robert Koch established in 1878–1879 that microorganisms, in their case cholera, were the causative agents of infectious diseases.[15] This led to the so-called germ theory at the time. However, it was only in October 1880 that Charles Louis Alphonse Laveran discovered a single-celled protozoan caused malaria.[11] Laveran, at the time, distinguished the three main parasite stages in patient samples: gametocyte, schizont, and trophozoite. Subsequently, Camillo Golgi affirmed that the rupture of asexual schizont-staged parasites was responsible for the onset of malarial fevers. Nonetheless, even with the protozoan's discovery in patients'

blood as being the causative agent of the fevers, it was unclear how the disease was transmitted.

This discovery came in August 1887, when Ronald Ross discovered malaria-like pigment bodies in the *Anopheles* mosquito.[11,16] Although initially sceptical of the germ theory, Ross demonstrated the propagation of malaria by the *Anopheles* mosquito with the use of birds. He dissected the mosquitoes used in the transmission experiments to show the presence of the parasite in the insect's salivary glands and its development in the stomach.[16] Notably, this discovery was inspired by the work of Patrick Manson, who had shown at the time that the filarial worm that causes elephantiasis could infect mosquitoes. Ross demonstrated the mosquito life cycle using *Plasmodium relictum*, a causative agent of malaria in birds.[11] Other investigators also worked on the mosquito life cycle at the time and demonstrated this for human malaria parasites, specifically *Plasmodium vivax*. This group of scientists consisted of Giovanni Battista Grassi, Amico Bignami, Giovanni Bastianelli, Antonio Dionisi, and Angelo Celli.[11,17] It was only in 1948 that a group from the Ross Institute of the London School of Hygiene and Tropical Medicine observed the presence of sporozoites in liver specimens of healthy human volunteers.[11] This served as a notable discovery that concluded the quest to discover the disease's causative agent and its mode of propagation in communities.

1.3. Species of *Plasmodium* and the life cycle

Malaria transmission occurs through the bite of an infected female mosquito of the genus *Anopheles*.[18] These infections transmit as sporozoites, a successful developmental stage of the gametocytes (male and female) acquired during a blood meal. Various species of the malaria parasite of the genus *Plasmodium* can affect humans: *Plasmodium vivax (P. vivax), Plasmodium falciparum (P. falciparum), Plasmodium ovale* (*Plasmodium ovale wallikeri and Plasmodium ovale curtisi*)*, Plasmodium malariae, and Plasmodium knowlesi*.[10] The deadliest species of the genus is *P. falciparum*, which accounts for most of the reported fatalities. Specifically, in 2021, within the WHO Africa region, where malaria cases are the highest globally (95% of global cases), it accounted for almost all the reported malaria cases, and *P. vivax,* the second deadly species in the genus, only accounted for 0.3% of cases.[1] However, *P. vivax* was more prevalent in the WHO South East Asia region and the WHO Americas region, accounting for 40% and 79% of the reported cases, respectively. Each vector species has a different geographical distribution globally, and *P. falciparum* and *P. vivax* are by far the most widespread species.[19] Figure 1.2 shows the global incidence distribution of *P. falciparum* and *P. vivax* species in 2020.

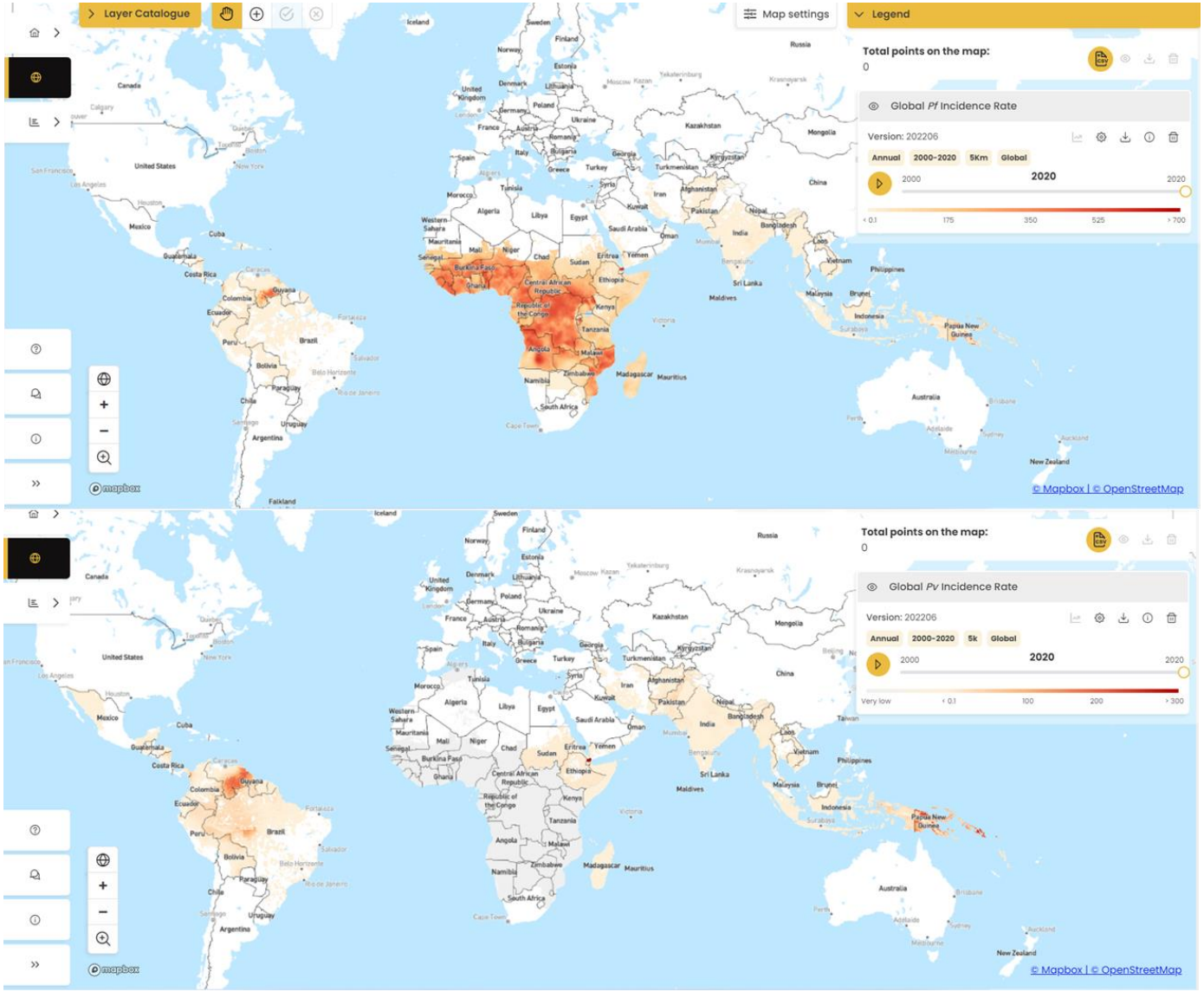

Figure 1.2: Global incidence distribution of *Plasmodium falciparum* and *Plasmodium vivax* malaria. (Top) The global incidence rate of *P. falciparum* infections is concentrated in sub-Saharan Africa. (Bottom) The incidence rate for *P. vivax*, which is prevalent in South America and South East Asia. The maps were reproduced from the Malaria Atlas Project website (malariaatlas.org/) under the creative commons attribution 3.0 licence (https://creativecommons.org/licenses/by/3.0/).[20]

The life cycle of *P. falciparum* malaria is complex, occurring in both the mosquito and human hosts. The human host's life cycle can further be divided into the liver and intraerythrocytic stages. Specific to the mosquito host, after a blood meal from an infected human host, the acquired gametocytes fuse in the mosquito (sexual life cycle) to form zygotes.[18,21] The zygotes then mature into ookinetes which develop into oocysts, which later become sporozoites.[18] The ruptured sporozoites are then transferred into the mosquito salivary glands, ready to be transmitted during the next blood meal. This multiplication stage of the parasite is called the sporogonic cycle.

Once in the mosquito's salivary glands, the extracellular sporozoites are transferred into humans through the epidermis when the mosquito takes a blood meal. These sporozoites are then transferred into the liver, where they infect the hepatocytes.[21] In the hepatocytes, the sporozoites mature into schizonts, later rupturing and releasing merozoites into the bloodstream, so completing the liver stage of the life cycle. During the intraerythrocytic phase (asexual life cycle), the merozoites invade healthy red blood cells (RBCs). Once in the RBCs, the parasite matures through the digestion of host haemoglobin (Hb) into ring-staged parasites. Over 24 hours, these ring-staged parasites develop into mature trophozoite-staged cells. These mature trophozoites then undergo mitotic division, resulting in schizont-staged parasites, which will rupture and give rise to merozoites that further perpetuate the intraerythrocytic cycle. Furthermore, a selection of the parasite population will differentiate to become gametocytes during each cycle, ready to infect a mosquito during a blood meal. These intraerythrocytic stages occur within 48 hours. A summary of the *P. falciparum* life-cycle events is illustrated in Figure 1.3.

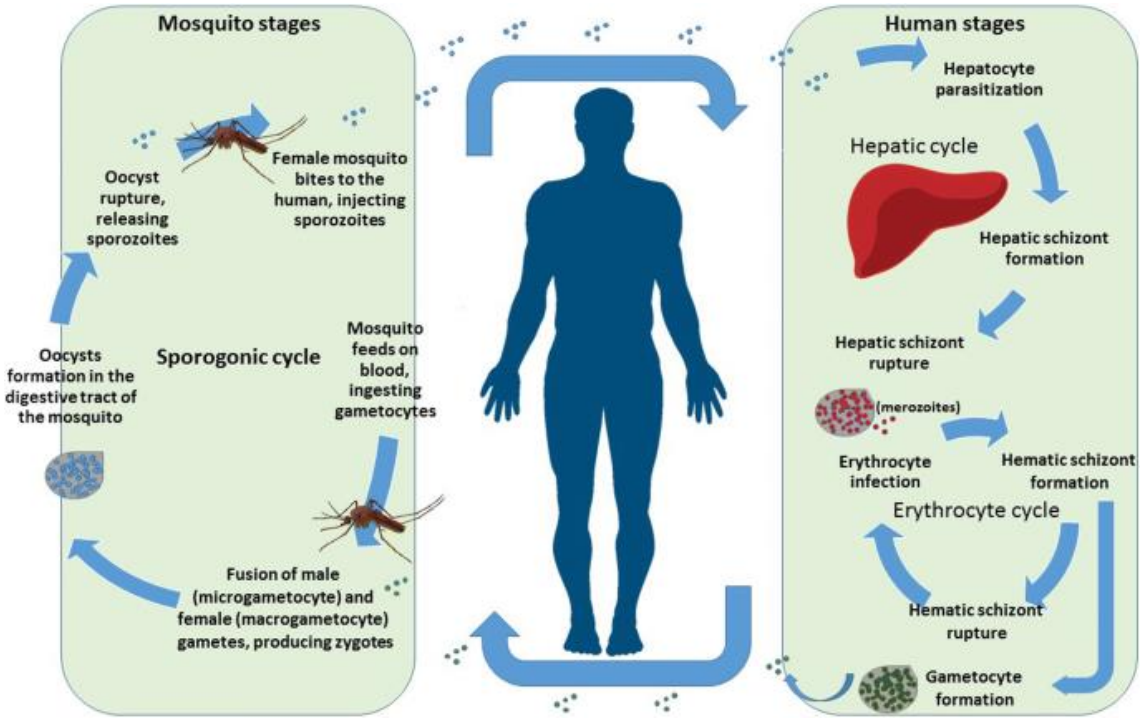

Figure 1.3: The *Plasmodium falciparum* parasite life cycle. The mosquito stage depicts the sexual cycle, and the human stage shows both the asexual hepatic and erythrocytic cycles. Reused with permission of Springer Nature, from Garrido-Cardenas, J. A.; González-Cerón, L.; Manzano-Agugliaro, F.; Mesa-Valle, C. Plasmodium Genomics: An Approach for Learning about and Ending Human Malaria. *Parasitol. Res.* **2019**, *118* (1), 1–27; permission conveyed through Springer Nature and the copyright clearance center.[21]

The onset of the intraerythrocytic stage is virulent and responsible for the typical clinical symptoms of malaria. Often these manifestations are characterised by an enlarged spleen and adhesion to the endothelium lining of blood vessels and other organs, which later induces the pathophysiology of the disease.[22,23] In the past, malaria interventions focused on treating the asexual stages, partly because of the safety and environmental health concerns of IRS and ITN agents at the time.[24] However, with the improvements in analytical tools and environmentally friendly chemical agents, each stage of the parasite life cycle presents a potential target for drug development. For example, ecologically friendly ITNs and IRS specifically target the malaria vectors (mosquitos), and different chemoprotection interventions and vaccines are used to intervene in the host life cycle, including the gametocyte stage.[24,25]

From here onwards, this literature review focuses on the intraerythrocytic stage of the *P. falciparum* parasite.

1.4. *Plasmodium falciparum* intraerythrocytic stages

The *P. falciparum* parasite is a complex unicellular protozoan that thrives in RBCs in four major stages (Figure 1.4). These stages are all distinct in the 48-hour life cycle: merozoites, rings, trophozoites, and schizonts. The significance of each stage of the life cycle is discussed below.

1.4.1. Merozoites

To invade the RBC, the merozoite, a tiny egg-shaped cell equipped with secretory vesicles, induces temporary disruptions of the standard structure of the RBC membrane.[26–28] Upon entry, the merozoite adheres and performs an apical orientation using merozoite surface proteins. After that, a chain of chemical events believed to be influenced by the rhoptries leads to the formation of a parasitophorous vacuole membrane (PVM).[27] Subsequently, dense granules are released by the merozoite into the parasitophorous vacuole (PV) to transition the cell into a ring-staged parasite.[27] This prepares it for nutrient acquisition and enlargement within the host cell.

1.4.2. Rings

Once adhered to the RBC, the parasite flattens into a biconcave disk-shaped cell with a thick cytoplasm that houses major organelles like the nucleus, plastids, mitochondrion, and ribosomes, to name a few.[27,28] Also developed at the ring stage are membrane structures like the tubulovesicular network that is interconnected to the PVM and sleeve-like structures called Maurer's clefts.[29] The clefts are secretory features responsible for trafficking proteins from the parasite lumen to the RBC membrane.[30]

During structural development at this time, the parasite also begins feeding on Hb for nutrients via the cytostome. Concomitantly, to avoid phagocytic clearance by the spleen, the parasite initiates cytoadherence of the infected RBC (iRBC) to the linings of blood vessels and other organs.[28,29] This adherence is associated with knob protrusions on the surface of the iRBC membrane, which embeds a cytoadherence protein called *P. falciparum* erythrocyte membrane protein 1 (PfEMP1). The parasite is then set for enlargement and to mature into the more metabolically active trophozoite cell.

1.4.3. Trophozoite

During its development, the parasite takes up the RBC cytoplasm, which mainly consists of Hb. It is estimated that this uptake is initiated in the mid-ring stage and that by the end of the 48-hour cycle it would have digested about 75% of the RBC cytosol.[31,32] The actual metabolism of Hb in *P. falciparum* parasites is discussed later in this review. However, aside from the peak Hb digestion, the trophozoite stage is also reported to be where the host RBC remodeling is at its peak.[26,27] Since the iRBC already adheres to the visceral organs at this point, part of its fundamental cellular processes is to continue to export to the surface crucial molecules that compromise the permeability of the RBC, thus increasing its chances of

survival and preparing for the release of its subsequent progeny. Therefore, to sustain the increased demand of trafficked molecules, the number of ribosomes and surface area of the endoplasmic reticulum substantially increases during this stage.[28] Concurrently, there is growth of the DV which is the compartment of Hb digestion, and enhanced development of structures like the Golgi body and exocytic vesicles, which are believed to be responsible for the transport of parasite proteins to and from the RBC surface.

As the parasite continues to digest Hb for nutrients, specifically amino acids, an increase in the secondary byproduct of Hb, namely haem, is also prominent. Given that haem is toxic to the parasite, an evolutionary mechanism of haem detoxification to produce haemozoin occurs in the parasite's DV.[33,34] Haemozoin, an inert and non-toxic biocrystal, continues accumulating in the parasite throughout the life cycle until the schizonts divide to form the merozoites.[28,35] Notably, there is no functional internal distinction between trophozoite and ring-staged cells other than in their metabolic activity, size and shape.[28]

1.4.4. Schizonts

Unlike the ring and trophozoite stages, schizogony is distinguished by nuclear division and multiple observable nuclei when viewed under a light microscope (Giemsa-stained). Specifically, during the schizont stage, the mature trophozoite undergoes nuclei divisions and synthesises molecules required for the next phase of RBC invasion.[27] Incidentally, the ingestion of Hb and the export of molecules still occurs throughout this stage. Also, the number of knobs on the surface increases, thus distorting the cytoskeleton and membrane of the RBC.[28] Furthermore, the above-mentioned endomitotic division results in 16 to 32 nuclei encompassed into merozoite buds. Remarkably, these will be released following multiple chemical processes. Salmon *et al.* reported that the merozoites' subsequent budding during the schizont stage depends on a proteolytic mechanism.[36] It is believed that the merozoites, still enclosed in the PVM, escape the RBC, and then through a proteolysis-dependent process, induce the rupture of the PVM. Consequently, this release enables the merozoite invasion of healthy RBCs to propagate the life cycle. All these asexual stages are shown in Figure 1.4.

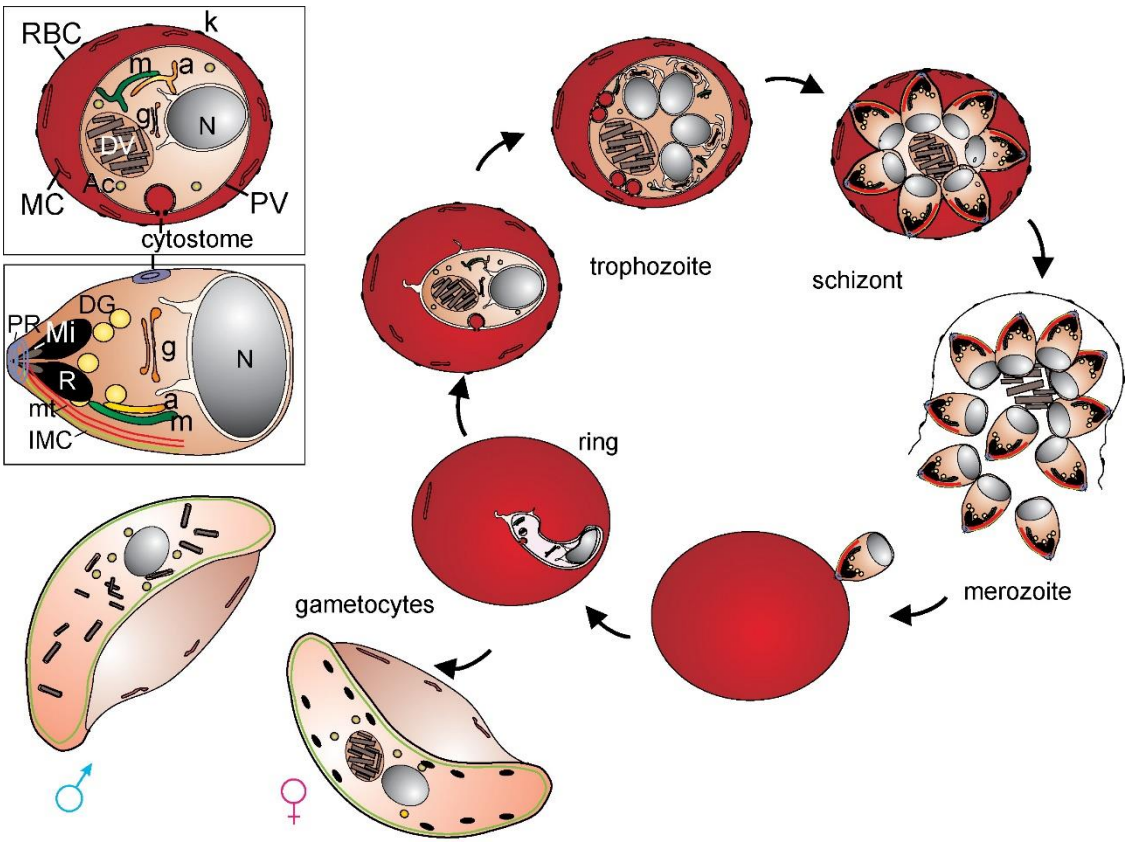

Figure 1.4: The intraerythrocytic stages of the *Plasmodium falciparum* parasite. The intraerythrocytic cycle begins when merozoites invade RBCs and develop into rings, which mature into trophozoites and schizont (mitotic division) stages. Selected parasites differentiate into gametocytes (male and female) that perpetuate the malaria transmissions when ingested by mosquitoes. The inserts illustrate a RBC infected with a trophozoite-staged parasite (upper insert) and an egressed merozoite stage parasite (lower insert). Keys for abbreviations: the nucleus (N), Golgi (g), digestive vacuole (DV), mitochondrion (m), apicoplast (a), acidocalcisomes (Ac), cytostomal invagination, parasitophorous vacuole (PV), Maurer's clefts (MC), knobs (k) indicated, rhoptries (R), micronemes (Mi), dense granules (DG), polar rings (PR), inner membrane complex (IMC) and lateral microtubules (mt). The Figure is reproduced with the permission of Elsevier, from Tilley, L.; Dixon, M. W. A.; Kirk, K. The *Plasmodium falciparum*-Infected Red Blood Cell. *Int. J. Biochem. Cell Biol.* **2011**, *43* (6), 839–842; permission cleared through the copyright clearance center.[34]

1.5. The digestive vacuole and haemozoin formation

Post-merozoite RBC invasion, the *P. falciparum* parasite transitions into a ring-staged cell that houses major organelles like the DV. Although the mechanism of origin of the DV is widely contested, it is reported that this organelle forms from the fusion of small, acidified vesicles that arise from the parasite's periphery.[32,37] Some evidence of these mid-ring stage acidic structures was presented by Abu Bakar *et al*. and Gruring *et al.* using various analytical techniques, and this supports the suggestion that the fusion of vesicles into a single large structure occurs in the mid to late ring stages, so resulting in a single large DV.[32,38] Furthermore, these small vesicles appear to be the first site of initial Hb digestion since they

had been observed to contain haemozoin crystals even before coalescing into the single DV. Therefore, both these occurrences corroborate the argument that Hb digestion starts during the ring stages and that this possibly precedes the formation of the single largest DV.

Interestingly, the DV plays two major critical roles in the survival of *P. falciparum* parasites. First, all the imported RBC cytosol (Hb) is trafficked by cytostomes for metabolism in the DV. The catabolism of Hb involves some utilised peptides and proteases and occurs throughout the asexual life cycle. Once digested, some of the freely hydrolysed amino acids are used for nutrients. However, Hb catabolism also gives rise to toxic haem species that threaten the parasite's viability. This leads to the second essential role played by the DV compartment — which is to detoxify the subsequent haem released during Hb digestion into the non-toxic haemozoin. Accordingly, the DV provides an exciting repertoire for drug development, and specific pathways like the haem detoxification route are unique to the parasite, thus making them suitable as direct molecular targets.

1.5.1. Haemoglobin uptake and digestion

Hb catabolism is more prolific during the trophozoite stage when the parasite is more metabolically active. However, as alluded to above, the transport and catabolism of Hb into the DV begins during the developmental ring stage. Here, cytostomes facilitate the ingestion of Hb into the DV *via* an endocytosis mechanism.[39–42] These cytostomes are believed to be extensions of the PVM and parasite plasma membrane (PPM), which was developed earlier in the ring phase.[32] The DV, having formed from multiple acidic vesicles, is a very specialised acidic environment, estimated to be maintained at a pH range of approximately 5.0–5.4.[39,41] The DV is thought to provide the optimal conditions necessary for the enzymatic processes involved in haemoglobin digestion. Notably, the catabolism of Hb is associated with major aspartic proteases: plasmepsins 1, 2, 3 and 4; zinc protease falcilysin; and falcipain proteases (cysteine).[41,43,44] These proteases are said to hydrolyse the ingested cytosolic Hb proteolytically into oligopeptides. Further evidence of the role played by the enzymes in Hb metabolism was given by Harbut *et al.,* they demonstrated the critical role of aminopeptidases in Hb metabolism using two metallo-aminopetidases.[45] They showed that specific inhibition of certain aminopeptidases prevented proteolysis of Hb-derived oligopeptides, leading to parasite death. This confirmed the critical role played by enzymes in Hb metabolism to preserve parasite survival.

Once the cleavage is complete within the DV, the process produces globin and ferrous haem. The parasite then uses some of the globin-derived peptides as nutrients and amino acids for protein synthesis. However, there are suggestions that some of the derived peptides are transported by *P. falciparum* chloroquine resistance transporter (PfCRT) into the parasite cytosol for further degradation by *P. falciparum* M1 alanyl aminopeptidase (*Pf*M1AAP) and M17 leucyl aminopeptidase (*Pf*M17LAP) – making the actual digestion of Hb a very complex

process.[43,46] Nonetheless, the whole process provides exciting opportunities as an antimalarial drug target. Indeed, recent efforts have been made to develop anti-aminopeptidase compounds specific to the malaria aminopeptidase homolog, specifically to the M1 and M17 aminopeptidase families.[45,47] Figure 1.5 summarises the processes involved in the iRBC during Hb metabolism in the DV.

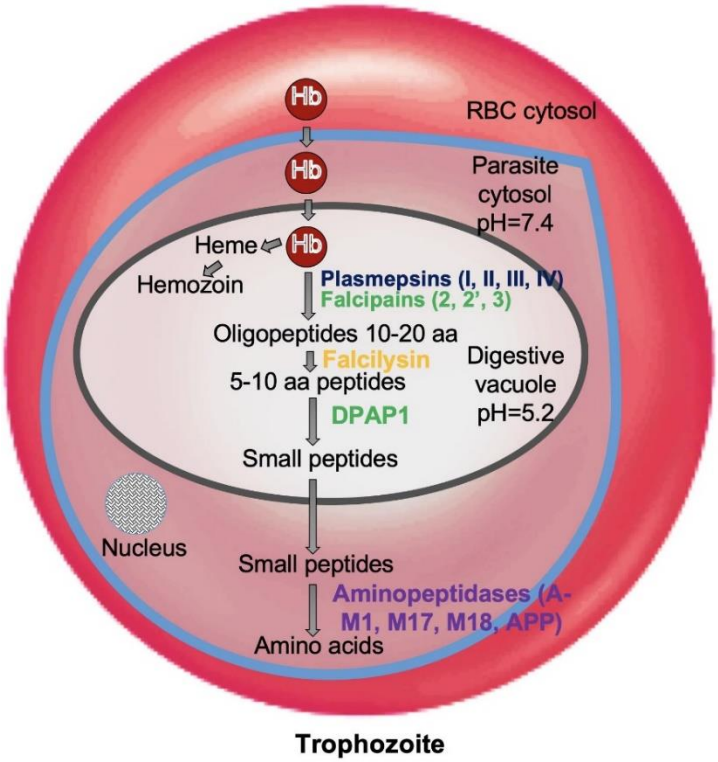

Figure 1.5: A *P. falciparum*-infected red blood cell. The schematic shows enzymes (proteases and other role players) that mediate the degradation of Hb. Hb degradation occurs in the digestive vacuole through the coordinated action of plasmepsins and falcipains into small peptides and heme (haem). These small peptides then get broken down into amino acids by aminopeptidases. Furthermore, the amino acids are transported to the parasite cytosol *via* an ATP-dependent mechanism. Republished from Mishra, M.; Singh, V.; Singh, S. Structural Insights into Key Plasmodium Proteases as Therapeutic Drug Targets *Front. Microbiol.* **2019**, *10* (MAR), 394, under the creative commons attribution licence (CC BY), Copyright (2019).[44]

1.5.2. Effects of haem from haemoglobin digestion

The proteolysis of Hb in the DV inadvertently leads to the production of haem as a ferroprotoporphyrin (Fe(II)PPIX) species. Haem is the primary source of oxidative stress in the malaria parasite. Essentially, haem-containing iron with a +2 oxidation state (Fe (II)) is autooxidised from Fe(II) to Fe(III), resulting in the formation of the ferriprotoporphyrin (Fe(III)PPIX) species (commonly referred to as haem or haematin).[43,48] Although the exact mechanism in which this oxidation takes place is yet to be fully understood, dioxygen (O_2) is believed to be the oxidant. This is supported by the fact that oxyhaemoglobin is oxidised to methaemoglobin at lower pH, producing quantities of superoxide (O_2^-).[49] Therefore, under the DV conditions in trophozoite cells, this spontaneously results in H_2O_2, which is highly toxic to the parasite. The parasite converts it to H_2O and O_2 via some catalytic activity.[49]

The resultant Fe(III)PPIX, like Fe(II)PPIX and H_2O_2,, possesses cytotoxicity risks to the parasite, thereby threatening its survival. Furthermore, although believed to be partly insoluble in aqueous conditions of the DV environment, Fe(III)PPIX is thought to associate with non-polar lipid membranes.[48] Free Fe(III)PPIX is proposed to cause lipid peroxidation and membrane destabilisation through a colloid osmotic process.[43,50] This critical hypothesis is supported by work from Oliveira *et al*. who showed that haemin increased lipid peroxidation significantly when added to phosphatidylcholine (PC) liposome, whereas haemozoin, the detoxified form of haem, presented with reduced capacity to impose any damage (Figure 1.6).[51] Notably, Fe(III)PPIX (interchangeably referred to as haem or haematin) differs from haemin in that the coordinating ion to the iron centre of haemin is chloride, while in haematin it is a hydroxide ion.[52] Nonetheless, this indisputably signifies the vital role of haemozoin detoxification in the parasite.

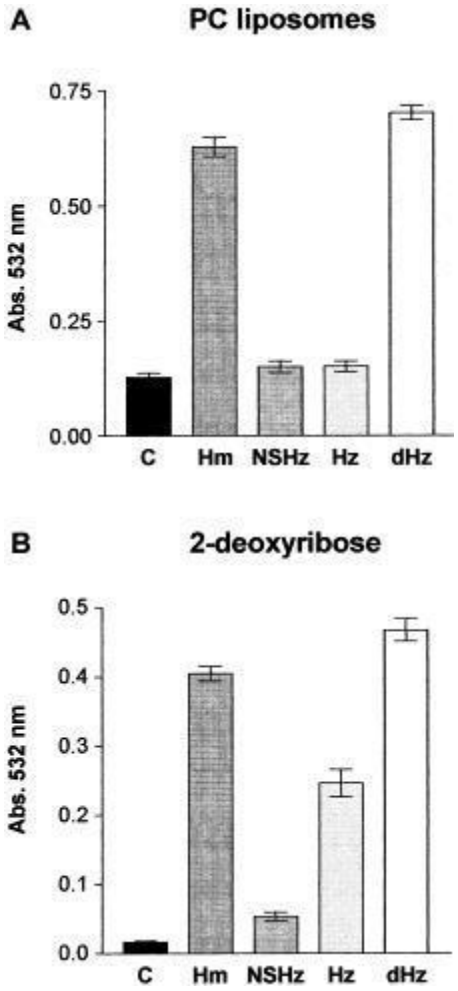

Figure 1.6: The effects on lipid peroxidation by haem compared to haemozoin. The two substrates used for the oxidation experiments were (a) phosphatidylcholine (PC) liposomes; and (b) 2-deoxyribose. The produced oxygen radicals were quantified by measuring thiobarbituric acid reactive substances (TBARS). In both substrates, haem produced significantly higher TBARS than haemozoin, thus demonstrating the strong pro-oxidant effects of haem versus haemozoin. Abbreviations: C = control samples without any additions; dHz = samples containing 15 µM de-aggregated haemozoin (solubilised using 0.1 M sodium hydroxide); Hm = samples containing 15 µM of haem (Hm); Hz = samples containing 15 µM of sonicated haemozoin; NSHz = samples containing 15 µM of non-sonicated haemozoin. Taken from: Oliveira, M. F.; Timm, B. L.; Machado, E. A.; Miranda, K.; Attias, M.; Silva, J. R.; Dansa-Petretski, M.; De Oliveira, M. A.; De Souza, W.; Pinhal, N. M.; Sousa, J. J. F.; Vugman, N. V.; Oliveira, P. L. On the Pro-Oxidant Effects of Haemozoin. *FEBS Lett.* **2002**, *512* (1–3), 139–144. Reprinting permission was granted by John Wiley and Sons Ltd, publishers, through the copyright clearance center.[51]

1.5.3. Haemozoin crystal and haemozoin formation

Haemozoin biocrystals serve as the detoxification by-products of the potentially toxic haem released during Hb degradation. Therefore, the mechanism of haemozoin formation in malaria parasites is critical for parasite survival, as is the globin for protein synthesis. This is because, as mentioned above, although rapidly autoxidised to Fe(III)PPIX, this still presents as a toxic insult to the parasite. This is especially given that it has been reported that within the DV of the parasite, haem (Fe(III)PPIX) can reach concentrations of up to 4 mM.[53] As alluded to previously, significant concentrations of haem in the parasite are lethal, as they result in oxidative stress, lipid peroxidation and cell lysis.[43,50,54,55] Remarkably, although in lower abundance to haem, some of these processes are believed to be contributed to by labile iron *via* the process of Fenton chemistry.[54] Nevertheless, here the focus is on the processes related directly to Fe(III)PPIX, specifically the haemozoin crystal and its formation.

1.5.3.1. Brief history of the haemozoin pigment

As previously mentioned, haemozoin pigmentation has been known within the scientific community for over a century. However, the first breakthrough in associating the brownish crystalline pigment as a blood product occurred during an autopsy in 1847 by Johann Heinrich Meckel.[56] Before then, the brown pigment deposit in the deceased organs of malaria patients was thought to have been a by-product of bile. Although Meckel did not associate the pigment with malaria infections, scientists Virchow and Frerichs discovered that the pigment's causal agent was the malaria parasites. Virchow likened the appearance of the pigment to haematin crystals. However, direct evidence of this association with haematin was later provided by Brown in 1911.[57] Thus, the conclusion was that the pigment was a haemoprotein and not necessarily pure haematin. However, the actual structure of haemozoin remained elusive for decades until the late 1980s.

In 1987, Fitch and Kanjananggulpan demonstrated for the first time, using elemental analysis, that haemozoin consists of purely Fe(III)PPIX (haem/haematin) molecules.[58] Furthermore, they concluded that this was likely identical to β-haematin, a synthetic form of Fe(III)PPIX, which, according to the literature, Hamsik had earlier described in 1937. Reportedly, at the time, Hamsik had used acetic acid precipitation to synthesise β-haematin from aqueous solutions.[48,58] Nonetheless, the actual evidence on the composition of haemozoin and its identical conformation to β-haematin was only produced in 1991 through Slater and colleagues using elemental analysis and x-ray diffraction, respectively.[59] In addition, they revealed that the structure is made up of Fe(III)PPIX molecules that are linked by coordinating to the iron centre (Fe(III)) of neighbouring haem propionate groups. Unfortunately, they incorrectly attributed the formation of haemozoin and β-haematin to polymerisation.

This hypothesised polymer structure remained as proposed and was further substantiated by Bohle *et al.* in 1997 using haem and haemozoin from intact lyophilised late trophozoites.[60] The structure was correctly predicted to be centrosymmetric. However, the elucidation of its arrangement still needed to be discovered. The breakthrough came in 2000 when the structure of β-haematin was established not to be a polymer but a cyclic centrosymmetric dimer of coordinating molecules linked by hydrogen bonds, as described above.[33] Thus, given that it was previously proven that both β-haematin and haemozoin were chemically identical, the inference to the latter's structure prevailed. Moreover, the structure of haemozoin was described as crystalline with defined faces. The illustration of the coordination of the dimeric molecules of haem is shown in Figure 1.7.

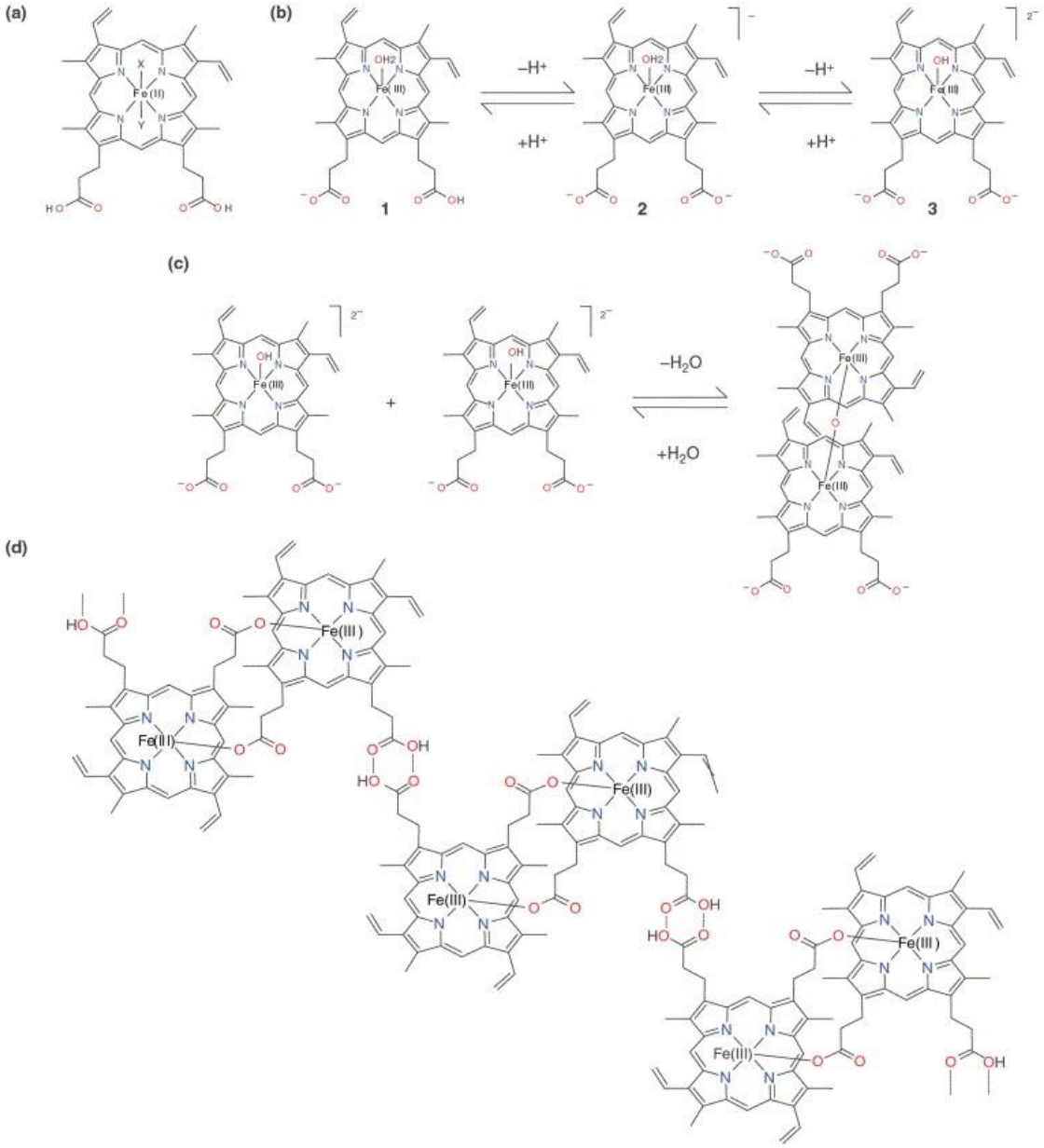

Figure 1.7: A schematic representation of detoxifying the haem species released from haemoglobin degradation. (a) Haem in haemoglobin (where Y is the proximal histidine residue of the protein and X is O_2 in oxyhaemoglobin). (b) The autooxidation of haem from Fe(II)PPIX to Fe(III)PPIX. (c) The haem dimers formed a μ-oxo bridge between the two Fe(III) ions through a dehydration process. (d) The formed dimers interact to produce a haemozoin structure, which appears as centrosymmetric haem dimers linked by hydrogen bonds. Reprinted with permission of Elsevier, from Egan, T. J. Haemozoin a Crystalline Drug Target. *Targets* **2003**, *2* (3), 115–124, through the copyright clearance center.[61]

1.5.3.2. Haemozoin formation process in the digestive vacuole

Although our understanding of the structure and composition of haemozoin has improved, the knowledge of its mechanism of formation still needs further understanding. This is especially given that chemical analysis has demonstrated that haemozoin accounts for ≥95% of all iron in mature trophozoites.[62] Interestingly, from earlier on, haem was believed to be polymeric in nature, and earlier studies suggested the involvement of a haem polymerase in its synthesis.[63] Other proteins had also been proposed at the time. Among these suspected proteins were the Histidine-rich proteins (HRPs).[64,65] For example, HRP II and III reportedly bound Fe(III)PPIX and mediated its sequestration into haemozoin (β-haematin) under acidic environments. However, Sullivan *et al.* demonstrated that *P. falciparum* field isolates lacking HRP II and III could still synthesise haemozoin.[66] This therefore highlighted that the presence of HRP is not necessarily required for crystal formation. Not surprisingly, in 2007, the same function was also attributed to the so-called haem detoxification protein (HDP).[67] And, more recently (2020), the role has also been attributed to the protein lipocalin, specifically its homologue PV5. PV5 is thought to be responsible for the unidirectional synthesis of the haemozoin crystal, thus giving the crystals their phenotypic morphology.[68] It was unequivocally shown that the genetic deregulation of this lipocalin-like protein in *P. falciparum* parasites resulted in multidirectional branching of the crystal. This therefore substantiates the essential role lipocalins play during haemozoin formation in the DV.

The other role players implicated in the detoxification of haem include lipids. It seems that the first demonstration of the involvement of lipids in haemozoin formation was performed by Bendrat *et al*. in 1995.[69] They synthesised β-haematin using lipid extracts from haemozoin. These findings initiated interest in the involvement of lipids in the sequestration of Hb-derived haem. Thus, in later work, the formation of β-haematin was mediated in the absence of proteins, using only lipids. These findings therefore suggested that the process of haemozoin formation was more complex than initially thought. Subsequently, Egan *et al*. employed an acetate solution and aqueous benzoic acid to form β-haematin.[70] This feat was not surprising as the DV had been proven to be acidic, meaning that these conditions are suitable for biomineralisation. Of course, this did not absolve the role of lipids in the haem sequestration process, as it was later demonstrated that lipid–water interfaces promoted β-haematin formation.[71] This was a process that was later achieved with many other solvents and detergents.[72,73] However, it is now believed that lipids may be responsible for providing fixed nucleation sites that promote haematin sequestration.

As Pisciotta *et al.* previously showed with lipids associated with haemozoin, the crystals were found at the lipid droplet surfaces.[74] Intriguingly, studies with β-haematin have shown a correlation between the lipid droplets and the crystal length.[75] But whether this was inferred in

the parasite during haemozoin formation remained to be discovered. This confirmation was later provided using a model for crystallite alignment derived from diffraction results in haemozoin clusters by Kapishnikov *et al.*[76] There, an X-ray pattern indicated the presence of hemozoin clusters, with each group comprising several crystals aligned along their needle c-axes, exposing their side faces (100) to a cylindrical-like surface that is suggestive of nucleation via a standard lipid layer. These observations affirmed that the haemozoin crystals, like the β-haematin crystals, constitute the same three faces: the (100), (001) and (011).[77] The modelled crystal structure of haemozoin is shown in Figure 1.8. Notably, it has been proposed that antimalarial drugs like chloroquine target some of these faces to impede parasite growth by inhibiting haemozoin formation.[78,79]

In conclusion, with all the above knowledge, our understanding of the haemozoin formation process is still limited and thus needs improving. Therefore, resolving all the limitations and the role of lipids and proteins in this process is crucial and will probably enhance our understanding of the mechanisms of inhibition in the detoxification pathway.

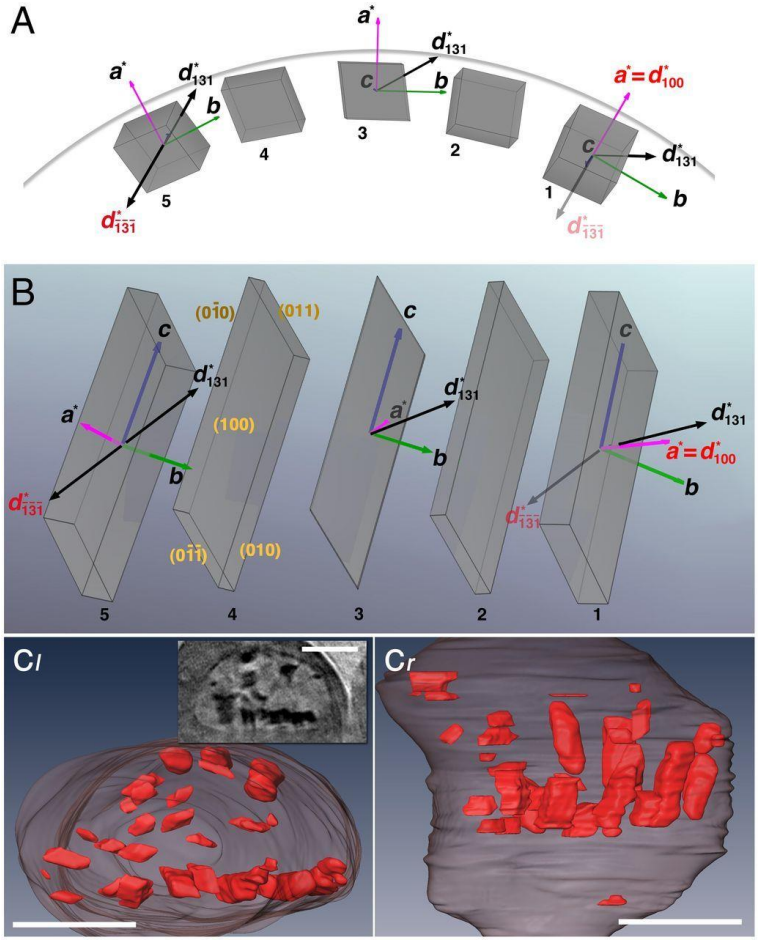

Figure 1.8: A model illustration of a hemozoin crystal structure in situ within RBCs. (A) Five crystals (labelled 1 to 5) are shown with their c-axes aligned almost parallel to the viewing direction, and their (100) crystal faces lying along a curved line. The crystal morphology [which exposes (100) and (010)

side faces and (011) slanted end faces] is based on a theoretical growth model of β-hematin and observed morphology of hemozoin. (B) The view of the five crystals along the radius of crystal 3. (C) A view of segmented cryo-XT of a trophozoite's DV, showing haemozoin crystals lining DV membrane, and (Inset) a reconstructed tomogram section viewed along the same direction. (Scale bars: 1 μm). Key: The model here denotes simultaneous diffraction of (100) and d^* ($\bar{1}\ \bar{3}\ \bar{1}$) reflections: The angle observed between the diffraction vectors d (100) of crystal 1 and d^* (131) of crystal 5 is 166°. Thus, the angle between d (100) and d^* (131) equal 14°. This is because the vector and label of d^* ($\bar{1}\ \bar{3}\ \bar{1}$) in crystal 1 are semi-transparent and belong to crystal 5; therefore, going from crystal 1 to 5, the crystals are rotated in steps of 14.5° about their c-axis (a total of 58°) and 3.3° about their b-axis, resulting in the observed angular difference of 14°. Taken from Kapishnikov *et al*., Aligned Hemozoin Crystals in Curved Clusters in Malarial Red Blood Cells Revealed by Nanoprobe X-Ray Fe Fluorescence and Diffraction. *Proc. Natl. Acad. Sci. U. S. A.* **2012**, *109* (28), 11184–11187, with the permission of PNAS (USA).[76]

1.6. Asexual stage infections: Prevention and treatment

Despite the high infection rates and virulence, malaria is preventable and curable. According to WHO, the current reductions in both incident rates and mortalities have strongly resulted from technologies that were unavailable in 2000 and before that.[1,4] These include, among others, ITNs (long-lasting), ACTs, and intermittent preventive treatment in pregnancy (IPTp). Of course, this is notwithstanding the crucial contributions of vector control measures with the IRS. Nonetheless, given that malaria is more prevalent in lower-income countries in sub-Saharan Africa, prevention is undoubtedly better than cure, mainly because these countries lack adequate access to healthcare. This is substantiated by the fact that in 2015 only 13% of febrile children in malaria-endemic regions had access to ACTs.[4] This is especially worrying given that the disease's victims are mostly children.

The purpose of this section is to review the current measures in place to prevent asexual-stage infections and treatment in cases of infections.

1.6.1. Prevention

To fight *P. falciparum* asexual stage infections, WHO recommends preventive measures in all malaria-endemic countries. As mentioned above, the commonly used preventive measures are ITNs, IRS, and IPTp for pregnant women. ITNs, specifically treated with the pyrethroid insecticide, are currently the most common prevention method, with a reported coverage of at least 68% of children in sub-Saharan Africa.[4,25] On the other hand, the use of the IRS has drastically decreased over the years due to concerns of its environmental impacts. However, in cases where the use prevails, WHO is recommended to prequalify the IRS of choice.[25] Furthermore, in endemic countries, pregnant women are provided extra protection as part of

antenatal care called IPTp. This involves giving antimalarial dosages during the second trimester of pregnancy at least once a month.

Notably, ITNs and IRS are vector control measures that serve as preventive measures against malaria infection, while the IPTp serve as chemoprophylaxis. Nonetheless, the above are only some of the measures recommended to prevent malaria cases and mortalities, although they are the most common practices. In some cases, prevention is done by performing either larviciding or mass drug administration (MDA) of the entire population, irrespective of the infection status.[25,80] One notable example of such an MDA campaign was the addition of CQ to table salt in the 1950s.[81] This is a measure that is believed to have contributed immensely to the subsequent rise in CQ resistance.

The next section focuses on chemoprophylactic preventive measures that help curb malaria infections.

1.6.1.1. Chemoprophylaxis

The most common chemoprophylactic preventive measures to protect against asexual stage infections include the following drugs: primaquine, pyrimethamine (PYR), sulfadoxine, and atovaquone (Figure 1.9). Primaquine is a unique 8-aminoquinoline in the quinoline family. Unlike most antimalarials in its class (used for asexual stage treatments), it is used for chemoprophylaxis of liver- and gametocyte-staged parasites.[82–84] Expectedly, its mechanism of action (MoA) differs from those of other quinolines since it is not used in asexual stage parasites.[82] Hence, unlike chloroquine (CQ), amodiaquine (AQ), and mefloquine (MQ), it is inactive against inhibition of β-haematin formation.[85,86] Also, contrary to the other quinolines, primaquine is reported to cause low haemoglobin levels in patients without glucose-6-phosphate dehydrogenase (G6PD).

On the other hand, sulfadoxine and PYR, like the major antimalarials used in ACTs, target the asexual stages of the parasite. However, these are used for chemoprophylaxis treatment in pregnant women as an IPTp.[87,88] The MoAs of sulfadoxine and PYR in the parasite are via inhibition of enzymes in the folate pathway, with this leading to impaired deoxyribonucleic acid (DNA) and ribonucleic acid (RNA) synthesis as a result of reduced pyrimidines (cytosine, thymine and uracil).[89] Interestingly, these two antifolates have beneficial non-malarial effects. They are reported to lead to improvements in birth outcomes, like birthweight, for example, which serve as beneficial characteristics that makes them superior prophylactic drugs compared to their rivals.[88,90] Nonetheless, like all the other antimalarials, these two drugs also face the challenge of resistant parasite mutants.[91–93] Genomic DNA analysed from resistant parasite isolates indicates that the resistance to the antifolates, specifically PYR, arises from point mutations that encode for the dihydrofolate reductase-thymidylate synthase gene.[94]

Lastly, atovaquone is a naphthoquinone antimalarial prophylactic with broad antiprotozoal activity.[95] It is reported to act on the parasite by inhibiting the mitochondrial cytochrome bc_1 complex.[96,97] Specifically, it depolarises the mitochondria by collapsing the electron transport chain, leading to cellular damage and death.[98] Despite its effectiveness, it is also challenged by emerging treatment failures because of resistant parasites. Furthermore, its resistance mechanism is associated with mutations in the cytochrome bc_1 complex.[99] Notably, atovaquone use is strictly recommended in non-endemic countries, where parasites remain sensitive to the drug.

Parasite resistance to antimalarials, being a major cause for concern, presents a challenge for all the prevention techniques mentioned above. The vectors, like the parasite, can develop resistance to the insecticides used, thus, leading to prevention failures.[1,4] When all the above prevention practices fail, and the asexual stage disease manifests, treatment with effective antimalarial drugs is the only option.

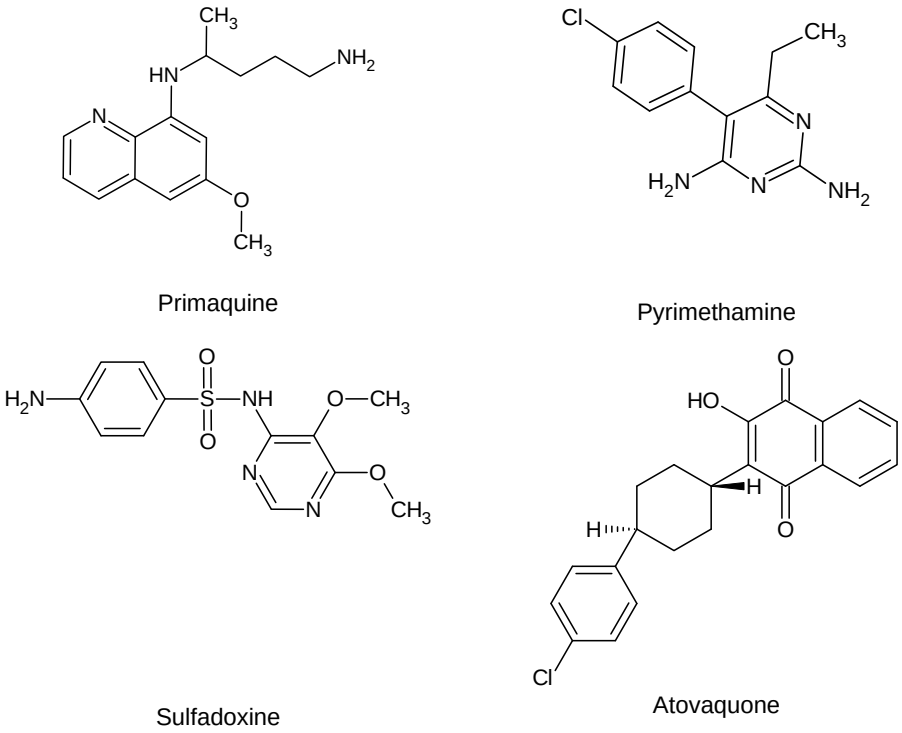

Figure 1.9: Structures of relevant antimalarials used for chemoprophylaxis.

1.6.2 Treatments

Once infected and when malaria progresses to the asexual stage, for those with access antimalarial therapy is their only hope of avoiding uncomplicated disease and even death. However, for some patients in endemic regions, infections present with lesser complications due to acquired immunity or sickle cell disease.[100,101] It is reported that in infected patients, both these conditions lead to the prolonged development of high parasitemia rates and

associated symptoms, although there have been no indications that sterile immunity has been achieved.[101] Nevertheless, the discovered immunity to malaria has led to the significant development of the RTS,S vaccine, which, although partially effective, will be very beneficial in endemic countries for helping with the future elimination of the disease.[102,103] Treatment via antimalarial drugs remains crucial for the time being, even with the recently approved vaccine and also for patients with less severe illnesses due to acquired immunity.

1.6.2.1. Artemisinin-based combination therapies (ACTs)

Current antimalarial therapies include the first-line WHO-recommended ACT drugs for uncomplicated *P. falciparum* malaria. These adopted ACT regimens are region or country specific. However, the most commonly used combinations in endemic regions are artesunate and amodiaquine (ASAQ) and artemether and lumefantrine (AL).[104–106] This is because they are the preferred first-line regimens used in most of the countries in the WHO African region to treat *P. falciparum* malaria, which accounts for more than 95% of the global cases. The other approved ACTs, artesunate and mefloquine, dihydroartemisin and piperaquine, and artesunate, sulfadoxine and pyrimethamine, are also efficacious and available for use in other endemic countries that prefer to adopt them as part of their first-line policies.[25] Notably, the choice of implementing ACT first-line treatment policies lies solely with the policy-makers in the specific countries, who normally make considerations based on several factors – like the costs and therapeutic efficacy of the ACT within their region. All these ACT combinations consist of a fast-acting drug (e.g., artesunate, artemether, dihydroartemisinin) for rapid reduction in parasitemia and a slow-acting, long half-life partner drug (e.g., amodiaquine, lumefantrine, sulfadoxine-pyrimethamine) that clears all parasites and protects against new infections for a limited period.[105] Despite their success, the ACTs' regimens, like the antimalarial drugs before them, face the threat of resistant parasites. Furthermore, a significant concern is the prevailing distribution of sub-standard antimalarial drugs, which may contribute to the development of parasite mutants.[107] Fortunately, the speed at which resistance has emerged or is emerging remains drug-specific (Figure 1.10).[108] Notably, a drug like CQ, previously used in monotherapy, is no longer in use today because of high treatment failures. Therefore, current treatment guidelines from WHO advise against using any current drugs for monotherapy.[25]

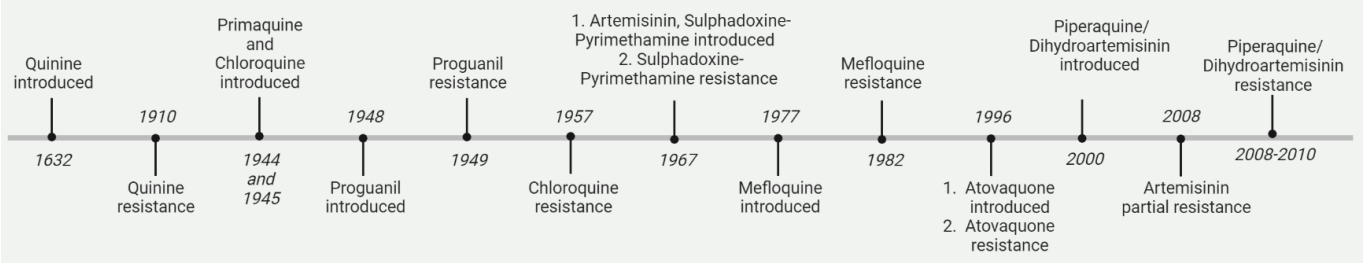

Figure 1.10: A timeline of the introduction of and independent evolution of antimalarial drug resistance. The timeline was reconstructed on biorender.com using data from Moss *et al.* and Leang *et al.*[108,109]

Historically, there has been a direct association between the widespread antimalarial resistance from Asia to Africa, as observed via molecular markers highlighted in Figure 1.11.[91,110] However, the recently detected partial resistance to artemisinin in Africa has been reported to have developed independently as the single-nucleotide polymorphism detected in Ugandan parasite mutants differed from those found in South East Asia.[111] In all artemisinin-resistant mutants, the encoded genetic mutations associated with resistance are in the kelch-13 protein (K13), irrespective of the country of origin (Figure 1.11a).[43,111–113] This resistance to the artemisinins is currently only associated with delayed parasite clearance of early ring-staged parasites and not full treatment failures.[113] However, this is concerning given that the artemisinins have a short half-life, which results in increased drug pressure from the longer-acting partner drug. This further threatens future malaria control since ACTs are the mainstay of malaria therapy.

Expectedly, artemisinins are just one of the combination drugs at threat of becoming obsolete owing to parasite resistance. The partner drugs piperaquine and amodiaquine have also shown select polymorphisms on the *P. falciparum* chloroquine resistance transporter (*PfCRT*) and the *P. falciparum* multidrug-resistant transporter 1 gene (pfmdr1), although selecting for different alleles (Figure 1.11b).[105,106,114] Interestingly, this is the same gene that was shown to encode CQ resistance by effecting significant changes in its DV accumulation through an efflux-mediated mechanism.[115] Therefore, for compounds like piperaquine and amodiaquine which share the same MoA as CQ, it is not entirely surprising that they are affected similarly in resistant parasites. Nevertheless, the resistance of these drugs is compound-specific and not necessarily linked to their haem target (haemozoin), which remains viable for developing new antimalarial drugs.[116] Although to our knowledge there are currently no mutations driving resistance to lumefantrine, there are reports that suggest that lumefantrine shares some cross-resistance with mefloquine.[25] This is a further indication of why there is urgency in developing new, effective antimalarial drugs. The details associated with the MoAs and resistance mechanisms for the above-mentioned drugs are discussed in the sections below.

1.6.2.2. Mechanism of artemisinins' partial resistance

As with the quinolines, the resistance mechanisms of the artemisinins are complex. However, they also present a primary determinant for resistance in the *k*13 gene.[43] This is a point mutation of the *P. falciparum* kelch protein gene on chromosome 13. Specifically, Ariey and colleagues associated these mutations with the *PF3D7_1343700* kelch propeller domain.[113] Although its role is unclear, the K13 protein is localised to the parasite's cytostomes and is thought to be essential for endocytosis or trafficking of proteins (Figure 1.11a).[117] Using parasite-resistant isolates, Ashley *et al*. found that the *k*13 mutation was associated with varying parasite clearance half-lives in different countries.[118] For example, isolates from the Democratic Republic of Congo showed parasite clearance that was about 1.9 hours, while it took 7.0 hours for isolates from the Thailand–Cambodia border to clear. The exact mechanism of this resistance is not fully understood. However, it is postulated that this is mediated through the reduced activation of artemisinin drugs or an evolved ability to remove damaged proteins.[43,119] Furthermore, as proposed by Yang *et al.* and Birnbaum *et al.,* decreased k13 levels impair haemoglobin digestion, so leading to lowered Fe(III)PPIX, and thus lowering artemisinin activation.[117,119] This is because, as mentioned above, one of the pleiotropic MoA of the artemisinins is hypothesised to be mediated *via* haem activation of the endoperoxide bridge on the artemisinin scaffold.[120] Although currently affected by only partially resistant parasites, the artemisinins are clearly at threat of full resistance in future. This is especially worrying since they are currently the mainstay of malaria treatments.

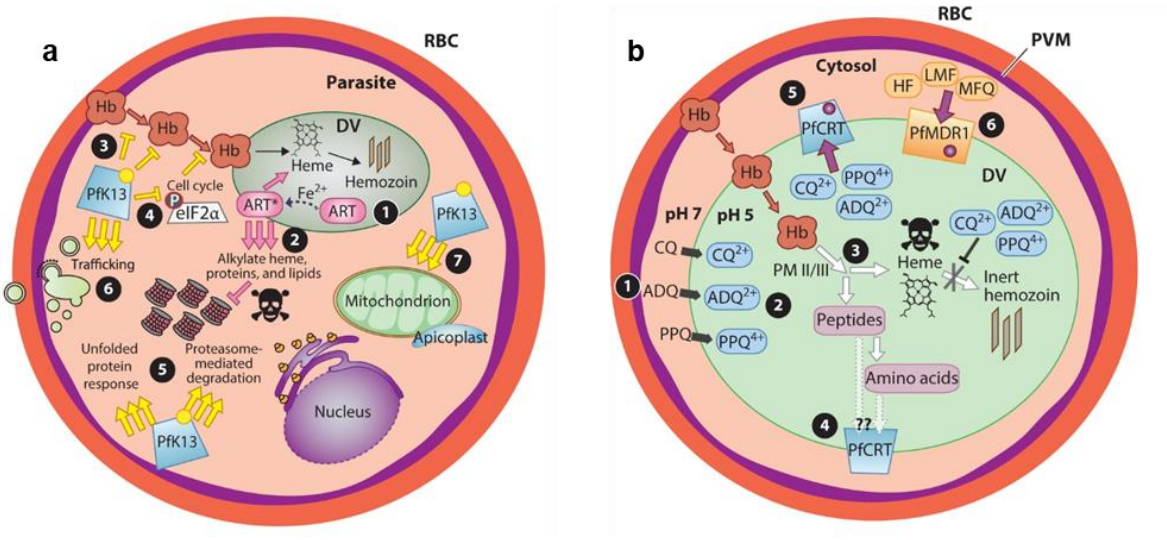

Figure 1.11: A model for the mechanism of action and resistant mechanism of ACT antimalarials – illustrating the roles played by PfCRT, PfMDR1 and K13. (a): (1) Showing the activation of artemisinin-based (ART) compounds by haem (Fe^{2+} and not Fe^{3+}) through cleavage of the endoperoxide ring. (2) The haem–ART alkylated species damages proteins and lipids, leading to parasite death. (3) In parasites with K13 mutations, Hb transport is reduced. (4) The K13 mutations lead to an extended duration of ring-stage development through a mediated eIF2α phosphorylation mechanism. Therefore, the changes result in decreased Fe(II)haem, which causes reduced ART activation. (5) K13 mutations can also lead to the activation of an unfolded protein response. (6) This can lead to drug and damaged protein removals through increased vesicular trafficking. (7) Mutations are also believed to help regulate mitochondrial physiology and to maintain membrane potential. (b): An asexual stage-infected RBC with a fully developed parasite PVM. (1) Quinoline-based antimalarials, chloroquine (CQ), amodiaquine (AQ) and piperaquine (PPQ) move from the cytosol to the acidic DV (pH 5). (2) Upon entry, these are protonated and accumulate (pH trapping), thus enabling them to move back into the cytosol. (3) The trapped protonated antimalarial molecules then bind to haem (heme), thus inhibiting haemozoin formation (hemozoin). (4) PfCRT is a DV membrane protein postulated to be responsible for transporting peptides from Hb degradation back into the cytosol. (5) A mutated PfCRT is believed to be responsible for the efflux of haemozoin-inhibiting antimalarials from the DV into the cytosol, away from their haem target. (6) In PfMDR1 mutant parasites, susceptibility to halofantrine (HF), lumefantrine (LF) and mefloquine (MF) are amplified as they are accumulated into the DV. Reprinted with Annual Reviews' permission from Wicht, K. J.; Mok, S.; Fidock, D. A. Molecular Mechanisms of Drug Resistance in Plasmodium Falciparum Malaria. *Annu. Rev. Microbiol.* **2020**, *74*, 431–454. Copyright permission requested was through the copyright and clearance center.[43]

1.6.2.3. Molecular mechanisms of chloroquine resistance and that of other quinolines

As alluded to in previous sections, historically, malaria elimination has been impeded by antimalarial resistance, and CQ was no exception. The first evidence of CQ resistance was reported in 1957 and was supposedly accelerated by the mass administration of the drug as a monotherapy, mainly as a table salt additive.[11,108] The exact mechanism of this resistance

in the parasites remained unknown for decades, albeit with the knowledge that CQR parasites accumulated less CQ than CQS parasites. However, in 2000, Fidock *et al.* elucidated the causal determinant mechanism in CQR parasites.[121] The study identified a mutation in the *P. falciparum* chloroquine resistance transporter PfCRT protein encoded by the gene *pfcrt*. This localised mutated vacuolar membrane transport protein mediates CQ efflux out of the DV into the cytosol, and away from the haemozoin target.[43,121–123] Notwithstanding the discovery of PfCRT, the protein structure remained elusive. The breakthrough in determining this structure has only been recent and was solved using single-particle cryogenic electron microscopy (cryo-EM). This implicated a vacuolar membrane protein containing 424 amino acids, 10 transmembrane helical domains, and 2 juxtamembrane helices (Fig 1.12).[124] Furthermore, the protein contains a negatively charged central cavity facing the DV, which allows it to transport positively charged species to the cytosol. Notably, all CQR isoforms, irrespective of origin, share an essential PfCRT K76T mutation.[125,126] Unsurprisingly, PfCRT is also said to be the primary driver of resistance to AQ.

For the 4-aminoquinoline and arylaminoalcohol antimalarials that interact with haem as their primary target, another marker that drives their observed resistance is reported to be the P-glycoprotein homolog (Pgh1), *P. falciparum* multidrug resistance 1 protein (PfMDR1), which is encoded by the *pfmdr1* gene.[127] Like PfCRT, PfMDR1 is also a transmembrane protein that lies on the DV. However, unlike PfCRT, its function is said to be transporting solutes from the cytosol into the DV.[43,128] Therefore, Pgh1 mutations affecting the inward transport of those molecules that exert their effects through associating with haem will hinder the molecules' ability to reach the target. On the other hand, this type of mutation will favour other quinolines like lumefantrine, halofantrine and mefloquine, which do not exert their antimalarial action via interactions with haem but on targets outside the DV. In contrast, Pgh1 mutations that promote transport into the DV have been linked with reduced susceptibility to halofantrine and mefloquine (probably the case for lumefantrine), because this inadvertently takes the drug away from its supposed target.[128,129] In general, most quinoline antimalarial resistance has been associated with selection for multicopy *pfmdr1*, irrespective of the fact that resistance remains somewhat drug specific.[43,105,106]

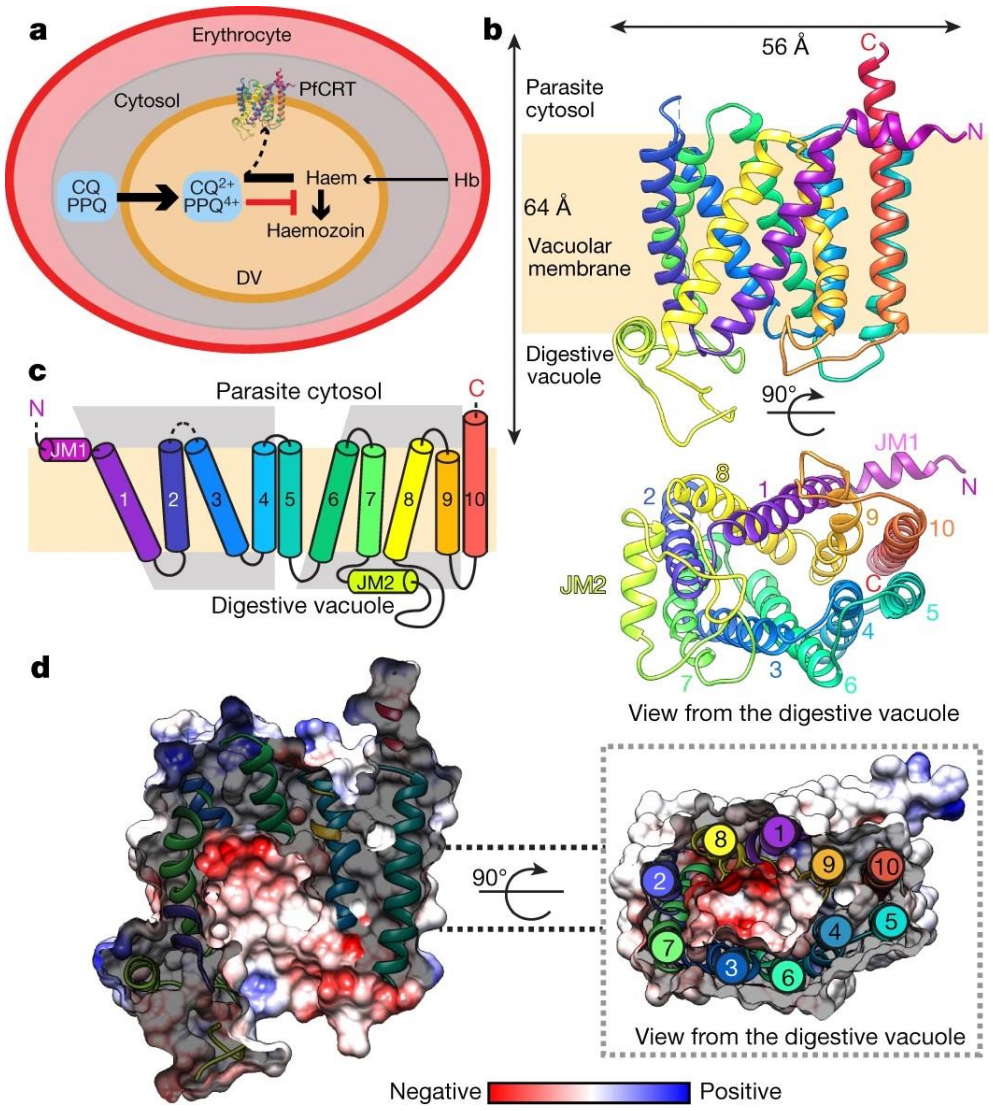

Figure 1.12: The Cryo-EM structure of PfCRT. (a) A PfCRT localised on the membrane of a *P. falciparum* intra-erythrocytic parasite's digestive vacuole (DV), through which haemoglobin (Hb) is transported into the DV and catabolised, thus releasing toxic unsequestered haem. Through a pH trapping mechanism, CQ and PPQ are believed to accumulate in the DV in a protonated state (CQ^{2+} and PPQ^{4+}), thus promoting incorporation into haemozoin to prevent haemozoin formation. In CQ-R parasites, PfCRT causes efflux of CQ from the DV into the cytosol away from the haem detoxification pathway. (b) The cryo-EM structure of PfCRT shows the 10 transmembrane (TM) helices in rainbow colours. Labels of the N and C termini are displayed. As viewed from the DV side, the rotated 90° structure of PfCRT is shown at the bottom, with the numbering of the TM and juxtamembrane (JM) helices (c) highlighting the topology of PfCRT's helices (TM1–TM10, JM1 and JM2). (d) A representation of the electrostatic potential on the surface of the central cavity; red and blue colours indicate negatively and positively charged residues, respectively. The inset on the right shows the arrangement of TM helices, labelled from N terminus to C terminus (the dotted lines represent a central slice through the structure to result in the inset view). Sourced from Kim *et al.,* Structure and Drug Resistance of the *Plasmodium falciparum* Transporter PfCRT. *Nat.* **2019**, *576* (7786), 315–320. The images were reused with the permission of Springer Nature publishers. The licence is granted through the copyright clearance center.[124]

Another worrying drug resistance trend is that of piperaquine, the partner drug of dihydroartemisinin. This came about because of growing resistance to the used primary artemisinin derivative ACT across South East Asia in the 2000s, which resulted in higher piperaquine selection pressure on parasites. Initially reported in Cambodia, piperaquine-resistant parasite isolates revealed amplification of potential resistance markers in plasmepsins 2 and 3 genes that encode for the aspartic proteases involved in Hb digestion.[130–132] These resistant parasites were reported to be linked to an increased risk of treatment failures. It is hypothesised that the observed decrease in piperaquine efficacy occurs because amplified plasmepsins allow the parasite to avoid the toxic effects of haemozoin inhibition by possibly decreasing the concentrations of unsequestered haem species for piperaquine binding.[108,132] This is because increased expression of plasmepsins (involved in Hb digestion) is believed to facilitate the rate of Hb digestion to counter the inhibitory effects of piperaquine on Hb digestion, since piperaquine-treated trophozoites (piperaquine-sensitive parasite) have been observed to contain packets of undigested Hb. These is a plausible hypothesis given that Mukherjee *et al.* found that the inactivation of the genes encoding plasmepsins 2 and 3 led to increased piperaquine sensitivity.[133]

Another marker suspected to be responsible for piperaquine resistance is an E415G mutation in the exonuclease gene.[131,134] However, an investigation by Boonyalai *et al*. revealed that insertion of this mutation in the *P. falciparum* exonuclease protein (PfEXO) was not associated with either increased parasite survival or 90% inhibitory concentration (IC_{90}) on piperaquine-treated parasites.[134] These results indicated that this mutation is insufficient to confer piperaquine resistance. It is believed however, that this mutation could still be an essential biomarker for monitoring piperaquine resistance when used simultaneously with other markers. This is because, in part, its role is not yet adequately understood as it has only been observed in Cambodian parasite populations and in edited parasite strains.[131,134]

The above discussion highlights the importance of MoA and MoR studies in helping with the discovery of future resistance mechanisms. For the quinolines, their resistance mechanisms are drug-specific and, intriguingly, not directly associated with their targets but rather via efflux mechanisms. This is true at least in the cases of CQ, amodiaquine and piperaquine. As a result, this makes haemozoin a viable target for future antimalarials given that it is immutable. Moreover, developing novel antimalarials with low resistance risks is crucial for future eradication of malaria, given the emerging resistance to artemisinins.

1.7. Looking ahead: Interventions to fight malaria resistance with current ACTs and future prospects

Resistant mutants compromise the efficacy of antimalarials. As a result, irrespective of the mechanism of action or resistance, there is a looming attrition to the current antimalarial arsenal, so threatening malaria eradication. Accordingly, the current cohort of antimalarials needs to be protected and new novel molecules need to be introduced. To combat this deadly parasitic disease despite the prevalence of resistant parasites, WHO introduced the Global Technical Strategy (GTS) for Malaria 2016–2030 (Table 1.1).[3,135] This strategy was briefly mentioned above and is discussed here in detail. The primary vision of the GTS envisages a world without malaria, and is arranged under three main pillars, which are sub-divided into goals, milestones and targets.[135] The pillars seek to address the following challenges (Table 1.1): (1) Ensuring equitable access to malaria tools for diagnosis and treatment, especially in endemic regions where these are often lacking and where sub-standard antimalarial drugs and diagnostic tools are prevalent. (2) Having member states accelerate towards malaria elimination to get malaria free-status. (3) Prioritising malaria surveillance.

The strategy specifies that the main objective for antimalarial treatment, prevention, and intervention should be achieving complete elimination and eradication of the disease, while protecting current antimalarial tools from becoming defunct because of resistance.[135] Most importantly, the sole intention of these aims is to pivot and provide an emphasis for drug discovery research programmes to start projects with existing ideas of end-products that will accelerate the process of achieving the targets set for 2030 by getting more desirable molecules in the malaria drug development pipeline. This is because it is believed that such interventions will help develop fully understood antimalarial drugs and tools that have the potential to be universally affordable in order to improve equitable access. However, notably, clear and specific guidelines for the drug discovery community are a requirement to help with the production of the type of antimalarial products needed.

Table 1.1: The World Health Organisation's (WHO) Global Technical Strategy for Malaria 2016–2030. The table was recreated from the 2019 World Malaria report. [135]

Vision – A world free of malaria			
Pillars			
Pillar 1	Ensure universal access to malaria prevention, diagnosis and treatment		
Pillar 2	Accelerate the process of eliminating and attaining malaria-free status		
Pillar 3	Transform malaria surveillance into a core intervention		
Goals	**Milestones**		**Targets**
	2020	**2025**	**2030**
1. Reduce malaria mortality rates globally compared with 2015	At least 40%	At least 75%	At least 90%
2. Reduce malaria case incidence globally compared with 2015	At least 40%	At least 75%	At least 90%
3. Eliminate malaria from countries in which malaria was transmitted in 2015	At least 10 countries	At least 20 countries	At least 35 countries
4. Prevent the re-establishment of malaria in all countries that are malaria-free	Re-establishment prevented	Re-establishment prevented	Re-establishment prevented

Interestingly, Burrows *et al.* gave clear guidelines for the drug discovery community by establishing what Medicines for Malaria Venture (MMV) describe as a target product profile (TPP), which may serve as a template for future drug discovery projects (see Table 1.2).[136] This involves, among other things, the need for the development and future provision of efficacious treatment against all species of human-causing malaria, including all the sexual and erythrocytic asexual stages.[3,136,137] There is also the need to solve the issue of recrudescent parasites, gametocytes and liver hypnozoites-staged parasites that often lead to relapses. Therefore, the goal would be to have a target candidate with the properties for single-exposure radical cure and prophylaxis (SERCaP), and this should be comparable to the current gold standard available for treatment of each stage. However, it should be remembered that these idealistic rationalisations do not limit or define the innovation of discovery projects. Rather, they provide a much needed guide to designing projects with a clear scope of the desired candidate product that will present with no potential cross-resistance to current antimalarial drugs.

Table 1.2: Medicines for Malaria Venture's (MMV) Target candidate profiles (TCPs) outlining the stringent set of biological attributes to select and prioritise during drug development projects. The table was recreated from Burrows, J. N.; Leroy, D.; Lotharius, J.; Waterson, D. Challenges in Antimalarial Drug Discovery. *Future Medicinal Chemistry*. 2011, under the terms of the creative commons licence (CC_BY: https://creativecommons.org/licenses/by/2.0). Copyright licence 2013.[136]

TPP / TCP	SERCaP			SEC
	Fast parasite clearance	**Long duration**	**Transmission blocking/ Relapse prevention**	**Chemoprotection**
Critical attributes	• Minimum 99.9% parasite clearance over 48 hours • >6 log total parasite reduction	• Time > MPC* critical • >80% ACPR day 28 monotherapy • Delivers>95% ACPR day 28 when combined with TCP1	• Gametocytocidal activity • Hypnozoitocidal activity without G6PD liability	• Liver schizontocide • Slow onset asexual blood stage • Supports 1x/ month use (min: 1x/ week) • High safety
Desirable attributes	• Gametocyte activity • Hypnozoitocidal activity	• Gametocyte activity • Hypnozoitocidal activity	• Vector-stage activity**	• Vector-stage activity to deplete mosquito reservoir • Gametocyte activity • Orthogonal MoA to minimise resistance development to drugs used for treatment
Current gold standard	Artemisinin	4-aminoquinolines	Primaquine	Atovaquone/Proguanil mefloquine

Key: MPC = Minimum Parasite Concentration, SEC = Single Exposure Chemoprotection, SERCaP = Single Exposure Radical Cure and Prophylaxis, TCP = Target Candidate Profile, and TPP = Target Product Profile.

1.8. The role of haem in antimalarial action

It has been well established that the detoxification of unsequestered haem (Fe(III)PPIX) to haemozoin accounts for the fate of haem in the DV. This is supported by evidence from electron spectroscopic imaging, chemical analysis, and Mossbauer spectroscopy that nearly all iron in trophozoites exists as haemozoin (≥95%).[62] In 1980, Chou *et al.* identified haem as a target for chloroquine and other antimalarials in its chemotherapeutic class.[138] In subsequent work, they attributed the activity to a resulting inhibitor complex with haem and showed that this led to haemolyses of cells.[139] However, as previously mentioned above, unsequestered haem alone is also toxic and has been shown to cause membrane damage and oxidative

stress.[50,54,55] Thus, disrupting or targeting the haem detoxification pathway at any stage during parasite development may be beneficial in developing new molecules.

Intriguingly, it has also been suggested that artemisinins are pleiotropic, and that they target haem and various proteins.[140] However, their interactions with haem are unique from the conventional mechanism that leads to inhibition of haem's sequestration into haemozoin. Instead, these have been reported to not necessarily interrupt haemozoin formation but to exert their action indirectly through interactions with Fe(II)PPIX. Although widely debated, it is said that Fe(II)PPIX is responsible for the cleavage of the endoperoxide bridge of artemisinins, resulting in haem-drug carbon-centred radicals.[120] These formed species then alkylate proteins and other molecules, so eventually leading to cell death. This is therefore one example of the diversified roles haem plays in the action of antimalarials. Conventionally, the MoA convolution associated with haem tends to focus on the complete inhibition of haemozoin formation by the inhibitor molecule. But, as is clear from the artemisinin example, the whole haem detoxification pathway presents an opportunity to discover novel molecules. Notably, it is crucial to emphasise that there may be various ways in which haemozoin formation may be inhibited.

1.8.1. Quinoline antimalarials

The quinoline class of antimalarial drugs are the oldest, most used and most well-known.[10] This antimalarial family is derived from quinine, which was first discovered in the early 19th century.[141] However, the use of quinine precedes its discovery, as it was isolated as the active ingredient of the bark of the cinchona tree, which was first introduced to Europe from South America in the 17th century for malaria treatment. Quinine and its stereoisomer quinidine were the primary ways of fighting the malaria endemic for centuries until the emergence of resistant parasites.[141] The distinctive identity of the quinoline group of antimalarials is *via* their heterocyclic aromatic rings in their organic structure (Figure 1.13). These quinoline antimalarials are divided into three groups: (a) 4-aminoquinolines including amodiaquine (AQ), chloroquine (CQ) and piperaquine among others; (b) aryl-amino alcohols including quinine, quinidine and mefloquine (MQ); and (c) and the 8-aminoquinolines that include pamaquine, primaquine and tafenoquine.[10,142]

The 4-aminoquinolines are inherently hydrophilic weak bases and are deprotonated at neutral pH, while aryl-amino alcohols are lipophilic weaker bases at neutral pH.[10,89] Coincidentally, the classification of these quinoline antimalarials happens to concur with the classification of their mechanism of action in the parasite. For example, the 4-aminoquinolines in general kill asexual-stage parasites by disrupting haem detoxification and leading to increased haem levels, whereas the aryl-amino alcohols exert their parasiticidal effects *via* a different MoA that

is currently not fully understood but is proposed to be outside of the DV (away from the haem target).[143–145] Regardless, the MoA of the 4-aminoquinolines is better understood than that of the aryl-amino alcohols and 8-aminoquinolines. Perhaps this is partly owed to CQ, which is by far the most popular drug of the family. Therefore, from here onwards, the review focuses on CQ and related antimalarials – specifically those that share similar MoA.

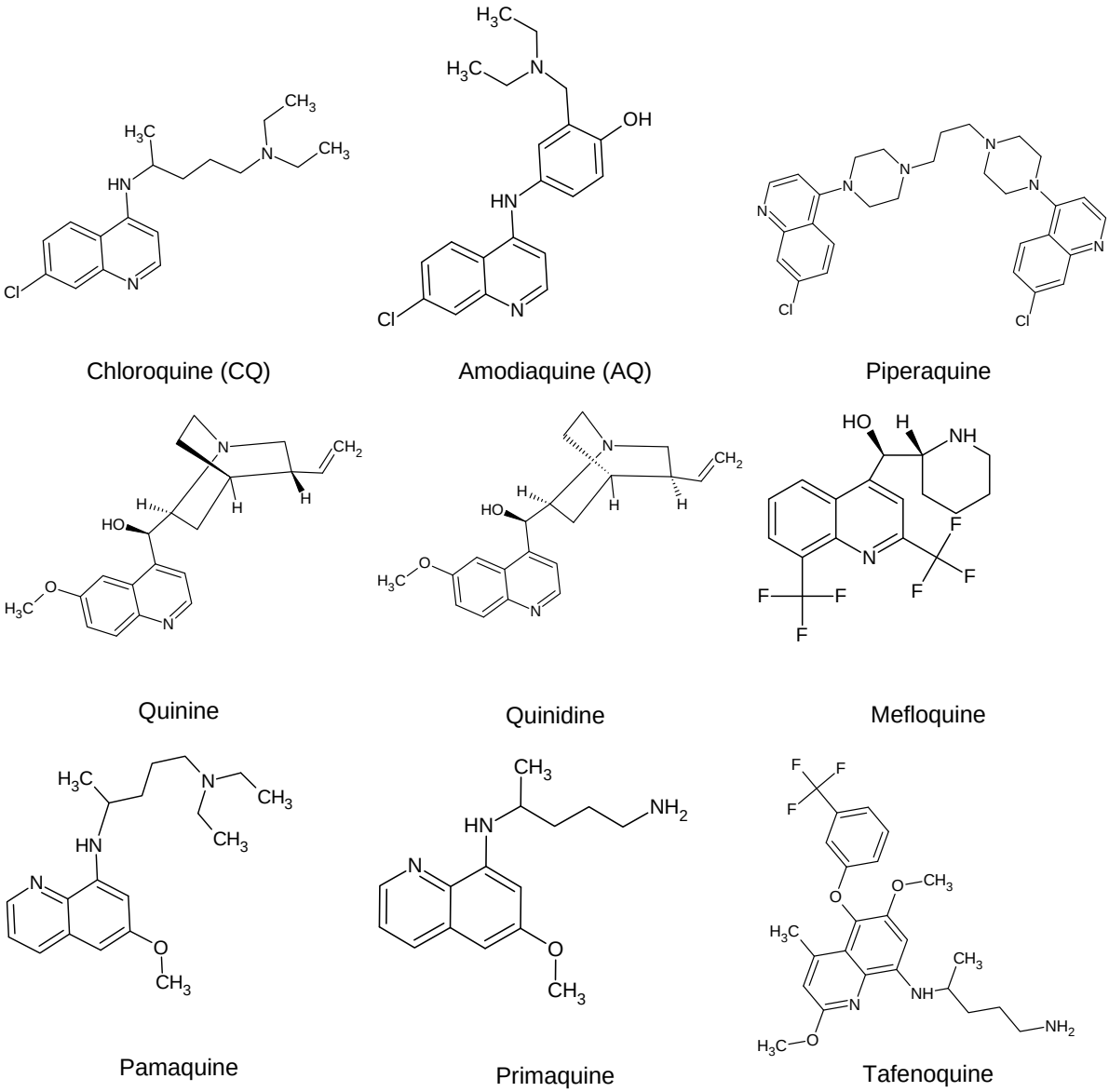

Figure 1.13: Structures of quinoline antimalarials.

1.8.2. pH trapping in the digestive vacuole

The DV is responsible for housing the metabolism of Hb and detoxification of haem, as well as being crucial in maintaining ion homeostasis.[37] For its homeostatic ion function, Saliba *et al.* reported that the DV is primarily acidified under physiological conditions through V-type H^+ ATPase and H^+-pyrophosphatase pumps.[146] Therefore, the subsequent inhibition of these

pumps with concanamycin A and sodium fluoride (NaF) proved detrimental to the homeostatic functions of the DV by resulting in alkalinisation. Given its inherently acidic nature, it is unsurprising that this vacuolar compartment plays a role in protonating basic molecules on entry. An example of one such molecule which has been extensively studied is CQ. This antimalarial drug is reported to accumulate to millimolar levels in the DV of treated parasites.[147]

It is believed that the same is true for the other 4-aminoquinolines. How this is achieved remains open to debate. However, the widely accepted mechanism is *via* pH trapping. This trapping mechanism is explained by the weak base properties of CQ (pK_{a1} = 8.1; pK_{a2} = 10.2), which allow CQ to readily diffuse across the membranes at neutral pH.[89,148] Thus, CQ gets doubly protonated (CQ^{2+}) and trapped inside the DV, where it cannot diffuse out in its protonated form. Alterations to the DV homeostasis expectedly lead to loss of function. Subsequent modifications of this intravacuolar pH gradient were shown by Yayon *et al.* to decrease the susceptibility of parasites to CQ concentrations. This therefore led to the critical deduction that the mechanism of CQ resistance observed may have been caused by decreased CQ accumulation in the DV.[148] However, it was unclear at the time how this occurred in the parasite. To explain these peculiarities in accumulation, a few studies at the time claimed that the pH of chloroquine-sensitive parasites (CQS) differed from that of chloroquine-resistant parasites (CQR), so leading to varying CQ accumulation.[149,150] However, this was later shown by Klonis *et al.* not to be the case. They found the pH of both CQS and CQR parasites to be the same, which led to a conclusion that the earlier observed differences in pH levels for the CQS and CQR parasites were method dependent.[151]

Notably, pH trapping is perhaps one of many mechanisms that lead to CQ's accumulation in the DV. This is because CQ heavily associates with haem in the parasite with a dissociation constant of 3.5×10^{-9} M, thus contributing to its accumulation.[138] This is not surprising given that CQ's MoA is through the inhibition of haem detoxification by capping the haemozoin crystals.

1.8.3. Mechanism of haemozoin inhibition

In 1980, Chou *et al.* discovered haem as a target for CQ and other antimalarial drugs.[138] In a later 1980 publication, they demonstrated that the complexation of CQ with haem in mouse erythrocytes led to haemolysis.[139] However, as alluded to in the earlier sections, the conclusive evidence of the inhibition of haemozoin formation by CQ was provided by Slater *et al.* in 1992, although, at the time, it was believed that this inhibition was directed at a haem polymerase enzyme.[63] Egan *et al.* subsequently showed that CQ (and other quinolines) inhibited the formation of haemozoin directly *via* pi-pi stacking interactions with synthetic haemozoin –

known as β-haematin.[152] However, it was not until after Pagola *et al*. discovered the structure of β-haematin that knowledge of this inhibition mechanism was improved.

The discovery of the β-haematin structure led to evidence showing that CQ and quinine interfered with the typical crystalline morphology of β-haematin crystals, so leading to the inhibition of the crystal growth.[153] The first crystal structure consisting of an inhibitor (CQ) capped to the β-haematin crystal (CQ-β-haematin complex), and grown as a DMSO solvate, was published by Gildenhuys *et al.* in 2013, and was obtained using a single-crystal X-ray diffraction technique.[78] Furthermore, they showed that CQ affected the crystal growth and was also found to decrease the first-order rate constant for the formation of the crystals. In particular, haemozoin formation inhibiting antimalarials are proposed to adsorb to the surface of the crystal.[79,154] Specifically, CQ was found to inhibit haematin sequestration by binding directly to the molecularly flat (100) surfaces.[79] Further evidence of the direct association of inhibiting drugs with haemozoin was reported by Kapishnikov *et al.* in 2019.[155] They demonstrated, using X-ray fluorescence microscopy with the bromine analogue of CQ, bromoquine, that even within parasites the drug adsorbs to the haemozoin crystal surfaces. These observations further support the suggestion that haemozoin-inhibiting antimalarials directly adsorb to the surfaces of the crystal to inhibit its growth, therefore resulting in an increase in unsequestered haem, which leads to parasite death.

1.8.4. Quantifying haem species for haemozoin-inhibiting antimalarials

The origins of the β-haematin methods can be traced back to the early 1990s when Slater *et al.* and Bendrat *et al.* used parasite extracts to synthesise β-haematin *in vitro*.[63,69] Of course, subsequent studies proved that the actual synthesis of these crystals without parasite extracts is possible and efficient.[70,156,157] The pioneering work came in the following years when various researchers developed techniques to synthesise β-haematin using only chemical reagents.[71–73] Although researchers have been measuring β-haematin inhibition by antimalarials and experimental molecules since the 1990s,[152,156] the quantification of haem species in parasites is more recent. Prior to this, predictions of haemozoin inhibition relied solely on *in vitro* β-haematin formation assays. These assays are based on a cell-free environment that mimics the low pH and lipophilic conditions of haemozoin formation in the DV.[73,158]

The commonest current method for measuring β-haematin inhibition *in vitro* employs a detergent-mediated assay with Nonidet P-40 (NP-40).[73,158] This method quantifies Fe(III)PPIX in aqueous solutions using pyridine, since in aqueous solutions pyridine forms a low-spin complex with haem but not β-haematin. However, despite its success, the method quantifies only extracellular inhibition, which is a considerable limitation since not all compounds can enter the DV to exert these inhibitory effects. This prompted the recent development of a

cellular haem fractionation assay by Combrinck *et al*.[143,159] The cellular haem assay, like the NP-40 assay, directly measures haem species in CQS parasites as a haem–pyridine complex. Here, experimental compounds can be tested at different dosing concentrations, which allows for the demonstrations of the haemozoin-inhibiting behaviour of the test compounds intracellularly. For example, the method has been applied to various antimalarials and experimental compounds, some of which turned out to have been falsely predicted to be haemozoin inhibitors by the β-haematin assay.[143,144,160,161] This revealed the inadequacy of using only β-haematin inhibition to demonstrate the cellular mechanism of haemozoin inhibitors.

The cellular haem fractionation assay showed that for some compounds, the increase in haem induces a corresponding decrease in parasite survival.[143] Moreover, another observed characteristic is that this increase in haem is directly correlated with signature decreases in haemozoin species. Figure 1.14 demonstrates these characteristic trends which were originally reported in Combrinck *et al.*[143] Notably, not every β-haematin inhibiting compound results in an increase of unsequestered haem, regardless of their effect on haemozoin levels. This was demonstrated with the β-haematin inhibitors, mefloquine and lumefantrine.[144] These two aryl-methanols resulted in decreased haemozoin formation without significant changes in unsequestered haem. This indicated that they were not true haemozoin inhibitors, given that their behaviour is like that of atovaquone (which also causes a decrease in haemozoin), a well-known mitochondrial cytochrome complex inhibitor. This highlights that the respective causative decreases in haemozoin are likely an indirect effect of the drug. For clarity, from here on, a haemozoin-inhibiting compound refers to a compound that causes a signature increase in unsequestered haem (or exchangeably called haem) and a concomitant decrease in haemozoin. Nonetheless, apart from quantifying haem and haemozoin, the cellular haem fractionation method also quantifies intracellular Hb (Figure 1.14a), which can also provide crucial information. For instance, it demonstrates whether the test molecule causes an increase in intracellular Hb levels or vice versa, which when considered using the first scenario may be an indication that the compound is affecting haemoglobin digestion.

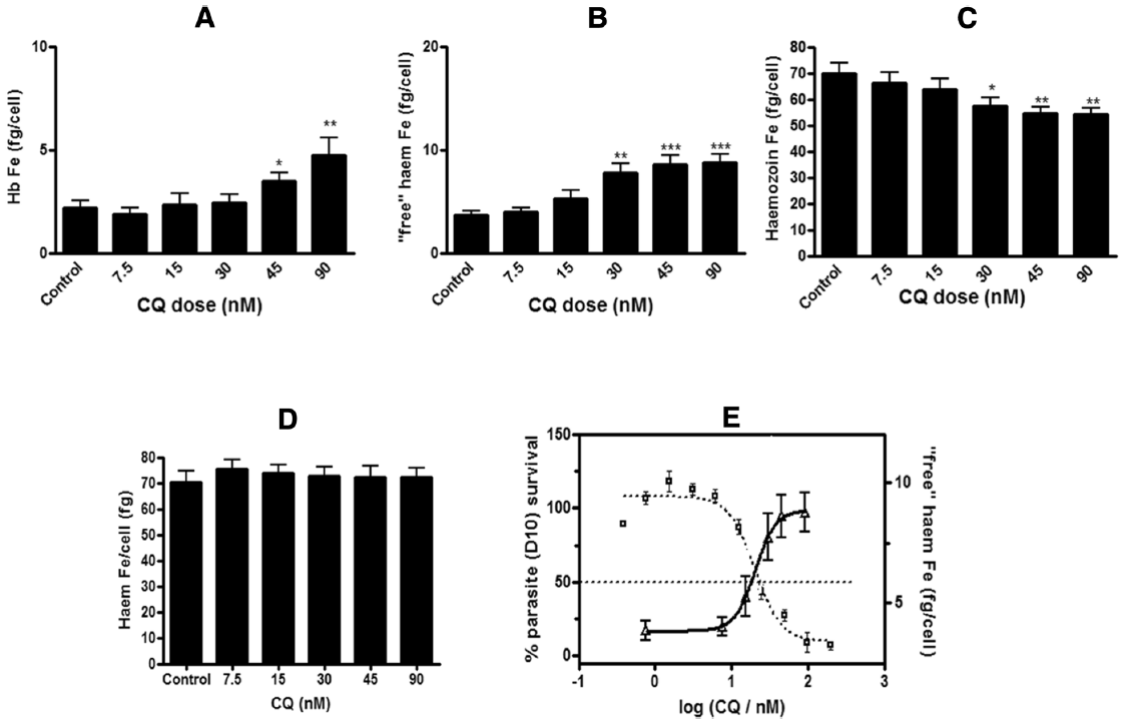

Figure 1.14: Plots of the intracellular haem species: (a) haemoglobin (Hb), (b) unsequestered haem, and (c) haemozoin in CQ-treated parasites. The total haem Fe (d) and parasite survival curve overlaid with unsequestered haem (e) are also shown. Reproduced from Combrinck *et al.*, *Malaria Journal* **2015**, *14* (1), 1–14, under the 2015 creative commons attribution licence (http://creativecommons.org/licenses/by/4.0).[143]

A few other methods for quantifying intracellular haem species have been reported, although these methods were not explicitly developed for determining haemozoin inhibition for antimalarials. Nonetheless, they are highlighted here as they are believed to be critical for the future of method development involving the quantification of haem species. The characterisation of Fe(III)-haem by electrospray ionisation mass spectrometry was apparently first reported by Pashynska *et al.* for noncovalent complexes of antimalarial artemisinin-based agents.[162] However, this was based on synthesised haem adducts, and not haem extracted from the parasite's DV. It was not until late 2018 that Heller *et al.* published two papers describing the quantification of haem extracted from the parasite using a mass spectrometer.[53,163] This was innovative given that the quantification of haem species usually relies on UV spectroscopic calorimetric evaluations. It was also a significant step toward encouraging the development of prospective liquid chromatography methods with either mass spectrometry or colourimetric detections to measure haem for haemozoin-inhibiting antimalarials. Ideally, analytical methods employing high-pressure liquid chromatography systems (HPLC) attached to a specific detector are favoured – given their sensitivity and selectivity.[164] Therefore, these techniques may be appropriate for developing a cellular haem assay that requires smaller biological materials for adequate haem detection.

In conclusion, not all β-haematin inhibitors are haemozoin inhibitors in the parasite. This strongly supports the need to validate the extracellular inhibition findings intracellularly. Furthermore, the developed pyridine-based cellular haem fractionation assay has allowed for the direct correlation between accumulated haem in the parasite and parasite survival, which has thus far proven to be a very essential approach for determining the actual MoA of novel compounds predicted to cause haemozoin inbition.[143]

1.8.5. Cellular mechanism of action of haemozoin-inhibiting compounds

It is widely believed that haemozoin-inhibiting antimalarials cause accumulation of unsequestered haem in the parasite and that this increased haem is toxic. It is further hypothesised that this accumulated haem leads to pro-oxidant effects, membrane destabilisation and osmotic pressure, which in turn kill the parasite.[55,165] However, many of these studies were based on extracellular observations and not necessarily on direct observations of the parasite. As explained in the section above, in 2013, Combrinck *et al*. demonstrated direct evidence of haemozoin inhibition in the malaria parasite for the first time.[159] This study unequivocally showed that CQ causes a dose-dependent increase in unsequestered haem, which coincides with decreased parasite survival. Later, this method was adapted for multi-well analysis and was applied to other antimalarial drugs and test compounds.[143,144,160,161] Surprisingly, all haemozoin inhibitors display unique levels of toxic unsequestered haem at their 50% inhibitory concentrations (IC_{50}). This suggests that haem toxicity may not be independent of the inhibitor, as initially proposed.

Presumably, if haem toxicity were independent of the inhibiting molecule, haem levels at the IC_{50} concentrations would be the same for all compounds. Therefore, the observations indicate the possible formation of haem–inhibitor complexes in treated parasites that drive the toxicity (Figure 1.15). Indeed, Chou *et al.* first reported (in 1980) the earliest notion of haem–inhibitor complex toxicity in mouse erythrocytes.[139] The existence of these complexes in the parasites was proposed by Kapishnikov *et al.* in 2019, based on the distribution of bromoquine with haem in the DV membranes of the parasite.[155] Nonetheless, previous efforts to definitively determine the crystal structures of the haem–inhibitor complexes have proven unsuccessful. Given the direct evidence of the inhibitors' association with haem and the observed variability in the haem levels for each inhibitor, it is clear that haem toxicity is more complex than commonly supposed. Moreover, it is clear that the measured increase in unsequestered haem (whether as Fe(III)PPIX, in complex form, or both) correlates with decreased parasite survival.[143] This suggests that haem toxicity is compound-specific and that the cellular mechanism of action of haemozoin-inhibiting compounds is unique given that haem–inhibitor complexes drive this toxicity.

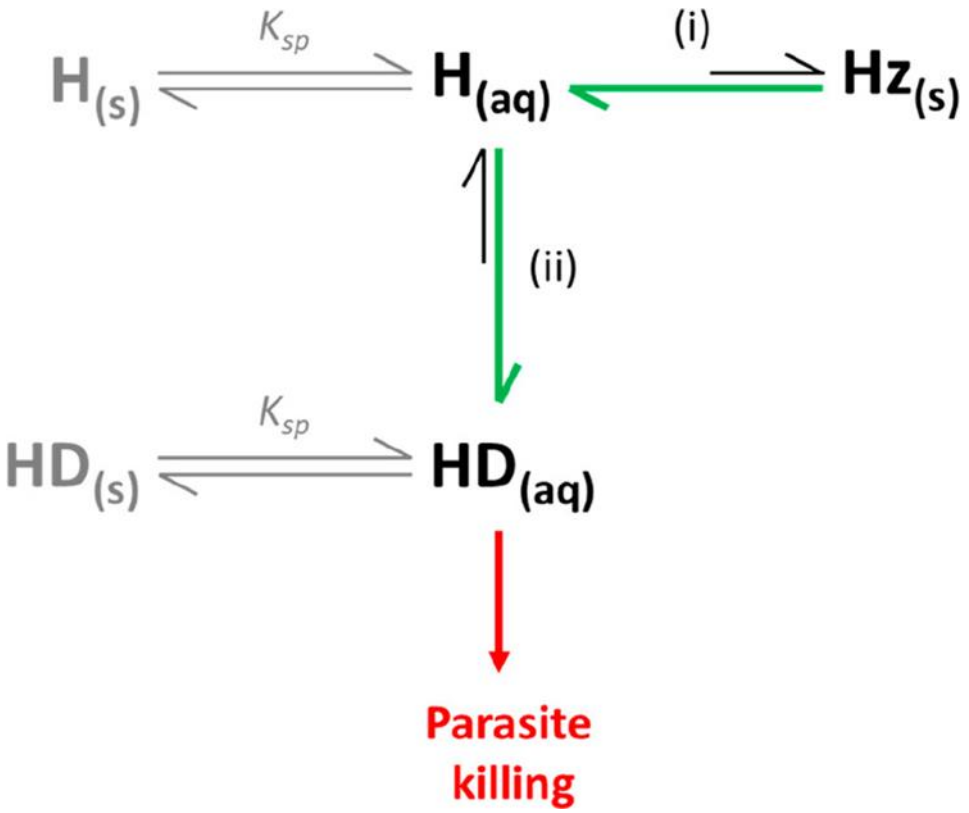

Figure 1.15: A representation of haem detoxification into haemozoin, and the proposed inhibition mechanism by chloroquine and related antimalarials (i). Haemozoin formation inhibiting antimalarials cap the haemozoin crystal *via* pi-pi stacking interactions leading to increased unsequestered haem (H(aq)) and decreased haemozoin levels (Hz(s)). These inhibitors are believed to complex unsequestered haem (ii) and produce a haem–drug complex (HD(aq)), which is possibly responsible for killing the parasite (red arrow). Green arrows show the proposed shift in equilibria when drug pressure is introduced. The processes displayed in grey represent proposed competing processes namely, the precipitation of unsequestered haem (H(s)) and haem-drug complex (HD(s)) that rely on their solubility products (*Ksp*). Reprinted with permission from De Villiers, K. A.; Egan, T. J. Heme Detoxification in the Malaria Parasite: A Target for Antimalarial Drug Development. Acc. Chem. Res. 2021, 54 (11), 2649–2659. Copyright (2021) American Chemical Society.[145]

1.9. Screening studies for β-haematin/haemozoin-inhibiting compounds

The effort to eliminate and eradicate malaria translates into three main/vital facets: discovering, developing, and distributing new medicines. These key aspects can be grouped into three branches: (1) control of blood-stage malaria by treatment of resistant mutants, (2) transmission-blocking of parasite life cycle between host and vector, (3) and radical cure of *P. vivax* malaria through the killing of persistent liver hypnozoites.[137] However, here the discussion will focus on the discovery of compounds aimed explicitly at the intraerythrocytic stage of the parasite life cycle. Specifically, this is focused on the haemozoin formation biology of the *P. falciparum* malaria parasite. This includes, in part, the investigation of the MOAs of newly discovered compounds identified from high-throughput screening campaigns. Through

this, it is believed we could further our understanding of how certain antimalarials kill the parasite via the haem detoxification pathway.

It is accepted that although antimalarial drug discovery and development has historically benefitted from whole-cell screening approaches, it presents a major challenge when it comes to therapeutic target identification in the parasite. This therefore results in clinical antimalarials which have targets that are not fully understood, or remain elusive. The artemisinins are a great example to this challenge, as their proposed MoA remains open to debate, especially given that recent studies have suggested that they (artemisinins) present as pleiotropic, and target several proteins and also haem to exert their toxic effects.[140] As such, their actual MoA remains unconventional. Nonetheless, traditionally, mechanistic investigations have provided crucial insights when elucidating possible future molecular resistance mechanisms in resistant mutants, specifically for compounds that exert their effects through haemozoin inhibition. The MoR studies of both CQ and piperaquine present as a case in point.[105,121,124,127,131] In any case, it is also crucial to mention that although a target-based approach provides an opportunity for selectively rationalising drug designs for a specific target, it has not been as successful as whole-cell screening in bringing clinical candidates to the drug market. This is largely because there are often issues relating to the disconnect between *in vitro/in vivo* target potency and cellular activity.[166] Therefore, conventional drug discovery and development programmes mostly leverage the two approaches to discover new leads. However, the scope of this work focuses on a target-based approach, especially in identifying compounds that inhibit the haem detoxification pathway.

1.9.1. Quantitative structure–activity relationship and high-throughput screening studies to discover β-haematin inhibitors

Historically, the fame and interest in the quinoline family is owed to CQ, which was undoubtedly the most successful antimalarial.[167] Despite its widespread resistance, it is now well known that this resistance does not associate with any change in the haemozoin formation process but rather from mutations of the membrane transport proteins that alter drug accumulation in the DV.[116,168] Therefore, the haemozoin formation pathway remains a viable target for developing new candidate molecules. This is because the haemozoin formation pathway is essential for parasite development and, as demonstrated with CQ and other inhibiting antimalarials, its disruption is detrimental to the parasite. Accordingly, putative studies have focused on developing various quinoline-based analogues that could emulate the superior antimalarial efficacy of this drug family.[169–171]

Unsurprisingly, studies on CQ analogues have been of interest and have resulted in informative structure–activity relationship models for parasite activity and β-haematin inhibiting

ability.[172,173] Intriguingly, these found that the 4-aminoquinoline moiety was critical for strong haem complexation, whilst the group substitution on position 7 of the quinoline ring is solely linked with activity. Intuitively, quantitative structure–activity relationship (QSAR) studies' significance is establishing predictive models of biological activity as a function of structural and molecular information for a compound.[174] Thus, the 4-aminoquinoline model proved interesting and produced some notable drug designs. In two subsequent studies, dibemethine and pyridodibemequine side chains were experimented with and yielded significant findings of value to drug discovery research efforts.[175,176] Specific to the dibemaquines, their dibemethine side chain chemosensitised CQR *P. falciparum* parasites and completely inhibited PfCRT, therefore demonstrating the usefulness of using structure–activity relationship (SAR) studies in finding novel derivatives for future applications. In 2013, studies by Nsumiwa *et al.* and Joshi *et al.* also synthesised different series of 4-aminoquinolines and quinoline triazole amide analogues with varying substituents at the 7-position, respectively.[177,178] Both these studies aimed to probe the SAR of association with ferriprotoporphyrin IX and inhibition of β-hematin formation by these newly synthesised analogues. Similarly, subsequent studies by Wang *et al.*, Wicht *et al.* and L'abbate *et al.* are also notable examples of SAR investigations that sought to discover novel molecules with inhibition activity against β-haematin (synthetic haemozoin) formation.[160,161,179,180] These are critically important studies because unlike many SAR studies before them, they instead focused on novel moieties like the indolo[3,2-*c*]quinolines, benzamides, triarylimidazoles and 2-phenylbenzimidazoles. Although none of the mentioned studies has yet provided a clinical candidate, they did provide pertinent insights into the development of molecules that inhibit the haemozoin formation pathway.

Another exciting application for exploring new haemozoin inhibitors is molecular docking studies. The prerequisite for docking applications is knowledge of a biological target structure, which is validated through crystallography or homology techniques.[181] Since the synthetic counterpart of haemozoin, β-haematin, has an identical chemical and spectroscopic crystal structure, it allows molecular docking studies for predictive in silico haemozoin inhibition to be performed instead on the β-haematin crystal.[33] The advantage of molecular docking (also known as virtual screening) is its ability to allow for high-throughput screening (HTS) of large chemical libraries to identify new leads for drug discovery. The first reported haemozoin-inhibiting compound to be discovered using this molecular docking technique was a benzoxazole derivative.[182] This is a molecule with a different scaffold to the conventional quinoline moiety. Also, a worthy mention is a recent study by Amod *et al*., were this technique was used to discover coumarin and iminodipyridinopyrimidine chemotypes which, although not yet tested intracellularly for haemozoin inhibition, displayed potent parasiticidal activity and

inhibited β-haematin formation *in vitro*.[183] Therefore, an attractive advantage of using virtual screening over traditional SAR lies in finding novel scaffolds that target haemozoin formation. Of course, this approach can also identify molecules for other targets, given that their structures are known and verified. However, what is indisputable is the critical relevance of these techniques in future applications to discover new molecules to replace currently resistant threatened drugs.

1.10. Rationale

As already demonstrated in this review, studies from past decades have explored novel and clinically effective antimalarials and their various targets in the parasite in order to enrich drug discovery research and development tools.[143,182,184–186] By far the most studied target in the parasite is the malarial pigment haemozoin.[62,143,159,187] Work in the Bioinorganic Research Group at the University of Cape Town (UCT) focuses on understanding the haem detoxification pathway as a potential target for various antimalarial compounds in the parasite. This is oriented towards performing QSAR studies, and developing both *in silico* methods and cellular assays which, when combined, will enable the synthesis, prediction and detection of novel haemozoin inhibitors. It is predicted that these could be of great utility in the target deconvolution of new compounds – especially if the techniques are readily transferable to the malaria drug discovery community. We believe this is of critical importance because the current predicament in drug discovery test cascades is the need for assays that do not exist or which may be highly specialised and limit access to the broader scientific community.[137,188]

As explained above, the degradation of host Hb in the parasite's DV leads to toxic Fe(III)PPIX species and rapidly assembles to haemozoin.[5] However, as earlier explained, many molecules, including CQ and AQ, inhibit this haem detoxification route by incorporating into the growing haemozoin crystal, so leading to parasite death. Although it is now possible to robustly measure the inhibition levels caused by many of these molecules and novel compounds in the parasite, unfortunately the currently available methods for quantifying Hb, unsequestered haem and haemozoin levels in the parasite are not readily transferable. First, these methods utilise pyridine, a toxic and volatile solvent to complex intracellular haem species, for colourimetric quantification as a monomeric species at selected wavelengths. The methods are also labour-intensive for wide application, suffers from low throughput, and have high demand for parasite starting material. These are significant disadvantages, given that various studies have been reported on HTS campaigns to identify β-haematin inhibitors and subsequently the lead compounds needed to be investigated intracellularly to ascertain the actual haemozoin inhibition MoA.[182,189,190] These factors drive the need for improved bioanalytical methods, because many compounds from HTS campaigns are seldom selected

for target validation in the parasite due to the inaccessibility and poor throughput of the techniques to perform these studies. This is critical, because the recent pyridine-based methods to quantify intracellular haem species have clearly showed that non-cellular β-haematin inhibitions are not always translatable in the cell.[143,144] Furthermore, performing phenotypic screening to discover new compounds ultimately necessitates target deconvolution, and haemozoin prediction assays are traditionally used in the process. Therefore, it is proposed that converting the current methods primarily to a high-performance liquid chromatography system with a diode array detector (HPLC-DAD) or tandem mass spectrometry detection (LC-MS/MS) will benefit wider applications, while also significantly improving the throughput and lead times.

On the other hand, although many quinolines and other antimalarials are known to act by inhibiting the haemozoin formation process, the exact mechanisms by which this inhibition process kills the parasite remain unknown.[191] Furthermore, the fact that a diverse range of haemozoin-inhibiting compounds lead to variable unsequestered haem levels (all haem other than Hb and haemozoin) in treated parasites at their IC_{50}s, is a further exacerbation of this incomplete knowledge in this pathway.[143,144,160,161,180,192] This is especially the case considering the observations that more active compounds often exhibit lower levels of unsequestered haem in comparison to less active compounds, which present higher levels of unsequestered haem. These findings fundamentally contradict the often simplified explanation that the activity for haemozoin-inhibiting compounds is as a result of a direct buildup of unsequestered haem. In fact, they support the suggestions discussed earlier in this chapter that haemozoin inhibitors form unique complexes with unsequestered haem. Since, if indeed detoxified haem was solely responsible for the parasiticidal effects of these compounds, then the unsequestered haem levels should be the same at their IC_{50} values. Based on this, it is evident that bioanalytical techniques should be developed to investigate the effects of the haemozoin-inhibiting compounds. Accordingly, it was proposed that to better understand the intricacies in the levels of unsequestered haem for haemozoin-inhibiting compounds, a flow cytometry-based assay should be developed. This was because it was believed that the observed differences could be better explained by studying the speed of killing and stage-specific effects of the compounds on ring-staged parasites.

In conclusion, it is indisputable that the haemozoin formation pathway as a direct target for antimalarial development remains a critical theme amid resistance associated with current antimalarials that exert their parasiticidal effects *via* this MoA. This is reinforced by the fact that resistance to those antimalarials is compound-specific and that the haemozoin formation process remains immutable.

1.11. Aims and objectives

1.11.1. Aims

This study aimed to: (1) Probe the biological effects of β-haematin inhibiting compounds against *P. falciparum* strains and further investigate the speed of killing and stage-specific effects of select inhibitors. (2) Develop a 96-well plate HPLC-DAD analytical method to quantify and detect intracellular haem species that will improve throughput and be readily transferable to research laboratories interested in its application.

1.11.2. Objectives

i. Determine the *in vitro* antiplasmodium activity of β-haematin inhibiting compounds against *P. falciparum* parasites and investigate the ability of the compounds to inhibit haemozoin formation using the pyridine-based cellular haem fractionation assay.
ii. Develop a stage specificity and speed of killing assay to probe selected haemozoin-inhibiting experimental compounds that exhibited variable levels of unsequestered haem at the IC_{50}.
iii. Develop a 96-well HPLC-DAD assay for quantifying intracellular Hb, unsequestered haem, and haemozoin in compound-treated *P. falciparum* parasites.
iv. Validate the 96-well assay with known haemozoin inhibitors and non-inhibitors.
v. Modify the developed bioanalytical assay to a higher-throughput method that is able to simultaneously determine haemozoin inhibition for 33 compounds at a single chosen concentration.
vi. Deploy the newly developed assays with novel compounds active against *P. falciparum* parasites.

Chapter 2: General Materials, Instrumentation and Methods

The HPLC assay methodologies are not discussed in this chapter, but later in Chapters 4, 5 and 6. However, the HPLC instrumentation and sample preparations are presented here.

2.1. Materials and instrumentation

All chemicals and solvents used in this study were of an analytical grade (AR) or higher and were used without further purification. The suppliers are listed below. The deionized water used was double distilled in-house.

Table 2.1: Reagents for tissue culturing of *P. falciparum* and *Plasmodium* Lactate Dehydrogenase (pLDH) assay.

Materials	Supplier
Tissue culturing of *Plasmodium falciparum*	
3-Acetylpyridine adenine dinucleotide	Sigma-Aldrich
Albumax II	Gibco
Calcium L-lactate	Sigma-Aldrich
Deionized water	In-house
Gentamicin	Micro Healthcare
Giemsa stain	Merck
D-(+)-Glucose	Sigma-Aldrich
Glycerol	Merck
HEPES	Sigma-Aldrich
Hypoxanthine	Sigma-Aldrich
Phosphate buffer saline (PBS tablets)	Sigma-Aldrich
Potassium chloride	Sigma-Aldrich
RPMI 1640 with glutamine (without sodium bicarbonate)	Sigma-Aldrich
Sodium bicarbonate	Sigma-Aldrich
Sodium chloride	Sigma-Aldrich
Sodium dihydrogen phosphate	Fluka
Sodium L-lactate	Sigma-Aldrich
D-Sorbitol	Sigma-Aldrich
Nitroblue tetrazolium salt (NBT)	Sigma-Aldrich
Phenazine ethosulphate	Sigma-Aldrich
Tris buffer	Sigma-Aldrich
Triton X 100	Merck
Instrumentation	
Modulus™ Microplate plate reader	Turner Biosystems
Thermo Scientific Multiscan GO UV-visible spectrophotometer with multi-plate	Thermo Fisher Scientific

Table 2.2: Reagents and instrumentation for the pyridine haem fractionation assay and stage specificity and speed of killing flow cytometry assay for haemozoin-inhibiting compounds.

Materials and instrumentation	Supplier
BD Accuri™ C6 Plus flow cytometer	Becton and Dickson Company (BD)
Chloroquine	Sigma-Aldrich
DNAse	Sigma-Aldrich
50% Glutaraldehyde	Sigma-Aldrich
Haematin Porcine	Sigma-Aldrich
HEPES	Sigma-Aldrich
Hydrochloric acid (HCl)	Merck
Phosphate buffer saline (PBS tablets)	Sigma-Aldrich
Pyridine	Sigma-Aldrich
Saponin	Sigma-Aldrich
Sodium chloride	Sigma-Aldrich
Sodium dodecyl sulfate (SDS)	Sigma-Aldrich
Sodium hydroxide	Sigma-Aldrich
SYBR green I	Sigma-Aldrich
Trucount tubes	Becton and Dickson Company (BD)

Table 2.3: Reagents and instrumentation for the HPLC-DAD haem assay.

Materials/instrumentation	Supplier
Acetonitrile (LC-MS grade)	Sigma-Aldrich
Haemin Porcine	Sigma-Aldrich
HEPES	Sigma-Aldrich
HPLC: HP Agilent 1100 series (Binary Pump), with Agilent 1200 series autosampler, an Agilent 1200 series analytical column compartment (temperature control), and Agilent 1290 infinity DAD detector (for UV detection).	Agilent Technologies
Imidazole	Merck
Methanol (LC-MS grade)	Sigma-Aldrich
Pre-column	Sigma-Aldrich (Supelco)
Silica gel (C18 particles)	Sigma-Aldrich (Supelco)
Phenomenex-Synergi 2.5 µm Hydro-RP 100 Å, LC 50 x 2 mm column	Phenomenex (*via* Promolab Pty Ltd t/a Separations)

Table 2.4: General instrumentation for experimental assays.

Instrumentation	Supplier
96-well round bottom plates (500 µL)	Lasec
96-well flat-bottom plates (400 µL)	Lasec
96-well v-bottom plates (2 mL; deep well)	Lasec
96-well v-bottom plates (1 mL; deep well)	Sigma-Aldrich
Centrifuge 5804	Eppendorf
Incubator (Memmert and Lasec)	Lasec
Light Microscope (BestScope)	Lasec
pH meter (Jenway 3510)	Thermo-Fischer Scientific
Sonicator (ultrasonic cleaner)	Scientech
UV-vis spectrophotometer (Cary 60 UV-Vis)	Agilent Technologies
Vortex (G560E)	Scientific Industries
Weighing balance)	Sartorius

2.2. Methods

2.2.1. Cultivation of *Plasmodium falciparum* parasites

2.2.1.1. Freezing of parasites

A freezing solution containing 1.6 g sodium lactate, 30 mg potassium chloride (KCl), 1.38 g sodium dihydrogen phosphate, and 57 g glycerol in 100 mL deionised water was prepared and filter-sterilised with a 0.22 µm filter. The glycerol forms a protective layer around the ring-staged parasitised red blood cells (PRBCs) and helps preserve the cells for later use. The parasites were further preserved by slowly adding 5 volumes of the freezing solution to 3 volumes of a 10% PRBC pellet. This was allowed to stand for 5 minutes on ice, and then was transferred to cryotubes suspended in propanol at -20°C overnight. The cryotubes were then transferred to a liquid nitrogen dewar the following morning until required for use in continuous culture.

2.2.1.2. Thawing of frozen parasites

Three different solutions containing varying concentrations of sodium chloride (NaCl) were prepared and filter-sterilised through a 0.22 µm filter. These solutions of 12%, 1.8% and 0.9% of NaCl, respectively, were required to break down the protective glycerol layer surrounding the frozen ring-staged PRBC. This was done by slowly adding 1 volume of 12% NaCl to 5 volumes of thawed parasites, while mixing. After 5 minutes of incubation, 10 mL of 1.8% NaCl was added and centrifuged at 400 ×g for 5 minutes. The supernatant was aspirated and 10 mL of 0.9% NaCl with 0.2% glucose was added, while swirling and allowed to stand for 5 minutes. The mixture was then centrifuged at 400 ×g for 5 minutes. The supernatant was removed and the pellet placed into culture.

2.2.1.3. Continuous culturing of parasites

Complete culture media (CM) was prepared with 0.4 g/L RPMI 1640 with glutamine (without sodium bicarbonate), 4 g/L glucose, 6 g/L HEPES, 0.088 g/L hypoxanthine, 1.2 mL gentamycin (for every 1 L), and 5 g/L Albumax. Just before use in parasite culture, 8.4 mL of 5% (*w/v*) sodium bicarbonate was added to 200 mL medium.

The culturing of parasite strains followed a modified method of Trager and Jensen for cultivation of *Plasmodium* parasites.[193] *P. falciparum* strains, the NF54 chloroquine sensitive (CQS) and K1 chloroquine resistant (CQR) strains were used. Cultures were maintained in washed O^+ red blood cells (RBCs) in culture medium at 2% haematocrit under aseptic conditions. For daily culturing, the pRBC medium was transferred to a sterile 50 mL centrifuge tube and centrifuged at 750 ×g for 5 minutes. The supernatant was aspirated off, and a thin blood smear was made on a microscope slide from the pellet and was subsequently fixed with

methanol. The slide was then stained with a 10% Giemsa stain solution (prepared with 1 mL Giemsa stain and 9 mL PBS) and allowed to stand for 10 minutes. The slide was rinsed with tap water, air dried, and then viewed using a 100x magnification under a light microscope to determine the predominant phase of the pRBC pellet and parasitemia. Cultures were maintained by diluting trophozoite-staged parasites between 5% and 10% parasitemia using O^+ RBCs for adequate growth.

To keep the parasite phases synchronous, the ring-staged parasites were treated with 10 mL of 5% sorbitol solution and allowed to incubate at 37°C for 10 minutes. Briefly, 50 g of D-sorbitol in 1 L of deionised water was filter-sterilised through a 0.22 µm filter membrane. Sorbitol selectively lyses the RBCs infected with the trophozoite and schizont phases of the parasite, as previously reported by Lambros and Vanderberg.[194] This is because RBCs infected with mature parasites have increased permeability towards sorbitol, thereby leading to an osmotic pressure that results in cell death.[195] The resultant suspension was centrifuged at 750 ×g for 5 minutes, and thereafter the supernatant and any debris were aspirated off. The pellet was resuspended with 40 mL of complete medium (CM) and transferred to a culture flask. The flask was gassed with a gas mixture of 3% O_2, 4% CO_2, and 93% N_2 for at least 60 seconds and then incubated at 37°C until the next culturing session or cells was ready to use for an experiment.

2.2.2. Test compound stocks for biological assays

All test compound stocks were prepared to 2 mg/mL in either 100% DMSO or an appropriate solvent and then stored at -20°C until required for experimental use. Just before use, these stocks were thawed and diluted accordingly to required experimental concentrations.

2.2.3. *Plasmodium* lactate dehydrogenase assay (pLDH assay)

The *in vitro* antiplasmodium activity in the CQS (NF54) and CQR (K1) strains was determined using a modified version of the method described by Makler *et.al.*[196] This allows for the indirect measurement of the pLDH using colourimetry. During glycolysis, both in the parasite and the RBC, the lactate dehydrogenase (LDH) enzyme indistinguishably catalyses the conversion of lactate to pyruvate using nicotinamide adenine dinucleotide (NAD) as a coenzyme.[196,197] Replacing NAD with its analogue, 3-acetylpyridine adenine dinucleotide (APAD) as a coenzyme, results in distinguishable activity between the parasite and RBC in their conversion of lactate to pyruvate.[196] Rapid conversion of lactate to pyruvate occurs in the parasite in the presence of APAD, while human red blood cells carry out this reaction at a very slow rate. Therefore, in the presence of APAD, as Figure 2.1 illustrates, live parasites can be monitored using this principle. For the assay, a Malstat reagent containing both the analogue coenzyme APAD and lactate was prepared using 400 µL Triton x 100, 4 g L-lactate, and 1.32 g Tris buffer

in 200 mL deionised water. Once all reagents were mixed to dissolve, 22 mg APAD was added, and the pH was adjusted to 9. The Malstat reagent was used as a source of APAD for the reaction, as described above. The substrate APADH is formed during the conversion of lactate to pyruvate (Fig 2.1), and Nitro Blue tetrazolium salt (NBT) was used as an oxidising agent.[196] Therefore, NBT is reduced by APADH, resulting in the formation of a blue/purple formazan salt which can be colourimetrically measured at 620 nm as an indicator of parasite survival.

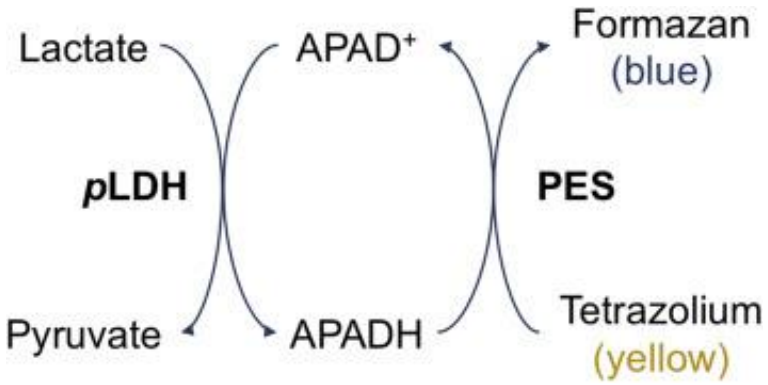

Figure 2.1: The biological reaction for the conversion of lactate to pyruvate using APAD as a coenzyme during the pLDH assay.[198]

Briefly, the pLDH assay was used to evaluate the activity of compounds by means of detecting the presence of *P. falciparum* after 48 h incubation in a 96-well plate. For each of the 96-well pLDH assay plates, 2% parasitemia was prepared in 2% haematocrit to 10 mL in CM. The reference standard CQ was prepared in deionised water at 2 mg/mL, and all other drug stocks were prepared as 2 mg/mL stocks in DMSO or supplier-specified solvent and stored at -20°C until use. On the day of use, CQ was diluted to 2 µg/mL and the test compounds to 20 µg/mL using the CM. From each of these diluted stocks, 200 µL was transferred to different wells in column 3 of the assay plate and further dilutions were performed as illustrated in Figure 2.2.

The 96-well plate set up was as follows: A blank column A containing 100 µL complete media and 100 µL of 2% RBC haematocrit (RBC diluted in complete media), a positive control (column B) with 100 µL complete media, and 100 µL of 2% parasitemia. Then 2-fold serial dilutions were performed from column 3 onwards for CQ and all the test samples. Test samples were tested at final in-well starting concentrations of 10 µg/mL (column 3), while CQ was tested from1 µg/mL. From column 3–12, 100 µL of 2% parasitemia was added, resulting in a final volume of 200 µL in each well. The plate was then covered with a lid and placed in an airtight gassing chamber and then gassed for about 5 minutes with a mixture of 3% O_2, 4% CO_2, and 93% N_2, and then was incubated at 37°C for 48 hours under sterile conditions.

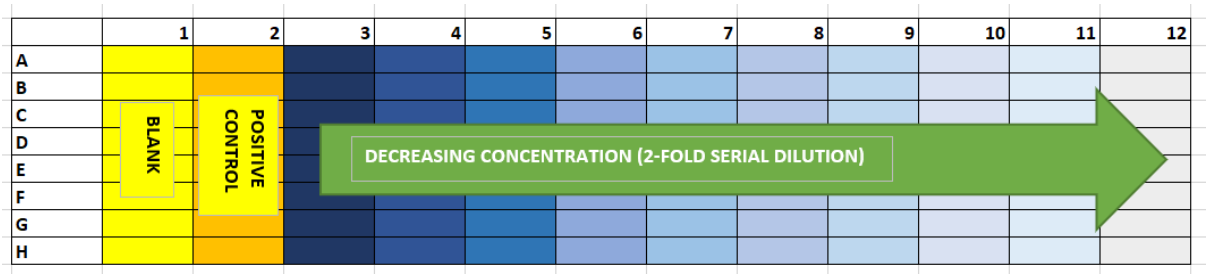

Figure 2.2: Illustration of the plate set up for a pLDH 96-well plate assay. The different shades of blue and arrow shape indicate the decrease in test compound concentration from column 3 to 12. The Blank column represents 2% RBC haematocrit (media diluted RBCs) and the positive control represents 2% *P. falciparum* infected RBCs in 2% RBC haematocrit.

After incubation, the plate was frozen at -20°C until required for development. On the day of development, each plate was thawed, each well resuspended using a pipette, and 25 µL aliquots of cell suspension were transferred to corresponding wells on a second 96-well plate where each well contained 100 µL of Malstat. To the mixture of cell suspension and Malstat, 25 µL of NBT was added and any air bubbles were removed to ensure accurate readings. Because of the light-sensitive nature of NBT the plates were either covered in foil or kept in a dark cupboard until fully developed. The absorbance was then measured at 620 nm using a Modulus™ Microplate plate reader (Turner Biosystems) or Thermo Scientific Multiscan GO UV-visible spectrophotometer with multi-plate. The data were then analysed in an Excel spreadsheet and plotted using a non-linear dose-response curve using GraphPad Prism v 6.0.0 software to determine the concentration required to inhibit 50% of parasite growth (IC_{50} value).

2.2.4. *In vitro* cytotoxicity assay

The selectivity of active compounds against *P. falciparum* was determined using the Chinese hamster ovary (CHO) cell line. CHO cell lines are derived from the epithelial cells of the ovary of the Chinese hamster, and they have a wide use in *in vitro* toxicology studies[199] and other scientific disciplines,[200] mainly because of their reported capacity for single-cell suspension growth.[201] Many biological assays require the quantification of surviving mammalian cells and in 1983 Tim Mosmann developed a rapid colourimetric assay based on the ability of the tetrazolium salt 3-(4,5-dimethylthiazol-2-yl)-2,5-diphenyl tetrazolium bromide (MTT) to quantify cell viability.[202] This colourimetric assay relies principally on the tetrazolium ring of MTT becoming cleaved by active mitochondria in living cells, but not dead cells, and thereby it selectively differentiates between viable cells and non-viable cells. Specifically, the MTT reagent, which has a pale yellow colour in media, is reduced by active mitochondria to form a dark blue formazan crystalline product that can be quantified spectrophotometrically at 595

nm. Therefore, the MTT-based assay[202] was used here to study the toxicity of selected compounds tested against *P. falciparum* in the pLDH assay.

Briefly, 10000 CHO cells were seeded in each well of a sterile, flat-bottomed 96-well plate and were incubated at 37°C under 5% CO_2 for 24 hours. Stock solutions of each test compound prepared as described above were thawed and diluted to 200 µg/mL in CHO cell culture media. The final DMSO concentration of each test compound was not greater than 0.2% after dilution in cell culture media. Diluted stock solutions were serially diluted further in 10-fold to result in a total of six concentrations. These six concentrations (highest and lowest in-well concentrations of 100 and 0.001 µg/mL, respectively) were then added to CHO cells on the corresponding wells of the 24 h incubated assay plate, and then further incubated for 48 h. Figure 2.3 below illustrates the CHO cell assay setup procedure.

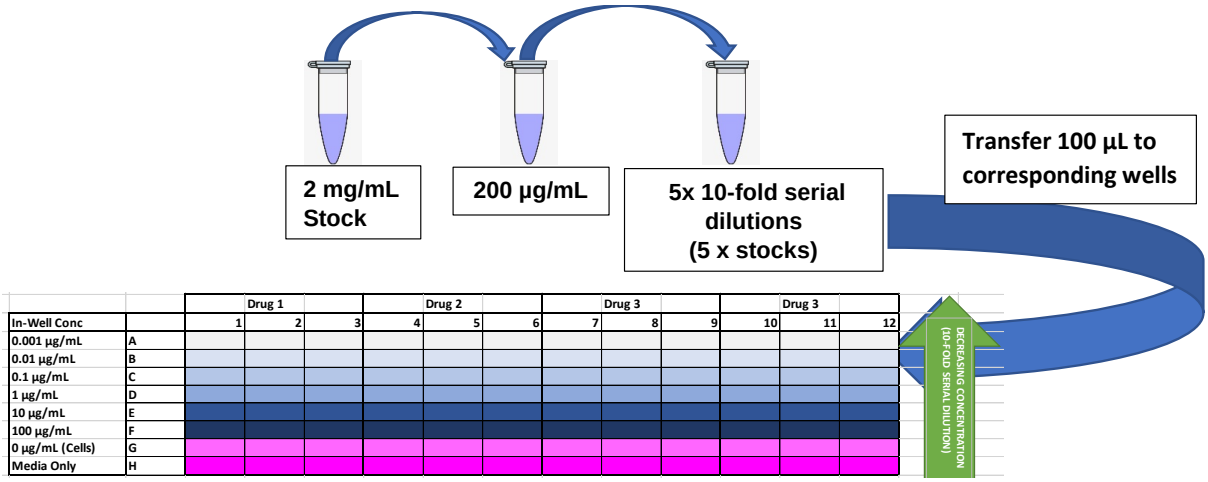

Figure 2.3: Illustration of the *in vitro* cytotoxicity assay setup in a 96-well plate. The varying shades of blue represent different dosing concentrations of drug – as shown by the green arrow (serial dilutions are performed from row F through A). The purple colour (column H) represents media only and the light purple colour (column G) represents cells in media. For these experiments, emetine was used as a positive control in all experiments.

After 48 h of incubation, the media was aspirated and 25 µL MTT solution was added to each well. The plates were incubated for 4 h, after which 100 µL of 100% DMSO was added to each well to help with solubilising the formed crystals. Importantly, the resultant colour of the fully solubilised crystals is proportional to absorbance, which in turn is proportional to cell survival. The absorbance of the solution was recorded at 595 nm, and the IC_{50} was determined using a non-linear dose-response curve fitting analysis on GraphPad Prism v6.0. Software.

2.2.5. Detergent-mediated β-haematin inhibition assay

The inhibition of the sequestration of toxic haem into non-toxic haemozoin remains a favourable MoA.[203] The β-haematin assay is the primary method used to probe haemozoin

inhibition using lipophilic chemical detergents to mimic the parasite DV conditions.[73,158,204] This is because haemozoin formation has been shown to closely associate with neutral lipids in the DV, and subsequently this has been replicated *in vitro* with β-haematin (synthetic haemozoin). Specifically, the NP-40 lipid detergent allows for the robust formation of synthetic haemozoin (β-haematin) under physiologically mimicked conditions.[204] Notably, under these assay conditions, the efficiency of any compound that can inhibit β-haematin formation can be assessed and quantified to predict cellular inhibition. This has been demonstrated with several classes of antimalarials, including CQ and AQ which inhibited the process.[73] Primarily, this is based on the fact that unreacted haematin can be quantified according to the pyridine haemochrome method previously described by Ncokazi and Egan, where, under neutral conditions, pyridine selectively complexes haematin in the presence of β-haematin.[158] The formed haem–pyridine complex results in an orange colour which can be detected spectroscopically at a maximum absorbance of 405 nm.

To set up the assay, all test samples were prepared as 20 mM stock solutions in DMSO (or in suitable solvent), while the reference standard CQ was prepared in distilled water. Subsequently, 20 µL of each compound solution was added to the wells in column 12 of a 96-well plate. Notably, these wells (column 12) already contained a mixture of 140 µL distilled water and 40 µL of the NP-40 detergent (307.3 µM). To the other wells (columns 1–11), 100 µL of a pre-prepared solution consisting of water (distilled), NP-40 and DMSO (7:2:1; v/v), was added. After that, serial dilutions of each compound (100 µL) were performed from column 12 to column 2, with column 1 serving as a blank (0 µM). Lastly, a 25 mM haematin stock was prepared by sonicating haemin in DMSO (for 1 minute) and then suspending 178.8 µL of this homogenous suspension in 1 M acetate buffer (20 mL, pH 4.8), before being added to all wells (100 µL). The plate was then covered and incubated for 5 h at 37°C. For analysis, 32 µL of a 50% buffered pyridine solution (v/v; pH 7.4) prepared using 10 mL pyridine, 4 mL water, 4 mL acetone, and 2 mL HEPES buffer (2 M; pH 7.4), was added to each well to solubilise any unreacted haematin. The UV-Vis absorbance of the plate was then read at 405 on a Thermo Scientific Multiscan GO UV-visible plate reader, and sigmoidal dose-response analysis was performed using Prism software to calculate the IC_{50} of each compound. Notably, the mechanistic evaluations of all test compounds were investigated initially for their inhibition of β-haematin formation, as a prerequisite for their intracellular mechanistic evaluation in the parasite using the pyridine-based cellular haem fractionation assay[143].

2.2.6. Pyridine-based cellular haem fractionation assay

The novel haem fractionation assay previously reported by Combrinck *et al.* was used for cellular mechanism of action studies in *P. falciparum* parasites.[143] Here, top ranked compounds predicted *in silico* to inhibit the formation of crystalline β-haematin and

subsequently tested *in vitro* using the colourimetric β-haematin assay[158] were prioritised. These compounds were chosen based on their pLDH and β-haematin assay activities for further mechanistic studies in the parasite. Prioritised compounds were only those that were predicted to strongly inhibit the formation of this process in *vitro* (presented sub-nanomolar IC_{50} values for the β-haematin assay).

The cellular fractionation assay allows for direct quantification of the three major haem species in *P. falciparum* isolated trophozoites: haemoglobin (Hb), unsequestered haem, and haemozoin. These haem species are quantified spectroscopically using the principle of the aqueous pyridine haemochrome method, which was previously reported by Ncokazi *et al*.[158] The principle follows that aqueous pyridine forms a low-spin coloured complex with unsequestered haem, but not haemozoin, and since the absorbance obeys Beer's law it allows for quantification of haem in solution. This published assay was used to probe the most active β-haematin inhibiting test compounds to determine whether these compounds inhibit the formation of haem in the malaria parasite.

2.2.6.1. Incubation and trophozoite harvesting

As shown in Figure 2.4, sorbitol synchronised early ring-staged *P. falciparum* parasites were incubated at 37°C with a probe compound of interest at multiples of the IC_{50} for 30–32 h, until the mature trophozoite stage was reached. The probe compounds were tested at final concentrations of 0.5 x IC_{50}, 1 x IC_{50}, 2 x IC_{50}, 2.5 x IC_{50} and 3 x IC_{50}. After incubation, matured trophozoites were harvested with a 1% saponin solution (0.1% in-well concentration) used to lyse the red blood cells and release the parasites. Thereafter, the extracellular red blood cell Hb supernatant was removed by washing the cell pellet three times using a PBS solution at pH 7.4, with subsequent centrifugation steps (650 ×g) between each wash.

To the washed trophozoite pellet, 100 µL of PBS was added to resuspend the cell pellet and this was then transferred to a 500 µL round bottomed 96-well plate, termed the stock plate. The stock plate was then used to prepare a second plate for flow cytometry cell counting, which was called the counting plate. This cell counting plate was prepared by aliquoting to each well 190 µL of a cell preservation solution made up as follows: 10 mL PBS (0.22 µm filtered), 25 µL 50% glutaraldehyde, and 50 µL ribonucleic DNAse. Thereafter, to each well containing the cell preservation (fixing) solution, 10 µL of resuspended trophozoite pellet from the stock assay plate was added (to 200 µL final volume) and then stored at 4°C for, at most, a week. The stock plate was stored at -80°C to facilitate the trophozoite cell lysis for the cellular haem fractionation procedure, because the lysis importantly results in the release of the parasite intracellular Hb, haem, and haemozoin.

2.2.6.2. Flow cytometry cell counting

Cell counts for the assay were performed using a flow cytometry method, as previously reported.[143] The significance of performing cell counts is to help determine the number of trophozoites per sample and therefore allow for the quantification of the amount of each haem species found in each individual cell in femtograms (fg/cell). Briefly, 160 µL of freshly prepared DNA-specific dye SYBR green I in 0.22 µm filtered PBS (1 µL SYBR green I: 10 mL PBS) was added to each well of a 96-well plate. To this, 20 µL of cell pellet (from cell counting plate) and 20 µL of Trucount beads (1 mL 0.22 µm filtered PBS to each tube containing 1 Trucount beads) were added. The BD Trucount beads are for estimation of the cell volume drawn per well by the flow cytometer allowing the determination of the number of trophozoites per mL. The plate containing the mixture of cells, SYBR green I and Trucount beads, was then covered with foil (SYBR green I is a light-sensitive fluorescent dye) and left to incubate for at least 30 minutes, in the dark, at room temperature. After incubation, the plate was resuspended and read on the BD Accuri™ C6 Plus flow cytometer with C-sampler software. The cell analysis was performed using Flowjo 10.8.0v software, which allowed for specific gating of cell populations. This follows from the fact that staining the cells with SYBR green I allows for the discrimination of cell populations from experimental debris (from possible cell lysate and PBS solution particles). For example, the trophozoite cells present much higher fluorescent intensity because of their nucleic acid content in comparison to rings or debris, which have lower fluorescence intensities. Therefore, the population gating facilitates the omission of debris to allow for the accurate determination of cell counting using intact cells. This methodology has been described in detail by Combrinck *et al*., as shown in Figure 2.4.[143]

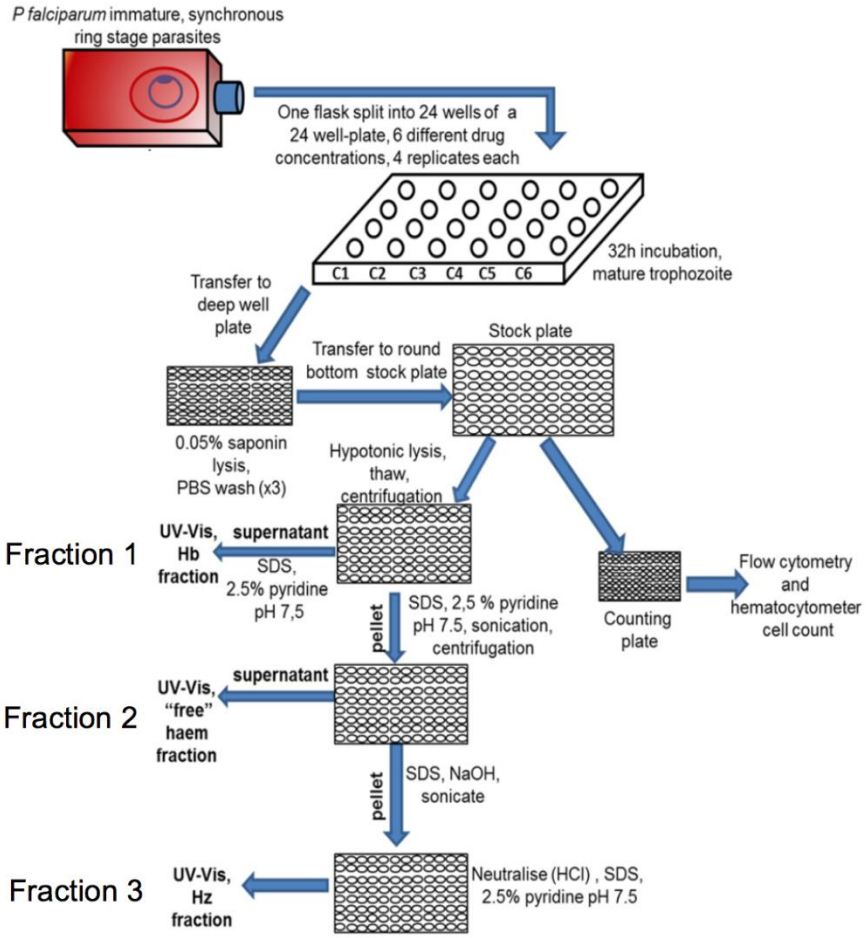

Figure 2.4: Flow chart for the pyridine-based haem fractionation assay protocol. Reproduced from Combrinck *et al.*, *Malaria Journal* **2015**, *14* (1), 1–14, under the 2015 creative commons attribution licence (http://creativecommons.org/licenses/by/4.0).[143]

2.2.6.3. Haem species fractionation

To recover all the haem fractions during the fractionation steps (Figure 2.4), the stock plate containing 100 µL of cell suspension in each well was removed from the freezer and thawed. Thereafter, 100 µL of water was added to help with cell lysis, and the suspension was sonicated for 5 minutes. Then, 50 µL 0.2 M HEPES buffer pH 7.5 was added, and the mixture was centrifuged at 2250 ×g for 20 minutes. The resulting supernatant containing soluble Hb (Fraction 1; Fig 2.4) was transferred to an adjacent set of wells on the same plate. To these wells 50 µL of each SDS (4% w/v), 0.3M NaCl, and 25% (v/v) pyridine were added, giving a final in-well volume of 400 µL. Of this volume, 200 µL was then transferred to a set of wells on a 96-well UV star plate. To the pellet containing both haem and haemozoin, a selective solubilisation of haem was performed. It is known that pyridine dissolves haem to form a low-spin complex, while the haemozoin remains and can be spun out by centrifugation.[158]

Haem solubilisation was facilitated by adding 50 µL of both water and 4% SDS to the pellet, and the mixture was resuspended and sonicated for 5 minutes. After sonication, 50 µL each of HEPES (0.2M pH 7.5), 0.3M NaCl, and 25% pyridine solutions were added to solubilise the haem fraction. The mixture was then centrifuged at 2250 ×g for 20 minutes. The supernatant (250 µL) containing haem (Fraction 2; Fig 2.4) was then transferred to adjacent wells on the plate and 150 µL of water was added to result in a final in-well volume of 400 µL. Then 200 µL of this solution was transferred to a set of wells adjacent to the Hb fraction on the 96-well UV star plate.

To the remaining haemozoin pellet (Fraction 3; Figure 2.4), which is a highly insoluble inert crystal except under highly basic conditions, 50 µL of water and 50 µL of a 0.3 M NaOH solution were added. The mixture was resuspended and sonicated for 15 minutes, after which the plate was incubated for 30 minutes at room temperature. After incubation, 50 µL each of 0.3 M HCl, HEPES (0.2 M pH 7.5), and 25% pyridine were added. To this, 150 µL of water was added (final volume of 400 µL) and 200 µL of this solution was transferred to a set of adjacent wells on a 96-well UV star plate already containing both the Hb and haem fractions. Finally, the plate was read on a Multiscan GO UV-Visible spectrophotometric plate reader at a maximum wavelength of 405 nm. The data was analysed, as previously described in Combrinck *et al*.,[143] in Microsoft Excel and GraphPad Prism v6.0 software.

2.2.7. Preparation of experimental test compounds for Chapters 5 and 6

All test compound stocks were prepared, as described in Section 2.2.2 above. The final in-well concentrations for the four-compound HPLC-DAD method in Chapter 5 were prepared similar to those of the pyridine assay at 0.5 x IC_{50}, 1 x IC_{50}, 2 x IC_{50}, 2.5 x IC_{50} and 3 x IC_{50}. These actual concentration values are summarised in Table 2.5 for each tested compound. Contrarily, for Chapter 6, the assay was performed at a single selected concentration of 2 x IC_{50}. The selected concentration values of only the control compounds used are summarised in Table 2.6.

Table 2.5: The prepared concentration values of each compound tested in the HPLC-DAD assay (Chapter 5). All the IC_{50} values were determined in the NF54 *P. falciparum* strain, using the pLDH assay.

Multiple of IC_{50}	CQ (nM)	AQ (nM)	LPT (nM)	LOM (nM)	PYR (nM)	LUM (nM)	MEF (nM)	THC (nM)
0.5x	7.5	12.5	170	300	25	13.5	12	394
1x	15	25	340	600	50	27	24	790
2x	30	50	680	1200	100	54	48	1580
2.5x	37.5	62.5	850	1500	125	67.5	60	1975
3x	45	75	1020	1800	150	81	72	2370

Table 2.6: The prepared concentrations of the control compounds tested in the 33-compound HPLC-DAD assay.

Positive Controls[a]		Negative Controls[a]	
Compound #	**2x IC_{50} Value (nM)**	**Compound #**	**2x IC_{50} Value (nM)**
1	30	10	1580
2	50	11	3600
3	680	12	100
4	1200	13	48
5	400	14	54
6	3400	-	-
7	9000	-	-
8	3000	-	-
9	818	-	-

a = All the control compound identities are described in detail in Chapter 6.

The other tested experimental compounds are not detailed here for reasons advanced in Chapter 6.

2.2.8. Speed of killing and stage specificity

The stage specificity and speed of killing for known haemozoin-inhibiting compounds were performed using a flow cytometry-based method with SYBR Green I staining. The method is a modification of earlier methods by Bennett *et.al.* and Johnson *et.al.* which focused on measuring activities of drugs using SYBR Green I fluorescence staining.[205,206] Briefly, SYBR Green I (Figure 2.5) is a nucleic acid intercalating dye that selectively binds to double-stranded DNA as opposed to single-stranded DNA (Thermo Fisher Scientific; thermofisher.com/handbook), and allows for a laser excitation (Max 497 nm) and emission (Max 520 nm) detection in the spectral region – as illustrated in Figure 2.5.

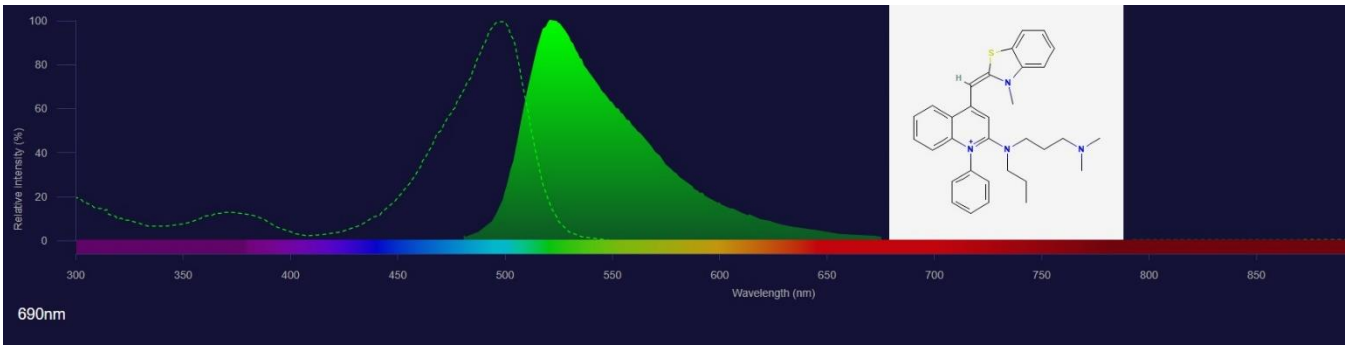

Figure 2.5: The SYBR Green I fluorescence stain's excitation (dashed green line) and emission (green shading) spectra between 300 nm and 850 nm. Maximum excitation wavelength at 497 nm and emission maximum at 520 nm. The image was reproduced using fluorescence spectraviewer from the Thermo Fisher Scientific online page (thermofisher.com/spectraviewer).

The principle for using a DNA-staining fluorescence dye is based on the lack of DNA in matured RBCs, so allowing for the selective binding of *P. falciparum* DNA in infected RBCs (iRBCs).[205] Therefore, using flow cytometry detection at 520 nm, allows for distinctive separation of *P. falciparum* iRBCs from non-infected RBCs, as illustrated by the population gating in Figure 2.6. Flow cytometry is an analytical technique that allows for the measurement and detection of both the physical and chemical characteristics of a cell population using the concepts of fluidics, optics and electronics,[207] when fluorescently labelled particles (electronics) flow individually (fluidics) in front of an area illuminated with a laser beam (optics).

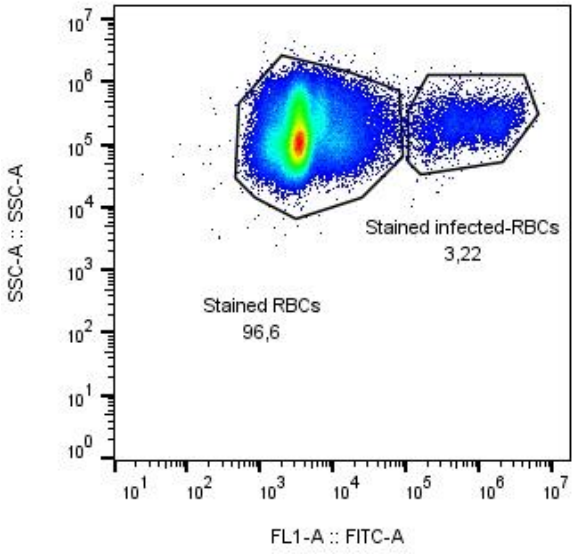

Figure 2.6: The separation of infected RBCs and non-infected RBCs using SYBR green I DNA staining for flow cytometric detection. Maximum excitation wavelength at 497 nm and maximum emission wavelength at 520 nm. The PRBC with increased fluorescence are distinguishable from the RBC.

2.2.8.1. Incubation of cells with test compounds

For sample preparations, an early ring-staged NF54 CQS sorbitol synchronised parasite culture at 2% parasitemia and 2% haematocrit was prepared (49 mL medium + 1 mL pellet) in CM. Aliquots of 200 µL from the culture were added to a 96-well flat-bottom plate. Exactly 20 µL of test compounds prepared at five concentrations – 0.5x, 1x, 1.5x, 2x and 3x multiples of each compound's IC_{50} in complete media – were added to the plate. The final volume in each well was 220 µL. Each assay plate had at least eight drug-free negative control wells (0 µM drug concentration) and CQ as a positive control (tested IC_{50} = 15 nM) on at least one of the plates. The assay plates were sealed and incubated at 37°C in a gassing chamber with a gas mixture of 3% O_2, 4% CO_2 and 93% N_2. Drug wash-out steps at specific times shown in Figure 2.7 below were performed by simply aspirating off the drug-containing medium and replacing it with new CM at the various time points. These were then left to fully incubate and complete a 72 h incubation period.

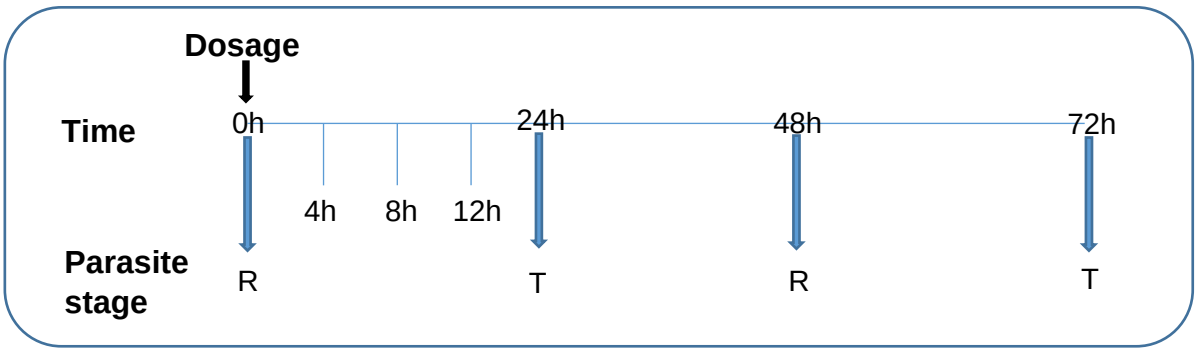

Figure 2.7: The various wash-out times during the incubation period of 72 h. Drug wash-out steps were performed at all the indicated times on the timeline between 0 h and 72 h. The 72 h time point was treated as a control. Abbreviations: R = ring-staged parasites; T = trophozoite-staged parasites.

2.2.8.2. Flowcytometry and data analysis

After the 72 h incubation, the plates were removed from the gassing chamber, the medium was aspirated and the pellet washed twice with 100 µL of 0.22 µm filtered phosphate buffered saline (PBS). Following this, 100 µL of the freshly prepared DNA-specific dye SYBR green I in 0.22 µm filtered PBS (1 µL SYBR green I: 9 mL PBS) was added to each well. The pellet was resuspended and left to incubate for at least 30 minutes in the dark and at room temperature. After incubation, the plates were resuspended and read on the BD Accuri™ C6 Plus flow cytometer with C-sampler software. For each flow cytometric sample measurement, 20 000 events were collected and analysed. Figure 2.8 summarises the step-by-step methodology for the assay.

Specific to the flowcytometry gating as illustrated in Figure 2.9, the FSC channel of the flow cytometer is representative of the size of a particle, while the SSC channel describes the complexity of the particle (Bio-rad; https://www.bio-rad-antibodies.com/introduction-to-flow-cytometry.html). However, for fluorescence detection the FL1 channel (FTC-A), which is specific for SYBR Green I fluorescence detection, was used. This is because it is critical in discriminating between SYBR Green I positive events in terms of their DNA binding. This phenomenon can be observed below (Figure 2.9), where stained RBCs and stained infected-RBCs fluoresce differently because of their DNA-specific abundance.

The acquired data was then analysed using FlowJo™ software version 10.5.3., using the gating methodology – as presented in Figure 2.9. The uninfected and infected red blood cells in each sample were characterised using forward (FSC) and side scatter (SSC), as well as the fluorescence intensity (FL1) parameter, in order to determine SYBR green I positive cells. Two independent experiments for each compound were performed, and each of the test compound concentrations were tested in triplicate. A non-linear dose-response analysis curve fitting of the specific gated events of interest (stained infected RBCs) was performed using

GraphPad Prism v6.0 software, in order to determine the IC_{50} values of each test compound. Further analyses were completed using Microsoft Excel software.

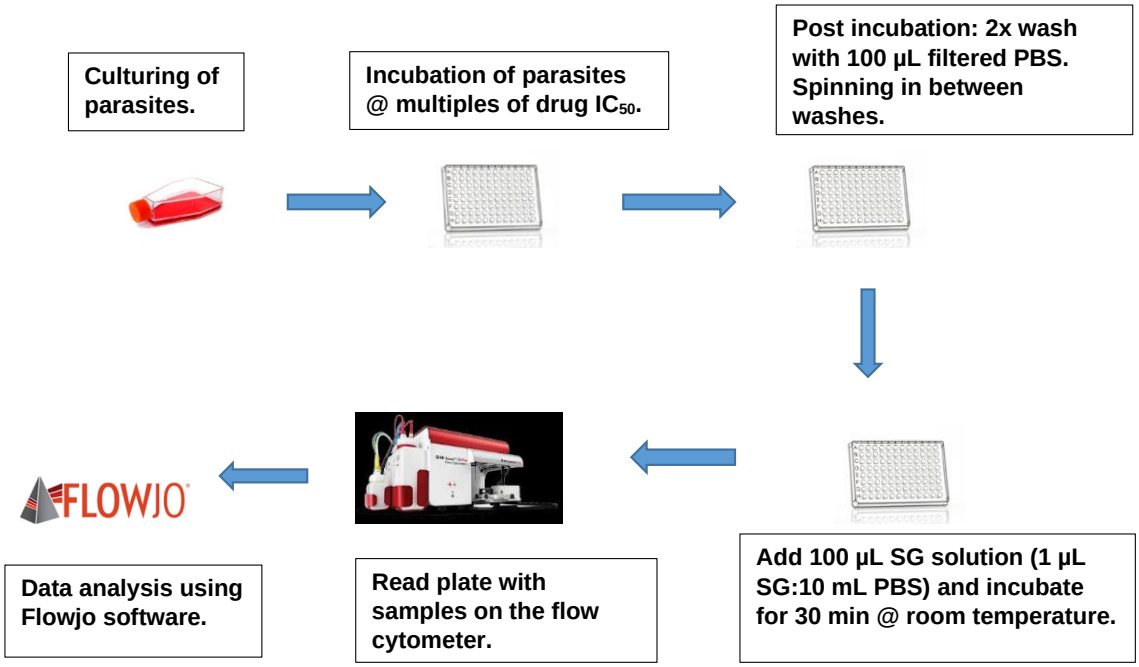

Figure 2.8: The step-by-step methodology for the speed of killing and stage-specificity assay.

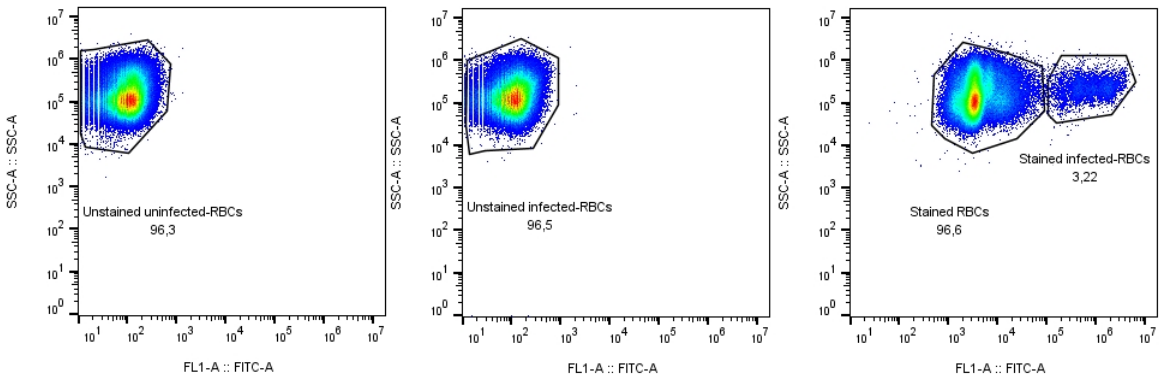

Figure 2.9: The gating controls for the flow cytometry result analysis of the speed of killing/stage specificity assay. Whereby: unstained uninfected-RBCs = no SYBR Green I staining of uninfected RBCs; unstained infected-RBCs = no SYBR Green I staining of infected RBCs; stained RBCs = uninfected RBCs with SYBR Green I staining; and stained infected-RBCs = SYBR Green I staining of *P. falciparum* infected RBCs. All *P. falciparum*-infected RBCs were analysed during the trophozoite stage.

Chapter 3: Measuring Intracellular *P. falciparum* Haem Species for *in Silico* Predicted β-haematin Inhibitors

3.1. Introduction

The current emergence of resistance by *P. falciparum* malaria to first-line treatment drugs is of great concern.[208] It is therefore essential that novel active compounds be discovered for future effective treatment of malaria. To achieve this, drug discovery laboratories use various techniques to find novel compounds. Mechanistic target-based screening is one such approach which can be broadly defined as a screening process using a single biological target that, when directly effected molecularly, results in a significant phenotypic and, ultimately, therapeutic effect.[209] Usually, activity predictions towards the specific targets are performed using computer models as structure- and ligand-based virtual screening tools, thereby allowing for large screens of chemical libraries.

A more directed approach – structure-based virtual screening – uses molecular docking to screen chemical libraries towards identifying target-docked ligands that are purchasable for testing.[210] However, for the technique to be successful, the structure of the biological target must be known, either via crystallographic approaches or homology modelling.[181] In the malaria parasite, the haem detoxification pathway, specifically the haemozoin crystal, presents as an attractive drug target. This is because resistance to currently effective haemozoin-inhibiting antimalarials does not arise from alterations in the haem detoxification process, but rather from mutations in transporter proteins located on the DV.[116,168] As previously mentioned in Chapter 1, quinoline-based antimalarials act by binding to the haemozoin crystal during haemoglobin degradation and interfere with this process, thus causing a build-up of unsequestered haem that kills the parasite.[211] This chapter reports on biological assay results of virtually screened compounds that are predicted *in silico* by de Sousa *et al.* to inhibit β-haematin formation and which were subsequently found to be active against β-haematin *in vitro*.[182,190,212]

β-haematin is the synthetic counterpart of intracellular haemozoin and has been shown to have an identical chemical and crystalline structure, and to be spectroscopically identical to haemozoin.[33] Therefore, inhibiting β-haematin extracellularly is a good indicator of a compound's ability to inhibit haemozoin in the whole-cell parasite. Resistance to antimalarials such as CQ, amodiaquine and piperaquine that act via this MoA in the parasite has been associated with mutations in the *P. falciparum* chloroquine resistance transporter protein (PfCRT). This digestive vacuole membrane transporter causes a structure-specific efflux of the drug from the parasite DV,[121] ruling out any direct relation of resistance to the therapeutic

target. Interestingly, in a comprehensive study by Chaparro *et al.,* the haemoglobin degradation pathway was reported as one of the targets in the parasite, which presented the highest probability of delivering successful new drug candidates.[203]

Herein, 39 *in silico*-predicted and β-haematin active compounds were evaluated for their activity against the pLDH assay, with the most active compounds evaluated for their haemozoin-inhibiting capabilities using the previously described (Chapter 2) pyridine-based haem fractionation assay. All the data presented in this chapter appears in three publications[182,190,212] that focused on structure-based virtual screening of the ZINC15 database and United States Food and Drug Administration (USFDA) database libraries to discover new β-haematin inhibitors.

3.2. Results

All materials, sample preparations and biological methods used in this chapter are detailed in Chapter 2. The β-haematin assay work for the reported compounds was performed by Ana de Sousa, a postdoctoral student in the Bioinorganic Chemistry Lab at UCT.

3.2.1. Determining *in vitro* activity against *Plasmodium falciparum*

The pLDH assay is used to assess the *in* vitro growth inhibitory activity of test compounds against *P. falciparum* strains, specifically by performing colourimetric measurement of pLDH activity in the presence of 3-acetylpyridine adenine dinucleotide (APAD) at varying test compound concentrations. As detailed in Chapter 2, the assay uses APAD as a coenzyme to convert parasite lactate to pyruvate in viable parasite cells, thus, allowing for the indirect measurement of parasiticidal activity of test compounds.[196] All 39 compounds were evaluated for their antiplasmodium activity against the NF54 CQS strain and, subsequently, a select group of compounds was assessed further for cross-resistance against the K1 CQR strain. Furthermore, a select few of the active compounds were evaluated for their cytotoxic selectivity towards the *P. falciparum* parasites using the Chinese hamster ovary (CHO) mammalian cell line. For the current work, an active test compound is defined as that with a less than 10 μM IC_{50} value, as determined using the dose-response curve fitting analysis.

3.2.1.1. Biological screening of the Zinc15 database compounds

The antiplasmodium results of the most promising β-haematin inhibiting compounds (Figure 3.1) from the Zinc15 database are shown in Table 3.1. These were chosen as top-ranked compounds based on their binding affinity and favourable interactions with the crystal structure, as described by de Sousa *et al.*[182] All 15 compounds were tested for antiplasmodium activity after being evaluated for their ability to inhibit β-haematin formation in the NP-40 detergent mediated assay, as described in Chapter 2. The most active compounds were

further evaluated for their general toxicity.

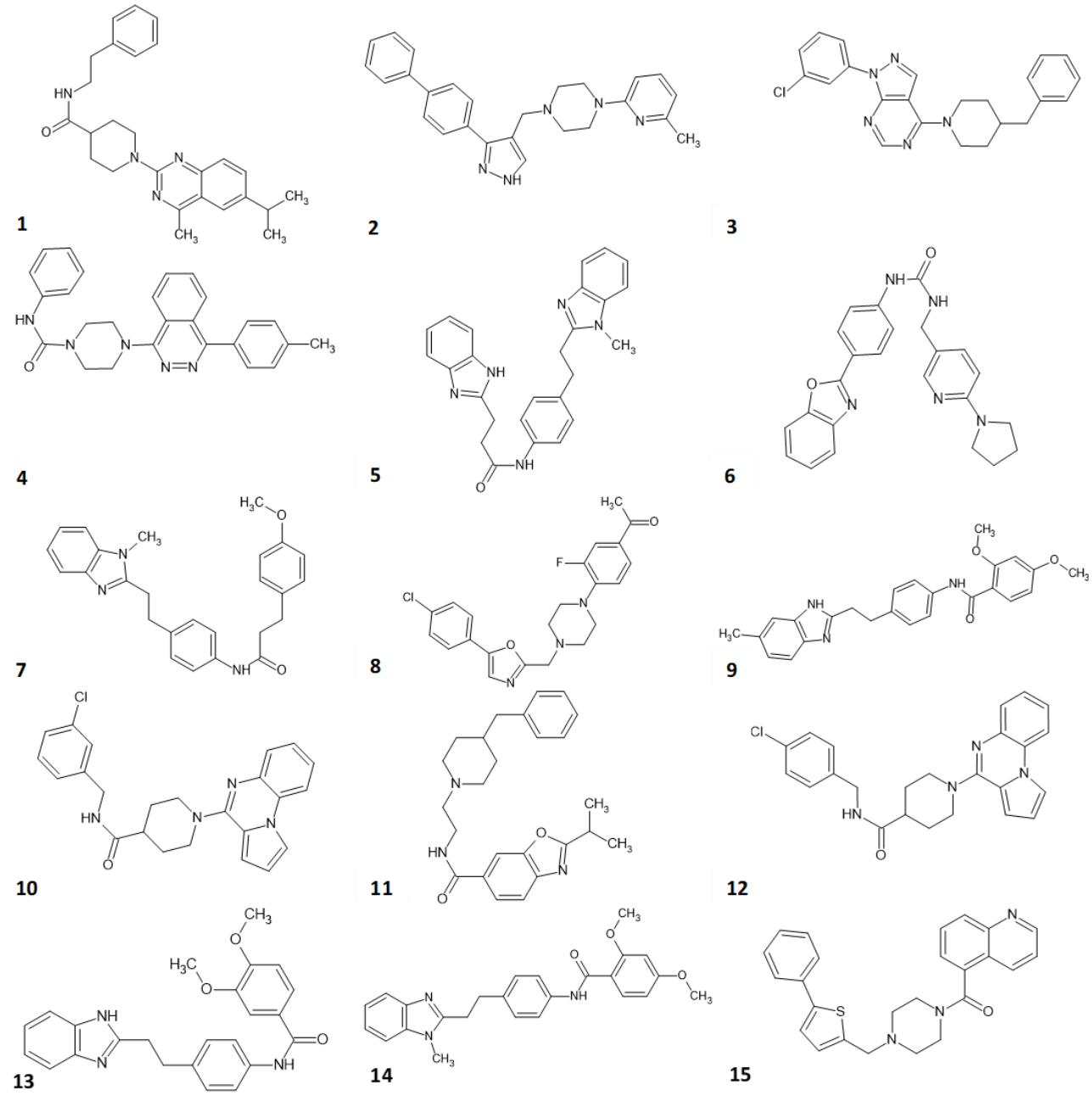

Figure 3.1: Top-ranked compounds from the Zinc15 database.[182]

Table 3.1: β-haematin antiplasmodium activity (NF54 (CQS) and K1 (CQR)) and cytotoxicity, and selectivity index (SI) results.

Compound	β-haematin IC_{50} (μM)	NF54 IC_{50} (μM)	K1 IC_{50} (μM)	CHO[a] IC_{50} (μM)	SI[b]
1	305 ± 37	>10	>10	-	
2	339 ± 7	4.4 ± 0.5	5.8 ± 0.002	323 ± 5	73
3	>1000	>10	>10	-	
4	288 ± 13	>10	>10	-	
5	>1000	>10	>10	-	
6	64 ± 3	3.5 ± 0.2	3.0 ± 0.9	18.8 ± 0.005	5
7	>1000	>10	>10	-	
8	139 ± 22	>10	>10	-	
9	66.3 ± 0.2	4.6 ± 0.5	4.9 ± 2	-	
10	394 ± 79	>10	>10	-	
11	212 ± 57	1.2 ± 0.02	2.3 ± 0.1	106 ± 6	87
12	605 ± 64	>10	>10	-	
13	313 ± 25	>10	>10	-	
14	>1 000	>10	>10	-	
15	563 ± 65	>10	>10	-	
CQ	22 ± 3	0.015 ± 0.002	0.17 ± 0.03	-	

a = Chinese hamster ovary cell line

b = Selectivity index = CHO IC_{50}/NF54 IC_{50}

Although the β-haematin results showed a remarkable hit rate (60%), with 9 out of 15 compounds showing activity below 500 μM, it was found that only 4 of the 15 compounds showed antiplasmodium activity below 10 μM, and none of the compounds had any sub-micromolar activity. However, no significant differences were observed between the activities in both the NF54 (CQS) and K1 (CQR) strains, so indicating a lack of CQ cross-resistance. Of the three selected compounds for cytotoxicity analysis, two (**2** and **11**) had selectivity indices above 70-fold. The selectivity index is defined as the ratio between the CHO activity (IC_{50}) and the antiplasmodium activity (IC_{50}). It is used as a measure of how selective a compound is towards the *P. falciparum* parasite relative to mammalian cells. Therefore, from the data, it was observed that compound **6** showed poor selectivity, while compounds **2** and **11** showed selectivity >70-fold.

3.2.1.2. Biological screening of compounds from the United States Food and Drug Administration (USFDA) and ChemDiv libraries

The structure-based virtual screening (SBVS) model was used to identify potential β-haematin inhibiting compounds from the USFDA database.[213] Here, 22 top-ranking compounds were chosen based on their association with the β-haematin structure for β-haematin evaluation and, subsequently, antiplasmodium testing as reported by de Sousa *et al.*[190] However, for the discussion in this chapter, only those compounds (10) that showed antiplasmodium activity below 10 μM are presented (Figure 3.2). Table 3.2 shows the antiplasmodium results of all the 10 β-haematin inhibiting compounds of the USFDA and ChemDiv set.

Most importantly, it should be noted that compounds **21–25** are not FDA-approved and were not found in the FDA database. These were, however, hit compounds generated from Ligand-based virtual screening (LBVS) using Lapatinib (**16**) and Nilotinib (**17**) as templates for shape and electrostatic similarities within the ChemDiv database.[190,214]

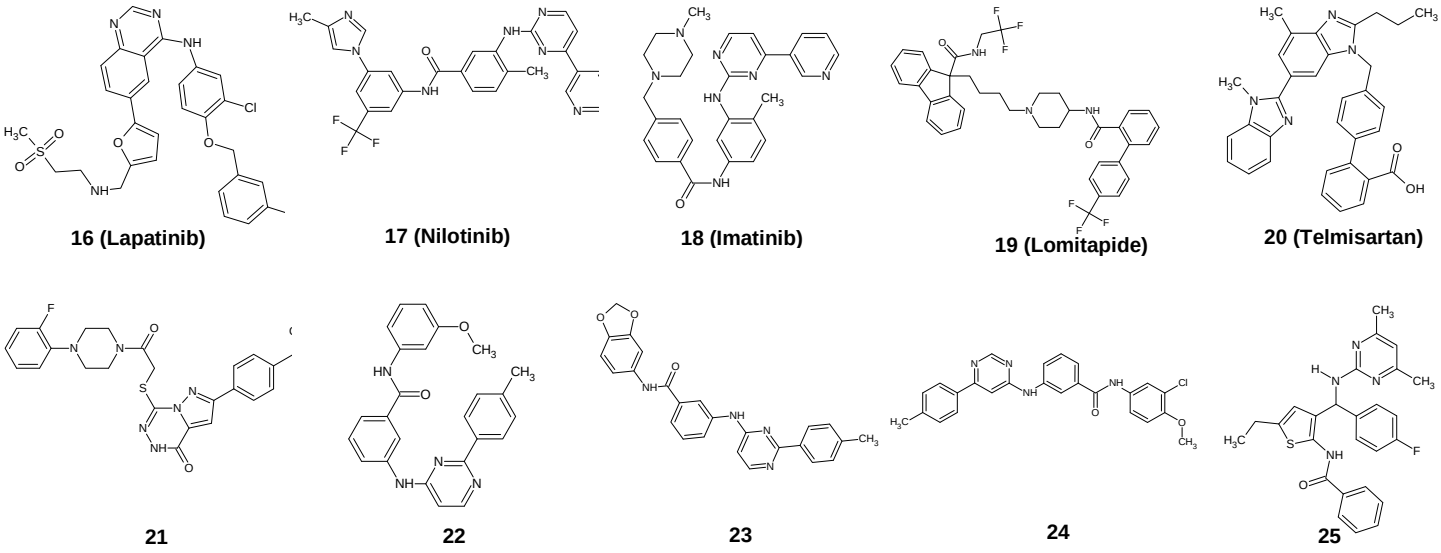

Figure 3.2: Active compounds (IC_{50} <10 µM) from the USFDA[213] (**16–20**) and ChemDiv[214] (**21–25**) databases.

Table 3.2: β-haematin activity, antiplasmodium activity and cytotoxicity results of the 10 most active selected compounds of the USFDA (**16–20**) and ChemDiv (**21–25**) databases.[213,214]

Compound	β-haematin IC_{50} (µM)	NF54 IC_{50} (µM)	K1 IC_{50} (µM)	CHO[a] IC_{50} (µM)	SI[b]
16	5.4 ± 0.03	0.26 ± 0.07	0.85 ± 0.02	21 ± 4	82
17	7.3 ± 1	0.28 ± 0.02	0.38 ± 0.06	17 ± 6	61
18	99 ± 5	3.9 ± 0.1	3.20 ± 0.03	NT	-
19	68 ± 0.9	0.56 ± 0.1	0.69 ± 0.1	19 ± 4	34
20	51 ± 0.7	5.0 ± 2	NT	NT	-
21	354 ± 60	4.9 ± 0.4	NT	NT	-
22	156 ± 2	6.4 ± 0.6	NT	NT	-
23	373 ± 98	8.1 ± 0.2	NT	NT	-
24	86 ± 40	3.9 ± 0.1	NT	NT	-
25	68 ± 6	3.8 ± 0.3	NT	NT	-
CQ	26 ± 0.3	0.015 ± 0.001	0.27 ± 0.005	NT	-

a = Chinese hamster ovary cell line
b = Selectivity index (SI) = CHO IC_{50}/NF54 IC_{50}
NT = Not tested

Of the 22 β-haematin active compounds, 10 were found to have antiplasmodium activity less than 10 μM against the NF54 CQS strain. Of these, three compounds (**16**, **17** and **19**) were found to have sub-micromolar activity. Subsequently, four compounds (**16**, **17**, **18** and **19**) were tested against the K1 CQR strain to assess possible cross-resistance with CQ. It was determined that only compound **16** displayed >2-fold increase in IC_{50} in the CQR strain. However, this fold increase was significantly below the increase shown by CQ (18-fold), thus presenting the minimal possibility of cross-resistance. Compounds **16**, **17** and **19** were then tested for their cytotoxicity against the CHO cell line, and all compounds had promising selectivity indices >34-fold.

Interestingly, through the SBVS of the USFDA database, the drug dronabinol was found among the top-ranked compounds with favourable binding affinity and interactions with the β-haematin structure. The main active ingredient of dronabinol capsules (Marinol®) is synthetic delta-9-tetrahydrocannabinol (THC), a distinct formulation of the natural marijuana.[215] Therefore, the two major occurring cannabinoids (THC and cannabidiol) (Figure 3.3) were purchased for β-haematin assay testing following an SBVS prediction study for their binding with the crystal structure. THC and cannabidiol (CBD) strongly inhibited the formation of β-haematin *in vitro* in ranges similar to quinine and CQ, and were taken for further antiplasmodium testing.[212] The summarised results are presented in Table 3.3. Here, THC was strongly active against both strains of *P. falciparum* with IC_{50} values in the nanomolar range compared to CBD, which showed poor activity in the CQS strain. Using the CHO cell line, the selectivity of THC against *P. falciparum* was found to be satisfactory and above 350-fold.

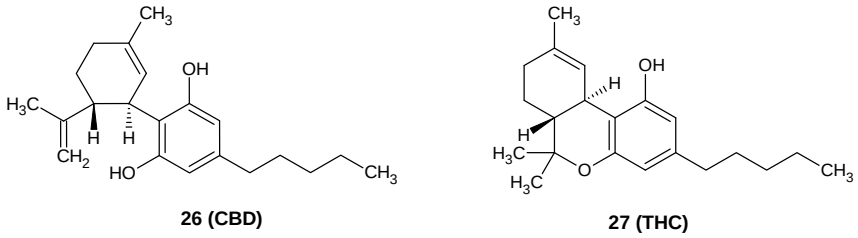

Figure 3.3: The structures of CBD and THC.

Table 3.3: The β-haematin activity, antiplasmodium activity, and cytotoxic activity of both THC and CBD.

Compound	β-haematin IC_{50} (μM)	NF54 IC_{50} (μM)	K1 IC_{50} (μM)	CHO[a] IC_{50} (μM)	SI[b]
THC (26)	11.3 ± 0.2	0.79 ± 0.04	0.72 ± 0.1	278[c]	352
CBD (27)	51.1 ± 0.7	4.1 ± 0.3	NT	NT	–
CQ	16.8 ± 0.2	0.020 ± 0.001	0.27 ± 0.05	NT	–

a = Chinese hamster ovary cell line

b = Selectivity index = CHO IC_{50}/NF54 IC_{50}

c = Tested once in triplicate (i.e., no repeat experiment)

NT = Not tested

Since all compounds reported in this chapter were found to be actual β-haematin inhibitors *in vitro*, as predicted through the SBVS models, performing intracellular MoA investigations was critical. A select group of the top active antiplasmodium compounds were chosen from each batch (Tables 3.1, 3.2 and 3.3) for mechanistic investigation in the malaria parasite. Therefore, six compounds were prioritised for investigation using the pyridine-based haem fractionation assay, relative to the positive control, CQ.

3.2.2. Probing the effects of β-haematin inhibiting compounds on the haem detoxification pathway

As previously mentioned, β-haematin is the synthetic counterpart of malaria haemozoin, making it a suitable chemical agent for predicting haemozoin inhibition *in vitro*. However, these predictions do not always translate into the intracellular haemozoin inhibition MoA, therefore necessitating the cellular measurements. Here, the unsequestered haem and haemozoin species profiles of compounds **6, 11, 16, 17, 19, 26** (published work[182,190,212]) and CQ are reported. This experiment aimed to ascertain that these compounds' actual MoA is via inhibition of haemozoin formation in the parasite, as predicted and, importantly, that this inhibition subsequently leads to increased parasite unsequestered haem. These determinations were obtained using the method published by Combrinck *et al.* for isolating drug-incubated trophozoites and performing haem species fractionations that can be colourimetrically quantified using pyridine.[143]

For reference, CQ was used as a positive control. Figure 3.4 shows the percentage species (%haem and %Hz) per well, the concentrations of unsequestered haem (haem Fe) and haemozoin (Hz Fe) per trophozoite, as well as the concentration of total haem Fe (sum of haemoglobin Fe, haem Fe and haemozoin Fe concentrations in fg/cell) in the trophozoite cell at different CQ dosing concentrations. The %haemoglobin (%Hb) and haemoglobin Fe (Hb Fe) concentrations are not reported here since they were not significance in the rationale of

this work. Briefly, the percentage values of each haem fraction (haemoglobin, unsequestered haem, and haemozoin) signify the abundance of each fraction in relation to the total haem Fe per well of trophozoites at that specific dosing concentration. To normalise this and report the actual haem fraction values in each trophozoite cell, the flow cytometry cell counting (Chapter 2; Section 2.2.6.2) data was used. It is important to mention that relying only on the percentage of unsequestered haem concentration values can be misleading in determining true haemozoin-inhibiting compounds, as previously explained by Combrinck *et al.* in the case of atovaquone.[143] Therefore, it is critical to report on the normalised haem Fe concentrations in femtograms per trophozoite cell (fg/cell) to identify haemozoin inhibitors.

Since CQ is a known haemozoin inhibitor, it was expected that the %haem and haem Fe concentrations increase with increasing dosing concentration, as observed (Figure 3.4), and that this phenomenon is followed by a decrease in %haemozoin (%Hz) and haemozoin Fe (Hz Fe) profiles as an indication of haemozoin formation inhibition. Moreover, the total Fe remained statistically indistinguishable, and only significantly decreasing at the 2.5x and 3x IC_{50} concentrations. The significant increase in haem Fe (fg/cell) and subsequent decrease in haemozoin Fe (fg/cell) over the increasing compound concentration (multiples IC_{50}) serve as an indicator of a true hemozoin inhibitor in the parasite cell.

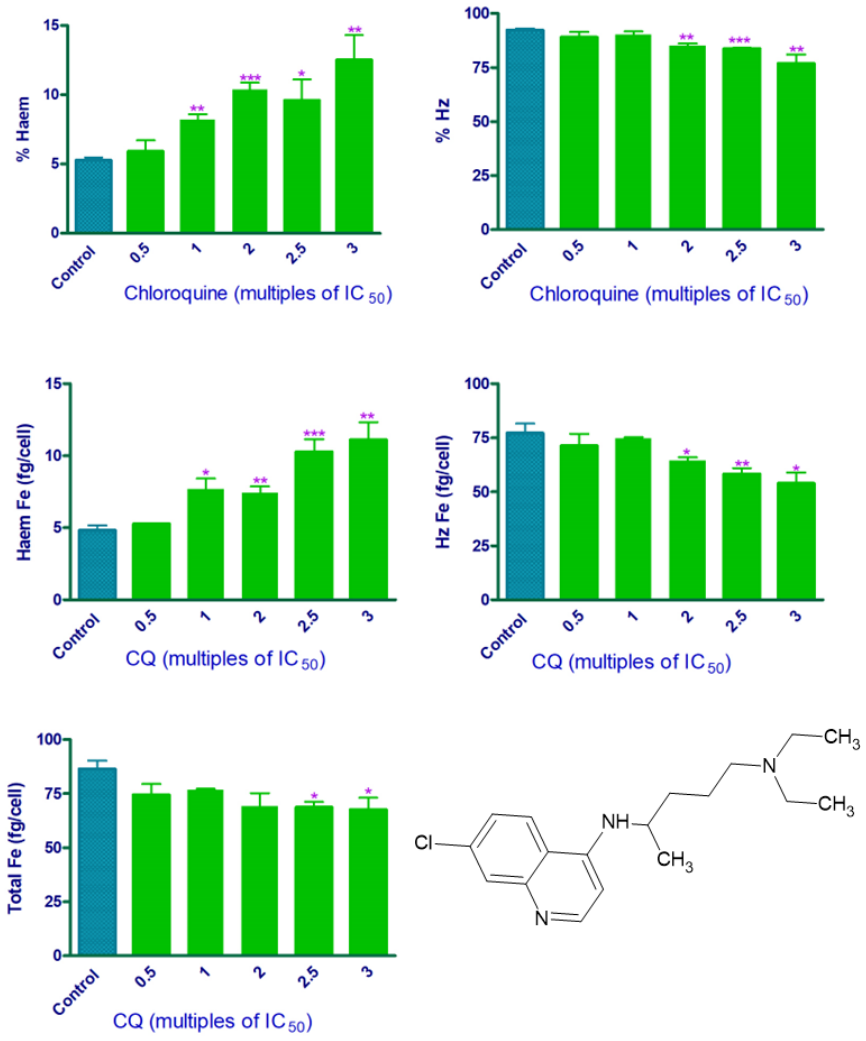

Figure 3.4: The *P. falciparum* isolated haem fraction profiles of unsequestered haem (haem) and haemozoin (Hz) expressed as percentage abundance (top panels) per well of trophozoites (represented at multiple of IC_{50}), haem Fe and haemozoin Fe per trophozoite cell in fg (middle panels). The total Fe (fg/cell; bottom panel) is the sum concentration of all major haem species (haemoglobin Fe, Haem Fe and haemozoin Fe) in an individual trophozoite cell. This follows from a 32 h incubation of early ring-stage *P. falciparum* parasites with CQ (attached structure) at multiples of IC_{50} and the subsequent isolation of mature trophozoites post-incubation. Control = untreated cells. Statistical significance was calculated relative to the control using the two-tailed t-test at a 95% confidence interval; this is expressed as an asterisk: * $p < 0.05$; ** $p < 0.01$; *** $p < 0.001$. Values represent the mean ± SEM and two repeat experiments were performed.

Similarly, the determination of the MoA was performed for compounds **6** and **11**, as depicted in Figures 3.5 and 3.6, respectively. For compound **6**, the %haem values increased with dosing concentration, whereas the haem Fe values at the various dosing concentrations were statistically indistinguishable from the control (untreated). The %haemozoin (%Hz) remained unchanged, while the haemozoin Fe (Hz Fe) decreased significantly. Lastly, the total Fe for

compound **6** decreased significantly across the tested concentrations. In contrast, the %haem and haem Fe values for compound **11** increased with dosing concentrations, while the %haemozoin and haemozoin Fe concentrations subsequently decreased, indicating a haemozoin inhibitor (Figure 3.6). The total haem Fe also declined significantly with increasing compound concentration.

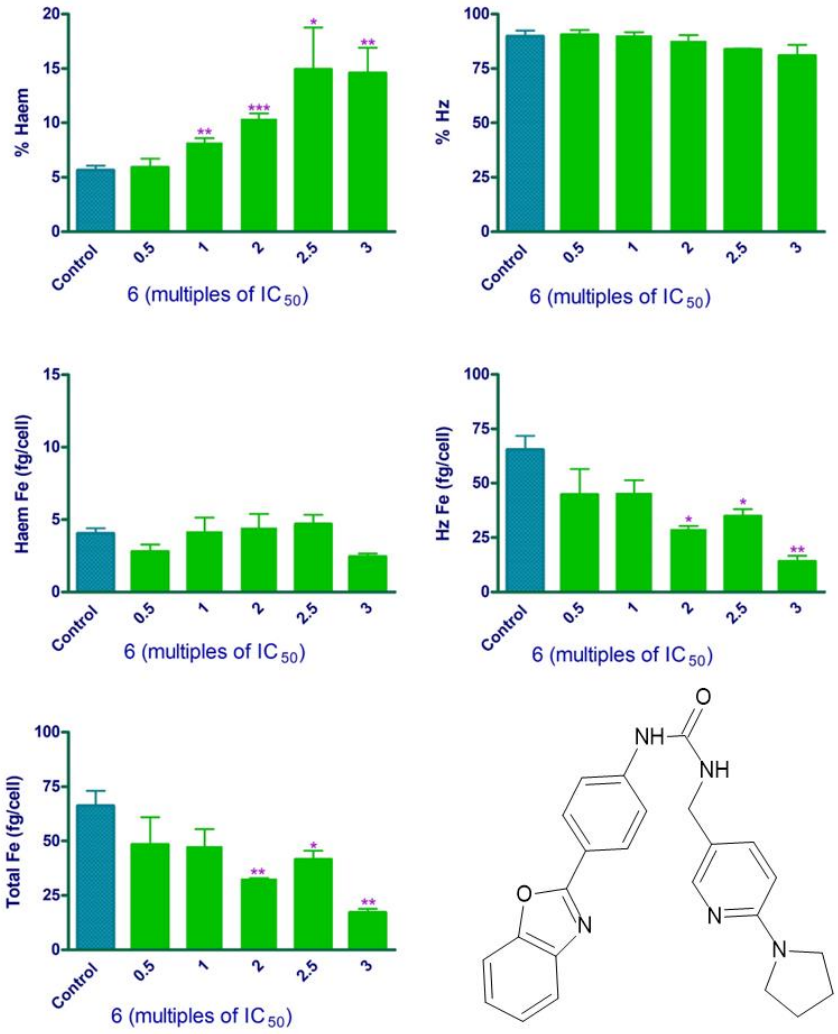

Figure 3.5: The profiles of unsequestered haem (haem) and haemozoin (Hz) expressed as percentage composition (top panels) per well of trophozoites, with haem Fe and haemozoin Fe in fg per trophozoite cell. The total Fe (fg/cell; bottom panel) is the sum concentration of all individual haem species in the trophozoite cell. This follows from a 32 h incubation of early ring-stage *P. falciparum* parasites with compound **6** (attached structure) at multiples of IC_{50} and the subsequent isolation of mature trophozoites post-incubation. Control = untreated cells. Statistical significance was calculated relative to the control using the two-tailed t-test at a 95% confidence interval; this is expressed as an asterisk: * $p < 0.05$; ** $p < 0.01$; *** $p < 0.001$. Values represent the mean ± SEM and two repeat experiments were performed.

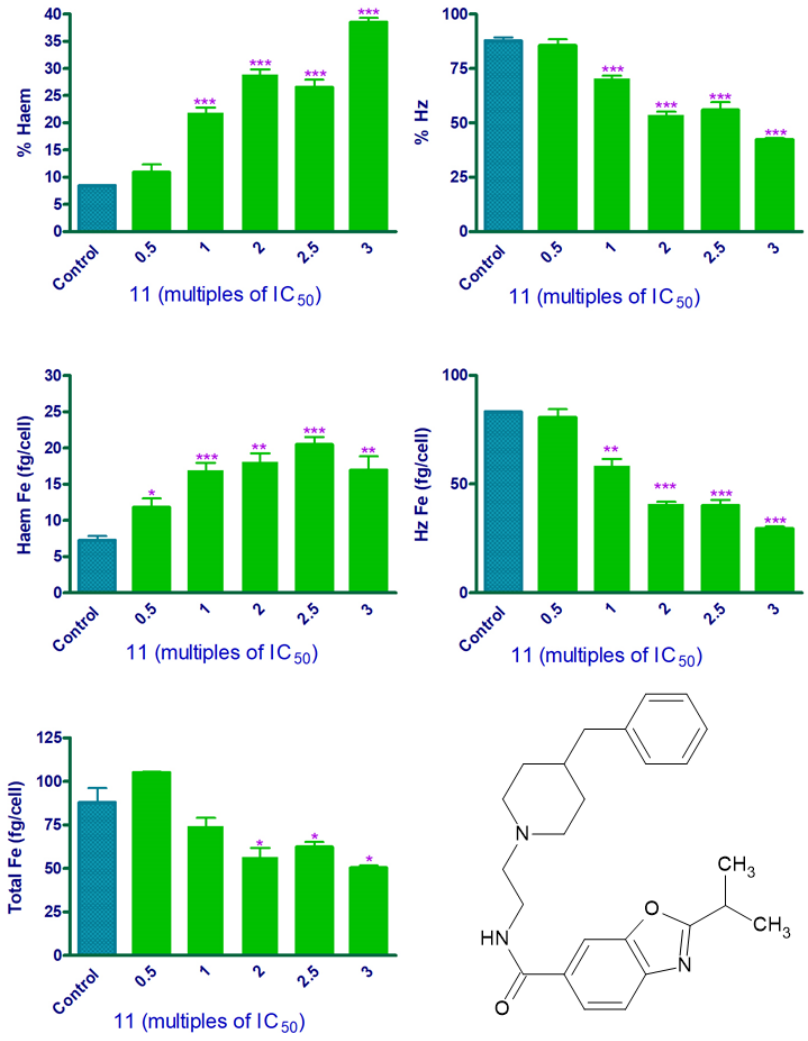

Figure 3.6: The levels of unsequestered haem (haem) and haemozoin (Hz) expressed as percentage abundance (top panels) per well of trophozoites, with haem and haemozoin Fe expressed in fg per trophozoite cell (middle panels). The total Fe (fg/cell; bottom panel) is the sum concentration of haem species in an individual trophozoite cell. This follows from a 32 h incubation of early ring-stage *P. falciparum* parasites with compound **11** (attached structure) at multiples of IC_{50}, and the subsequent isolation of mature trophozoites post-incubation. Control = untreated cells. Statistical significance was calculated relative to the control using the two-tailed t-test at a 95% confidence interval; this is expressed as an asterisk: * $p < 0.05$; ** $p < 0.01$; *** $p < 0.001$. Values represent the mean ± SEM and two repeat experiments were performed.

From the antiplasmodium results of the USFDA database (Table 3.2), compounds **16**, **17** and **19** were chosen for mechanistic evaluations. In all these compounds (**16**, **17** and **19** represented in Figures 3.7, 3.8 and 3.9) the %haem and haem Fe values increased significantly with increasing dosing concentration, while the %haemozoin and haemozoin Fe decreased considerably under similar conditions. For **16** and **17,** the total Fe remained unchanged, although showing a significant gradual decrease for **19** at the 2.5x and 3x IC_{50}.

Effectively, all three selected test compounds from this set displayed inhibition of the haem detoxification pathway as initially predicted by the *in silico* models.

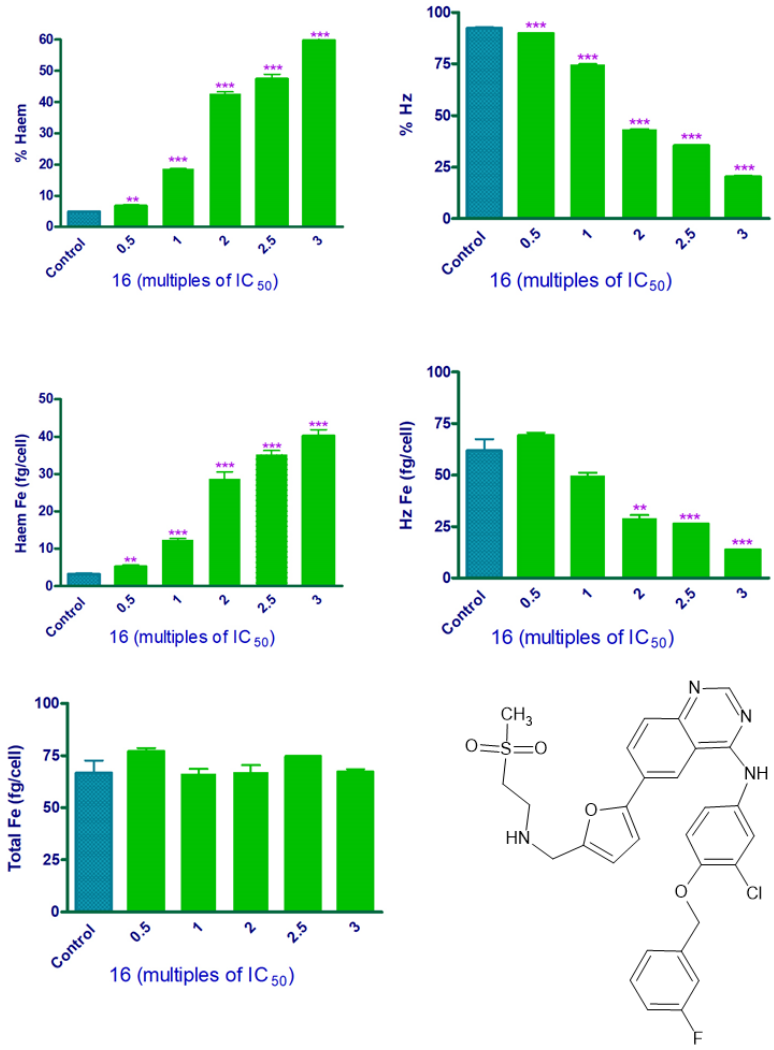

Figure 3.7: Intracellular levels of unsequestered haem (haem) and haemozoin (Hz) expressed as percentage abundance (top panels) per well of trophozoites, and fg/cell for both haem Fe and haemozoin Fe (middle panels). The total Fe (fg/cell; bottom panel) is the sum concentration of all the haem species in each trophozoite cell. This follows from a 32 h incubation of early ring-stage *P. falciparum* parasites with compound **16** (attached structure) at multiples of IC_{50}, and the subsequent isolation of mature trophozoites post-incubation. Control = untreated cells. Statistical significance was calculated relative to the control using the two-tailed t-test at a 95% confidence interval; this is expressed as an asterisk: * $p < 0.05$; ** $p < 0.01$; *** $p < 0.001$. Values represent the mean ± SEM and two repeat experiments were performed.

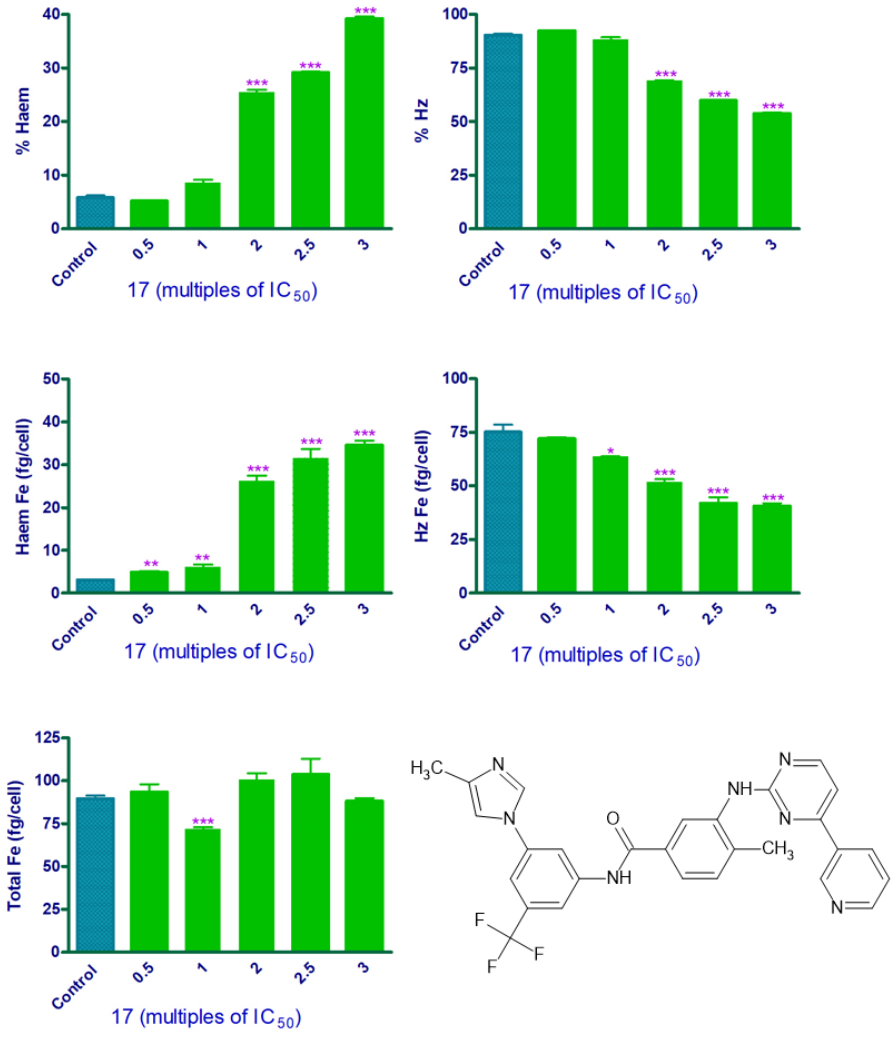

Figure 3.8: The haem fractionation profiles of unsequestered haem (haem) and haemozoin (Hz) expressed as percent abundance (top panels) per well of trophozoites, while haem and haemozoin Fe are expressed in fg per trophozoite (middle panels). The total Fe (fg/cell; bottom panel) is the sum concentration of all haem fractions per trophozoite cell. This follows from a 32 h incubation of early ring-stage *P. falciparum* parasites with compound **17** (attached structure) at multiples of IC_{50}, and the subsequent isolation of mature trophozoites post-incubation. Control = untreated cells. Statistical significance was calculated relative to the control using the two-tailed t-test at a 95% confidence interval; this is expressed as an asterisk: * $p < 0.05$; ** $p < 0.01$; *** $p < 0.001$. Values represent the mean ± SEM and two repeat experiments were performed.

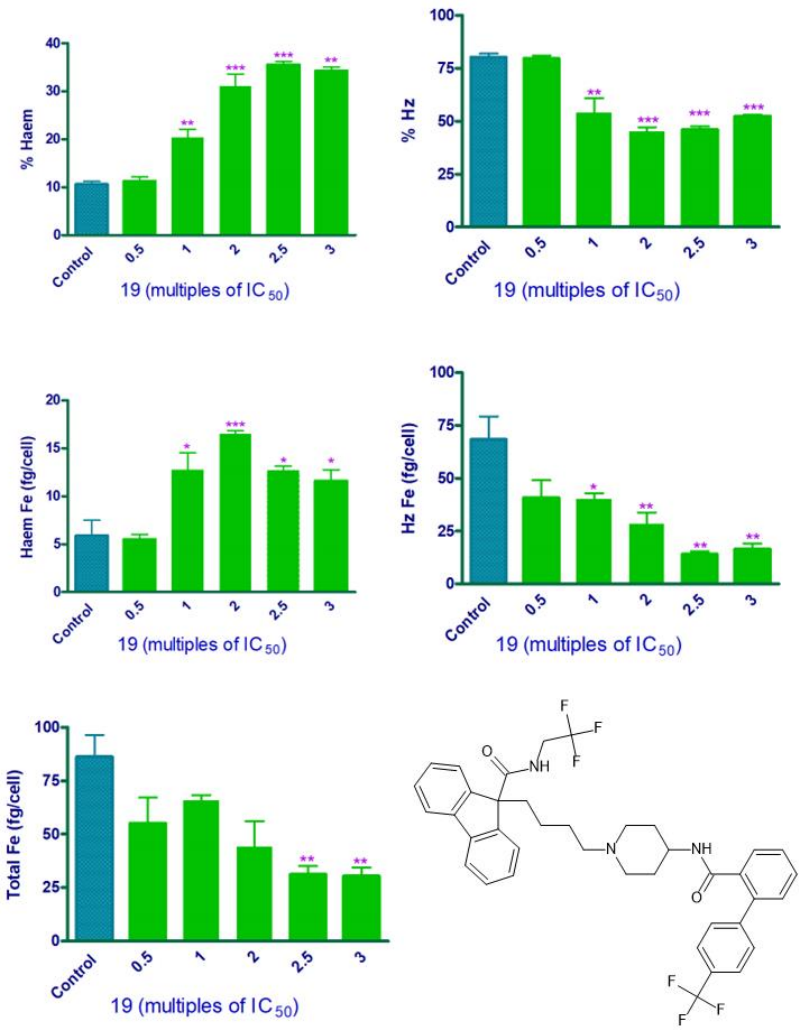

Figure 3.9: The fractionation profiles of unsequestered haem (haem) and haemozoin (Hz) expressed as percent abundance (top panels) per well of trophozoites, and fg/cell for haem and haemozoin Fe (middle panels). The total Fe (fg/cell; bottom panel) is the sum concentration of the haem species in a trophozoite cell. This follows from a 32 h incubation of early ring-stage *P. falciparum* parasites with compound **19** (attached structure) at multiples of IC_{50}, and the subsequent isolation of mature trophozoites post-incubation. Control = untreated cells. Statistical significance was calculated relative to the control using the two-tailed t-test at a 95% confidence interval; this is expressed as an asterisk: * $p < 0.05$; ** $p < 0.01$; *** $p < 0.001$. Values represent the mean ± SEM and two repeat experiments were performed.

Lastly, from the SBVS dataset (Table 3.3), **26** was chosen ahead of **27** for mechanistic evaluation based on its antiplasmodium activity. The significant limitation in the pyridine assay's slow and labour-intensive throughput makes it difficult to study every compound of interest for mechanistic determinations. The %haem values of **26** increased while haem Fe values were indistinguishable at various dosing concentrations. Similarly, the %haemozoin remained unchanged. At the same time, haemozoin Fe and total Fe values significantly

decreased over the increasing concentration range. Therefore, compound **26** does not kill the parasite by inhibiting haemozoin formation, as it shows no increase in haem Fe with increasing drug dosage. Figure 3.10 shows the different haem species profiles for compound **26**.

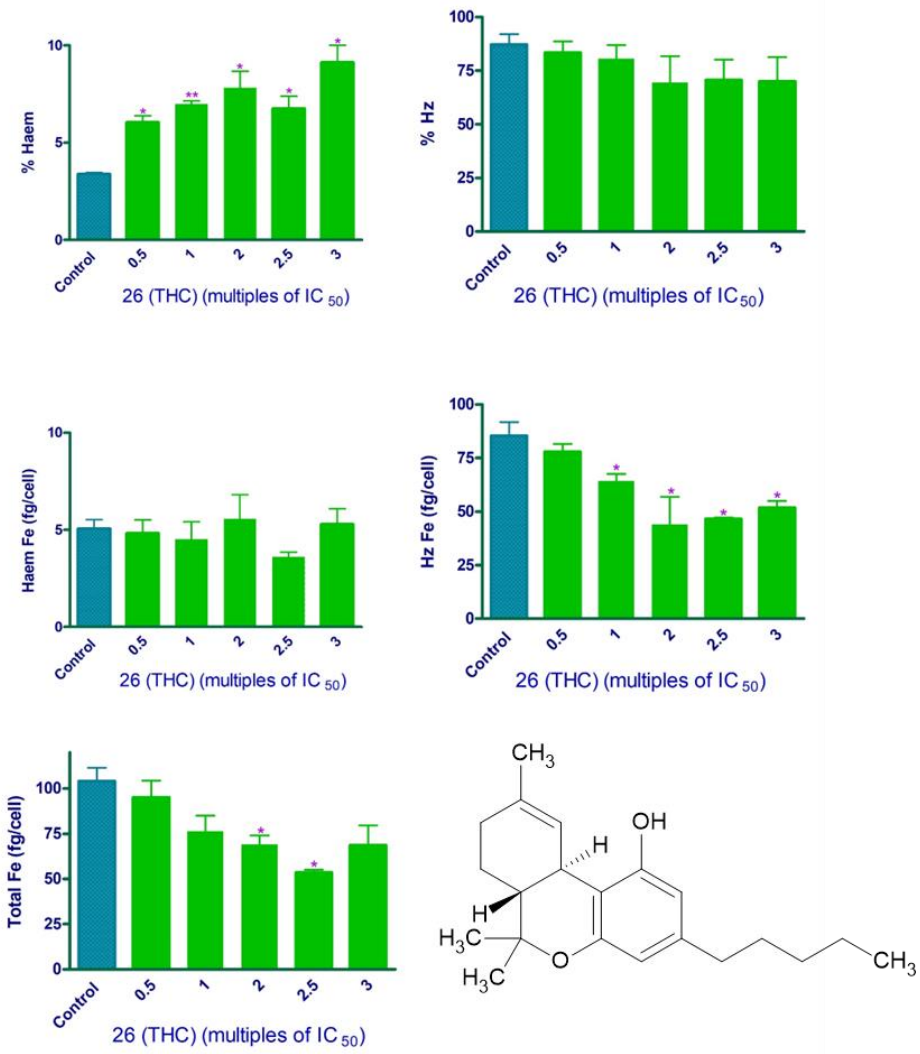

Figure 3.10: The unsequestered haem (haem) and haemozoin (Hz) fractions expressed as percentage abundance (top panels) per well of trophozoites, and in fg/cell for both haem Fe and haemozoin Fe (middle panels). The total Fe (fg/cell; bottom panel) is the sum concentration of all major haem species in an individual trophozoite. This follows from a 32 h incubation of early ring-stage *P. falciparum* parasites with compound **26** (attached structure) at multiples of $IC_{50,}$ and the subsequent isolation of mature trophozoites post-incubation. Control = untreated cells. Statistical significance was calculated relative to the control using the two-tailed t-test at a 95% confidence interval; this is expressed as an asterisk: * $p < 0.05$; ** $p < 0.01$; *** $p < 0.001$. Values represent the mean ± SEM and two repeat experiments were performed.

3.3. Discussion

The cellular mechanistic determination of novel compounds active against *P. falciparum* is an important aspect to drug discovery, especially in the face of emerging resistance to the artemisinins, which still have MoAs that are poorly understood.[216] Such mechanistic determinations may help with the challenges brought about by future threats of resistance. Therefore, using an *in silico* target-based approach to identify novel β-haematin compounds proved useful for target identification in the parasite.[182,190,212] Specific to this study, 39 *in vitro* β-haematin formation inhibiting compounds that were predicted *in silico* using SBVS models, were investigated in three studies for antiplasmodium activity against the NF54 CQS and K1 CQR strains. Furthermore, six of these antiplasmodium active and β-haematin inhibiting compounds were selected to determine their haemozoin formation inhibiting ability in the NF54 CQS strain as a potential MoA.

Sixteen compounds (41% hit) out of 39 showed antiplasmodium activity of less than 10 µM. Four compounds (10% hit) had sub-micromolar activities of 0.26 µM, 0.28 µM, 0.56 µM and 0.79 µM for **16**, **17**, **19** and **26,** respectively. Although these were not superior to the activity shown by CQ (0.015 µM), they still proved to be promising starting points for drug discovery, since three (**16**, **17**, and **19**) of the top-performing compounds were all from the USFDA database and thus were approved for therapeutic use in cancer (**16** and **17**) and familial hypercholesterolemia (**19**).[217–219] Intriguingly, the fourth top-performing compound (**26**) was THC, a known psychoactive constituent of cannabinoids. THC is widely used for various treatments, including as a constituent in dronabinol capsules used for stimulating appetite, and many other applications for specific disease conditions.[215] Perhaps these observations present an exciting prospect for future reconsiderations in repurposing or repositioning these drugs for use in malaria treatment, primarily given the observed minimal possibility of cross-resistance with CQ, as shown by the negligible resistance indices (RI; K1 IC_{50}/ NF54 IC_{50}) when the data from the CQS NF54 and CQR K1 strain is collated. Drug repurposing in drug discovery and development is attractive as a result of its potential to rapidly bring new medicines with known safety profiles to patients.[220,221] Furthermore, unlike in normal development for new molecules, repurposing potentially lowers development costs and shortens timelines, since the pharmacokinetics are already optimised for patients.[221,222] Thus, evaluating the future prospects of currently approved compounds for repurposing as antimalarials may be advantageous or even necessary.

The selectivity of the most active compounds against the *P. falciparum* parasite from each dataset (Tables 3.1–3.3) was good, except for compound **6** (SI = 5), which showed a lower activity margin against the CHO cell line. A selectivity index measures the toxicity of potential

antiplasmodium compounds towards mammalian cells, since less toxic compounds will allow for adequate cell proliferation, whereas highly toxic compounds may lead to reduced mammalian cell survival. Therefore, such a determination indicates a compound's ability to selectively discriminate between the target (*P. falciparum*) and the mammalian cells. Unfortunately, in the case of compound **6**, some of the observed activity may be attributable to its toxicity towards the cells in general. However, it still served as an attractive compound for further mechanistic investigation.

Six of the most biologically active and β-haematin inhibiting compounds from the different datasets (Tables 3.1–3.3) were selected for determination of haemozoin formation inhibiting ability in the NF54 CQS strain towards potential MoA elucidation. This is because, although the β-haematin assay is effective and highly selective in predicting haemozoin formation inhibitors, it is still inconclusive about the exact mechanism in the cell owing to factors such as cell permeability, compound accumulation and the presence of other targets. As previously shown by Vanaerschot *et al.*, both lumefantrine and mefloquine inhibited β-haematin formation *in vitro*, but not intracellular haemozoin formation. This suggested the role of other targets and pathways in the activity of these drugs.[144] Therefore, it is crucial to perform the pyridine-based haem fractionation assay to determine the MoA. Moreover, as explained by both Combrinck *et al.* and de Villiers *et al.*, a true haemozoin inhibitor is defined by a signature increase in unsequestered haem (or exchangeable haem), with a subsequent decrease in haemozoin.[142,144]

In this chapter the pyridine-based haem fractionation method was first used to test CQ, a known haemozoin inhibitor, as a positive control. As shown in Figure 3.4, CQ caused a dose-dependent increase in unsequestered haem and a subsequent decrease in haemozoin. This observed increase in unsequestered haem can be correlated with decreased parasite survival, as reported previously by Combrinck *et al.*[143] The method was then used to assess the haemozoin formation inhibiting ability of compounds **6**, **11**, **16**, **17**, **19** and **26**. Compounds **6** and **26** showed no significant increase in unsequestered haem at increasing compound concentration. This indicated that their MoA in the parasite is likely not *via* haemozoin inhibition. However, it was observed that the haemozoin Fe and total haem Fe decreased with increasing concentration for both these compounds. This phenomenon was previously demonstrated in the case of atovaquone, a known inhibitor of parasite mitochondrial cytochrome complex, which resulted in a decrease in haemozoin, although not even inhibiting β-haematin formation *in vitro*.[143] Therefore, it can be stated that the observed reduction in haemozoin and total haem of compounds **6** and **26** is probably because of an indirect effect, or perhaps even because of reduced Hb uptake by the parasite.

Interestingly, compounds **11**, **16**, **17** and **19** showed a significant dose-dependent increase in unsequestered haem Fe (fg/cell) and a subsequent decrease in haemozoin Fe (fg/cell), indicative of true haemozoin inhibitors, in resembling the action of CQ and other known haemozoin inhibitors.[143,159] It can be concluded that these observed increases in unsequestered haem infer decreased parasite survival with respect to compounds **11**, **16**, **17** and **19**. It is debatable how this increased unsequestered haem kills the parasite. However, earlier work by Chou *et al.* attributed the activity of CQ to a CQ-haem complex that leads to damaged biological membranes.[139] This has been supported by the recent work of Openshaw *et al.* which demonstrated using both electron spectroscopic imaging (ESI) and transmission electron microscopy (TEM) that a haem–inhibitor complex existed in treated parasites – thus allowing for a direct correlation between parasite death and the formed haem–inhibitor complex.[187] Fundamentally, the above observations were rather intriguing, specifically for compounds **16** (lapatinib) and **17** (nilotinib), which are used for cancer treatments and are known tyrosine kinase inhibitors.[217,218] Although tyrosine kinases are absent in the malaria parasite,[223] it was initially presumed that these could potentially have inferred activity on other protein-related kinases available in the parasite. Nevertheless, these results proved the specificity of the compounds for different targets in both diseases, which may prove interesting for future studies.

Compound **19** is used to treat familial hypercholesterolaemia and is known to exert its therapeutic effects in the human liver. However, here it was found to inhibit intraerythrocytic-staged parasite growth with a sub-micromolar IC_{50} of 0.56 µM by inhibiting haemozoin formation in the DV. This suggests that these compounds not only localise but may also accumulate in the parasite DV. Notably, it may prove interesting to determine the DV physiological processes that lead to the accumulation of this haemozoin formation inhibitor. This is in light of the fact that recent evidence by Alder *et al.* suggests that the long-believed phenomenon that a pH trapping mechanism[224,225] leads to substantial increase in the concentration of vacuolar CQ (or other drugs with basic pharmacophores) may be invalid.[226] The authors showed that the loss of the DV proton gradient had only a minor impact on both drug uptake and drug susceptibility. This, however, has no direct implications on our current findings. It is also believed that the results presented may likely prompt future investigations against liver-stage and transmission-stage parasites for **19** to determine its effectiveness against multiple stages of the life-cycle, which can lead to repositioning the drug for malaria. However, since haemozoin formation is the putative primary mode of action, the compound is unlikely to act against stages other than the blood stage where hemozoin formation occurs. Nonetheless, the hemozoin inhibitors presented above could be evaluated for their *in vivo* efficacy and further developed to be used in combination with a compound targeting other

stages. This is idealistic but is based upon the important role that the haemozoin formation pathway plays in the detoxification of unsequestered haem in the malaria parasite. Thus, haemozoin presents as a desirable target for antimalarial development, primarily because it is unique to the parasite.

Unsurprisingly, some of the most effective clinical antimalarials used to fight malaria in endemic regions in the last century are known haemozoin inhibitors, and these include chloroquine, amodiaquine and piperaquine.[108,143,192] Although chloroquine is no longer used for treatment as a result of resistance, it has been unequivocally shown that this resistance is not related to the haemozoin formation pathway.[121] This is also evident for the emerging resistance observed with amodiaquine and piperaquine in Africa and South East Asia, respectively.[105,112,130] This further proves that resistance is compound-specific and not directly associated with haemozoin formation.[116] Ultimately, the observed resistance to amodiaquine and piperaquine will definitely compromise the future use of these drugs in ACT regimens, thus prompting the need for new partner drugs. Since haemozoin remains a viable drug target for novel compounds, the above compounds may serve as critical templates for the development of future lead compounds to replace the current resistance threatened haemozoin-inhibiting clinical antimalarials. This is especially because one of the critical aspects of ACT combinations is the need for the partner drugs to have independent MoAs and molecular targets, while displaying synergistic or additive parasiticidal effects.[227] However, it is accepted that isobolographic analysis and *in vivo* efficacy investigations are still required for all the compounds presented in order to further substantiate their potential development or repositioning.

3.4. Summary and conclusions

Thirty-nine compounds inhibiting β-haematin formation, and previously predicted *in silico* using SBVS models to interact with the crystal, were investigated in this chapter for their antiplasmodium activity. Sixteen (41% hit) had activity below 10 µM. Of these, a total of six which showed nanomolar parasiticidal activity, as well as compounds **6** and **11**, were selected for MoA investigation using the pyridine haem fractionation assay. In addition, the selectivity of seven of the compounds prioritised from each of the different studies was also determined. In general, the compounds showed no significant mammalian cell toxicity and were largely selective towards *P. falciparum*. Moreover, the activity of all the compounds in the CQR (K1) strain was satisfactory, showing minimal to no cross-resistance with CQ.

Of the six compounds investigated for their MoA, four (**11**, **16**, **17** and **19**) inhibited haemozoin formation with the signature increase in unsequestered haem and decrease in haemozoin. This was despite the fact that all six compounds inhibited β-haematin formation *in vitro*, as a

pre-requisite for the haem fractionation assay. This confirms that to identify haemozoin inhibitors, it is inadequate to demonstrate β-haematin inhibition only. This is because the investigated compound may not even have the ability to enter and accumulate in the parasite DV of treated parasites to directly interact with the haemozoin crystal. Therefore, it is crucial to demonstrate inhibition of haemozoin formation in the parasite. It is also of utmost importance to mention that it is still not fully understood how unsequestered haem kills the parasite. Therefore, future studies on this front must be carried out to help improve our understanding. Nevertheless, the *in silico* predictions for β-haematin inhibition will still prove useful for future medicinal chemistry projects, as the aforementioned results in this chapter have successfully demonstrated the use of virtual screening as an effective technique to predict for novel haemozoin inhibitors. Of course, this could also be applicable to predicting other targets in the parasite. Moreover, significant insights were obtained using these techniques, specifically for compounds **6** and **26,** which did not cause any increase in unsequestered haem. Still, they resulted in a decrease in both haemozoin Fe and total haem Fe, which may indicate that the MoA of these compounds occurs upstream in this pathway, perhaps by interfering with Hb trafficking into the parasite or Hb digestion processes.

Lastly, the complicated nature and low throughput of the haem fractionation method hinders the evaluation of more compounds for haemozoin inhibition. This is a particular drawback, since virtual screening produces a substantial number of compounds with promising parasiticidal activity, as demonstrated here. Furthermore, this is exacerbated by the fact that demonstrating only β-haematin inhibition *in vitro* is inadequate to identify true haemozoin inhibitors. Accordingly, there is a need for improved haemozoin assays (or haem quantification assays) which will increase the throughput to accommodate hits from virtual screening techniques. This will be crucial in improving our understanding of the haemozoin detoxification pathway, including the role of lipids and proteins and the inhibition thereof by test compounds.[145] Also, there are various places along the haem detoxification pathway (apart from haemozoin inhibition) that can be inhibited. This will result in changes in haem species and may consequently require improved methods to quantify these changes. For example, a study by Heller *et al.* required an improved analytical technique to quantify haem species in artemisinin-sensitive versus delayed clearance phenotypes of *P. falciparum* parasites. Contrarily, there is also a general need for analytical assays that are readily available for easy application in quantifying haem species in many physiological and pathological scientific settings for diseases such as porphyria and those affecting haem proteins in general.

Finally, it is inevitable that understanding the role of the haemozoin formation process in the parasite and how compounds interfere with this pathway will be important going forward. Furthermore, it remains undeniable that there is potential for future virtual screening methods

that can help medicinal chemists select for better drug discovery candidates, especially in cases where this may aid with target deconvolution of compounds discovered in phenotypic screenings. Accordingly, this current work sought to highlight the potential for MoA determination of prioritised hits via virtual screening against a known target that can be experimentally tested in the laboratory.

Chapter 4: Development of a 96-well HPLC-DAD Assay for Quantification of Intracellular Haem Species in *P. falciparum*

4.1. Introduction

A primary concern in drug discovery is the need for assays that do not currently exist or which have limited access for many researchers.[137] As a result, many drug molecules have poorly understood mechanisms of action (MoAs). The inhibition of the haemozoin formation process in the malaria parasite remains an attractive drug target for developing new antimalarials.[203] This is especially because it is immutable, and several important antimalarials, such as CQ, AQ and the cinchona alkaloids quinine and quinidine, exert their therapeutic effect by disrupting this process, so causing an increase in unsequestered haem which impedes parasite survival.[139,145,211] These directly act by coordinating with the iron centre of Fe(III)PPIX, therefore inhibiting the incorporation of Fe(III)PPIX into crystalline haemozoin.[211]

The pyridine-based method of Combrinck *et al.* is currently used (detailed in Chapter 2) to measure Hb, unsequestered haem and haemozoin concentrations in the malaria parasite, in order to determine if new compounds can be classified as haemozoin inhibitors.[143] This cellular haem fractionation assay measures haem (all solubilised haem species) colourimetrically as a low-spin complex formed between Fe(III)haem and pyridine[143,158], with a 1:2 association[228]. The method, however, is not readily transferable to other laboratories because of the need for specific knowledge in haem chemistry, highly specialised training, and the labour-intensive nature of the assay. Therefore, this highlights the need for new methods to be developed based on techniques readily transferable to the malaria drug discovery community.

This chapter focuses on improving the throughput of the current haem fractionation assay by converting it to a 96-well HPLC-DAD platform. It also reports on the partial development of an LC-MS/MS-based method. These modifications have further improved the assay by eliminating the use of toxic pyridine while also reducing quantities of parasite starting material four-fold and increasing output by four-fold (in the case of the HPLC-UV method). However, only the partial development of the LC-MS/MS method is discussed for technical reasons that are explained further in the following sections. The increased output of the fully developed HPLC-DAD method, which allows for measurement of four compounds per 96-well plate, will help provide an efficient procedure for studying the haem detoxification pathway and help elucidate the mechanism of haemozoin inhibitors (compounds which displayed activity as inhibitors of β-haematin). Moreover, this improved assay will be necessary for determining the haemozoin inhibition MoA and ruling out this MoA when other novel MoAs are sought.

The improved assay is necessary because, as already mentioned, the current method is not only cumbersome but also lacks in throughput which affects the turnaround time for haemozoin MoA investigations. Consequently, the conventional β-haematin inhibition determinations are insufficient to demonstrate the haemozoin MoA, since β-haematin serves as a qualitative extracellular MoA prediction. Therefore, an improved throughput assay will allow for increased intracellular haemozoin MoA quantifications for active compounds that would have been excluded from cellular MoA investigations under the standard fractionation methods, which prioritise only lead compounds. Such advancement in the technique will be important for target validations as it would help enrich the development of more efficient machine learning models used for the predictive virtual screening campaigns of finding β-haematin inhibiting compounds.

Inevitably, all three haem species, Hb, haem and haemozoin, exist independently in the parasite DV (most probably also in transport vesicles) in different proportions at any time during the parasite life cycle. This haem fractionation assay will selectively separate each species using organic solvents compatible with use in HPLC instrumentations.

4.2. Method development

4.2.1. LC-MS/MS haem detection

The current pyridine-based assay consumes considerable parasite material to ascertain reliable sensitivity and selectivity for spectrophotometric detection. This led to the decision to investigate the option to develop a sensitive and selective LC-MS/MS assay to improve throughput.

Infusions of the analyte haematin (dissolved in acetonitrile:water), were performed on an AB Sciex API 3200 mass spectrometer using a Hamilton syringe pump at a flow rate of 10 µL/minute to obtain precursor and product ion spectra in the positive ionisation mode. The product ion scan of haematin (Figure 4.1) showed a molecular peak $[M+H]^+$ at a mass-to-charge ratio (m/z) of 616.8, similar to the results previously observed by Heller *et al.*[53] The observed fragmentation pattern of the parent ions is shown in Figure 4.2, where a predicted cleavage of the first propionate group resulted in product ions at 558.0 and the cleavage of the second propionate group resulted in product ions at 499.0. The minor peaks at 483.4 and m/z 452.8 correspond to the predicted further loss of a single methyl group (CH_3), and three methyl groups, respectively.

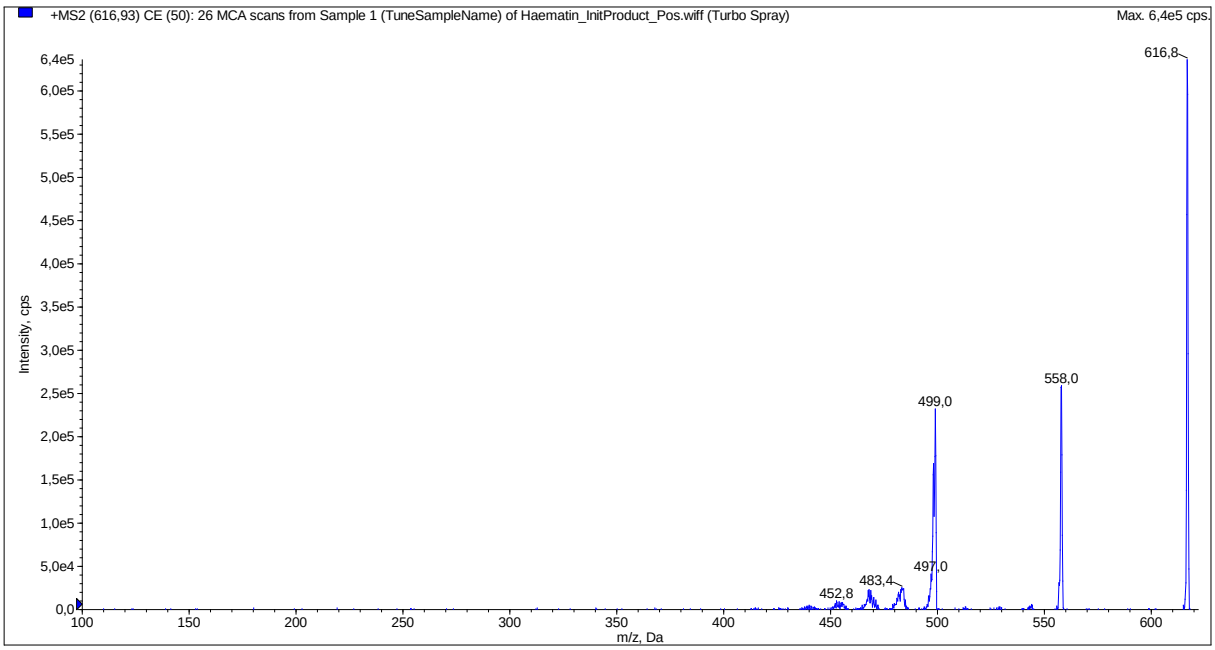

Figure 4.1: Product ion mass spectra of haematin dissolved in a mixture of acetonitrile and water (1:1 v/v) with 0.1% formic acid (FA). The molecular ion peak of haematin is at 616.8 and propionate fragmentation peaks are at m/z 558.0 and 499.0.

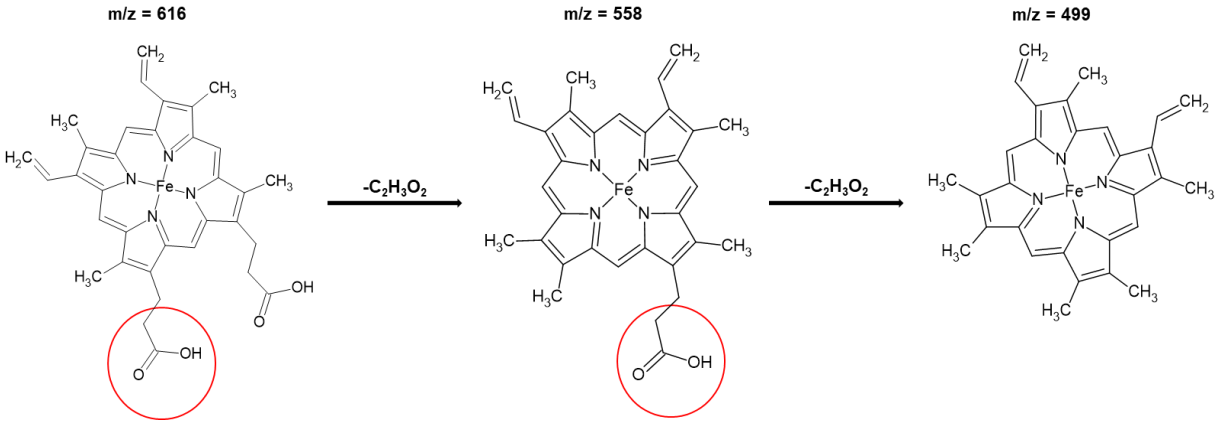

Figure 4.2: Fragmentation pattern of haematin, showing the step-wise loss of the -$C_2H_3O_2$ ethanoic fragments (circled in red).

Multiple reaction monitoring was used to monitor the two transitions from 616.8 to 558 and 499. Haematin was dissolved in a mixture of acetonitrile and water (1:1 v/v) with 0.1% FA and was infused at a concentration of 1000 ng/mL at a flow rate of 10 µL/min. Electrospray ionisation in the positive ionisation mode was used. The optimised mass spectrometer parameters were: Curtain gas, 10; Electrospray voltage, 5500 V; Temperature, 450°C; Gas 1 and Gas 2, both at 30 psi; Collision-activated dissociation (CAD), 5 psi; Declustering potential, 100 V; Entrance Potential, 12 V; Collision energy, 85 eV; and Cell exit potential, 36 V.

An HPLC system with an Agilent 1100 LC binary pump, Agilent 1200 series autosampler and Agilent 1200 series analytical column compartment was used for chromatographic analysis. A C18 reversed-phase Hydro-RP (Phenomenex) analytical column was selected with the following specifications: 2.5 µm, 100 Å, 50 mm x 2 mm. An aqueous mobile phase of 0.1% FA in water (Mobile phase A) and an organic mobile phase of 0.1% FA in acetonitrile (Mobile phae B) were pumped at a flow rate of 300 µL/min. As shown in Table 4.1, gradient elution was used to separate the expected common phospholipids and membrane residues in the haemoglobin fraction, which have the potential to cause ion suppression or enhancement. The analyte retains at 3.1 minutes, as depicted by two extracted ions with m/z 558 (blue) and 499 (red), as illustrated in Figure 4.3.

Haem extracts from parasite material were obtained using various optimised fractionation solvents. The chromatograms in Figures 4.4 and 4.5 represent the unsequestered haem fraction corresponding to m/z 558 and 499. The Hb and haemozoin fraction injections were not performed because of previously described concerns relating to the ability of these samples to contaminate the instrument. Further purification steps were required for these fractions. However, the project was halted because of major contamination that impaired the instrument. Furthermore, the use of sodium hydroxide to solubilise haemozoin was another contamination risk.

Table 4.1: Gradient method.

Time (min)	Mobile phase A (%)	Mobile phase B (%)
0.00	75	25
0.25	75	25
1.00	5	95
2.50	5	95
2.75	75	25
5.00	75	25

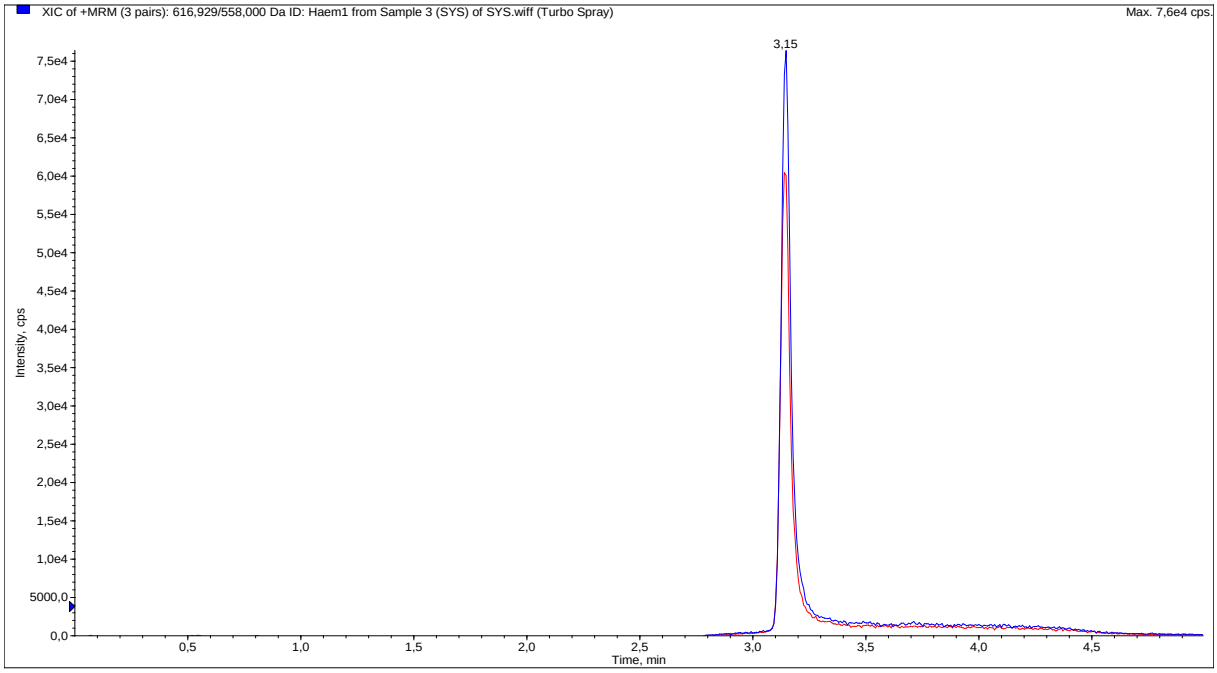

Figure 4.3: A chromatogram of haematin using gradient elution, representative of two MRM transitions from m/z 616.8 to to 558 (blue) and 499 (red) at 1000 ng/mL.

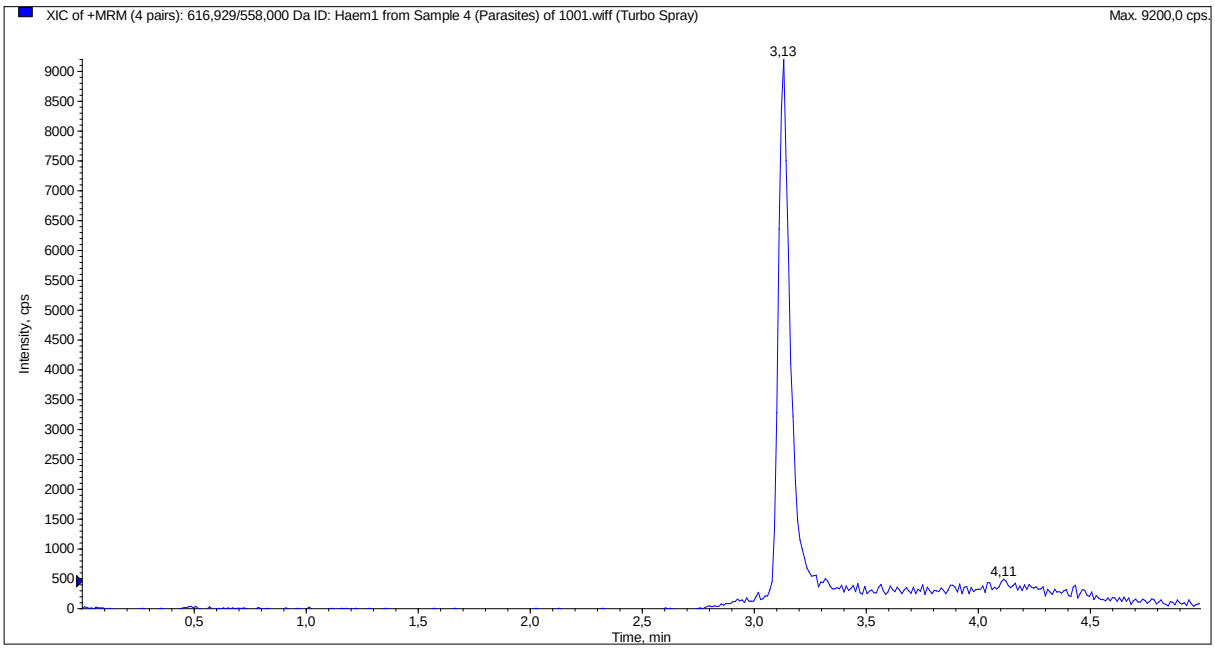

Figure 4.4: Chromatographic representation of extracted parasite haem (most abundant product ion; m/z 558).

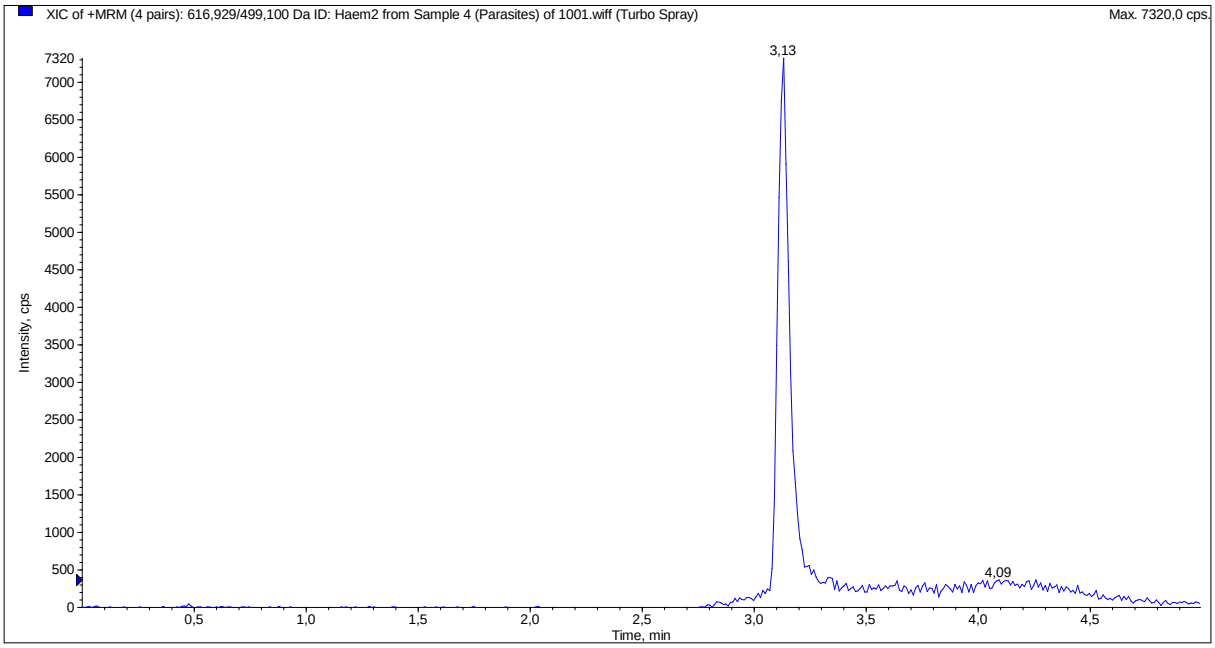

Figure 4.5: A chromatogram of extracted parasite haem (less abundant product ion; m/z 499).

4.2.2. HPLC-DAD method development for quantification of haem species

Considering the challenges experienced with mass spectrometry detection, HPLC-DAD analysis was preferred. It is expected that HPLC-UV systems are more commonly available to the malaria drug discovery communities than LC-MS/MS systems. Therefore, it presents as a more suitable analytical technique for easy transfer to other laboratories. Fortunately, preliminary experiments showed that the sensitivity and selectivity of the detection method would be adequate for the selected sample volume. However, as previously reported, quantifying haem colourimetrically in aqueous conditions is very challenging.[228] This is because haem tends to undergo aggregation, making it impossible to selectively quantify it as a monomeric species. Therefore, complexation of haem to keep it in its monomeric form is important, although this had to be done without using pyridine.[143,158]

4.2.2.1. Haem ligand titrations

The currently used cellular haem fractionation and β-haematin assays measure Fe(III)haem and aqueous pyridine as a low-spin complex.[143,158] However, given the toxicity associated with pyridine, imidazole was considered a viable non-volatile substitute. Imidazole was also previously shown by Kuter *et al.* to form a low-spin complex with haem, with a relatively similar association as pyridine.[228] It was then sought to establish optimal reaction conditions that were to result in the formation of a Fe(III)haem-(bis)Imidazole low-spin complex, by performing various titrations of haem with imidazole. It was important to form a monomeric haem species, given that haem aggregates under aqueous conditions.

Considering the previous findings on the sensitivity of low-spin haem complexes to pH, various titrations with 4-(2-hydroxyethyl)-1-piperazineethanesulfonic acid (HEPES) were performed for optimal complex formation.[158] Figures 4.6 and 4.7 illustrate the UV-Vis spectra obtained from these titrations for Fe(III)haem-(bis)Imidazole and Fe(III)haem-HEPES, respectively. The maximum absorbance of the Fe(III)haem-(bis)imidazole complex was observed at 410 nm. Further confirmation of the Fe(III)haem-(bis)imidazole low-spin complex was supported by the observation of the Q and charge transfer bands in the region between 500 nm and 600 nm, respectively, which indicate the formation of a low-spin haem complex.

The molar extinction coefficient was then calculated using the final optimised conditions determined during titrations at 5 µg/mL haematin. An approximate value of 112258 $M^{-1}cm^{-1}$ was determined. This was higher than the 90800 $M^{-1}cm^{-1}$ value reported with a pyridine ligand by Asakura *et al*.[229] This can be expected, given the differences in haem–ligand binding (Fe(III)haem-(bis)imidazole vs Fe(III)haem-(bis)pyridine), which resulted in a shift in the maxima absorbance wavelength from 405 nm with pyridine to 410 nm with imidazole. It is noteworthy that under these experimental conditions, the determined value was similar to the 109000 $M^{-1}cm^{-1}$ value reported by Erman *et al.* for binding recombinant forms of cytochrome c peroxidase (rCcP) and imidazole.[230] Furthermore, the binding of imidazole to various haem proteins had previously been reported to be more intricate than other ligands due to the ability of imidazole to exist in three different forms in solutions.[230]

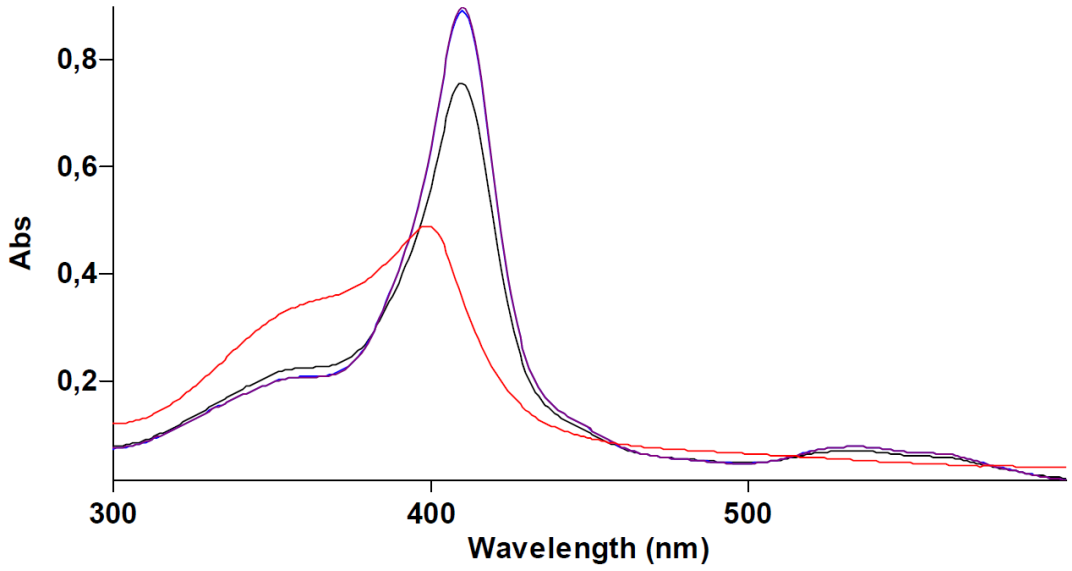

Figure 4.6: Fe(III)haem-(bis)imidazole titrations to establish the optimal formation of a stable low-spin complex. The concentration of haematin was 5 µg/mL, and that of HEPES was kept constant at 50 mM across all experiments. The concentrations of imidazole were varied accordingly: 0 mM (red); 5 mM (green); 30 mM (blue); 50 mM (purple).

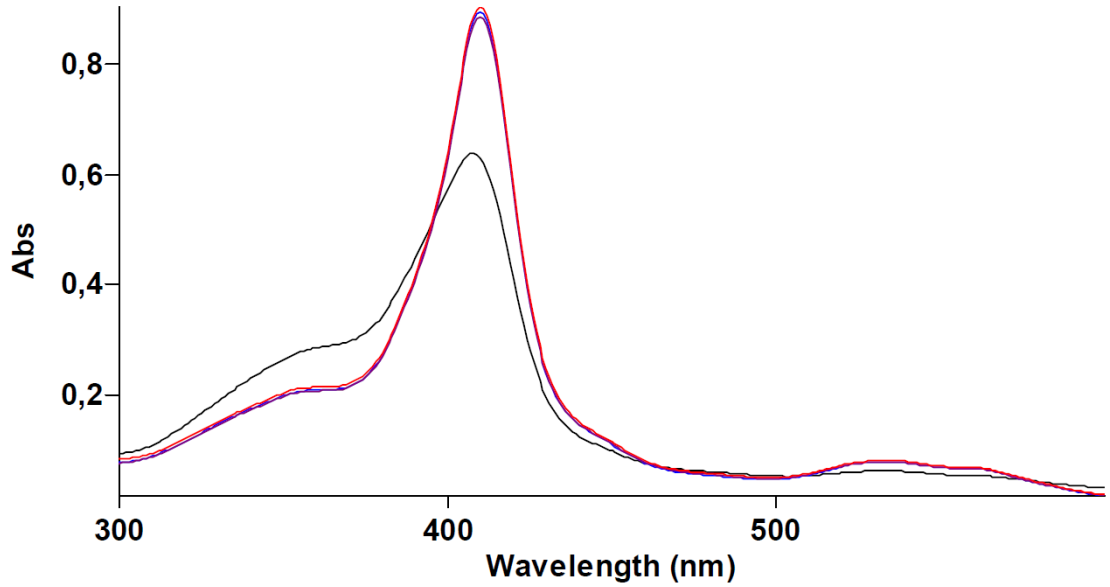

Figure 4.7: Spectroscopic titrations of HEPES buffer for the formation of a stable Fe(III)haem-(bis)imidazole low-spin complex. The concentration of haematin was 5 µg/mL, and that of imidazole was kept constant at 50 mM across all experiments. The concentrations of HEPES were varied as follows: 5 mM (green); 25 mM (blue); 50 mM (purple); 100 mM (red).

Lastly, a 2 mL pellet from a trophozoite parasite culture at 5% parasitemia was harvested and fractionated to recover the haemozoin fraction (as discussed later in this chapter). The haemozoin pellet was then solubilised to form a Fe(III)haem-(bis)imidazole complex (Figure 4.8). This was done to determine similarities to the Fe(III)haem-(bis)imidazole complex formed using haematin, especially the confirmation of the soret band, which was found to be the same at 410 nm. As a result, the final reaction concentrations of 30 mM and 50 mM for imidazole and HEPES, respectively, were selected based on the optimised experimental conditions.

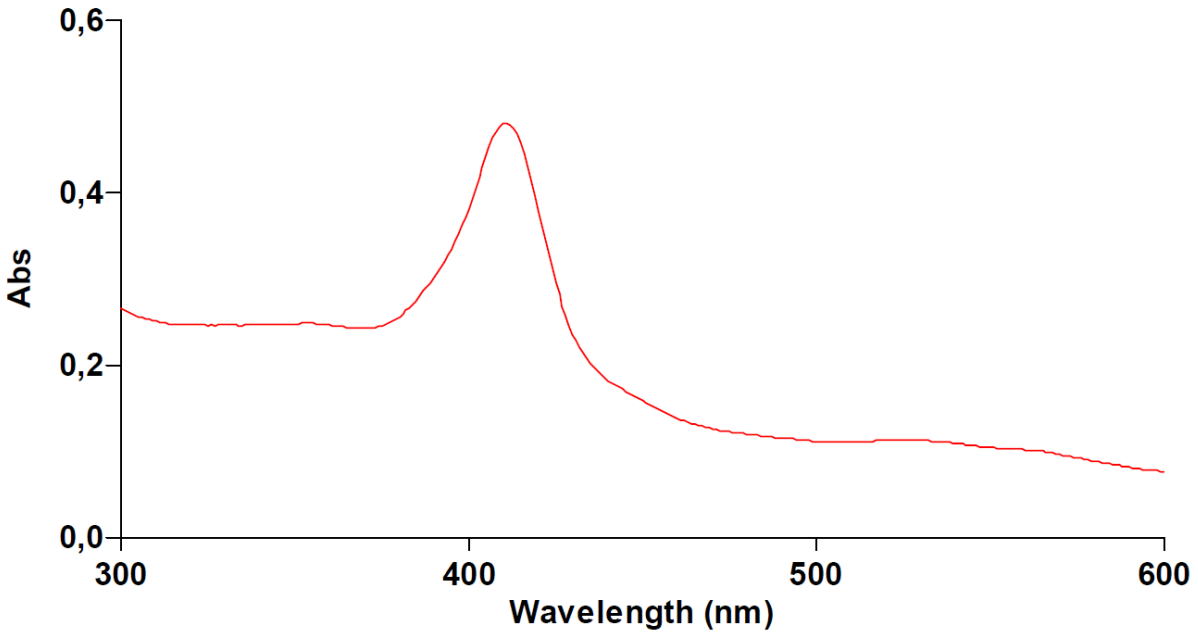

Figure 4.8: Solubilisation of isolated parasite haemozoin to form a stable low-spin Fe(III)haem-(bis)imidazole complex, with maximum wavelength observed at 410 nm. HEPES and imidazole concentrations used were 50 mM and 30 mM, respectively.

4.2.2.2. Fe(III)haem-(bis)imidazole chromatographic development

An HPLC-DAD system with an Agilent 1100 LC binary pump, Agilent 1200 series autosampler, Agilent 1200 series analytical column compartment, and Agilent 1290 infinity diode array detector was used for the chromatographic development and detection of monomeric Fe(III)haem-(bis)imidazole. A C18 reversed-phase analytical column was selected, with similar specifications – as mentioned above for the LC-MS/MS method. A pre-column packed with C18 silica material was used to protect the analytical column, and was freshly packed before injecting each analytical batch. An aqueous mobile phase composition of 30 mM imidazole, 50 mM HEPES and 5% dimethyl sulfoxide (DMSO) in water, and an organic mobile phase spiked with 30 mM imidazole, 50 mM HEPES and 5% DMSO in methanol (MeOH) and acetonitrile (15:5:40:40 (v/v) was pumped at a flow rate of 350 µL/min. Buffers were dissolved in a small volume of water and filtered through 0.22 µm MILLEX® filters using a syringe before being added to either of the mobile phases. The aqueous mobile phase was adjusted to pH 7.5 using a 5 M NaOH solution.

Gradient elution with a six-minute run time was used, with the wavelength of detection set at 410 nm. A reference wavelength of 485 nm was used to correct any baseline drift during the gradient elution. A 20-second needle rinse comprising methanol:2-propanol:H_2O:DMSO (50:30:15:5; v/v) between each sample was performed to reduce any carryover, since Fe(III)PPIX is known to adsorb to surfaces and accumulate. The column compartment temperature was set at 30°C. Thus, the subsequently observed chromatograms were obtained

using the final optimised HPLC-DAD conditions described in Table 4.2. The analyte was found to retain at 3.4 to 3.5 min, as depicted by the Fe(III)-(bis)imidazole chromatogram shown in Figure 4.9.

Table 4.2: Gradient and detection parameters of the HPLC-DAD method (aqueous mobile phase (%A) and an organic mobile phase (%B)).

Time (min)	Mobile phase (%A)	Mobile phase (%B)	Detection parameters
0.00	45	55	Wavelength: 410 nm
0.25	45	55	Ref wavelength: 485 nm
0.75	5	95	Mobile phase A: pH 7.5
2.50	5	95	Analytical column temp: 30°C
3.00	45	55	Flow rate: 350 µL/min
6.00	45	55	Injection volume: 10 µL

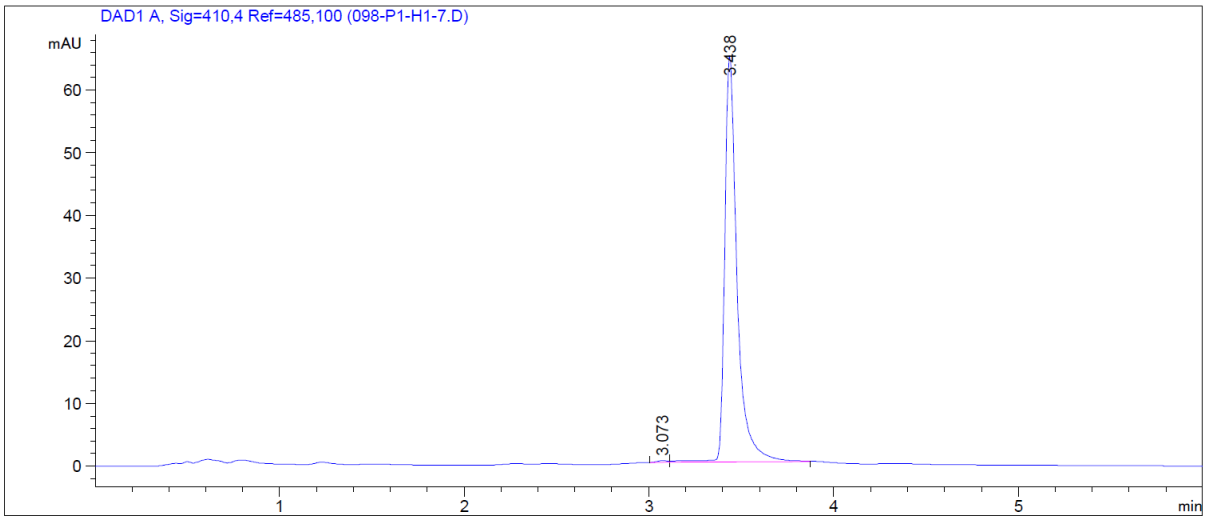

Figure 4.9: A chromatographic representation of a haem–imidazole low-spin complex at 1000 ng/mL haematin with an absorbance wavelength of 410 nm and reference wavelength of 485 nm. The retention time was at 3.4 minutes.

4.2.2.3. Extraction of haem fractions from *P. falciparum*

As mentioned above, all three haem species – Hb, haem and haemozoin – coexist in the parasite in different proportions during the parasite's intraerythrocytic life cycle. Therefore, various organic solvents were chosen to achieve selective species separation and its HPLC compatibility.

Trophozoite cell harvesting (or recovery of trophozoite cells):

This fractionation assay procedure was adapted from the method of Combrinck *et al.*, but with significant changes.[143] Mature trophozoite-stage synchronous parasite culture at 5%

parasitemia and 2% RBC haematocrit was prepared (49 mL medium + 1 mL pellet) in complete medium. Five hundred microlitres of parasite culture aliquots were added to each well of a 96-deep-well round bottom plate. No test compounds were added; thus, the parasite cells serve as controls.

The plate was then centrifuged at 650 ×g for 15 minutes to allow for the cells to settle. After centrifugation, the excess culture medium was carefully aspirated without disturbing the layer of cells on the bottom of the plate. After that, the parasite pellet from each well was resuspended by adding 450 µL of phosphate-buffered saline (PBS) at pH 7.4 and, subsequently, RBCs were lysed to harvest trophozoites. Cell lysis was performed by saponin lysis by adding 50 µL of a 1% (w/v) saponin solution into the wells. Plates were incubated for 2 minutes at room temperature and were then centrifuged at 650 ×g for 15 min. The supernatant was then carefully removed, and the pellet was washed three times with 500 µL PBS (spinning in-between at 650 g for 15 min) to remove any traces of leftover Hb contributed by the lysed RBCs. A hundred microlitres of PBS was added to the washed pellet and the cell lysate transferred to a 500 µL round bottom 96-well plate and stored at -80°C, until the day of the trophozoite cell lysis.

Cellular haem fractionation procedure:

Notably, the prior freezing and thawing of the trophozoite pellet aids with DV membrane lysing and results in the release of the parasite intracellular Hb, haem and haemozoin through hypotonic cell lysis. Therefore, on the day of performing the fractionation procedure, the plate was removed from the freezer and was thawed to recover the haem fractions as follows:

Specific to the Hb fraction (Fraction 1 in Figure 4.10), 25 µL of deionised H_2O was added to help lyse any remnant intact cells (those not lysed during freeze/thaw) and, importantly, to solubilise the intracellular Hb. Thereafter, the plate was sonicated for 5 minutes, and then 15 µL HEPES (1 M at pH 7.5) was added. The plate was centrifuged at 2250 ×g for 20 minutes. Then, without disturbing the pellet, the resultant supernatant containing soluble Hb was transferred into a new 96-well plate. Haem and haemozoin are insoluble in an aqueous medium and were retained in the pellet. To the Hb supernatant, each of the following solvents and solutions was added: 25 µL methanol:acetonitrile (30:70, v/v), 14 µL DMSO:tert-butanol (4:1, v/v), 25 µL 0.3 M NaCl, and 6 µL 1 M imidazole – giving a final in-well volume of 200 µL. This Hb fraction is essential for quantifying any Hb species in the parasite, which were previously derived from the red blood cells (RBC) and not yet digested. Notably, the addition of methanol and acetonitrile solvents was to help degrade any residual haem proteins in the samples. In the pyridine-based method, this was performed using sodium dodecyl sulfate (SDS).

To the remaining pellet, selective solubilisation of the haem fraction (Fraction 2 in Figure 4.10) was performed. This follows from an earlier report that pyridine dissolves haem to form a low-spin complex, while the haemozoin remains can be isolated.[158] However, in this study, pyridine has been replaced with imidazole to achieve the solubilisation of haem from haemozoin. Here, 25 µL each of H_2O (deionised), methanol:acetonitrile(30:70, v/v) and DMSO:tert-butanol (4:1, v/v) were added to form aqueous DMSO to help with solubilising haem, since some of the haem from the parasite may be charged. The plate was sonicated for 10 min and then incubated for 20 min at room temperature. Thereafter, each of the following solvents and solutions was added: 15 µL HEPES (1 M at pH 7.5), 25 µL NaCl (0.3 M), and 6 µL imidazole (1 M). After that, the contents of each well were resuspended, and the plate was centrifuged at 2250 ×g for 20 minutes. The supernatant (containing haem; 121 µL) was transferred to a separate 96-well plate. To this, 79 µL of injection solvent was added to a final in-well volume of 200 µL, and the plate was stored at -20°C until required for analysis. The injection solvent referred from here onwards constitutes an equal composition (1:1; mobile phase A: mobile phase B) of the mobile phase solvents without the buffers (HEPES and imidazole). Importantly, this fraction will quantify any unsequestered haem that was not converted to haemozoin.

To the remaining pellet containing haemozoin only (Fraction 3 in Figure 4.10), 50 µL of H_2O and 0.3 M NaOH were added, respectively. As mentioned previously, haemozoin is an inert biocrystal that is highly insoluble except in the presence of a strong base. Therefore, each well was resuspended in the aqueous base, the plate sonicated for 15 minutes and then incubated for 15 minutes at room temperature to help solubilise haemozoin. After incubation, each of the following solvents and solutions was added: 25 µL of 0.3 M HCl, 15 µL HEPES (1 M at pH 7.5), 25 µL DMSO:tert-butanol (4:1, v/v), 25 µL methanol:acetonitrile (30:70, v/v), 6 µL imidazole (1 M), and 54 µL injection solvent to a final in-well volume of 200 µL. Subsequently, a 1:4 dilution of the haemozoin fraction was performed using the injection solvent, and the final diluted plate was stored at -20°C until required for analysis. The haemozoin fraction will quantify any of the sequestered haem resulting from Hb degradation.

Lastly, all the plates containing the various fractions (Hb, haem and diluted-haemozoin) were analysed using the HPLC method described above. Figure 4.10 illustrates the flow chart for the fractionation procedure. Further analysis of samples is discussed in Chapter 5. However, on the day of analysis, before each haem fractionation batch was analysed, five injections of a reference standard (1000 ng/mL haem-(bis)imidazole) were run to equilibrate the instrument.

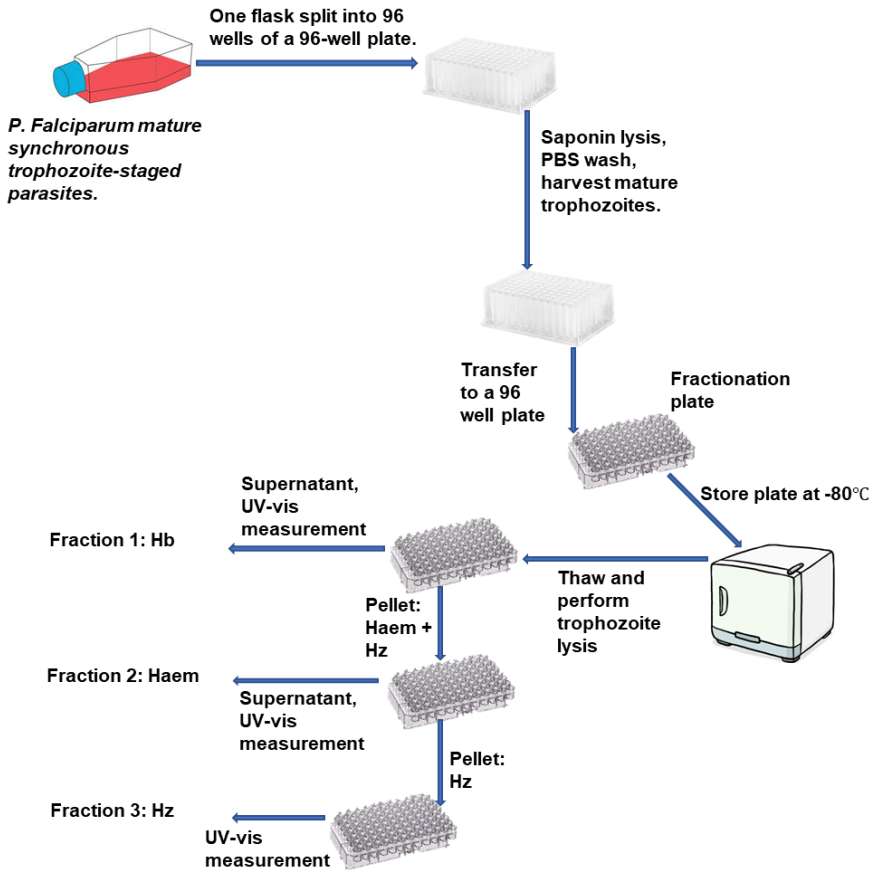

Figure 4.10: A flow chart illustrating the haem fractionation procedure for the selective recovery of all the major haem species of *P. falciparum*.

Following the successful optimisation of the extraction procedure, parasite cellular haem extracts (Hb, haem and haemozoin) were obtained for HPLC analysis. Separate injections of these fractions resulted in similar chromatograms to those of haematin (Figure 4.9), as expected (Figures 4.11–4.13). There was no observed significant shift in the retention times of all the fractions as initially presumed, because of the different natures of their matrices. This was significant since it was experimentally implausible to prepare the fractions uniformly. This is especially the case given that the formation of a haem complex in aqueous matrices is problematic and any slight changes to the matrix composition may infer changes in absorbance wavelengths, so leading to variations in the absorbance spectrum. These fractionation results were used to inform the decision-making process in choosing the calibration range. Moreover, exploratory experiments were further performed to establish the lowest limit of quantification (LLOQ). A concentration of 1 ng/mL was chosen, as the peak was clearly distinguishable from the baseline and the signal-to-noise ratio was determined to be approximately five. Figure 4.14 shows both chromatograms of the blank (solvents only) and the LLOQ.

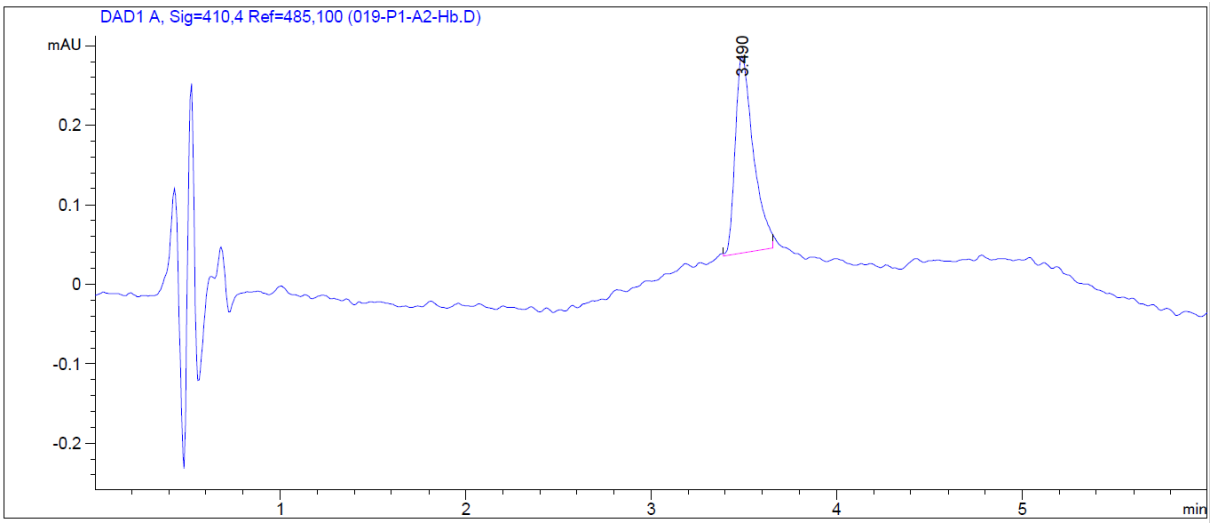

Figure 4.11: Representative chromatogram of a low-spin complex of extracted cellular parasite haemoglobin (as haem Fe). Maximum absorbance observed at 410 nm (Ref wavelength = 485 nm).

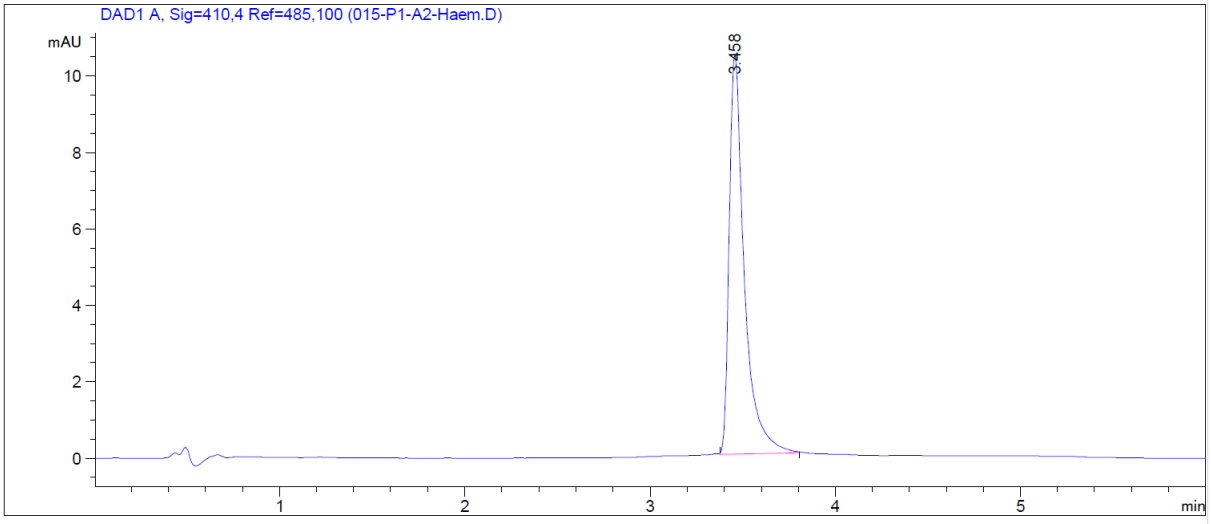

Figure 4.12: Representative chromatogram showing a low-spin complex of extracted cellular parasite haem. Maximum absorbance at 410 nm (Ref wavelength = 485 nm) and 3.5 min retention time.

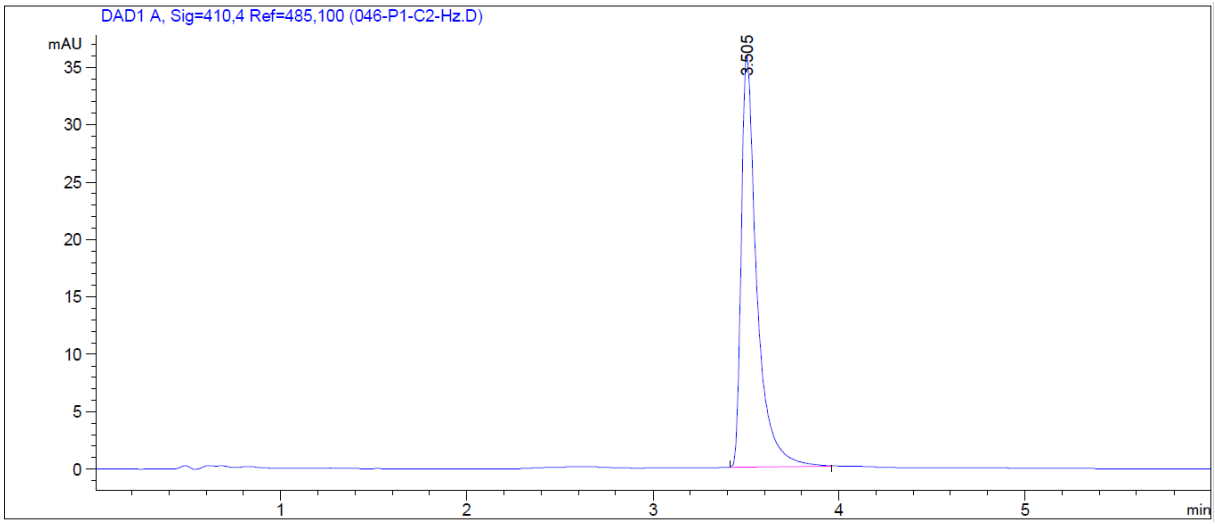

Figure 4.13: Chromatographic representation of a low-spin complex of extracted cellular parasite haemozoin (4-fold dilution), which was solubilised using NaOH and neutralised using HCl. Maximum absorbance at 410 nm (Ref wavelength = 485 nm) and 3.5 min retention time.

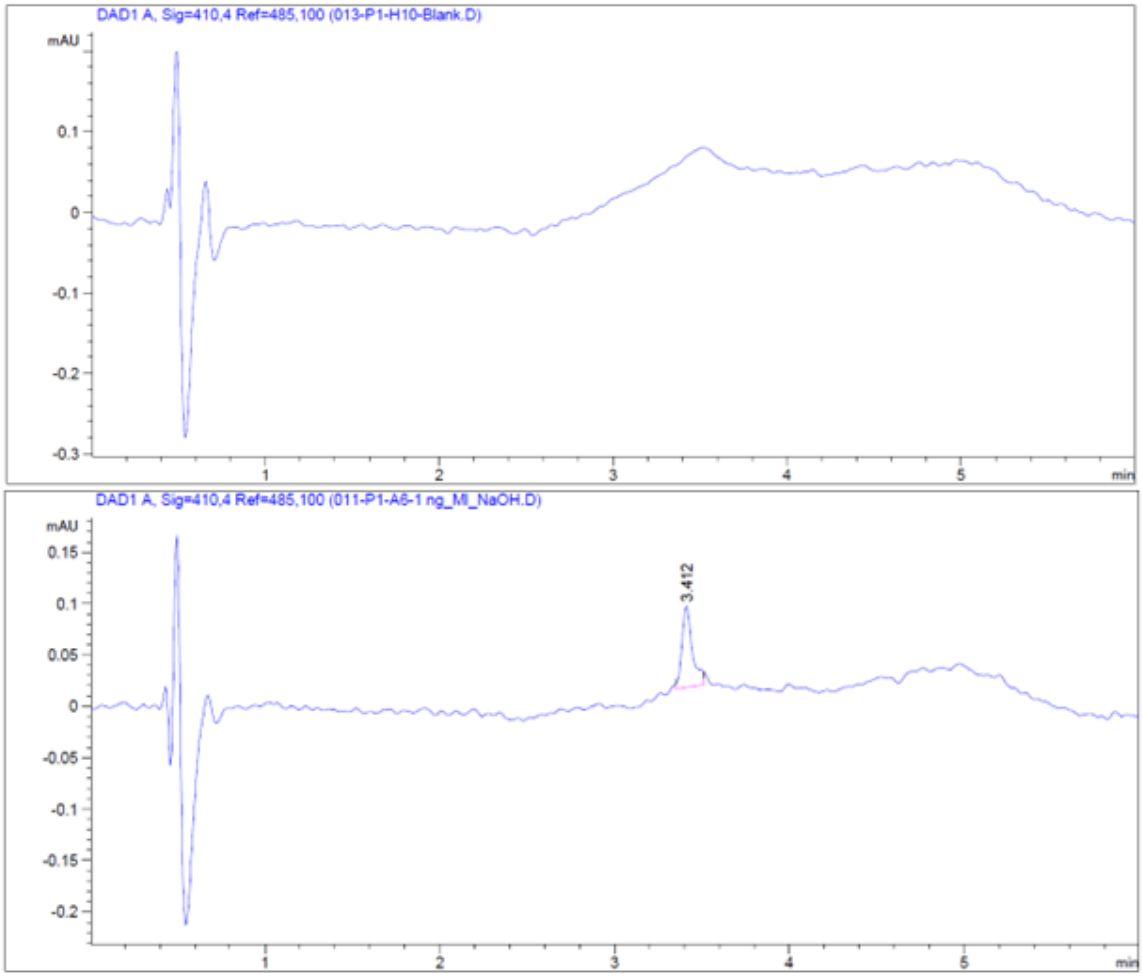

Figure 4.14: Chromatograms of the blank (0 ng/mL haem; top) and the lowest level of quantification (1 ng/mL; bottom).

4.2.2.4. Robustness and selectivity of the extraction procedure for fractionation of haem species

Based on the nature of the assay's fractionation procedure, it was crucial to address the question of the robustness and selectivity of the assay for the different haem species. This was to ascertain whether the fractionation steps can selectively allow for the separation of each haem component. This is because the robust selectivity will confer the specificity of the fractionation procedure in quantifying each haem fraction with high certainty. Therefore, demonstrating no significant cross-contamination between the haem fractionation steps was critical. These assessments were previously discussed in detail by Combrinck *et al.* in the multi-well colourimetric pyridine-based assay.[143]

Specifically, the focus here was on two sources in the fractionation steps that may pose significant cross-contamination. These were contamination of the Hb fraction (intracellular Hb) by host Hb (extracellular Hb) after RBC saponin lysis of trophozoites and the contamination of the haem (unsequestered) fraction by the possible breakdown of haemozoin during sonication in the presence of the organic solvents. Given that the culturing and sample preparation techniques are similar to those previously reported, the investigation on the cross-contamination by haemozoin after synchronisation of the ring-culture was excluded.[143]

Contamination by host RBC after saponin lysis:

The host Hb fraction (RBC Hb) is the majority source of haem in the total culture, therefore presenting as a potential source of cross-contamination.[143] To investigate if the PBS washing steps were efficient in removing the extracellular Hb in the harvesting of trophozoites during saponin lysis, the following procedure was performed: a 20 µL pRBC pellet at 5% parasitemia was spiked with 30 µL of RBC up to 500 µL in PBS (2.5 x the normal haematocrit). The mixture was then subjected to the usual fractionation procedure described above (Figure 4.10 as reference illustration). Figure 4.15a shows no significant change between the standard control (at 2% haematocrit) and the spiked samples, therefore demonstrating that like the previous results cross-contamination by extracellular Hb was negligible – provided the washing procedure is followed.[143]

Contamination of unsequestered haem by the breakdown of haemozoin:

For the cross-contamination of unsequestered haem by the breakdown of haemozoin, the following procedure for isolating mature trophozoites was performed: mature synchronous parasite culture was prepared in CM at 5% parasitemia and 2% haematocrit. The cells were harvested as described above (Figure 4.10), with no deviation. Two separate pellets were obtained for analysis from 500 µL aliquots of the prepared culture. The first pellet was a

mixture of haem and hemozoin and the second pellet was isolated haemozoin. The pellet containing unsequestered haem and haemozoin was then spiked with the isolated haemozoin pellet before the addition of solvents and ultrasound treatment. The isolated haemozoin was obtained from a control sample prepared as described for the haem fractionation procedure but before any NaOH solubilisation. This resulted in a two-fold increase in haemozoin in the experimental samples described in these specific experiments. As shown in Figure 4.15b for haem, the spiked samples showed no significant difference relative to the non-spiked controls. This confirmed that, using the current solvents, the haemozoin fraction does not cross-contaminate (breakdown to haem) the unsequestered haem fraction. These findings are similar to those previously reported by Combrinck *et al.*[143]

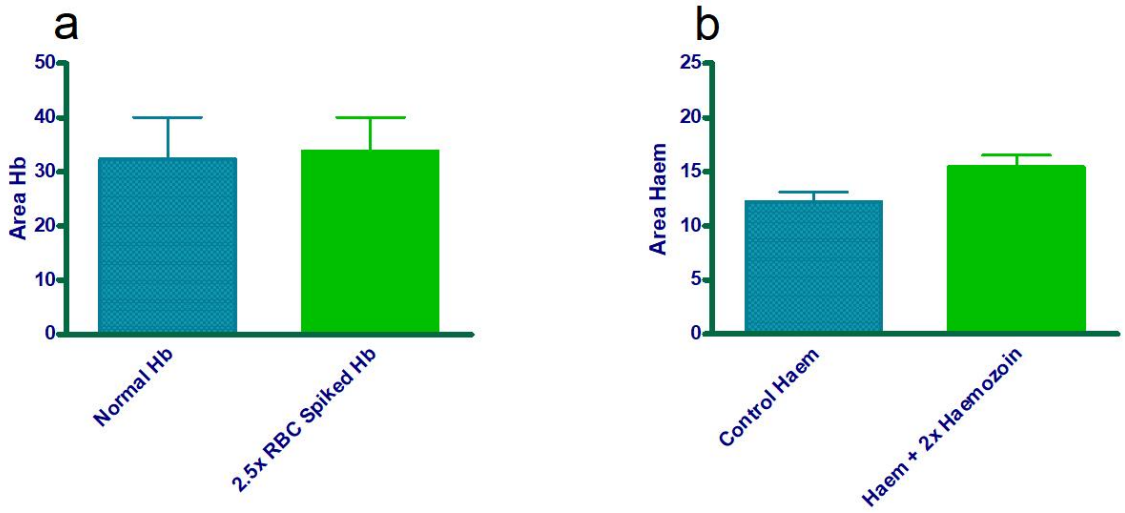

Figure 4.15: The cross-contamination experiments for (a) Hb fraction of sample spiked with 2.5-fold RBCs (5% haematocrit) compared to control of 20 µL of 5% pRBCs (2% haematocrit), and (b) haem fraction spiked with a two-fold haemozoin pellet. The plots represent the average areas of the chromatograms (n = 5). The statistical values were determined using GraphPad Prism software using an unpaired 2-tailed t-test at 95% CI analysis. For Hb analysis (a): P-value = 0.88. For haem analysis: P-value = 0.08. A *P*-value greater than 0.05 represents no significant differences in the means.

4.2.3. Calibration standards

4.2.3.1. Preparation of calibration standards

The calibration curve range was established using theoretical estimations based on the observed haem species' concentrations from the pyridine assay, and the exploratory parasite experiments described above. Eight different calibration concentrations of haematin-(bis)imidazole complex ranging between 1 and 2500 ng/mL were selected. Critically, the highest calibration concentration was chosen on the basis that a four-fold dilution of the haemozoin fraction, which contains the most haem when solubilised, would fit within the calibration range.

In preparing the calibration standards, the following haematin concentrations were selected: 1 ng/mL, 15 ng/mL, 30 ng/mL, 50 ng/mL, 100 ng/mL, 500 ng/mL, 1000 ng/mL and 2500 ng/mL. Briefly, the two highest calibration concentrations (1000 and 2500 ng/mL) were prepared using a 20000 ng/mL standard solution of haematin dissolved in 0.3 M NaOH, and the six remaining lower calibration standards were prepared from a 1000 ng/mL working solution diluted (dilution of the 20000 ng/mL standard solution of haematin) in a solution matrix on the day. The solution matrix used for preparing the 1000 ng/mL working solution was similar to the matrix used for preparing the standards, but without the presence of imidazole. All the standards were prepared by spiking the 20000 ng/mL or 1000 ng/mL standard solutions into a volume of a blank solution matrix for each respective standard in 10 mL conical bottom centrifuge tubes up to a total volume of 5 mL. Specifically, each standard was prepared using different volumes of the following solvents and solutions to give the final solution matrix composition: 1 M HEPES, pH 7.5, 1 M imidazole, MeOH:ACN (30:70, v/v), 0.3 M NaCl, DMSO:tert-butanol (4:1, v/v), and injection solvent. No serial dilutions were performed in preparing the calibration standards. Therefore, the complexation reaction of haematin with imidazole for each standard happened independently. This was to mimic the exact complexation reaction conditions occurring in each extracted sample of Hb, haem and haemozoin. All standards were prepared in duplicate. The details for each calibration standard are shown in Table 4.3.

Table 4.3: Preparation of individual haematin-(bis)imidazole calibration standards in selected solvents or reagents.

	Volumes of solvent or solution used at each concentration of haem (µL)							
Solvent/ Reagent	**1 ng/mL**	**15 ng/mL**	**30 ng/mL**	**50 ng/mL**	**100 ng/mL**	**500 ng/mL**	**1000 ng/mL**	**2500 ng/mL**
Water	995	925	850	750	500	0	997	994
MeOH:ACN	625	625	625	625	625	625	625	625
NaCl (0.3M)	625	625	625	625	625	625	625	625
DMSO:But	625	625	625	625	625	625	625	625
Injection solvent	1725	1725	1725	1725	1725	225	1725	1725
HEPES (1M)	250	250	250	250	250	250	250	250
Imidazole (1M)	150	150	150	150	150	150	150	150
Haematin stock[b]	5[a]	75[a]	150[a]	250[a]	500[a]	2500[a]	3	6
Total (µL)	5000	5000	5000	5000	5000	5000	5000	5000

a = Volume taken from a 1000 ng/mL haematin solution prepared in all the above solvents, but without imidazole.

b = 2 mg/mL stock prepared in 0.3M NaOH and stored at -20°C.

Abbreviations: MeOH:ACN = methanol:acetonitrile (30:70, v/v); DMSO:But = dimethylsulfoxide:*tert*-butanol (4:1, v/v); injection solvent = a composition of the solvents used in the mobile phases but without any buffers (HEPES and imidazole).

Lastly, for the calibration curve plot, the calibration concentrations (Table 4.3) were first converted to amount haem Fe per sample using the composition of Fe (MW = 55.85) in haematin (MW = 633.51). This was because this would allow for easier interpolation from the calibration curve when determining for amount of haem Fe per trophozoite (fg/cell) during sample analysis. The calibration curve (Figure 4.16) was plotted using GraphPad Prism software. A linear regression equation was used for the best-of-fit line (y = mx + c), resulting in a correlation coefficient (r^2) of 0.9993.

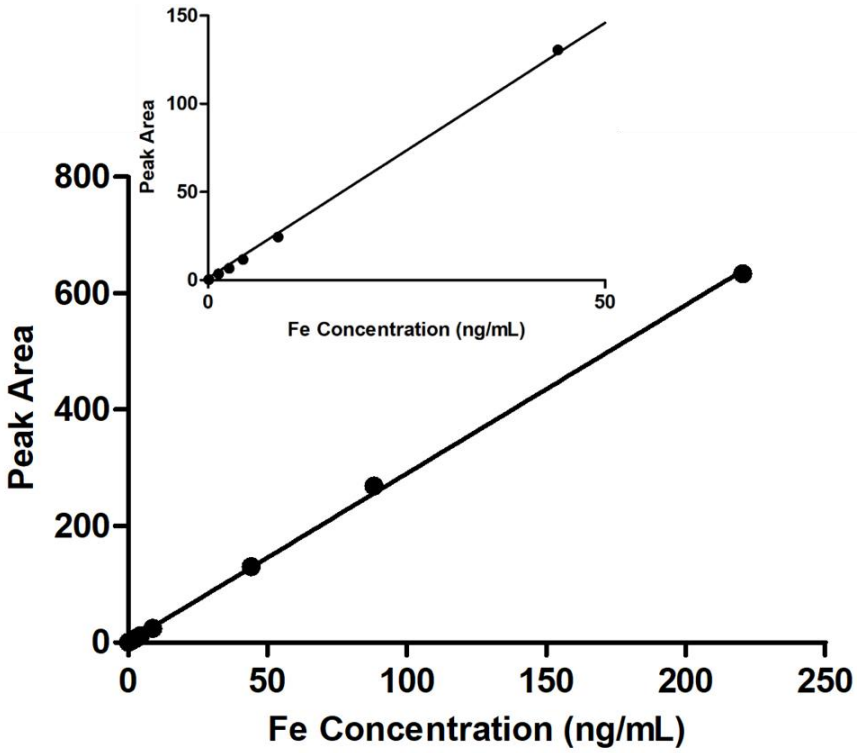

Figure 4.16: A calibration curve of haematin standards for the calibration range of 1 ng/mL to 2500 ng/mL. The haematin standard concentrations in Table 4.3 were converted to haem Fe concentrations using the composition of Fe (Mw = 55.85) in haematin (Mw = 633.51). The linearity correlation (r^2) was established across the range at 0.9993. A linear regression equation (y = mx + c) was used. Figure Insert demonstrates linear conformity at the lower calibration concentrations on the left of the graph.

4.2.4. Accuracy and precision

The accuracy of an analytical method across the calibration range indicates the proximity between the measured value (interpolated) and the nominal value of the analyte and is expressed as a percentage. On the other hand, the precision of a method indicates the method's reliability to repeatedly reproduce the measured values with proximity to the nominal value (%CV; percentage coefficient of variation).[231] Therefore, the accuracy and precision of the method were assessed over two days by freshly preparing calibration standards as previously described (Table 3) and quality control samples (QCs) at low (QCL), medium

(QCM) and high (QCH) concentrations on each day.

4.2.4.1. Preparation of quality control standards (QCs)

The QCs were prepared by spiking the 20000 ng/mL haematin standard solution into a 5 mL volume of a blank solution matrix in conical bottom centrifuge tubes. These were prepared at the following haematin concentrations: QCH = 1700 ng/mL, QCM = 850 ng/mL, and QCL = 3 ng/mL. For the solution matrix, the composition was the same as for the calibration standards. Similar to the standards, no serial dilutions were performed in preparing the QCs. Table 4.4 details the preparation of the chosen QC concentrations, with each concentration prepared in sexpartite. The concentrations of the QCH and QCM samples were adjusted to correct for the pipette volumes used. The following revised concentrations for each QC were determined: QCH = 1680 ng/mL, QCM = 880 ng/mL, and QCL = 3 ng/mL.

Table 4.4: Quality control standards (QCs) preparation at the low (QCL), medium (QCM), and high (QCH) concentrations from 2 mg/mL haematin standard solutions in solvents or reagents.

	Volumes of solvent or solution used at each haem concentration (µL)		
Solvent/ Reagent	**QCH[a] (1700 ng/mL)**	**QCM[a] (850 ng/mL)**	**QCL (3 ng/mL)**
Water	995.8	997.8	850
MeOH:ACN	625	625	625
NaCl (0.3M)	625	625	625
DMSO:But	625	625	625
Injection solvent	1725	1725	1725
HEPES (1M)	250	250	250
Imidazole (1M)	150	150	150
Haem stock[b]	4.2	2.2	15[c]

a = Concentrations corrected for pipette volumes: QCH = 1680 ng/mL and QCM = 880 ng/mL.

b = 2 mg/mL stock prepared in 0.3 M NaOH and stored at -20℃.

c = Volume taken from a 1000 ng/mL haematin solution prepared in all the above solvents but without imidazole.

The purpose of these experiments was to choose relatively low, medium and high concentrations to cover the calibration range. These could then be effectively used to determine the measured concentrations by interpolation from the calibration curve and to subsequently compare them to the nominal concentration value. The accuracy and precision of the QCs need to be within 15% (85–115%) of the nominal concentration to be accepted as per analytical method criteria stipulated in the United States Food and Drug Administration (US FDA) validation guidelines.[232] Therefore, the results from the experiments showed acceptable accuracy and precision over the entire calibration range, as displayed in Table 4.5, with all QC concentrations falling within the 15% requirement of the nominal concentration.

Table 4.5: Accuracy and precision results at the QCH, QCM and QCL concentrations.

		QCH[a]	QCM[a]	QCL
	Nominal Conc. (ng/mL)	**1680 (ng/mL)**	**880 (ng/mL)**	**3.0 (ng/mL)**
	Replicates	Observed Conc.	Observed Conc.	Observed Conc.
Batch 1	1	1531	1064[b]	3.45
	2	1501	781	3.17
	3	1787	880	3.12
	4	1498	876	3.13
	5	1795	782	2.97
	6	1508	1028[b]	2.78
Batch 2	1	1346[b]	889	3.25
	2	1589	997	3.29
	3	1449	902	3.13
	4	1453	892	2.91
	5	1349[b]	997	2.94
	6	1607	887	2.73
All	n	12	12	12
	Mean	1534	915	3.07
	STD	144	90.0	0.210
	%CV[c]	9.4	9.8	6.7
	%Accuracy[d]	90.3	107.6	102.2

a = Concentrations corrected for pipette volumes.

b = Failed the 85% acceptance criteria.

c = 100*(STD/mean)

d = ((mean observed concentration – nominal concentration)/nominal concentration) *100

4.2.5. Proposed 96-well four-compound method

As proposed above, a 96-well four-compound method was developed to increase throughput. This method allows for the quantification of the major haem species in the parasite for four compounds simultaneously, so increasing throughput by four-fold. The assay was adapted from the method reported by Combrinck *et al.*, with significant changes.[143] Early ring-stage (0-6 h rings) sorbitol synchronised parasite culture at 5% parasitemia and 2% haematocrit was prepared (49 mL medium + 1 mL pellet) in complete medium. Contrary to the previous setup, 500 µL (previously 2 mL) of parasite culture aliquots was added to each well of a 96-deep-well round bottom plate, which amounts to a four-fold reduction in sample volume of starting parasite material. Test compounds were prepared at multiples of each compound's IC_{50} value in the complete medium, as described earlier in Chapter 2. However, each drug concentration was tested as three replicates, as opposed to the four-replicate setup previously used. The final test concentrations were kept the same as previous levels, with each test well at 0.5x, 1x,

2x, 2.5x and 3x of their IC_{50} value. Therefore, each compound was investigated at five different concentrations. This type of detailed analysis (at five concentrations) is termed the full-dose response. A summarised version of the plate setup is shown in Figure 4.17. Previously, the assay could only determine haemozoin inhibition for a single compound at a time in a 24-well plate. The detailed validation experiments for this new 96-well four-compound method are further discussed in Chapter 5.

Dosing Concentrations											
0	0	0.5x	1x	2x	2.5x	3x	0.5x	1x	2x	2.5x	3x
RBC	Control	Drug 1	Drug 1	Drug 1	Drug 1	Drug 1	Drug 2	Drug 2	Drug 2	Drug 2	Drug 2
RBC	Control	Drug 1	Drug 1	Drug 1	Drug 1	Drug 1	Drug 2	Drug 2	Drug 2	Drug 2	Drug 2
RBC	Control	Drug 1	Drug 1	Drug 1	Drug 1	Drug 1	Drug2	Drug2	Drug2	Drug2	Drug2
RBC	Control	Drug 3	Drug 3	Drug 3	Drug 3	Drug 3	Drug 4	Drug 4	Drug 4	Drug 4	Drug 4
RBC	Control	Drug 3	Drug 3	Drug 3	Drug 3	Drug 3	Drug 4	Drug 4	Drug 4	Drug 4	Drug 4
RBC	Control	Drug 3	Drug 3	Drug 3	Drug 3	Drug 3	Drug 4	Drug 4	Drug 4	Drug 4	Drug 4
Cal 1	Cal 1	Cal 2	Cal 2	Cal 3	Cal 3	Cal 4	Cal 4	Cal 5	Cal 5	Cal 6	Cal 6
Cal 7	Cal 7	Cal 8	Cal 8	empty	empty	empty	empty	Blank	Blank	Ref Std	Ref Std

Figure 4.17: An example of the haem species fractionation plate setup for four test compounds. Key: RBC = uninfected red blood cells, Control = parasite infected-RBCs with no drug, cal 1–8 = calibration curve standards, Blank = solvents without any analyte, Ref std = 1000 ng/mL of haem–(bis)imidazole complex, Drug 1–4 = all the test compounds and dosing concentrations are represented as multiples of the IC_{50} for each drug per column.

4.3. Conclusions

Mechanistic determinations are crucial in malaria drug discovery since they are an invaluable source for monitoring the emergence and spread of antimalarial drug resistance.[191] However, many existing antimalarials have poorly understood mechanisms of action, making target deconvolution difficult. Contrarily, in cases where the target is known, target validation may be impeded by a lack of appropriate assays or assays that require specialised skills.[137] The parasite's haem detoxification pathway remains an exciting drug target for potential future antimalarials. However, the pyridine-based assay used to elucidate inhibitors, as described in Chapter 2, is tedious, suffers reduced throughput, and requires specialised knowledge of haem chemistry. As a result, there is a need to develop a method with improved throughput, and which is readily transferrable and uses smaller parasite material.

This chapter reported on the development of an HPLC-DAD assay and a partially developed LC-MS/MS assay for detecting haem species. Although detected successfully using LC-MS/MS with four-fold reduced parasite starting material, haem quantification was classified as a risk for the instrumentation and was therefore abandoned. Nevertheless, HPLC-DAD analysis presented an alternative, less risky approach with adequate sensitivity for quantifying all the intracellular haem species. Also, it is believed that this approach will be easily

transferable and user friendly. Therefore, a six-minute gradient elution reverse-phase chromatographic method for detecting Fe(III)PPIX-(bis)imidazole at 410 nm was successfully developed, as reported above. As demonstrated, the technique proved robust and selective for the three intracellular haem species since there was no significant cross-contamination during the fractionation procedure and no deviations in retention time by either fraction during chromatographic analysis. Furthermore, the method was shown to be accurate and precise in determining measurements. Its validation with known haemozoin and non-haemozoin inhibitors against the parasite will be discussed in Chapters 5 and 6 for the 96-well four-compound-based and 96-well 33-compound-based methods, respectively.

Chapter 5: Validation of 96-well HPLC-DAD Assay for Quantifying Haem Species with Known Haemozoin Inhibitors and Non-Haemozoin Inhibitors

5.1. Introduction

Target deconvolution of new antimalarial drug candidates has proved to be invaluable, especially in predicting future drug resistance.[191] The difficulty, however, is that many suspected antimalarial targets have not been validated and are thus inaccessible to the drug discovery community.[137] Therefore, it is essential to have strategies focused on identifying known parasite-specific targets and to reinforce them through assay development and validation for potential use in drug discovery hit identification programmes. As initially highlighted in Chapter 1, Hb catabolism in the malaria parasite is crucial, especially as a rich nutrient source in the form of amino acids.[233] However, it is also a source of unsequestered haem, which threatens parasite survival when it is not detoxified via the formation of crystalline haemozoin.[62] The haemozoin crystal presents as a centrosymmetric structure of sequestered haem that is chemically inert and therefore presents no threat to parasite viability. As previously reported in the literature and in Chapter 3, certain clinically approved antimalarials like CQ and AQ exert their therapeutic effects by interrupting this process.[143] These antimalarials are reported to adsorb to the fastest growing face of the haemozoin crystal, thereby inhibiting further crystallisation of the released haem.[145] The inhibition therefore results in a signature increase in unsequestered haem followed by a subsequent decrease in haemozoin abundance. This distinct phenomenon was reported by Combrinck *et al.* using a pyridine–ferrochrome method of quantifying haem species in the parasite.[143] This quantification is based on the haem-(bis)pyridyl low-spin complex, which is colourimetrically determined in an aqueous environment. Although highly reliable, the original method lacks in throughput, is tedious, uses relatively large volumes of cell culture and reagents, and employs volatile, toxic pyridine for the quantification of haem species.

In this thesis, as detailed in Chapter 4, imidazole was used as a viable substitute to colourimetrically measure monomeric haem as a low-spin complex. Therefore, the aim of this Chapter is to employ known haemozoin-inhibiting antiplasmodium compounds to validate this imidazole-based protocol, which has improved throughput, uses reduced parasite starting material, and eliminates the use of pyridine. This will be a significant step towards a method that can reproducibly and efficiently discriminate haemozoin inhibitors from non-inhibitors.

During optimisation of this improved method, a cellular fractionation procedure for isolating trophozoites released from RBCs using saponin lysis was achieved in four times smaller cell sample volumes when compared to the original method (Chapter 4, Section 4.2.5). Furthermore, the protocol was optimised to analyse four compounds simultaneously per 96-well plate, as opposed to one compound per 24-well plate in the pyridine-based method. To directly compare these three fractionated haem species, the conversion of each fraction to a monomeric haem-(bis)imidazole species was performed. The protocol reported in Chapter 4 (Section 4.2.2b) details the six-minute reverse-phase chromatographic analysis to quantify a Fe(III)PPIX-(bis)imidazole complex at 410 nm in an aqueous medium. Although the method was determined to be robust and selective for quantification, given that no significant cross-contamination was observed, full validation using known haemozoin inhibitors and negative control compounds is required and is demonstrated below.

5.2. Materials and methods

The detailed fractionation procedures used in this chapter were described in the method and development section in Chapter 4, Section 4.2.2c, while the materials and sample preparations were discussed in Chapters 2 (Sections 2.2.1, 2.2.2 and 2.2.6) and 4 (Sections 4.2.2, 4.2.3 and 4.2.5). The 96-well plate setup for the haemozoin inhibitors and non-inhibitors is discussed here, followed by the data analysis of the flow cytometry cell counting and haem fractionation results of the positive and negative controls.

5.2.1. 96-well four-compound assay setup

As previously mentioned in Chapter 4, this assay was adapted from the method reported by Combrinck *et al.,* with significant changes.[143] Thus, early ring-stage sorbitol synchronised parasite culture at 5% parasitemia and 2% haematocrit was prepared (49 mL medium + 1 mL pellet) in CM. Next, 500 µL of parasite culture aliquots of the mixture was added to each 1 mL well of a 96-deep-well round bottom plate. Test compounds were prepared in stock solutions in complete medium as described earlier in Chapter 2 (Sections 2.2.2 and 2.2.6), and 20 µL of each was added to the corresponding wells such that the final volume in each well was 520 µL and the final concentration was at multiples of each compound's IC_{50} value. Each compound concentration was tested as three replicates, with final concentrations in each well at 0.5x, 1x, 2x, 2.5x and 3x of their IC_{50} value. The actual concentration values for the compounds (at each IC_{50} multiple) are detailed in Chapter 2, Section 2.2.6. Following the preparations, the plates were incubated for 30 hours at 37°C in a gas chamber with 3% O_2, 4% CO_2, and 93% N_2. The summarised versions of the 96-well plate setup for the haemozoin inhibitors and non-inhibitors are shown in Figures 5.1 and 5.2, respectively.

Dosing Concentrations											
0	0	0.5x	1x	2x	2.5x	3x	0.5x	1x	2x	2.5x	3x
Blank	Control	CQ	CQ	CQ	CQ	CQ	AQ	AQ	AQ	AQ	AQ
Blank	Control	CQ	CQ	CQ	CQ	CQ	AQ	AQ	AQ	AQ	AQ
Blank	Control	CQ	CQ	CQ	CQ	CQ	AQ	AQ	AQ	AQ	AQ
Blank	Control	LOM	LOM	LOM	LOM	LOM	LPT	LPT	LPT	LPT	LPT
Blank	Control	LOM	LOM	LOM	LOM	LOM	LPT	LPT	LPT	LPT	LPT
Blank	Control	LOM	LOM	LOM	LOM	LOM	LPT	LPT	LPT	LPT	LPT
Cal	Cal	Cal	Cal	Cal	Cal	Cal	Cal	Cal	Cal	Cal	Cal
Cal	Cal	Cal	Cal	empty	empty	empty	empty	empty	empty	Ref std	Ref std

Figure 5.1: The 96-well plate setup for the four known haemozoin inhibitors used in the method validation. Key: Blank = lysed uninfected red blood cells (will contain only solvents during analysis; all solvents are described in Chapter 4 for calibration standards' preparation), Cal = the eight haematin calibration curve standards used (the calibration standards concentrations are described in Chapter 4, Section 4.2.3), Control = parasite-infected RBCs with no drug, Ref std = 1000 ng/mL of the haem-bis-imidazole complex. All the test compounds' dosing concentrations are represented as multiples of the IC_{50} for each drug per column. CQ = chloroquine, AQ = amodiaquine, LOM = lomitapide, and LPT = lapatinib. This is a representative layout and does not necessarily translate to the layout in which compounds were routinely tested using this method. As during the routine testing, the positions of the test compounds were changed as follows: two inhibitors were paired with two non-inhibitors.

Dosing Concentrations											
0	0	0.5x	1x	2x	2.5x	3x	0.5x	1x	2x	2.5x	3x
Blank	Control	PYR	PYR	PYR	PYR	PYR	THC	THC	THC	THC	THC
Blank	Control	PYR	PYR	PYR	PYR	PYR	THC	THC	THC	THC	THC
Blank	Control	PYR	PYR	PYR	PYR	PYR	THC	THC	THC	THC	THC
Blank	Control	MQ	MQ	MQ	MQ	MQ	LUM	LUM	LUM	LUM	LUM
Blank	Control	MQ	MQ	MQ	MQ	MQ	LUM	LUM	LUM	LUM	LUM
Blank	Control	MQ	MQ	MQ	MQ	MQ	LUM	LUM	LUM	LUM	LUM
Cal	Cal	Cal	Cal	Cal	Cal	Cal	Cal	Cal	Cal	Cal	Cal
Cal	Cal	Cal	Cal	empty	empty	empty	empty	empty	empty	Ref std	Ref std

Figure 5.2: The 96-well assay setup for the four known haemozoin non-inhibitors. Key: Blank = lysed uninfected red blood cells (contains only solvents during analysis; all solvents are described in Chapter 4 for calibration standards' preparation), Control = parasite-infected RBCs with no drug, Cal = the eight haematin calibration curve standards used, Blank = solvents without any analyte, Ref std = 1000 ng/mL of the haem–imidazole$_2$ complex. All the test compounds' dosing concentrations are represented as multiples of the IC_{50} for each drug per column. PYR = pyrimethamine, THC = delta-9-tetrahydrocannabinol, MQ = mefloquine, and LUM = lumefantrine.

After incubation, the excess culture medium was carefully aspirated without disturbing the layer of cells on the bottom of the plate. Thereafter, Giemsa-stained blood smears of only representative wells with control parasites (no drug) and the representative wells with 3x IC_{50} concentration for each compound were prepared on a glass slide to confirm the erythrocytic stage of the cells. The parasite pellet from each well was resuspended by adding 450 µL of phosphate-buffered saline (PBS) at pH 7.4 and subsequently RBCs were lysed to harvest trophozoites as described in Chapter 4. Following recovery of trophozoite cells, 100 µL of PBS

was added, and the resuspended pellet was subsequently transferred to a 500 µL round bottom 96-well plate, referred to as the stock plate. The stock plate was then used to prepare a second plate for flow cytometry cell counting, called the counting plate – as described in Chapter 2, Section 2.2.5. Thereafter, the stock plate was stored at -80°C until the day of the trophozoite cell lysis for the cellular haem fractionation procedure described in Chapter 4 (Section 4.2.2c).

5.2.2. Flow cytometry counting

The cell counting plate was set up by adding 10 µL of the harvested trophozoites to corresponding wells of a 96-well flat-bottom plate containing 90 µL of counting diluent. The counting diluent was prepared in 10 mL filtered PBS (pH 7.5) using 25 µL of 50% glutaraldehyde solution and 50 µL of deoxyribonuclease I and bovine recombinant (DNAse). The counting plate was then stored at 4°C until further analysis. Cell counting was performed on a BD Accuri C6 Plus flow cytometer – as described in Chapter 2, Section 2.2.5b. Figure 5.3 shows the flow chart for the 96-well four-compound procedure.

For this chapter, cell counts' sample analyses were performed as described in equation (1) below. This followed the earlier validated flow cytometry counting methodology developed by Combrinck *et al.*, which was used to normalise the amount of total haem in fg/cell.[143] The samples were analysed on a BD Accuri C6 Plus flow cytometer with C-Flow software. Each sample contained a fixed amount of fluorescent Trucount beads in a final volume of 200 µL. To estimate the concentration of cells in each acquired sample, equation 1 was used:

$$C_{flowcytometry} = (T/B) \times C_{T.beads} \qquad (1)$$

Where:

$C_{flowcytometry}$ = Concentration of cells in mL, determined using flow cytometry

T = Gated parasite cells

B = Number of gated Trucount beads from sample acquisition

$C_{T.beads}$ = Concentration of Trucount beads in the calibrated tube, as specified by the supplier

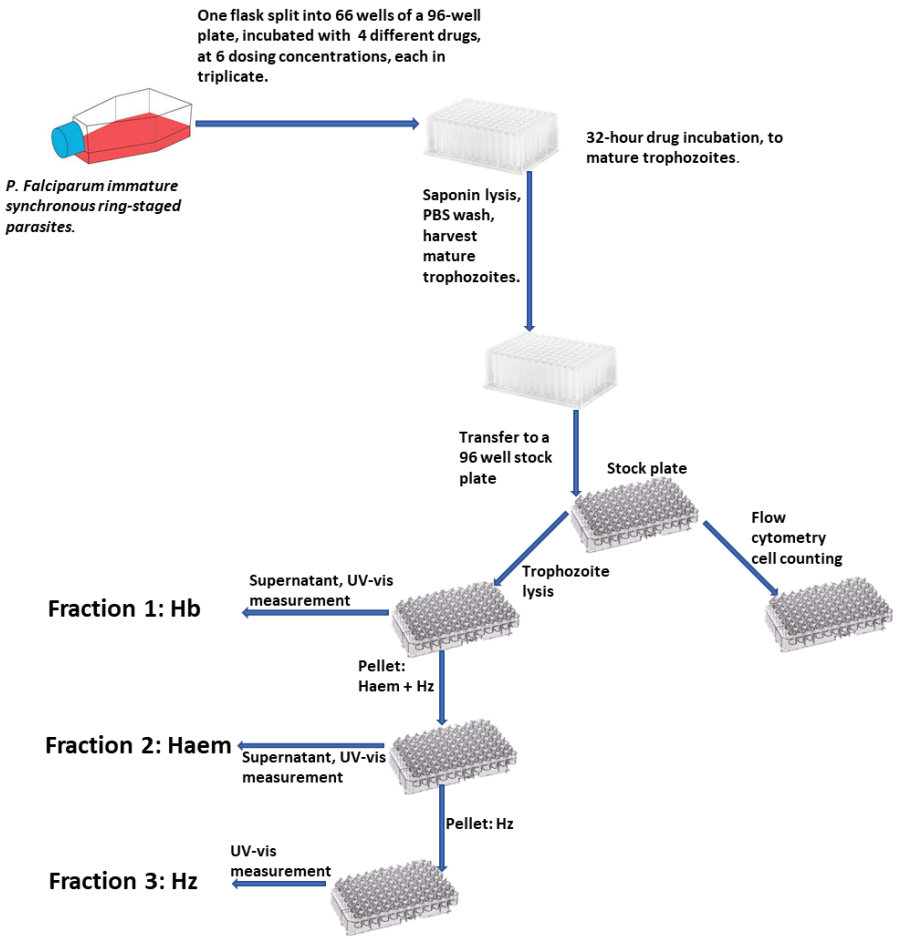

Figure 5.3: A flow chart illustrating the haem fractionation species assay setup and selective fractionation procedure of all the major haem species of *P. falciparum*.

5.2.3. Haem fractionation data analysis

Following successful cell count estimations, a subsequent sample analysis of fractionated samples was performed on the HPLC system. Post-analysis, the area was recorded for each haem species (Hb, haem and haemozoin) as per the chromatographic peaks of all analytical samples. From these areas, the sum (Area Hb + Area haem + Area haemozoin) of these species was calculated at each individually tested concentration: 0x, 0.5x, 1x, 2x, 2.5x and 3x IC_{50} values. From this, the percentage abundance of each species was calculated as follows:

%Hb = [(Area Hb) / (Total area (Hb + haem +haemozoin))] x 100

%haem = [(Area haem) / (Total area (Hb + haem +haemozoin))] x 100

%haemozoin = [(Area haemozoin) / (Total area (Hb + haem +haemozoin))] x 100

Where: Total Area = Area Hb + Area Haem + Area haemozoin

Subsequently, the amount of total haem Fe per cell (Total Fe in fg/cell) was determined by dividing the total haem Fe (interpolated from the calibration curve using the Total Area of haem

species) by the number of cells determined for each sample concentration. Therefore, the amount of each fraction in a sample (per tested concentration) was determined as follows:

Hb Fe (fg/cell) = %Hb x Total Fe (fg/cell) x V

Haem Fe (fg/cell) = %haem x Total Fe (fg/cell) x V

Haemozoin Fe (fg/cell) = %haemozoin x Total Fe (fg/cell) x V

Where:

V is a 0.2 normalising constant for the amount of Fe present in the 200 µL volume.

5.2.4. Statistical analysis

Following validation of the 96-well method with the four positive and four negative haemozoin-inhibiting controls, the Bland and Altman method[234] was used to determine the agreement between the pyridine ferrochrome and the current HPLC-DAD methods (Chapter 4). A two-tailed t-test (95% CI) was used for the statistical assessment of measurement differences that may present significance relative to the controls. The significant differences are displayed as asterisks on graphs: * $p < 0.05$; ** $p < 0.01$; *** $p < 0.001$. The data presented was from a minimum of two repeat experiments performed in triplicate and subsequently analysed using Microsoft Excel and GraphPad Prism version 9.0 software.

5.3. Results and discussion

5.3.1. Validation of method with haemozoin inhibitors

The 96-well HPLC-DAD four compounds method was validated using NF54 CQS *P. falciparum* parasites with previously identified haemozoin-inhibiting compounds. These were discussed earlier in Chapter 3 and can also be found in various publications[143,190] as validated haemozoin inhibitors. These include CQ, AQ, lapatinib (LPT/compound **16** in Chapter 3) and lomitapide (LOM/compound **19** in Chapter 3). The plots for the dose-response determinations of the haem species are reported for all compounds.

5.3.1.1. Chloroquine (CQ)

All the quantified haem species (Hb, haem and haemozoin) for CQ-treated parasites are shown in Figure 5.4. The Hb levels represented here indicate intracellular Hb taken up into the DV but not yet digested. The haem fraction represents the unsequestered haem released from Hb catabolism but not yet converted into haemozoin. Lastly, the haemozoin levels indicate the haem sequestered into the crystal for detoxification. Here, the %Hb (Figure 5.4a) and Hb Fe (Figure 5.4b; fg/cell) increased with increasing compound concentration. This was previously observed for CQ, which was found to interfere with Hb catabolism – thereby causing

an increased abundance of undigested Hb in *P. falciparum*.[143] The exact mechanism of how this happens has yet to be elucidated. However, it could be speculated that CQ has secondary effects on the parasite that lead to interference with Hb digestion but not uptake. Furthermore, since the parasite cell would be in distress from the parasiticidal effects of the drug, the regular cellular processes that allow for Hb ingestion and degradation are likely to be negatively affected as a result. The latter scenario is highly probable, since such fluctuations in Hb may be reminiscent of the negative feedback mechanism that underpins many biological homeostatic functions.[235]

The primary indicator of haemozoin inhibition is significantly increased levels of unsequestered haem measured in fg/cell in treated parasites relative to untreated parasites. For CQ, the levels of %haem (Figure 5.4c) and haem Fe (Figure 5.4d; fg/cell) were found to significantly increase with dosing concentration. These were followed by the expected concomitant decreases in %haemozoin (Figure 5.4e) and haemozoin Fe (Figure 5.4f; fg/cell). These observed effects were similar to those previously reported by Combrinck *et al.*, where the observation was first made that CQ causes a dose-dependent increase and decrease in unsequestered haem and haemozoin in the cell, respectively.[143,159] It was also demonstrated that these increased unsequestered haem levels coincided with a decrease in parasite survival. Unsurprisingly, CQ was found to negatively interfere with the growth and morphology of haemozoin crystals in the process.[159] These findings provide validation for this method and further evidence that the MoA of CQ is via haemozoin inhibition, with a direct increase in toxic haem (Figure 5.4).

It should be noted that less is known about how this unsequestered haem kills the parasite, but most of the evidence points to the possibility of a haem–compound complex being responsible for the parasiticidal effects.[187] This is not an uncommon phenomenon, given the MoA for artemisinin-based compounds which also depend on unsequestered haem activation,[43] with direct evidence of haem–artemisinin adducts having been reported.[163] Lastly, it was also observed that the Total haem Fe (sum of all haem fractions) in CQ-treated cells was statistically indistinguishable from untreated control cells, with exceptions at the two highest concentrations. This again agreed with previous observations.[143] The slight decrease in total Fe concentrations at 2.5x and 3x IC_{50} may be attributable to experimental variation and the low levels of haem in the solutions at the limit of detection, since very few trophozoites are expected to survive at high drug concentrations.

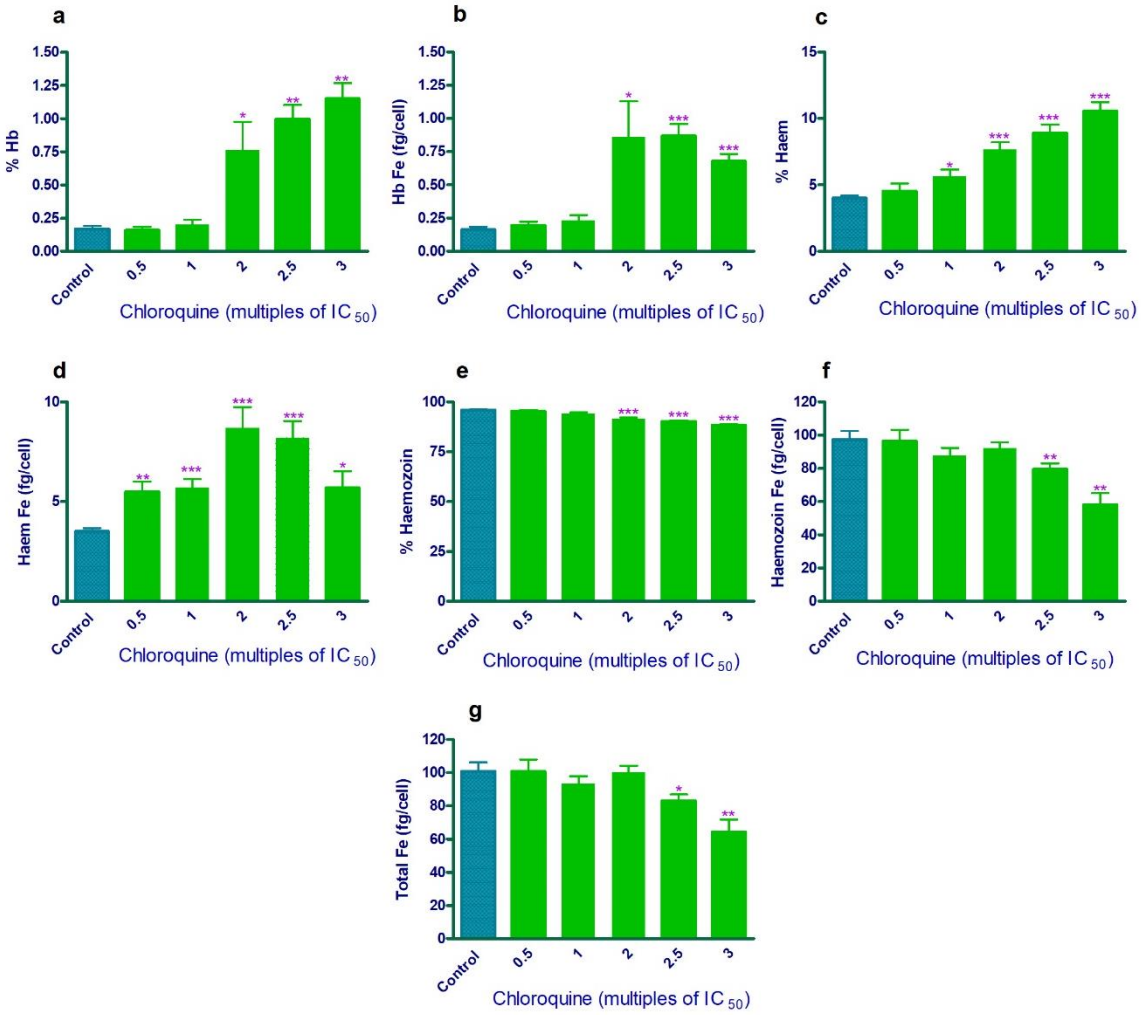

Figure 5.4: Profiles of various haem species from chloroquine-treated parasites. The Hb, unsequestered haem (haem) and haemozoin (Hz) fractions are expressed as percentages (a, c, and e) per well of trophozoites (represented at multiple of IC_{50}), and as Hb Fe, haem Fe and haemozoin Fe per trophozoite cell in fg/cell (b, d and f). The Total Fe (g) is the sum concentration of all major haem species (haemoglobin Fe, Haem Fe and haemozoin Fe) in an individual trophozoite cell. This observation follows from a 32 h incubation of early ring-stage *P. falciparum* parasites with CQ at multiples of IC_{50} and the subsequent isolation of mature trophozoites post-incubation. Control = untreated cells. Statistical significance was calculated relative to the control using the two-tailed t-test at a 95% confidence interval; this is expressed as an asterisk: * $p < 0.05$; ** $p < 0.01$; *** $p < 0.001$. Data represent the mean ± SEM from two repeat experiments.

5.3.1.2. Amodiaquine (AQ) vs Lapatinib (LPT) vs Lomitapide (LOM)

The optimised 96-well method was also validated with AQ, LPT and LOM, which are all known inhibitors. As described in Chapter 1, AQ is a 4-aminoquinoline previously shown to inhibit haemozoin formation in the parasite,[143] whereas LPT is an FDA-approved drug used in breast cancer treatment, and was shown in Chapter 3 (as compound **16**) to exert its parasiticidal effects *via* haemozoin inhibition. Lastly, LOM is also an FDA-approved drug that is commonly

used for treating familial disease by lowering low-density lipoprotein (LDL) cholesterol and was also reported in Chapter 3 (as compound **19**) to inhibit haemozoin formation.[219] The haem fractionation results of parasites treated with AQ, LPT and LOM are shown in Figures 5.5, 5.6 and 5.7, respectively. Expectedly, the full-dose response profiles confirmed that AQ, LPT and LOM, like CQ above, inhibited haemozoin formation. These resulted in increasing levels of %haem (5.5a, 5.6a and 5.7a) and most importantly the haem Fe (5.5b, 5.6b and 5.7b) concentrations in the trophozoite cell, as well as the subsequent concomitant decrease in %haemozoin (5.5c, 5.6c and 5.7c) and haemozoin Fe (5.5d, 5.6d and 5.7d).

Interestingly, contrary to what was previously reported by Combrinck *et al.,* it was found that the total haem Fe from the control parasites was statistically distinguishable from the AQ-treated parasites (Figure 5.5e).[143] This may suggest that less Hb is taken up in AQ-treated cells, so leading to less total Fe. A similar phenomenon was also observed for LPT and LOM. Most notably, the determined LPT haem Fe profiles using the bis-pyridine assay and the bis-imidazole assay were significantly different at the three highest concentrations (2 x, 2.5 x and 3 x IC_{50} values). This is not of any concern given that the conclusions reached by the two methods are the same. Unfortunately, we could not determine or explain the cause of these observed differences in the current work, and therefore future experiments should be planned to elucidate the muted response in the bis-imidazole results. This, however, was specific to LPT and not the other tested positive control compounds. Accordingly, the current results demonstrate indisputably that the bis-imidazole assay profiles are comparable to the pyridine-based assay and more importantly that the conclusions reached between the assays are similar. In both methods, it was robustly determined that AQ, LPT and LOM's MoA in the parasite cell is via haemozoin inhibition as previously determined.[143,190]

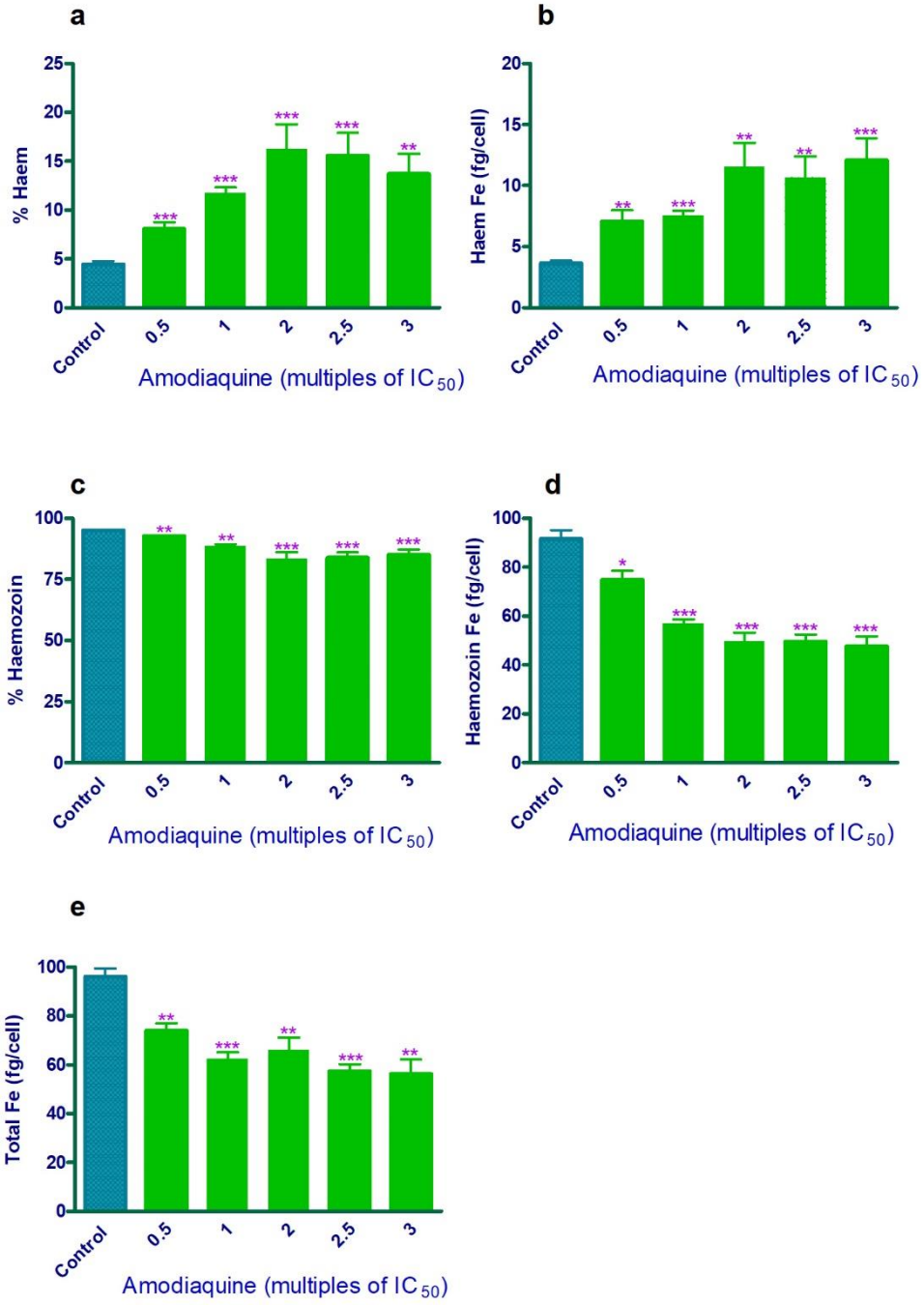

Figure 5.5: The haem fractionation profiles of parasites treated with amodiaquine. The percentages of haem (a) and haemozoin (c) are shown at multiples of AQ concentrations. Amounts of haem Fe (b) and haemozoin Fe (d) at increasing AQ concentrations are also shown. The total Fe (e) represents the sum of all the haem species per trophozoite. Control = untreated cells. Statistical significance was calculated relative to the control using the two-tailed t-test at a 95% confidence interval; this is expressed as an asterisk: * $p < 0.05$; ** $p < 0.01$; *** $p < 0.001$. Data represent the mean ± SEM from two repeat experiments.

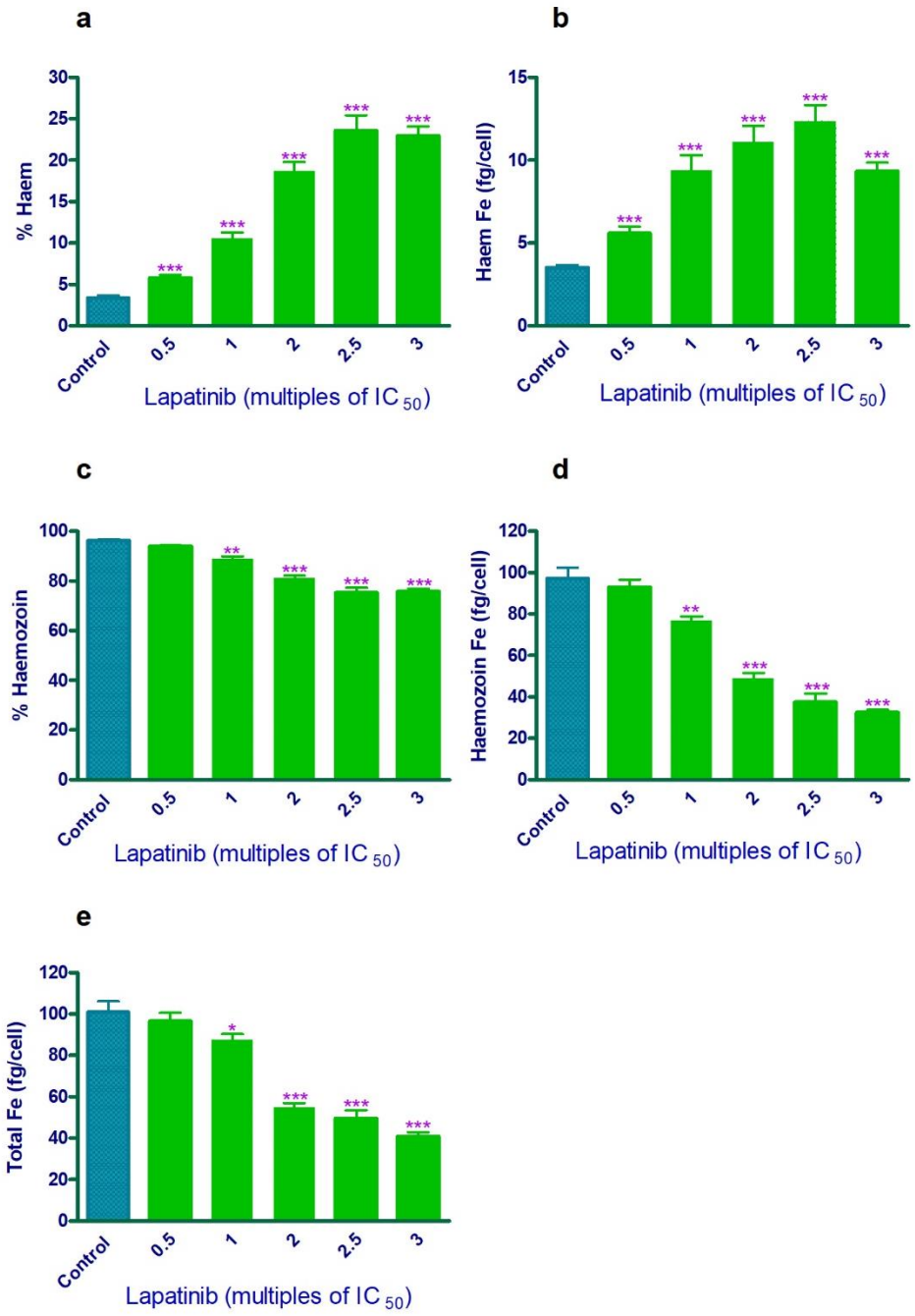

Figure 5.6: Unsequestered haem (a and b), haemozoin (c and d) and total Fe (e) of lapatinib-treated parasites expressed as fg per cell in isolated *P. falciparum* trophozoites. Control = untreated cells. Statistical significance was calculated relative to the control using the two-tailed t-test at a 95% confidence interval; this is expressed as an asterisk: * $p < 0.05$; ** $p < 0.01$; *** $p < 0.001$. Data represent the mean ± SEM from two repeat experiments.

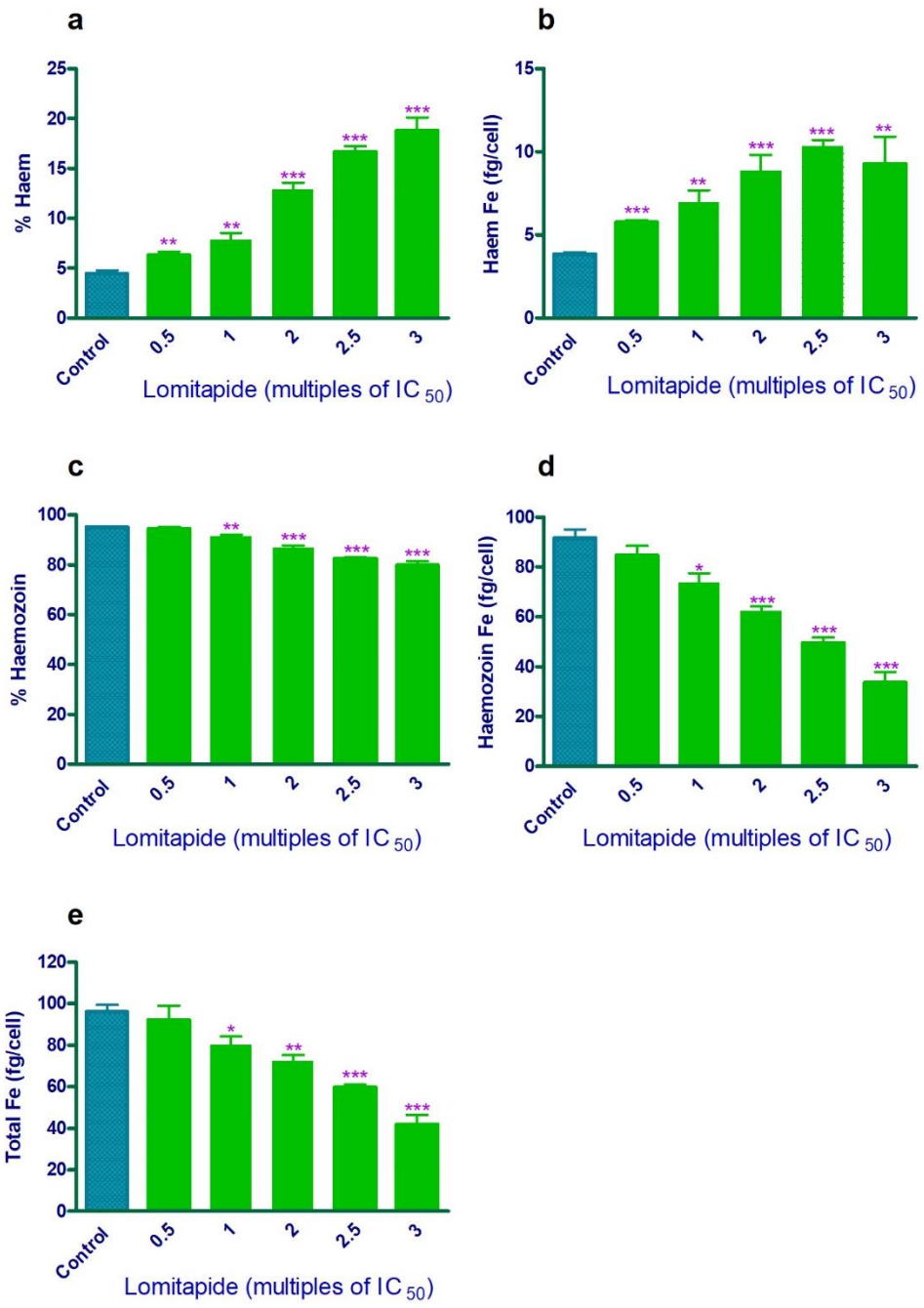

Figure 5.7: *P. falciparum* intracellular unsequestered haem (a and b), haemozoin (c and d), and total Fe (e) haem profiles. Control = untreated cells. Statistical significance was calculated relative to the control using the two-tailed t-test at a 95% confidence interval; this is expressed as an asterisk: * $p < 0.05$; ** $p < 0.01$; *** $p < 0.001$. Data represent the mean ± SEM from two repeat experiments.

5.3.2. Validation of 96-well method with the haemozoin non-inhibitors PYR, THC, MQ, and LUM

To determine whether the 96-well HPLC-DAD method could discriminate between haemozoin inhibitors and non-inhibitors, four known non-inhibitors were selected for validation. These comprised PYR, THC, MQ, and LUM, whose intracellular haem species profiles have previously been reported in the literature using the pyridine-based method.[143,144,212] The full-dose response haem fractionation profiles for the compounds are reported below.

5.3.2.1. PYR vs THC vs LUM vs MQ

PYR is an antifolate antimalarial drug that is well known to be a non-β-haematin and non-haemozoin inhibitor.[73,143,159] Contrarily, THC is a recently discovered non-haemozoin inhibitor and a well established psychoactive molecule which was discussed earlier in Chapter 3.[212] The other negative inhibitor, LUM, is an effective antimalarial drug used in artemisinin combination therapy (ACT) and has also been widely reported in the literature as not exerting its parasite toxic effects through inhibition of haemozoin formation.[144] Lastly, MQ is a potent approved antimalarial drug which like LUM is used in combination therapy. Moreover, like the other non-haemozoin inhibitors, MQ is a well known β-haematin inhibiting compound *in vitro*, although not inhibiting haemozoin formation in the parasite cell.[144]

The respective haem fractionation results for all these negative haemozoin inhibitors are shown in Figures 5.8, 5.9, 5.10 and 5.11 for PYR, THC, LUM and MQ, respectively. Unsurprisingly, the observed profiles demonstrate the ability of the 96-well bis-imidazole method to discriminate robustly between haemozoin inhibitors and non-inhibitors. As presented in the plots, all the tested compounds generally exhibited no persistent increase in %haem concentrations (Figure 5.8a, 5.9a, 5.10a and 5.11a), with exceptions for PYR and LUM which showed significant increases only at the highest concentrations. However, normalising for haem Fe concentrations (Figure 5.8c, 5.9c, 5.10c and 5.11c) in the trophozoite cell revealed no statistically significant increase in unsequestered haem compared to the untreated parasites in all the compounds reported. Unconventionally, it was apparent that the levels of haem Fe for MQ (Figure 5.11c), like those of haemozoin Fe (Figure 5.11d), decreased significantly in the cell with increasing drug concentration. These effects on the haem and haemozoin fractions were because of the drastic decrease in total Fe (Figure 5.11e) in treated parasites compared to the control parasites, thus suggesting less uptake of haem-Fe in MQ-treated cells. The fact that the percentage haem levels remain unchanged and haem Fe concentrations decreased with dose suggests that there is very little accumulation of haem in cells treated with MQ. This is substantiated by previous work from Vanaerschot *et al.* where it was observed that in parasites treated with MQ there was a significant decrease in the

accumulation of haem compared to control cells, and that this reduction was not related to decreased endocytosis of intracellular Hb but the reduction in total haem Fe.[144] This perhaps suggests an alternative cellular mechanism that remains unknown, but which causes secondary effects on haem sequestration downstream in the pathway. Nonetheless, what is evident from the current measurements is that the data is consistent with MQ being a non-haemozoin inhibitor as per my previous definition.

The same conclusions can be reached for PYR, LUM and THC, which displayed no significant increases in haem but rather statistically significant reductions in haemozoin Fe. Likewise, these reductions in haemozoin are not related to any interference of the compounds' haemozoin-inhibiting ability but rather to the significant reductions in total Fe profiles (Figure 5.8e, 5.9e, 5.10e and 5.11e), and perhaps other secondary inhibitions that have a significant impact on the haem detoxification pathway. More importantly, the observations of the above compounds further substantiate the importance of measuring the fg/cell data when discriminating between inhibitors and non-inhibitors, rather than reporting only on the percentage (%) data which could often be misleading. This phenomenon has been highlighted in detail by Combrinck *et al.* in the case for atovaquone (a non-haemozoin inhibitor).[143] Hence, it was explicitly stated by these authors and elsewhere that the indicators of a direct haemozoin inhibitor in the parasite cell are the concurrent decrease in haemozoin and increase in unsequestered haem measured in fg/cell.[143,145] These are criteria that the current tested compounds (PYR, THC, LUM and MQ) do not meet, thus making them non-inhibitors of haemozoin formation.

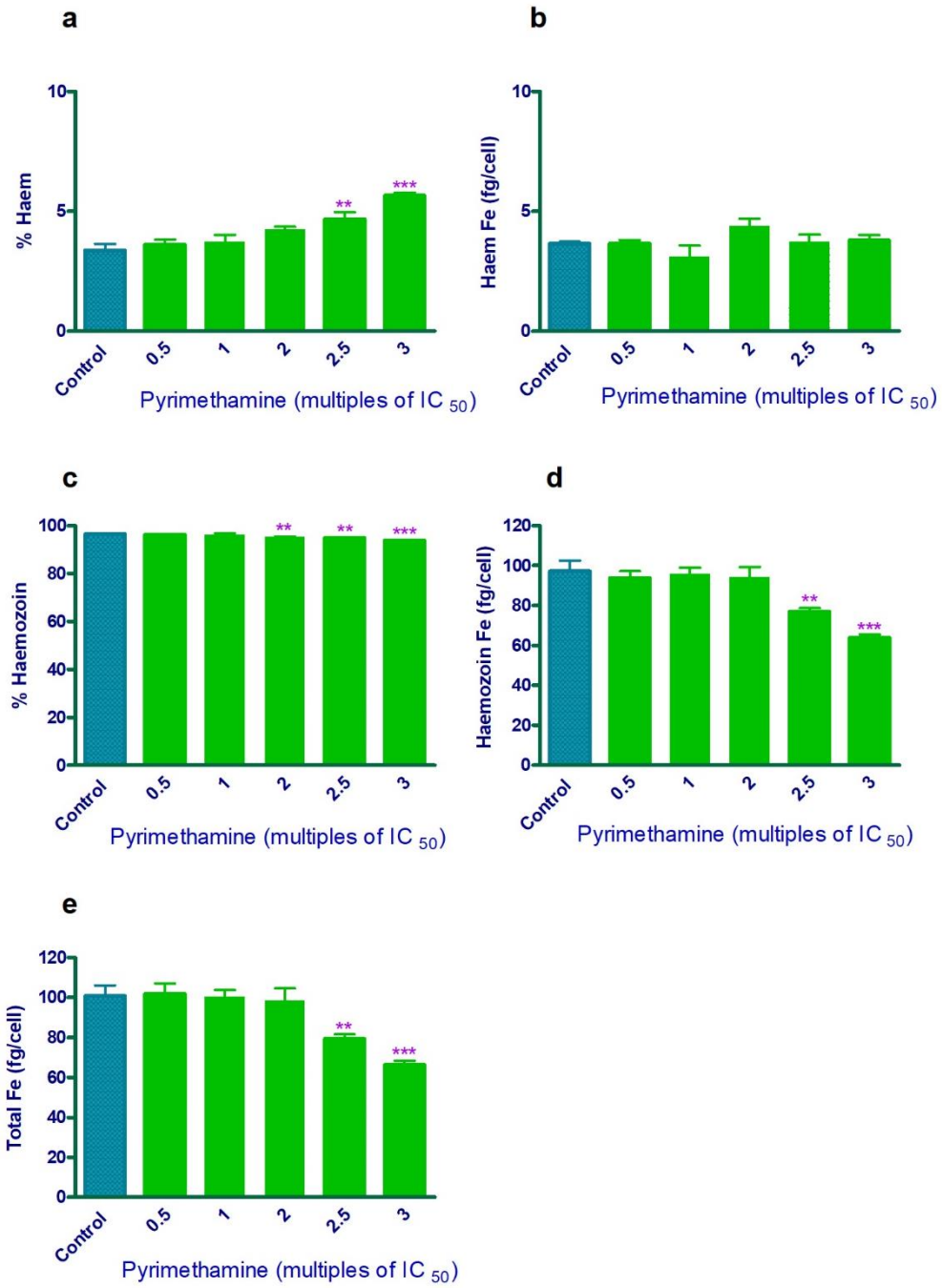

Figure 5.8: The intracellular unsequestered haem (a and b), haemozoin (c and d) and total Fe (e) haem species of the haemozoin non-inhibiting antimalarial, pyrimethamine. Statistical significance was calculated relative to the control using the two-tailed t-test at a 95% confidence interval; this is expressed as an asterisk: * $p < 0.05$; ** $p < 0.01$; *** $p < 0.001$. Data represent the mean ± SEM from two repeat experiments.

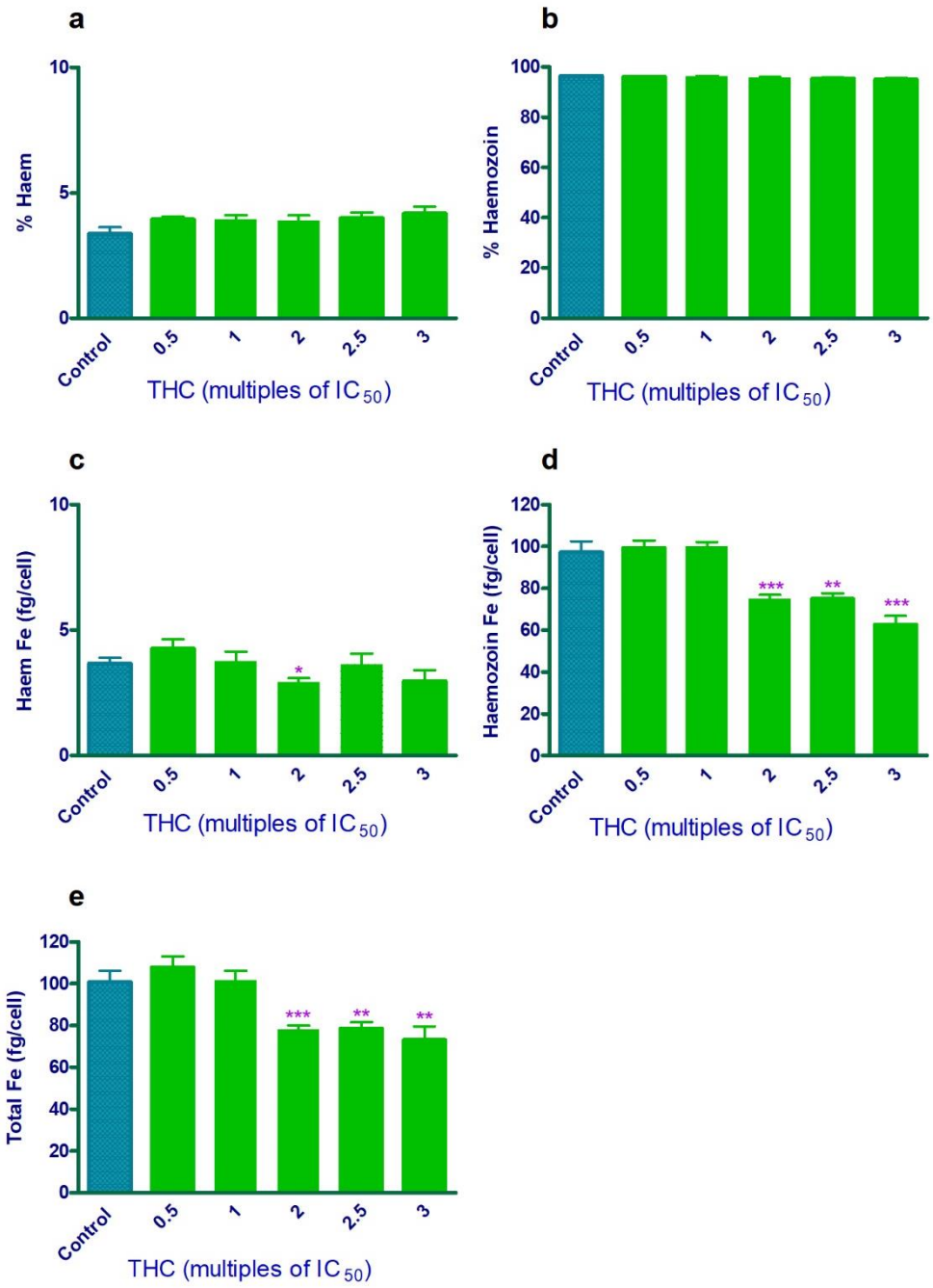

Figure 5.9: Haem fractionation profiles of the two abundant haem species in *P. falciparum*, unsequestered haem and haemozoin, in THC-treated cells. These are expressed as percentages of haem (a), haemozoin (b), amounts of haem Fe (c) and haemozoin Fe (d), as well as the total Fe (e) of all the major haem species (Hb, haem and haemozoin) at multiples of THC IC_{50} concentrations. Statistical significance was calculated relative to the control using the two-tailed t-test at a 95% confidence interval; this is expressed as an asterisk: * $p < 0.05$; ** $p < 0.01$; *** $p < 0.001$. Data represent the mean ± SEM from two repeat experiments.

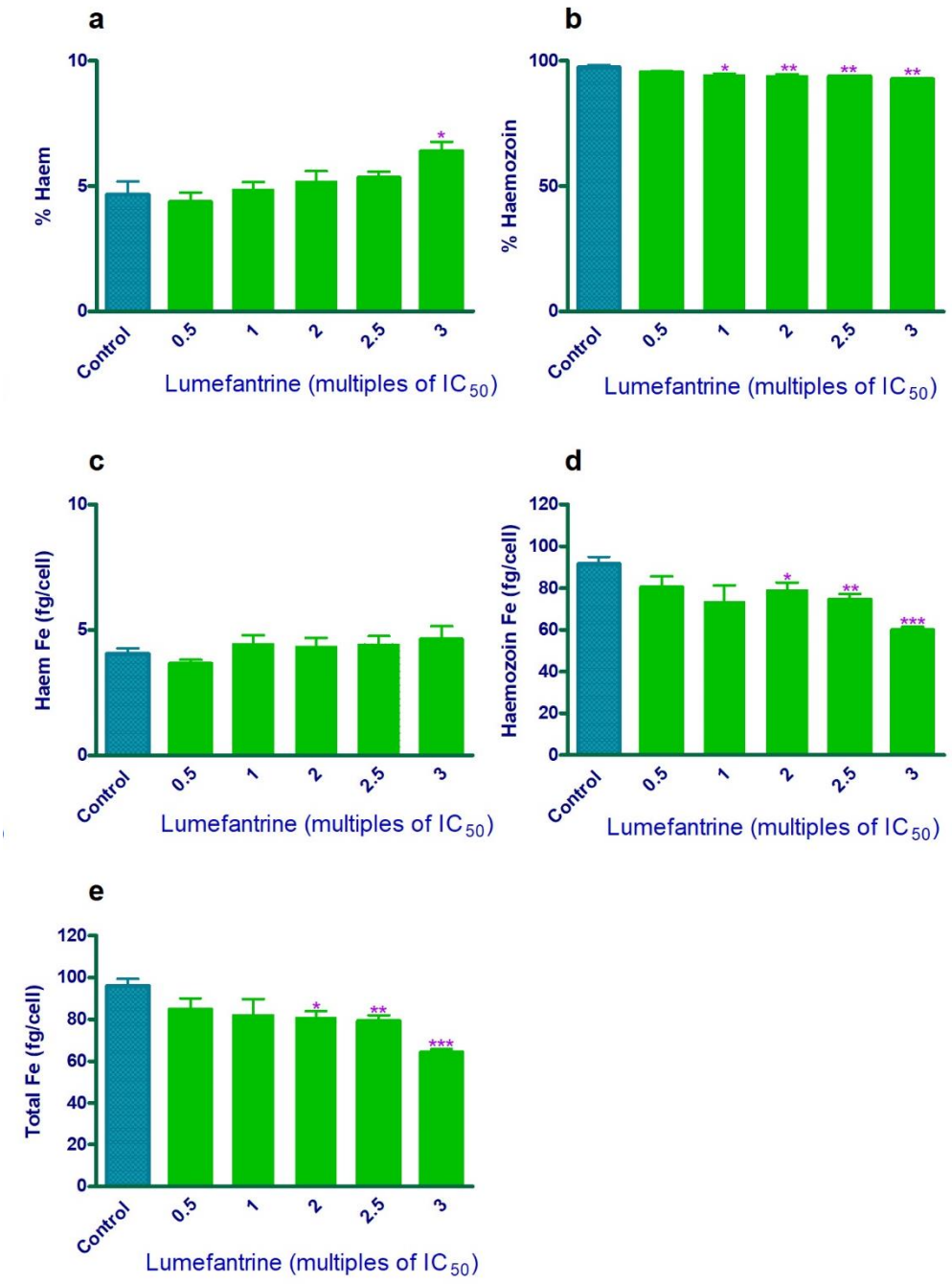

Figure 5.10: Haem fractionation profiles for lumefantrine. Percentages of haem (a) and haemozoin (b) are shown at increasing lumefantrine concentrations. The amounts of haem Fe (c), haemozoin Fe (d) and total Fe (e), as determined using flow cytometry cell counts, are also shown. Statistical significance was calculated relative to the control using the two-tailed t-test at a 95% confidence interval; this is expressed as an asterisk: * $p < 0.05$; ** $p < 0.01$; *** $p < 0.001$. Data represent the mean ± SEM from two repeat experiments.

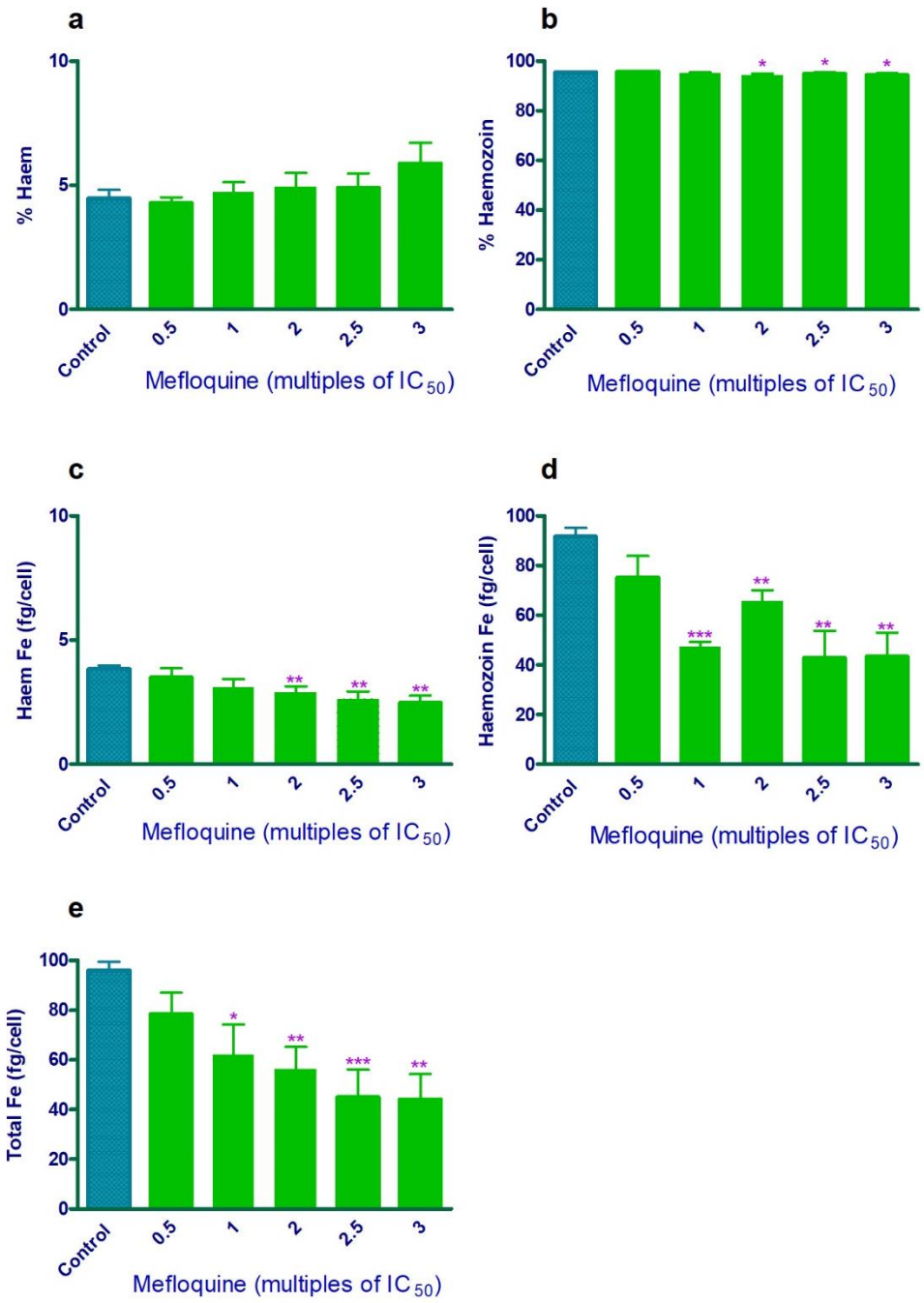

Figure 5.11: The profiles for the two major intracellular haem species, haem and haemozoin, of mefloquine-treated cells. These are expressed as percentage haem (a), percentage haemozoin (b), haem Fe (c), haemozoin Fe (d) and total Fe (e) per trophozoite. Statistical significance was calculated relative to the control using the two-tailed t-test at a 95% confidence interval; this is expressed as an asterisk: * $p < 0.05$; ** $p < 0.01$; *** $p < 0.001$. Data represent the mean ± SEM from two repeat experiments.

5.3.3. Comparison of pyridine plate method with 96-well HPLC-DAD method

Since it was successfully established that the 96-well method could robustly distinguish between haemozoin inhibitors and non-inhibitors with high reproducibility, a direct comparison of the results obtained with the pyridine plate method and the 96-well HPLC-DAD method was performed using the Bland-Altman statistical analysis (B&A). The B&A statistical analysis method is used to assess the agreement between two methods and therefore is critical in identifying any underlying differences that may exist.[234,236] However, as explained in the literature, the B&A analysis does not specify if the determined agreement or differences between the two methods makes the new method suitable to use or to be rejected.[236] Instead, the purpose of the B&A analysis is to quantify the bias (mean difference) and range of agreement (95% limits of agreement). Thus, only analytical, biological, and clinical objectives define the suitability of the method to either be used or rejected for the required purposes. Consequently, as mentioned above, our goal is to develop a robust and improved throughput method that reproducibly discriminates haemozoin inhibitors from non-inhibitors, with a reduced quantity of parasite starting material that eliminates the use of pyridine to complex haem.

The full-dose response profiles for direct comparison of the 96-well and pyridine-based plate method in CQ-treated *P. falciparum* parasites are shown in Figure 5.12. The results of both methods showed an equivalent dose-dependent increase in haem and a concomitant decrease in haemozoin (Figure 5.12b, c, e and f). A 7.22% increase in haem compared to the control was attained in the pyridine-based method, while a maximum increase of 6.56% was observed with the 96-well method, so indicating minimal differences between the methods. However, there were substantially larger differences in the Hb fractions (Figure 5.12a and d) between the two methods, with the 96-well method presenting very low concentrations of quantified Hb in comparison. This is probably attributable to the current method's four-fold decrease in the sample volume. The phenomenon of the effect by sample volume was reported by Combrinck *et al.* during the development of the pyridine-based method, where it was noted that smaller sample sizes tend to associate with larger errors since significant sample losses probably occur during the fractionation steps.[143] Therefore, given the already reduced presence of undigested intracellular Hb, this effect will likely be a significant contributory factor compared to the other fractions, which are present in larger quantities. This can be seen when statistically comparing the percentages of each haem species for the two methods in the B&A plots shown in Figure 5.13.

Here, the differences in the averages of the results obtained from the pyridine method and the 96-well method were plotted against the mean for each haem species. This showed an observed broader bias of 5.56 for the Hb fraction (Figure 5.13a), indicating that the 96-well

plate method consistently results in lower concentrations in comparison. This was very high, given the measured intracellular concentration of Hb in mature trophozoites. Nevertheless, this proved insignificant as the conclusions reached by both methods were similar. The agreement between both methods for the haem (Figure 5.13b) and haemozoin (Figure 5.13c) fractions was fair, with narrower biases of 1.77 and -6.36, respectively. Thus, given the fair agreement for both the haem and haemozoin fractions and the fit for purpose, the 96-well method is suitable for identifying true haemozoin inhibitors from non-inhibitors. As mentioned above, the larger errors and muted response in the Hb fractions were anticipated as potential challenges for quantification when the sample volumes were to be decreased.[143] However, in order to better understand the observed broader differences in Hb concentrations for both methods, further investigations using a suitable internal standard in the 96-well method may suffice. This may reveal whether these quantification differences are associated with sample losses or otherwise. Nevertheless, it is believed that given the robustness and reproducibility of the 96-well method, the muted response in Hb is a minor compromise. This is especially the case when considering that the conclusions reached for the fraction by both methods are similar. More importantly, the essential indicators of a haemozoin inhibitor are the haem Fe and haemozoin Fe fractions measured in fg/cell, which presented as not problematic.

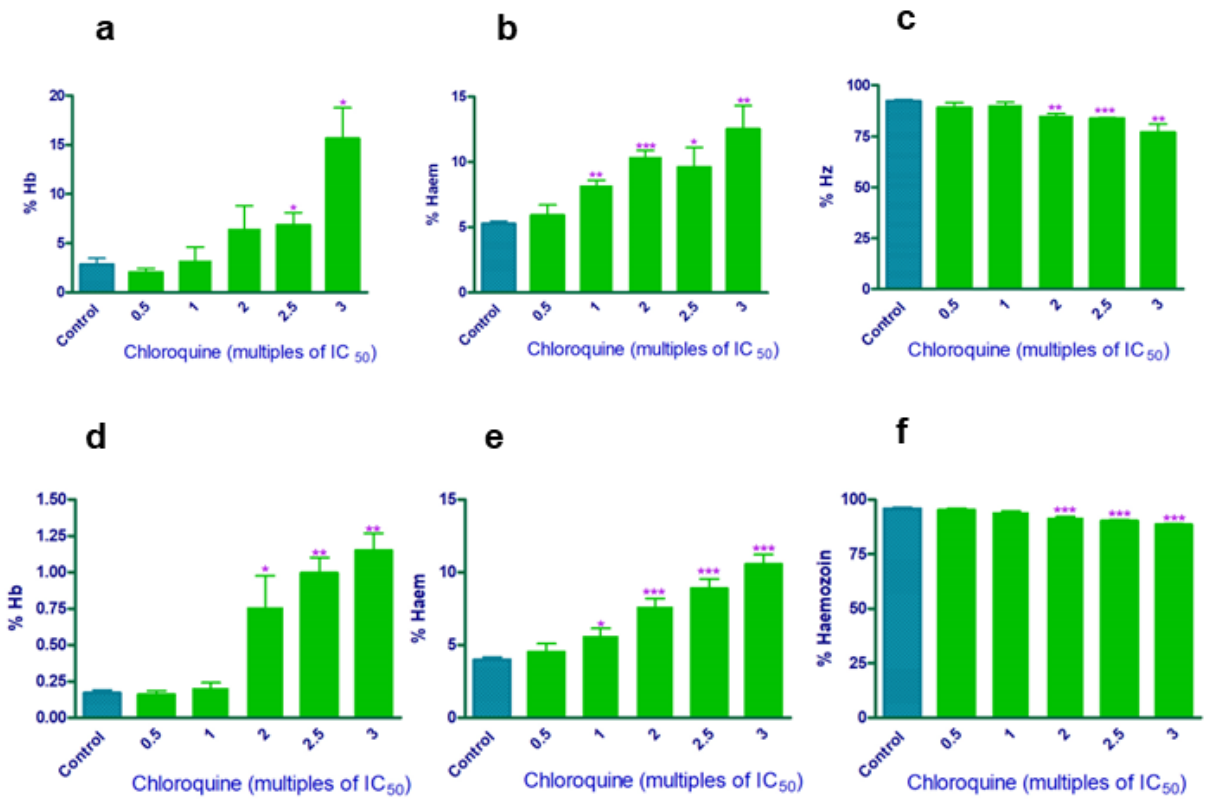

Figure 5.12: The percentage of haem species in chloroquine-treated parasites obtained using the pyridine-based method (a, b and c) and the improved 96-well method (d, e and f) at increasing chloroquine concentrations. These are expressed as %Hb (a and d), %haem (b and e) and %haemozoin (c and f) relative to the total haem found in the isolated parasites. Statistical significance was calculated relative to the control using the two-tailed t-test at a 95% confidence interval; this is expressed as an asterisk: * $p < 0.05$; ** $p < 0.01$; *** $p < 0.001$.

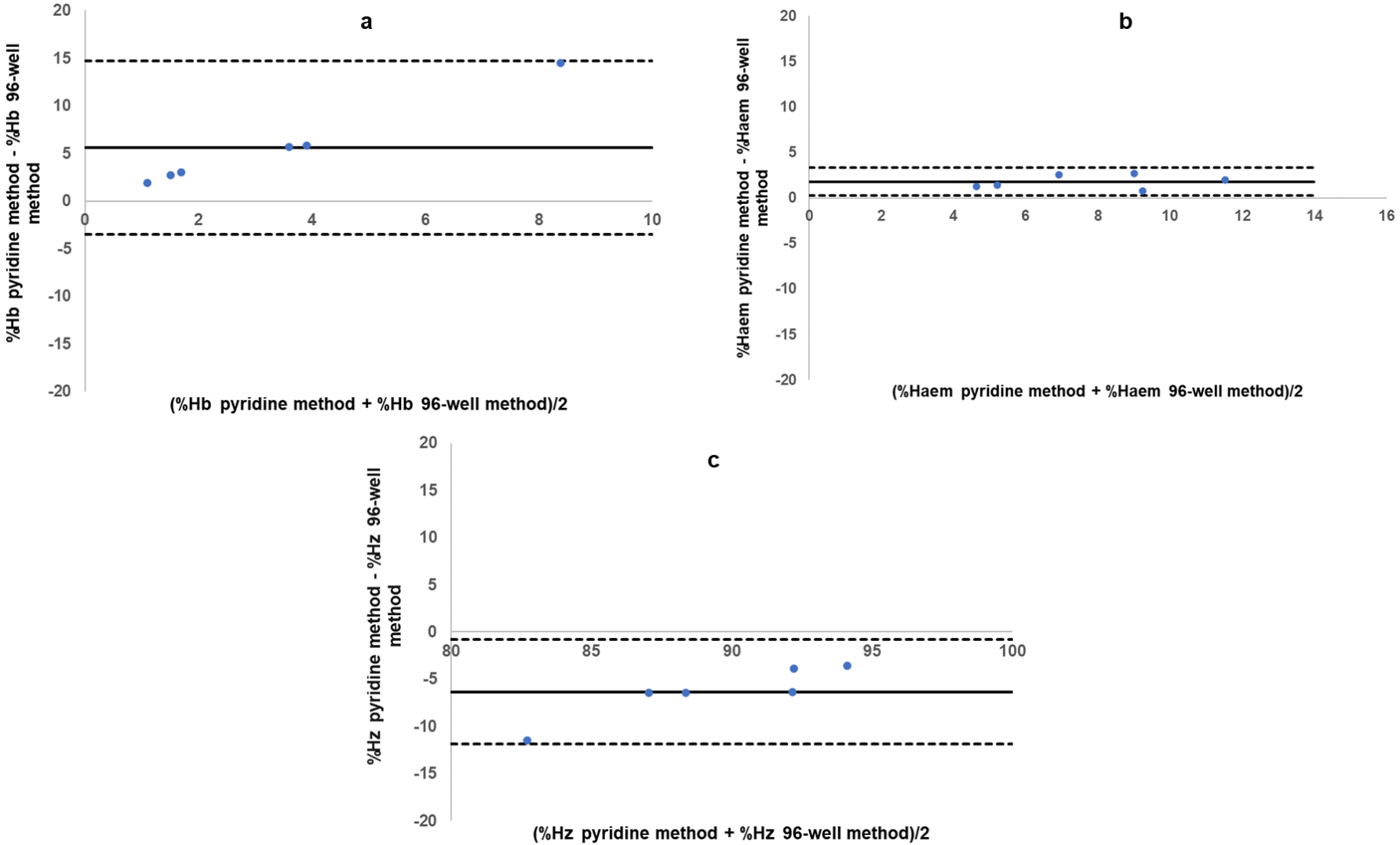

Figure 5.13: Bland and Altman plots showing the differences between the results of the pyridine-based method and the 96-well method at each concentration measurement of the individual fraction; %Hb (a), %haem (b) and %Hz (c). The solid line represents the mean (bias), and the dotted lines represent the upper and lower 95% limits of agreement between the two methods. The biases: Hb fraction = 5.56, haem fraction = 1.77, and Hz fraction = -6.36.

5.4. Conclusion

The pyridine-based haem fractionation method was optimised to the increased throughput 96-well HPLC-DAD method and validated using four positive and four negative haemozoin formation inhibiting controls. This improved 96-well method has eliminated the use of pyridine, reduced parasite starting material four-fold, and increased output by four-fold. The method is robust and reproduces the main results and conclusions obtained using the pyridine-based method, although there were some observed differences in the concentration levels for the Hb fraction and total Fe between methods. These were, however, hypothesised to be a result of the reduced sample size, and had an insignificant impact on the overall conclusions reached. Interestingly, results from the collated data demonstrated the crucial significance of determining haem Fe levels per cell using flow cytometry cell counting rather than just using percentages of haem species to interpret haemozoin inhibition. Lastly, as previously stipulated, this assay will be helpful even in cases where novel targets are needed since it will help to completely rule out the possibility of haemozoin inhibition. Furthermore, this method and the 33-compound high-throughput method (Chapter 6) will complement the insights gained from the β-haematin assay, especially in cases where medium to high throughput screening is a priority. It is hoped that these techniques will be readily accessible and user-friendly for adaptations in many drug discovery programmes.

Chapter 6: Adaptation of the 96-well HPLC-DAD Assay to a Single-concentration Medium High-throughput Assay

6.1. Introduction

Drug discovery and development programmes have relied on cell- and target-based high-throughput screening for years.[237] Target-based screening is applied when molecular targets are known and their therapeutic effects can be measured *in vitro* using biochemical assays or conditional knockdown approaches.[209] On the other hand, cell-based phenotypic screens determine the activity of drug compounds and experimental molecules against *in vitro* whole-cell parasites.[237] The downside is that whole-cell screens present challenging target deconvolution. Therefore, target-based high-throughput screening has become an essential tool in drug discovery processes due to the increasing number of validated drug targets.[238] On the upside, target-based screening allows the discovery of innovative leads by probing interactions with specific targets.[239]

Virtual screening, where computer models are employed in early-stage drug development to search for new molecules, is becoming increasingly valuable. As previously mentioned in Chapter 3, the directed approaches of ligand and structure-based virtual screening use molecular docking against known biological target structures to identify suitable lead compounds in chemical libraries.[210,239] The haemozoin crystal in the malaria parasite is a promising target for antimalarial development, especially for generating leads from virtual screenings *in silico*. As demonstrated by de Sousa *et al*., its chemical equivalence to the synthetic β-haematin crystal allows for a directed ligand or structure-based virtual screening approach.[182,190,212] This allows for the identification of many lead compounds that are predicted as unique inhibitors of haemozoin formation in the malaria parasite. However, a confirmatory *in vitro* β-haematin formation assay is initially required for the *in silico* discovered lead compounds. These confirmatory predictions of haemozoin formation inhibitors are performed using the NP-40 detergent-mediated synthetic haemozoin (β-hematin) inhibition assay because it mimics the physiological conditions in the parasite's digestive vacuole.[158] Although a high-throughput confirmatory assay to test β-haematin inhibition for selected leads is available in the Bioinorganic Research Group at UCT, a directed intracellular prediction method is still unavailable to determine haemozoin inhibition at a high-throughput level. Such a method is necessary because, despite its success, the β-haematin prediction is still not conclusive on the actual mechanism of action in the cell since any compound that directly interacts with the crystal will result in positive inhibition. It is worth noting that for any interaction to occur in the parasite cell, the compound must first enter the DV, where haemozoin formation

occurs. An example of this is illustrated in the results previously discussed in Chapters 3 and 5, specifically in the case of THC, which inhibited β-haematin formation *in vitro* but not haemozoin formation in the cell.

This chapter focuses on validating a 33-compound high-throughput method, whose development was initially described in Chapter 4. The technique was repurposed from the successfully developed and validated four-compound HPLC-DAD assay (Chapter 5). This adapted medium high-throughput method aims to predictively quantify intracellular haem species in *P. falciparum* cells for 33 compounds tested simultaneously at a single-point concentration. Therefore, it is proposed that the technique, in conjunction with the extracellular β-haematin assay, will be essential for triaging compounds for further dose-response evaluation of haemozoin formation – towards determining the actual mechanism of action in the cell. Moreover, there is a need to supplement the previously reported *in silico* screening methods[182,190] designed to discover new β-haematin inhibitors (Chapter 3). This is significant since such models generate many compounds that are seldom evaluated for mechanistic determinations in the cell. Therefore, since the currently proposed prediction will be primarily made intracellularly by quantifying haem species at a single dose concentration, the results from this assay will be valid, irrespective of whether haemozoin inhibition is desired. As previously alluded to in Chapters 4 and 5, when new (non-haemozoin-based) targets are sought, this haem fractionation method will allow researchers to avoid further development of compounds that inhibit haemozoin formation. Furthermore, this medium high-throughput assay will also help reduce false positives generated from the β-haematin assay, thus leading to the attrition of compounds claimed to be haemozoin inhibitors based solely on their β-haematin inhibition.

Notably, this high-throughput method needs to address whether, at the tested concentration, the experimental compound causes any statistically significant increase in unsequestered haem compared to the untreated control. Therefore, this method will be a qualitative intracellular predictive tool for haemozoin inhibition in medium high-throughput screening since it is performed at only one concentration. Thus, it will differ from a quantitative high-throughput screening (qHTS) approach that profiles many compounds in a dose-response format.[240] The four-compound dose-response assay discussed in Chapter 5 will have to be subsequently performed to determine the actual MoA in *P. falciparum*.

6.2. Materials and methods

The materials, sample preparations and culturing techniques used in this chapter were described earlier in Chapter 2. The HPLC detection, sample analysis and fractionation

procedure to recover the cellular haem species are detailed in Chapter 4. This section focuses on the plate setup with all the compounds, which is discussed in further detail.

Briefly, the 33-compound medium high-throughput single-point haem quantification assay was performed similarly to the four-compound assay described in Chapter 5, with only minor changes in the assay plate setup. Likewise, for the high-throughput assay plate setup, early ring-staged (0-6 h) sorbitol synchronised parasite cultures at 5% parasitemia and 2% RBC haematocrit were prepared (49 mL medium + 1 mL pellet) in complete medium. Again, aliquots of 500 µL from the cell culture were added to each of the 72 test wells of a 96-deep-well round bottom plate. Contrary to the four-compound 96-well assay, here 33 compounds were investigated simultaneously at a single concentration. These 33 test compounds were prepared at 2x each compound's IC_{50} value in control medium – as discussed in Chapter 2 (Section 2.2.7.), and 20 µL of these individual concentrations was added to the plate to afford a final in-well volume of 520 µL. A 2x IC_{50} concentration was chosen for experimental testing because it is two-fold above the minimum required inhibitory concentration to confer parasiticidal activity. Also, it is expected that if haemozoin inhibition is not observed at this concentration, then the compound can be excluded as exerting its parasiticidal effects by haemozoin inhibition. Moreso, this concentration was expected to result in minimal sample losses as a direct effect of parasite death. Each compound was tested in duplicate, with the final concentration in each well at 2x IC_{50}. After this, the 96-well assay plates were incubated for 30 h at 37°C in a gas chamber with 3% O_2, 4% CO_2 and 93% N_2. Figure 6.1 shows the setup of the high-throughput single-point assay.

	2x IC_{50} Dosing Concentrations										
Control	CQ (1)	AM (2)	LPT (3)	LOM (4)	5	6	7	8	9	THC (10)	NIL (11)
Control	CQ (1)	AM (2)	LPT (3)	LOM (4)	5	6	7	8	9	THC (10)	NIL (11)
Control	PYR (12)	MQ (13)	LUM (14)	15	16	17	18	19	20	21	22
Control	PYR (12)	MQ (13)	LUM (14)	15	16	17	18	19	20	21	22
Control	23	24	25	26	27	28	29	30	31	32	33
Control	23	24	25	26	27	28	29	30	31	32	33
Cal	Cal	Cal	Cal	Cal	Cal	Cal	Cal	Cal	Cal	Cal	Cal
Cal	Cal	Cal	Cal	empty	empty	empty	empty	empty	empty	Ref std	Ref std

Figure 6.1: The 33-compound high-throughput haem fractionation assay plate setup for the simultaneous investigation of 33 compounds. These were dosed at 2x IC_{50} concentration using the NF54 strain of *P. falciparum*. The assay was performed in duplicate. Key: Blank = solvents without any analyte, Cal 1–8 = calibration curve standards, Control = iRBC with no drug, and Ref std = 1000 ng/mL of the haem-imidazole$_2$ complex. The compounds are separated into different colours for visualisation of the various groups tested: mustard = Positive controls (1-9), yellow = negative controls (10-14), and grey = experimental test compounds (15-33). Abbreviations: AQ = amodiaquine, CQ = chloroquine, LPT = lapatinib, LOM = lomitapide, LUM = lumefantrine, MQ = mefloquine, NIL = nilvadipine, PYR = pyrimethamine, and THC = delta-9-tetrahydrocannabinol.

After incubation, the excess culture medium was carefully aspirated without disturbing the layer of cells on the bottom of the plate, as mentioned in previous chapters. A Giemsa-stained blood smear of only the control wells was prepared on a glass slide to confirm the correct erythrocytic stage of the parasites. The fractionation procedure, flow cytometry cell counting and HPLC analysis followed was described in Chapters 4 and 5 with no further modifications. The quantification of haem Fe per cell was also performed as described in Chapter 5. Likewise, a two-tailed t-test (95% CI) was used and is displayed on graphs using an asterisk (*$p < 0.05$). Thus, the significant indicator for the high-throughput graphs is meant to denote mean differences between the tested concentration (2x IC_{50}) against the control, irrespective of whether the significance went below $p = 0.01$ or $p = 0.001$. This is especially given that the interest for this work was to report if the p-value from the t-test was less than 0.05, so representing statistically significant results.

Lastly, it was decided that only the two major haem species, haem and haemozoin, would be analysed in this assay. This decision was driven by the fact that the haemoglobin fraction was unlikely to offer any insightful information for this method. Figure 6.2 (below) illustrates the flow chart for the high-throughput haem quantification assay.

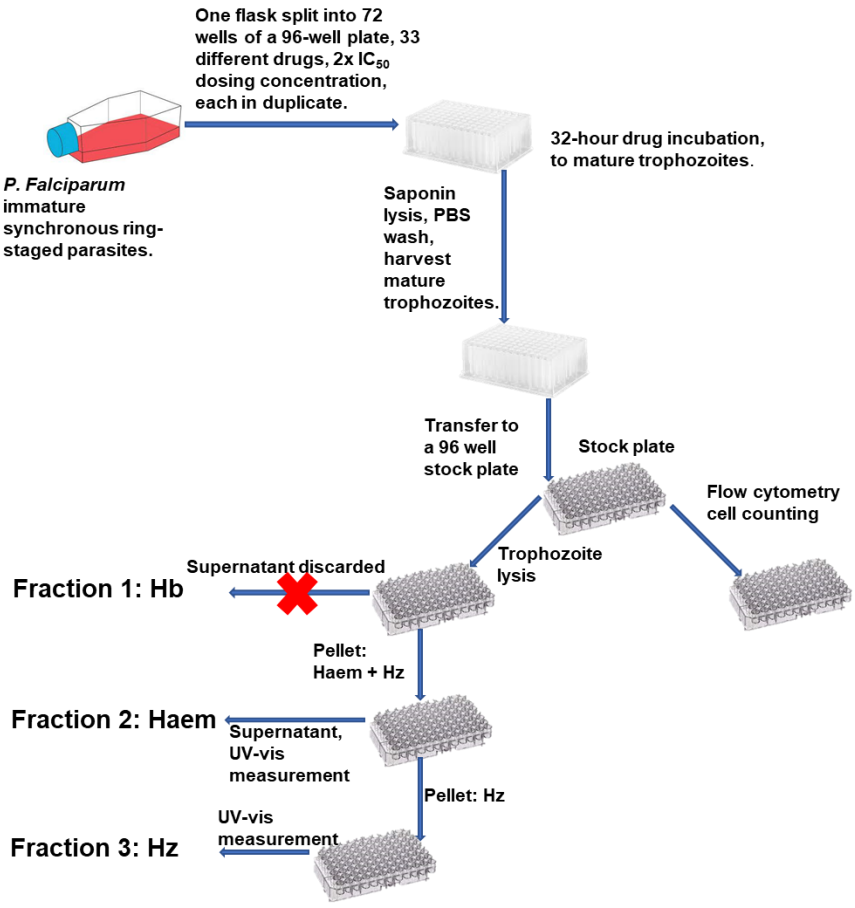

Figure 6.2: A flow chart detailing the steps used in this high-throughput assay during the setup and the selective fractionation procedure of all the major haem species of *P. falciparum*.

6.3. Results and discussion

The 33-compound high-throughput HPLC-DAD 96-well assay was validated in NF54 CQS *P. falciparum* parasites. It was validated using nine positive controls, five negative controls and 19 test compounds generated from various projects of UCT research groups. The positive controls used included CQ (**1**), AQ (**2**), LTP (**3**), LOM (**4**), and five other inhibitors (**5**-**9**) that were previously published and reported in Chapter 7.[160,180,187,190] These five other inhibitors belong to the following scaffolds: quinazoline (**5**), triarylimidazole (**6**), benzamide (**7**), benzothiazole (**8**), and benzimidazole (**9**). The negative controls used for validation included THC (**10**), nilvadipine (**11**), PYR (**12**), MQ (**13**), and LUM (**14**). All the negative controls had previously been shown not to inhibit haemozoin formation in the parasite using the pyridine-based assay.[143,144,212] Of the non-haemozoin inhibitors, THC has been previously reported in Chapter 3 and the literature, while nilvadipine has not previously been reported.[212] Lastly, 19 test compounds were solicited from different research groups at UCT. Their identities and biological data will not be revealed since they are part of ongoing projects and are subject to intellectual property (IP) protection. However, permission was granted to report on their haem fractionation profiles to demonstrate the application of the current method. For clarity, the compounds will be labelled **1–33** as follows: positive controls (**1-9**), negative controls (**10-14**), and test compounds (**15-33**).

The aim of adapting the method to a high-throughput mode is primarily for cases when larger sets of β-haematin inhibitors need to be evaluated for their ability to inhibit haemozoin in the cell. Therefore, a workflow that allows for compounds to be prioritised for full-dose response cell fractionation is required. Of the 19 test compounds, eight compounds (**25**-**33**) were novel molecules acquired from an online database which allows access to physical compounds libraries for screening. This was akin to the work reported in Chapter 3, but with some modification. The compounds were obtained for high-throughput screening, first in the single-point β-haematin assay.[189] Active compounds (showing >50% inhibition) were subjected to the full dose-response β-haematin assay[73] for IC_{50} determinations. Then the most active compounds (β-haematin activity <500 µM) were tested for antiplasmodium activity using the pLDH assay. Thereafter, all the compounds acquired from the database were subjected to *in silico* structure-based virtual screening (SBVS) via docking to the β-haematin crystal using the established virtual screening tools[182,190,212] used to select the compounds reported in Chapter 3. These results provided the proof-of-concept for the workflow and were used to further evaluate the effectiveness of the SBVS methods in predicting β-haematin inhibitors. For the current work, the most active compounds in both the β-haematin assay and pLDH assay were selected for evaluation with the 33-compound medium to high throughput assay. Following the single-point screening, selected compounds were prioritised for the four-compound 96-

well cell fractionation assay, allowing the demonstration of their haemozoin formation interfering ability in the parasite. This is because the chosen compounds were predicted active by the *in vitro* β-haematin assay and active or inactive in the single-point 96-well method. These data provided the proof-of-concept for the application of the developed HPLC-DAD analytical assays.

The crucial question to be answered by the high-throughput method is whether there is a significant increase in haem Fe (fg/cell) in the cell relative to the untreated control at the tested concentration. As discussed in the method section above, the 2x IC_{50} concentration was chosen because it is two-fold above the minimum required inhibitory concentration to confer parasiticidal activity. Thus, if haemozoin inhibition is not observed at the 2x IC_{50}, the compound does not exert its toxic effects through the increase in unsequestered haem. This is because the requirement for haemozoin inhibition necessitates the correlation between unsequestered haem and parasite death, and that the overlay of the parasite survival curve with the haem Fe curve intersect at 50% parasite survival.[143,145] Moreover, this was a concentration at which it was predicted that minimum loss of parasite cells would occur because of cell death caused by the long incubation periods with the compounds.

6.3.1. Validation with positive controls

The positive control compounds were all compounds that have been previously shown to inhibit haemozoin formation. All their respective quantified haem species profiles at 2x IC_{50} compound-treated parasites are reported in Figure 6.3 (A-D). The partial dose response carried out at the single-point concentration showed a correlated increase in percentage haem, followed by a subsequent subtle but significant decrease in percentage haemozoin. This was expected since all the current positive control compounds are known inhibitors. Subsequently, using cell counts determined by flow cytometry to quantify the amount of haem Fe per trophozoite at each dose of the individual compound showed a statistically distinguished increase compared to the untreated control. Similarly, a significant concomitant decline in haemozoin Fe was observed. Thus, the current results confirmed the method's ability to identify haemozoin inhibitors at the single-point concentration.

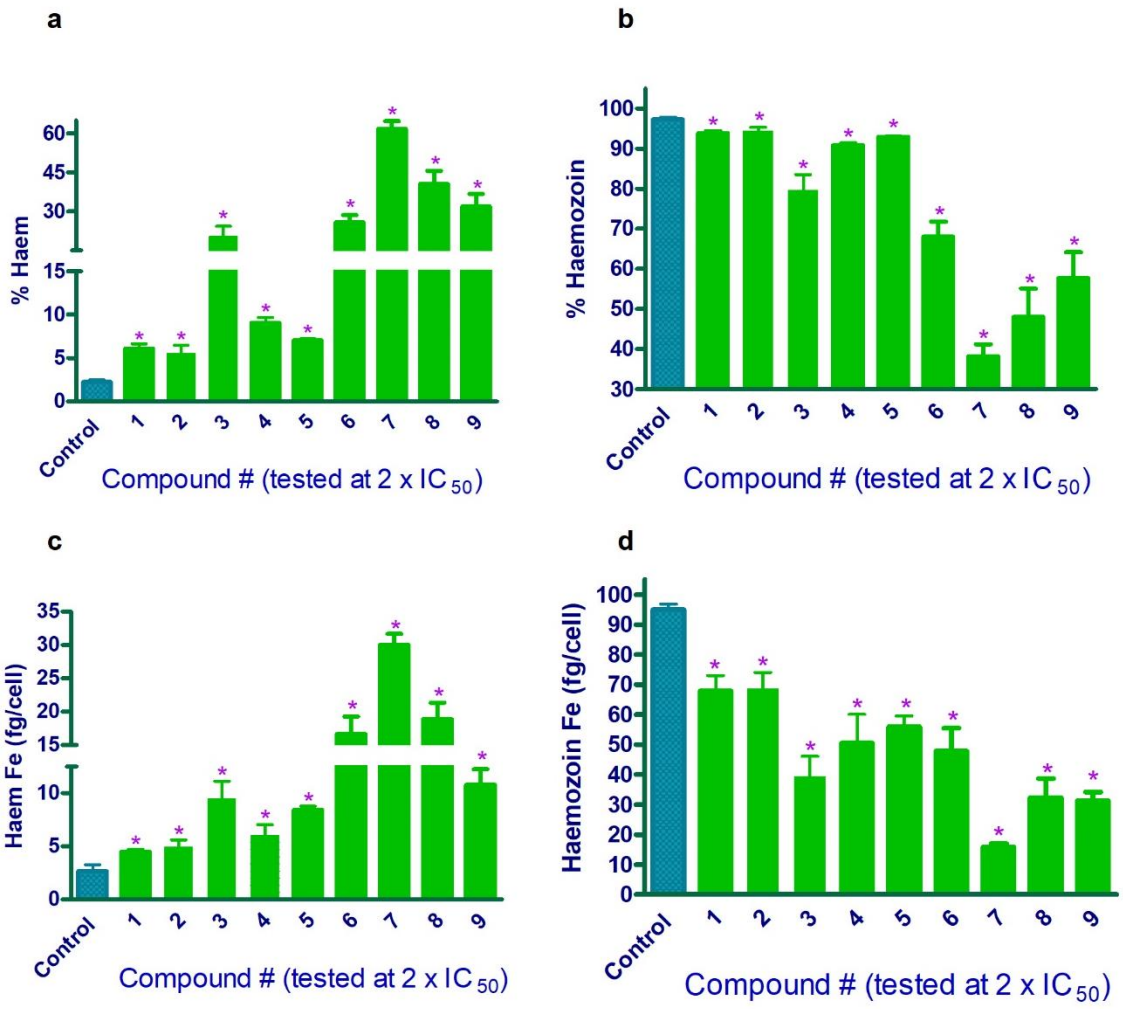

Figure 6.3: The high-throughput haem fractionation profiles of *P. falciparum* trophozoites treated with positive control compounds (1-9) at 2x IC_{50} concentration for each compound. Percentages of haem (a) and haemozoin (b), as well as the amount of haem Fe (c) and haemozoin Fe (d) at the 2x IC_{50} for all compounds, are shown. Control bar = haem species in untreated cells. Statistical significance was calculated relative to the control using the two-tailed t-test at a 95% confidence interval; this is expressed as an asterisk: * $p < 0.05$. These significant indicators were irrespective of whether the significance went below $p = 0.01$. Thus, the interest was to report whether the p-value from the t-test was less than 0.05. Data represent the mean ± SEM from two repeat experiments.

6.3.2. Validation with negative controls

The new method was also applied to compounds used as negative controls. All negative controls reported here were previously shown not to inhibit haemozoin formation in the parasite.[143,144,212] PYR (**12**) does not even confer any interactions with the β-haematin crystal.[73] As shown in Figure 6.4 (A-D), all compounds displayed a dose-dependent increase in percentage haem and an insignificant decrease in percentage haemozoin. However, as observed in the case of the percentage haem values, these results contradict previous observations (Chapter 5) at the individual concentrations. Therefore, it is believed that these

minor but significant increases may be treated as experimental-related errors, especially since there were no observed statistical increases in haem Fe which remained constant for all compounds (Figure 6.4c). Therefore, this indicates the importance of looking at haem Fe (fg/cell) to indisputably identify a wide range of haemozoin inhibitors in medium high-throughput mode. Furthermore, this phenomenon is clearly articulated by Combrinck *et al.* with respect to atovaquone.[143] Nonetheless, a significant decline in haemozoin Fe was observed. As previously explained in Chapters 3 and 5, this is attributable to the decrease in total haem Fe in the parasite at the treated concentrations rather than because of inhibition in haemozoin formation. Unsurprisingly, the method demonstrated that the negative control compounds did not inhibit haemozoin formation at the tested concentration, as shown by the lack of any significant increase in their haem Fe profiles.

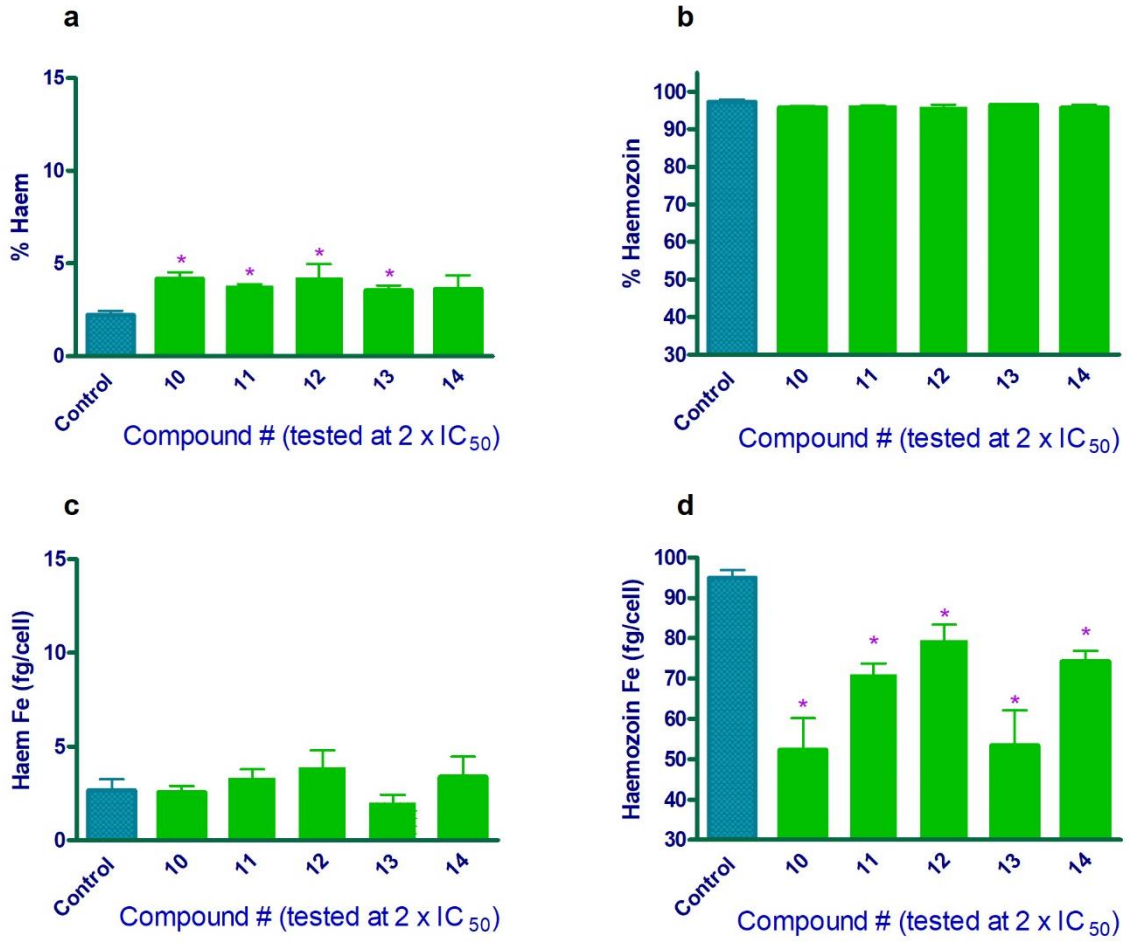

Figure 6.4: *P. falciparum* intracellular haem species of negative control compounds (10-14). These were generated using the 96-well 33-compound high-throughput method. The percentage and values of each of the two major haem species at the 2x IC_{50} are shown: haem (a), haemozoin (b), haem Fe (c) and haemozoin Fe (d). Control = untreated cells. Statistical significance was calculated relative to the control using the two-tailed t-test at a 95% confidence interval; this is expressed as an asterisk: * $p < 0.05$. The shown significant indicators indicate differences between means and not the significance level. Data represent the mean ± SEM from two repeat experiments.

6.3.3. Using the 96-well medium high-throughput method on experimental test compounds

The method was subsequently applied to 19 test compounds sourced from various research groups at UCT. Importantly, these compounds had never been tested for haemozoin inhibition in the malaria parasite. However, these did show β-haematin inhibition activity when tested with the NP-40 detergent-mediated assay[73]. Thus, the compounds were selected based primarily on their β-haematin inhibition activity and NF54 CQS parasiticidal activity as a second factor. The aim of including them in the assay was to allow for more intracellular haem data to be generated qualitatively for all the active compounds in order to enrich the selection of compounds for complete dose-response determinations in the 96-well four-compound method. This is because it was established from previous observations that it is insufficient to demonstrate only β-haematin inhibition as an exact MoA, as β-haematin predictions serve as a qualitative MoA determinant.[144,145,212]

The haem speciation profiles for compounds **15–24** and **25–33** are shown in Figures 6.5 and 6.6, respectively. These were separated into different figures for presentation purposes only. Experimental work and analyses relating to these compounds were performed simultaneously with positive and negative controls. All compounds, except **15,** showed a dose-dependent increase in percentage haem. However, only **15** and **16** showed insignificant decreases in the percentage of haemozoin. Furthermore, when quantitatively determining haem Fe per trophozoite, compounds **15**, **16**, **21**, **24**, **25** and **26** displayed no significant increase in unsequestered haem (haem Fe) relative to the control (untreated parasites). This observation demonstrates the importance of determining haem Fe per cell, as relying solely on the percentage results could be misleading. The observations on the five compounds were reminiscent of the behaviour of non-haemozoin inhibitors. Thus, compounds **15**, **16**, **21**, **24**, **25** and **26** do not exert their parasiticidal activity in the parasite *via* the haemozoin inhibition MoA. Intriguingly, all other compounds were found to increase the haem Fe concentration significantly, thus, highlighting their haemozoin-inhibiting potential in *P. falciparum*.

Furthermore, it was observed that the haemozoin Fe concentrations decreased substantially for all the respective compounds at the tested concentration – except for **16**. This suggests that as a non-haemozoin inhibitor, **16** is reminiscent of a compound with no secondary effects on the total haem Fe, especially downstream in the pathway, like interfering with the trafficking of Hb or its digestion. Nevertheless, the unprecedented hit rate of haemozoin inhibitors discovered was favourable. This stood at a remarkable ~68% (13 of 19) of all the tested compounds. This also indirectly revealed the ability of the β-haematin assay to predict haemozoin formation in the parasite. It also demonstrated the significance of having a method

that quantifies these predictions in the cell, further supporting and adding confidence to the predicted data. An exemplary display of this is with compounds **25**–**33** (78% hit rate), which were specifically acquired from an online database for β-haematin high-throughput screening to discover novel compounds that inhibit haemozoin formation. Applying all the above techniques – β-haematin assay, pLDH assay, and the 33-compound 96-well assay – further illustrates the versatility and importance of these tools in discovering new antiplasmodium compounds.

The data generated here is crucial since, under standard techniques, many of these compounds would never have been tested for inhibition in the parasite, because it would be time-consuming and costly – especially with a vast library of compounds. There would still be uncertainty about whether these even inhibit haemozoin formation in the cell. What is evident with the help of the current data at the concentrations tested, is that the haemozoin-inhibiting test compounds enter the digestive vacuole to interact with the haemozoin crystal. Thus, these results provide crucial information on selecting compounds to be tested using the full-dose response 96-well four-compound assay for conclusive MoA determinations.

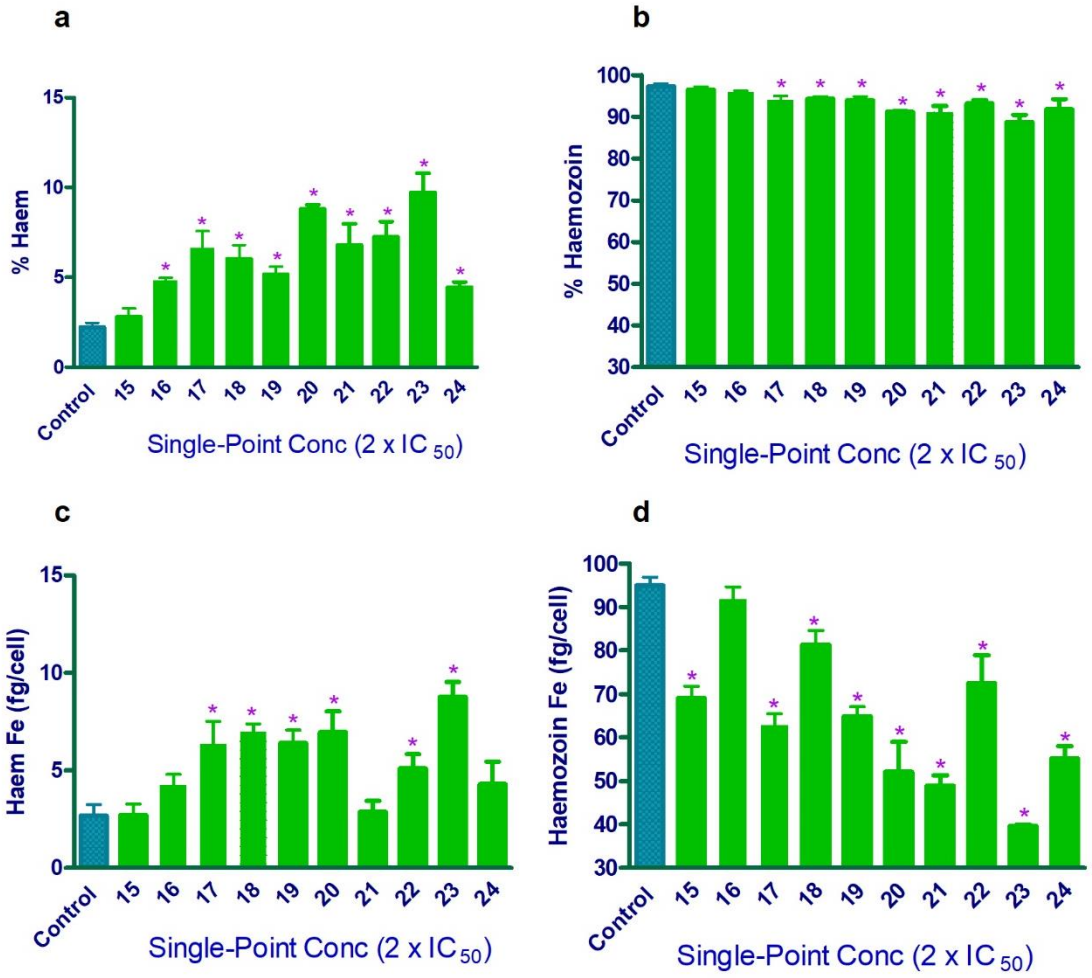

Figure 6.5: Haem fractionation profiles for the ten experimental compounds, 15–24, at 2x IC_{50} parasite dosing concentration. Each of the following plots for each compound is shown at the 2x IC_{50}: (a) %haem, (b) %haemozoin, (c) amount haem Fe, and (d) the amount haemozoin Fe. Control bar = untreated parasite cells. Statistical significance at each concentration was calculated relative to the control using the unpaired two-tailed t-test at a 95% confidence interval; this is expressed as an asterisk above each bar: * $p < 0.05$. This was irrespective of the level of significance. Data represent the mean ± SEM from two repeat experiments.

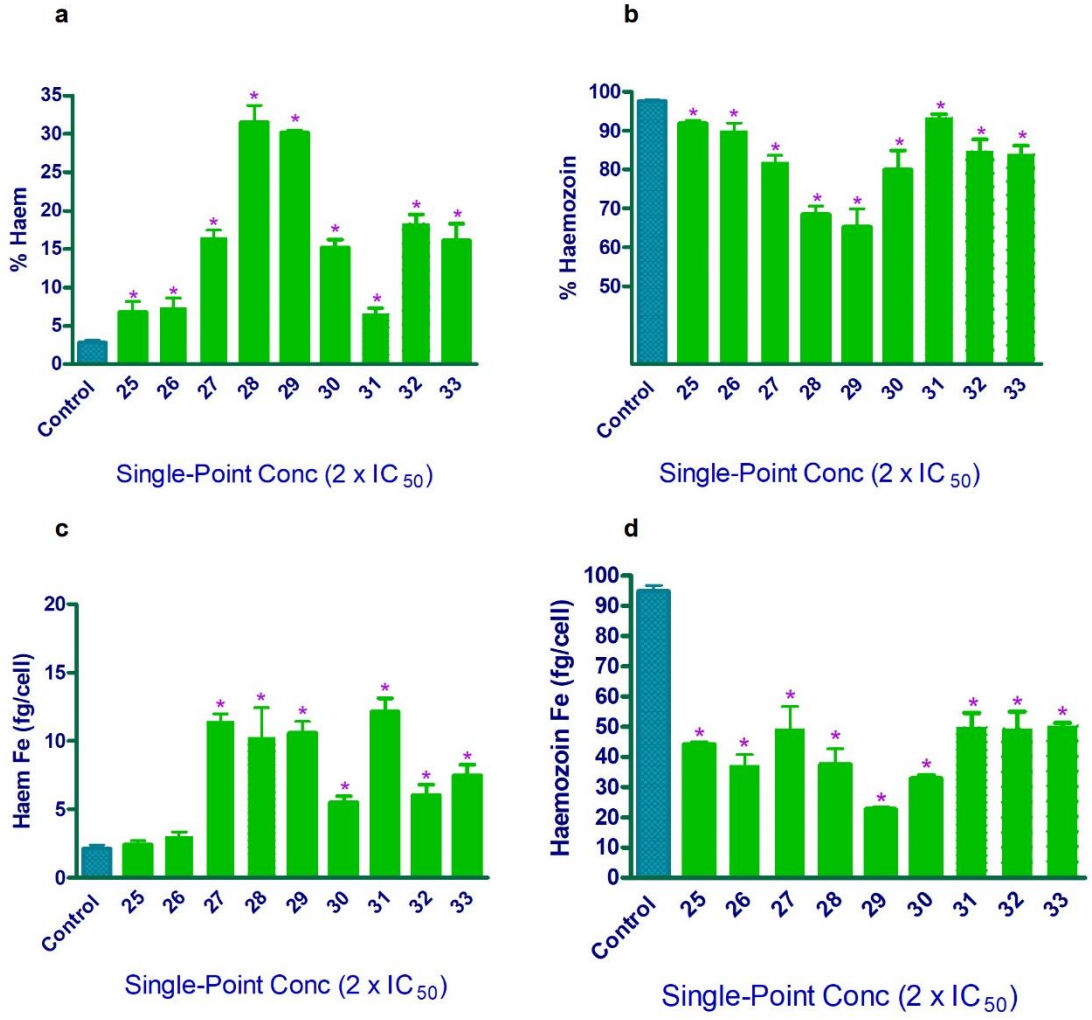

Figure 6.6: The haem fractionation profiles of eight experimental compounds (25–33) continued from Figure 6.5 above. For each compound, the plots of the two major haem species are represented as follows: percentages of haem (a) and haemozoin (b), the amount of haem Fe (c) and haemozoin Fe (d) at the 2x IC_{50} value. Control = untreated cells. Statistical significance was calculated relative to the control using the two-tailed t-test at a 95% confidence interval; this is expressed as an asterisk: * $p < 0.05$. Data represent the mean ± SEM from two repeat experiments.

6.4. Applying the 96-well HPLC-DAD method to test compounds 26, 27, 31, and 32

Subsequent to the above data, compounds **26**, **27**, **31** and **32** were selected for full-dose response mechanistic evaluation in the 96-well four-compound method. These were selected based on multiple factors, including parasiticidal activities and structure variabilities. More importantly, these were the group of compounds that had been predicted *in silico* and *in vitro* using the NP-40 detergent-mediated β-haematin assay to inhibit the formation of haemozoin in the parasite. Therefore, it was essential to establish whether these compounds inhibited haemozoin formation as initially predicted. The non-inhibiting compound **26** (as predicted by

the 33-compound high-throughput cell assay) was solely chosen to demonstrate the accuracy of the high-throughput technique for discriminating inhibitors from non-inhibitors. Again, the selected compounds were those to which permission was granted for further investigations.

The haem fractionation results for the four compounds are shown in Figure 6.7. The profiles for Compound **26** (Figure 6.7a) showed no significant increase in haem at the 2x IC_{50} concentration and lower. However, the highest doses (2.5x and 3x IC_{50}) showed a distinguishable increase in unsequestered haem. These considerable increases observed at these high dosages are unlikely to be a result of classical haemozoin inhibition (discussed in Chapter 1; Section 1.8.4) but could be because of other factors in the parasite at these high dosing concentrations. Characteristically, there is no correlation between the decrease in percentage parasite survival and the observed increase in unsequestered haem as shown in the overlay of the parasite survival curve and haem Fe concentrations (Figure 6.7a-3). Instead, the increase in haem Fe for **26** occurs only at higher concentrations above the minimum concentration required to inhibit parasite growth, which demonstrates that this is as a result of secondary effects. For example, it could be argued that since the parasite is in distress because of the compound's parasiticidal toxicity, there is probable cause to allow for an influx of the compound into the DV at these high concentrations. This is because it is presumed that the DV membrane loses its integrity and becomes highly permeable. Hence, this resultant influx is believed to allow direct interaction between the compound and haemozoin, thus causing increased levels in unsequestered haem. This then becomes similar to the conditions observed with the β-haematin assay when predicting inhibition. Therefore, it can be concluded with certainty that the MoA of compound **26** is not *via* haemozoin formation, as correctly predicted by the 33-compound medium high-throughput assay above. However, further investigations are required to establish the actual cause of the minor significant increase in haem Fe at the higher doses.

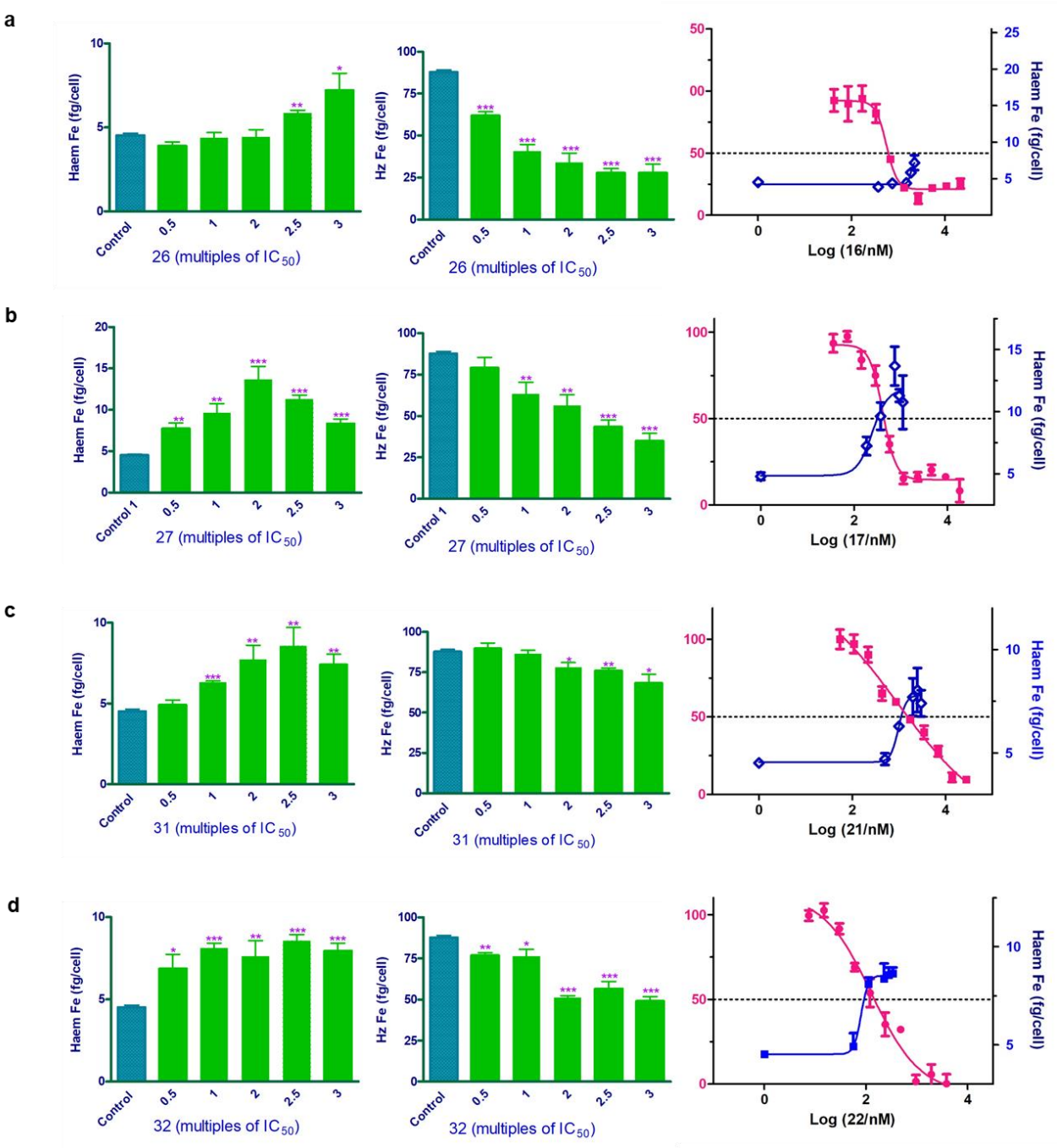

Figure 6.7: The unsequestered haem (left panels; a-1, b-1, c-1, and d-1), haemozoin (middle panels; a-2, b-2, c-2, and d-2), and the overlay of the parasite survival curve (pLDH assay) and unsequestered haem Fe levels (right panels; a-3, b-3, c-3, and d-3) of compounds **26**, **27**, **31** and **32** treated cells. These fractions are expressed as fg haem iron per trophozoite cell at multiples of their IC_{50} concentrations. Control = untreated cells. Statistical significance was calculated relative to the control using an unpaired two-tailed t-test at a 95% confidence interval; the level of significance is expressed as an asterisk: * $p < 0.05$; ** $p < 0.01$; *** $p < 0.001$. Data represent the mean ± SEM from two repeat experiments.

Unsurprisingly, compounds **27**, **31** and **32** were found to be haemozoin inhibitors. They cause dose-related increases in unsequestered haem that are mirrored by significant declines in haemozoin (Figure 6.7b-d). Furthermore, like the case of CQ, the increases in unsequestered haem concentrations correlate with decreases in parasite survival curves, as shown in their parasite survival curves versus haem Fe curves in Figure 6.7b-d. These results are in line with the observations in the medium high-throughput method, thus confirming the robustness and reliability of this method to discriminate haemozoin inhibitors from non-inhibitors. However, it is important to reiterate that in the high-throughput assay, as in the four-compound assay (Chapter 5), it is essential to look at the fg/cell data rather than the percentage haem data, as mentioned above. Nonetheless, despite the false positive activity of **26** in the β-haematin method, there was still an impressively higher hit rate observed (~78%), as seen in the medium high-throughput method and now with the four-compound method.

Notably, the current study was meant to serve as a proof-of-concept in applying the analytical techniques developed in the Bioinorganic Chemistry and Pharmacokinetic Research Groups (Clinical Pharmacology) at UCT. Although robust and effective, it may be more beneficial in future to perform the high-throughput single-point assay in triplicate – and not duplicate as reported here. This is because at least three experiments were required to reduce variations between data points for statistical analysis and this is not ideal for application in a high-throughput mode scenario. This is important because although the assay reaches an acceptable level of quality, many compromises often need to be made in high-throughput screening implementations based on opposing factors.[238] Thus, in this case the throughput (number of test compounds) of the reported 96-well medium high-throughput HPLC-DAD assay may need to be revised.

6.5. Conclusions

This chapter sought to validate a 96-well medium high-throughput 33-compound assay using nine positive controls, five negative controls, and 19 test compounds. This was validated to simultaneously determine haemozoin inhibition at a single-point dosing concentration (2x IC50) for the 33 compounds. The main objective of the investigation was to develop a robust technique that would allow for the predictive discrimination of haemozoin inhibitors from non-inhibitors for application in medium high-throughput mode. Fundamentally, such determinations were sought for advancing a qualitative intracellular predictive assay for haemozoin inhibition screening at a single concentration.

The high-throughput assay was successfully validated using positive and negative haemozoin controls at the single chosen concentration (2x IC_{50}). All the positive controls were found to inhibit haemozoin formation as expected, and the negative controls did not inhibit the formation of haemozoin. It was also established that to definitively identify haemozoin inhibitors in high-throughput mode, it is necessary to determine haem Fe in fg/cell. This proposition is based on the fact that relying only on percentage haem results can be misleading, as seen with the profiles for the negative controls. Accordingly, these observations highlight the significance of performing cell counting *via* flow cytometry.

Furthermore, the successful identification of novel haemozoin inhibitors was achieved from the 19 investigated test compounds. These were a cohort of compounds still subject to ongoing projects and have never been evaluated for haemozoin inhibition. The hit rate was impressive, with ~68% (13/19) showing positive inhibition. This was relatively higher at 78% (7/9) for the compounds (**25**–**33**) acquired from the high-throughput screening investigation. This study permitted a proof-of-concept on the effectiveness of this assay to determine actual haemozoin inhibition definitively, while also limiting the identification of false positives as real inhibitors. The 96-well four-compound method (Chapter 5) was applied to four compounds of the *in silico* predicted cohort. These included three identified inhibitors (**27**, **31**, and **32**) and one non-inhibitor (**26**) per the 33-compound method results. The negative inhibitor was selected to determine if this compound was indeed an actual non-haemozoin inhibitor or if it was falsely classified by the method. It was established that the three compounds were haemozoin inhibitors, as predicted. The one compound was also a non-haemozoin inhibitor, as indicated before by the high-throughput assay.

In conclusion, it is accepted that although efficient and robust in discriminating between inhibitors and non-inhibitors, the method's limitations should be considered when it is applied. This is because performing the assay in duplicate requires at least three repeats to minimise variance between data points for statistical analysis. Consequently, for future use, performing the assay in triplicate is advised. This will allow for the simultaneous evaluation of 22 compounds instead of 33. Nonetheless, this chapter successfully demonstrated the method’s potential for enriching the prediction process intracellularly on whether haemozoin formation is the actual mechanism of action in the cell. This was essential for highlighting the importance of developing high-throughput cell assays in supplementing *in silico* target screening methods in drug discovery and development. However, it is essential to remember that the four-compound dose-response assay (Chapter 5) is still a requirement for conclusive MoA determinations.

Chapter 7: Stage Specificity and Speed of Killing of Haemozoin-inhibiting Compounds

7.1. Introduction

The parasite's haem detoxification pathway presents as a therapeutic target for chloroquine (CQ) and other antimalarials. These antimalarials inhibit the sequestration of Hb-released haem into haemozoin, as discussed in Chapter 3. The resultant increase in unsequestered haem is believed to kill the parasite *via* oxidative stress and membrane disruptions.[165,241] However, the exact mechanism for this remains unclear. There is therefore a need to better understand the overall haem detoxification pathway to aid with target deconvolution specific to changes in cellular haemozoin, irrespective of whether the changes result via its direct inhibition or not.[145] Intriguingly, the levels of unsequestered haem at the IC_{50} value of all haemozoin-inhibiting compounds, are quite variable, as seen in Chapters 3, 5, 6 and other reported work[143,160,161,180] produced by the Bioinorganic Chemistry Research Group at UCT. It has been observed that compounds displaying lower IC_{50} values (more active) produced lower levels of unsequestered haem, while those displaying higher IC_{50} values (less active) resulted in higher levels of unsequestered haem. This therefore raises the issue of the specific mechanism of haem toxicity and the parasiticidal effects exerted by unsequestered haem.

The toxicity of haem in the parasite appears to be compound-specific, as seen in the data presented in earlier chapters. Moreover, it is expected that if unsequestered haem released from the inhibition of haemozoin was solely responsible for parasite death, then the levels of unsequestered haem should be equal at the IC_{50} values of the compounds under study. Openshaw *et al.* proposed that the dose-dependent inhibition of haemozoin formation generates increased levels of unsequestered haem in the form of a compound–haem complex and that it is this unique complex that is responsible for the antimalarial activity observed.[187] Indeed, this suggestion was supported by the earlier work of Chou *et al.,* which determined that the activity of CQ was attributable to a complex formed with haem.[139] This probably suggests that complex formation and possible haem complex redistribution in the parasite food vacuole are compound-specific. Therefore, they may not be distributed to the same compartments, so leading to the observed varying IC_{50} values which would depend on the location of toxicity of the drug–haem complex. Consequently, the observed IC_{50} variance could be highly substantiated since the extent of accumulation in the DV for each compound is expected to be variable.[187] The toxicity of haem would, in any case, have to remain the same if it was solely responsible for parasite death, which is not what was previously observed in the work mentioned above. Therefore, to further investigate whether the haem–inhibitor

complexes were responsible for parasite death, a stage-specific speed of killing mechanism was hypothesised. This is because a haem complex that kills the parasite later in the life cycle would enable Hb digestion, so leading to the accumulation of more haem to form a complex with the inhibiting molecule.[187] The opposite would be observed for fast-acting compounds.

This chapter focuses on the results of a flow cytometry method which used SYBR green I staining (Chapter 2: Section 2.2.8). The study was performed specifically in RBCs infected with ring-staged parasites to determine the stage-specific speed of killing for a selected group of haemozoin-inhibiting compounds. Parasites were incubated with these compounds which were washed out at the following selected washout times: 4, 8, 12, 24 and 48 h, while a 72 h incubation (no washout) served as a control. It was expected that this flow cytometry method could be implemented to help understand the effects of these observed varying unsequestered haem levels in the parasite at different incubation times after invasion.

7.2. Materials and methods

The specific methods and materials for this chapter were discussed in detail in Chapter 2, Section 2.2.8. The figure below (Figure 7.1) summarises the stage-specific speed of killing procedure.

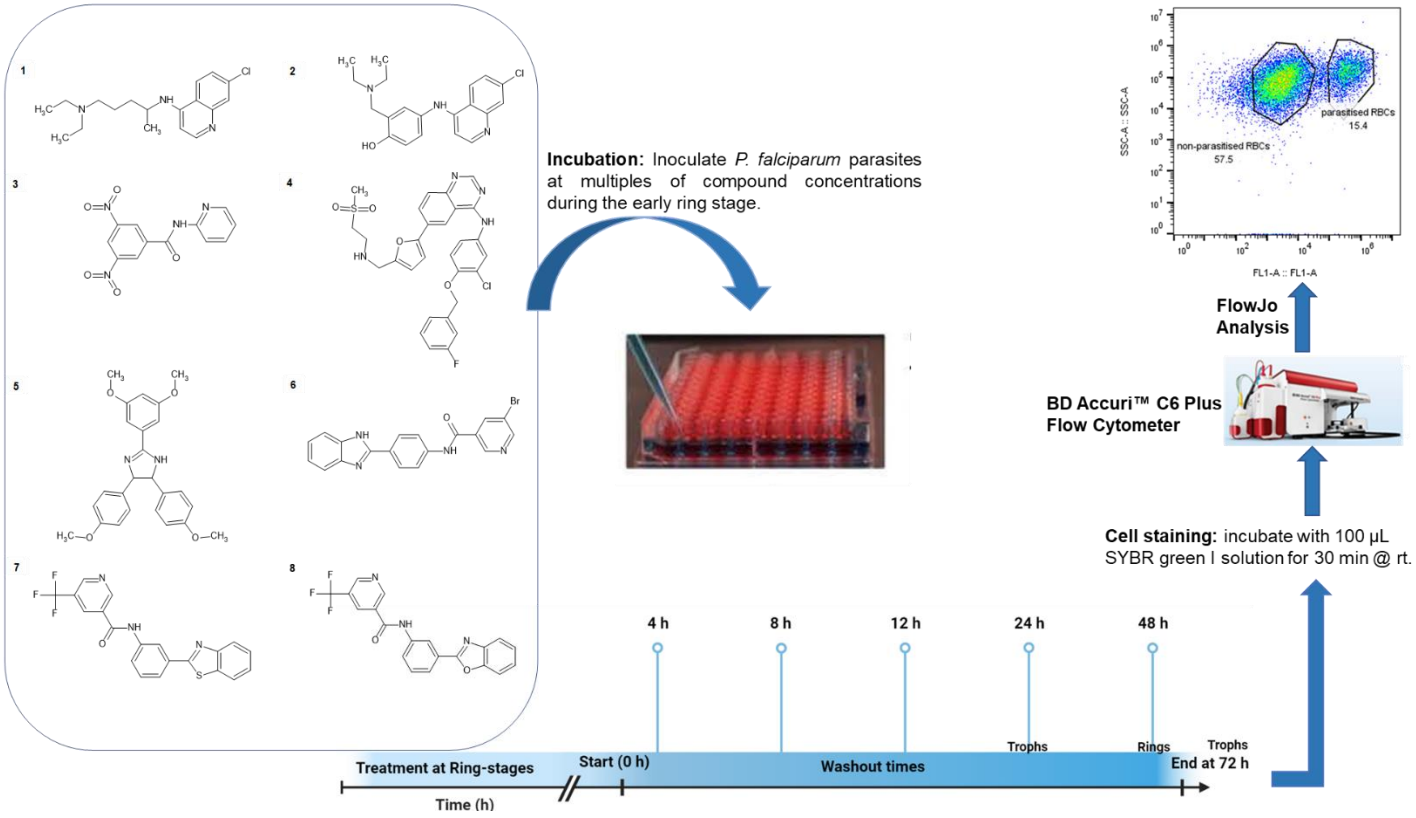

Figure 7.1: A flow diagram illustrating the various steps of the stage-specific speed of killing flow cytometry assay. Compounds 1–8 were used during the early ring inoculation and the selected incubation periods before washouts were observed. Thereafter, a cell staining procedure and flow cytometric detection were carried out before the final analysis using the FlowJo software was performed.

7.2.1. Data analysis and dose-response curve fitting

As briefly described in Chapter 2, the SSC channel of the flow cytometer is representative of the complexity of a cell or event, while the FL1 channel is descriptive of the fluorescent intensity of the SYBR green I dye staining the cell DNA. For data analysis, a dot plot of the SSC channel (y-axis) against the FL1 channel (x-axis) was performed, and a gating procedure was applied for infected RBCs (iRBCs), as shown in Figure 7.2. The iRBCs' gate represents the number of parasitised RBCs per sample analysed. Therefore, the number of events at each of the five tested concentrations (Chapter 2) was used to calculate the percentage parasite survival (%Survival), which was subsequently used for the dose-response curve plot – assuming 100% survival in the untreated samples. From the dose-response curve, a non-linear curve fitting analysis in GraphPad Prism software was performed to estimate the IC_{50} values at each washout time point. The 72 h time point IC_{50} was used as a standard control. In order to visualise the parasiticidal effects of the compounds

at each washout time, histogram plots of the FL1 channel of the iRBC gates were plotted using FlowJo software.

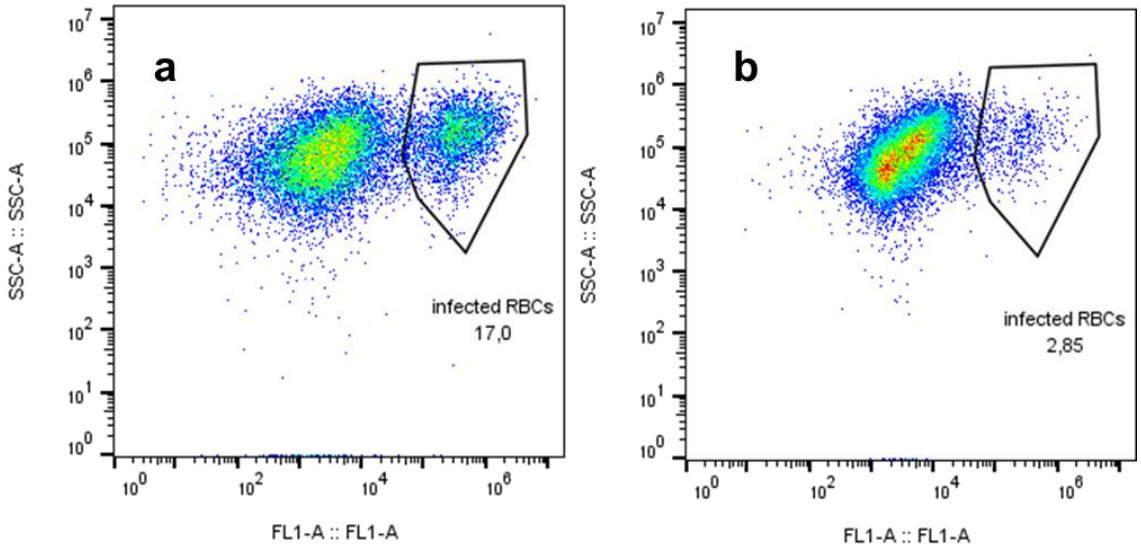

Figure 7.2: Distinct separation of SYBR green I positive infected RBCs and non-infected RBCs using flow cytometry. Maximum excitation wavelength at 497 nm and maximum emission wavelength at 520 nm for SYBR green. The illustration in (a) shows gated untreated infected RBCs, while (b) shows the gated infected RBCs treated with a test compound.

7.3. Results

Eight compounds (Figure 7.3) were selected for investigation of their stage-specific speed of killing against the NF54 CQS strain. The levels of unsequestered haem at the IC_{50} were found to be compound-specific and thus variable among haemozoin inhibitors. It was believed that these variations could be associated with the killing rate of a haem–inhibitor complex (or haem–compound complex), which could help explain the relationship between the levels of haem and the IC_{50} values. The compounds used in this study were selected from the following previously reported haemozoin inhibitors: CQ (**1**), amodiaquine (**2**; AQ), benzamide (**3**), FDA-approved lapatinib (**4**; reported in Chapter 3 as compound **16**), triarylimidazoles (**5**), benzimidazole (**6**), benzothiazole (**7**), and benzoxazole (**8**).[143,160,180,190] Compounds **7** and **8** were first reported by Openshaw *et al.* and led to the current work.[187] The IC_{50} values and levels of unsequestered haem for all compounds are listed in Table 7.1, as well as their β-haematin inhibition activities. As seen (Table 7.1), compounds **1** (CQ) and **2** (AQ), which displayed lower IC_{50} values at 0.019 and 0.020 µM, showed lower unsequestered haem levels at 0.15 and 0.14 fmol/cell, respectively. However, compounds **3** and **8**, which had higher IC_{50} values at 5.0 and 7.5 µM, exhibited higher unsequestered haem levels: 0.86 and 1.1 fmol/cell, respectively. The remaining compounds (**4**, **5**, **6** and **7**) with moderate activities of 0.26, 1.7, 0.41 and 1.3 µM also displayed intermediate haem levels at 0.22, 0.26, 0.23 and 0.25 fmol/cell,

respectively, as reported in Table 7.1. Considering these data, it is apparent that the explanation that the accumulation of unsequestered haem directly kills the parasite may not be entirely accurate – further highlighting the complexity of this pathway.

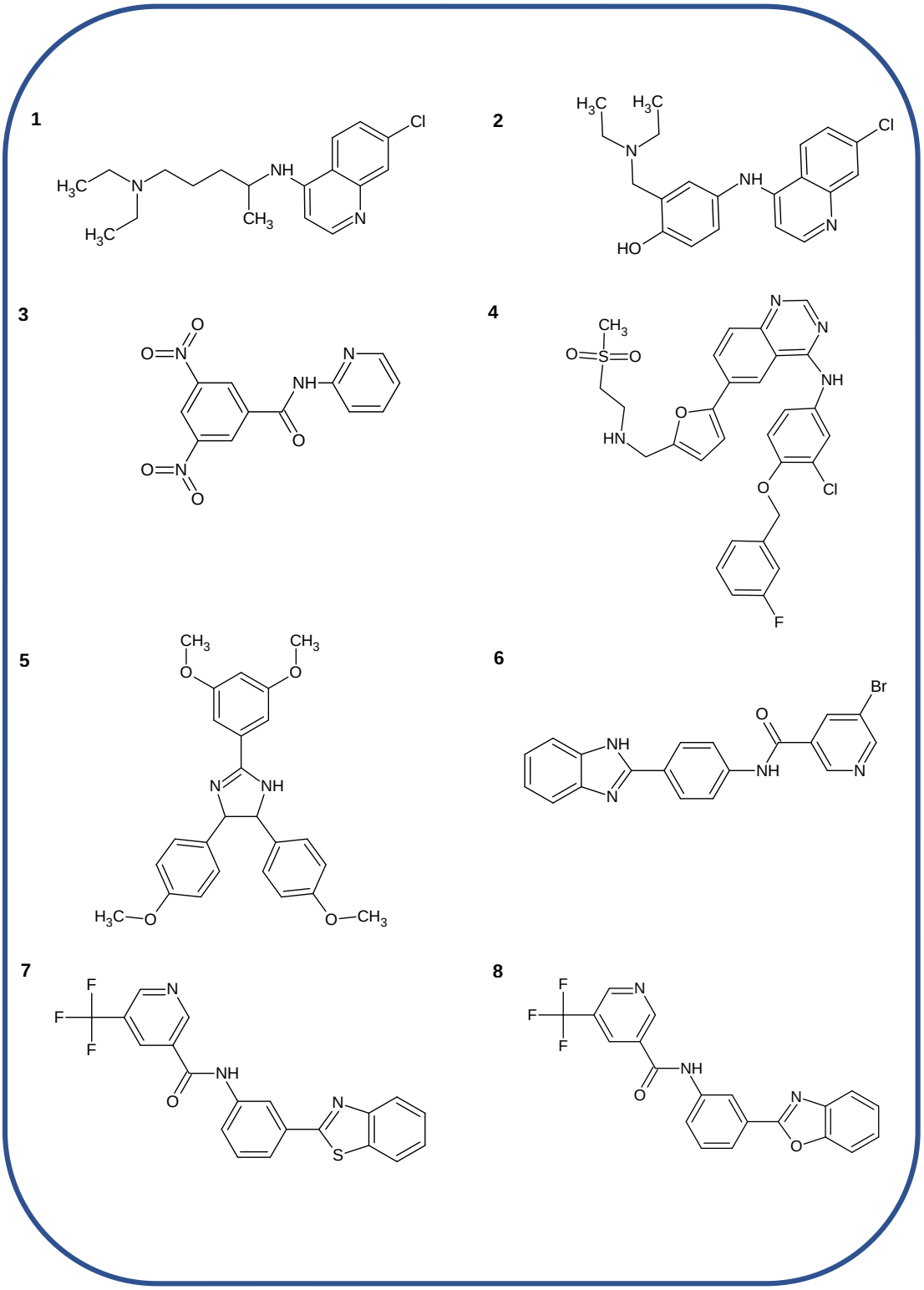

Figure 7.3: The structures of the selected haemozoin formation inhibiting compounds investigated in this study.

Table 7.1: IC_{50} values of each compound following testing in the NF54 CQS strain of *P. falciparum*, β-haematin inhibition IC_{50}s and the unsequestered haem values at the respective IC_{50} concentrations.

Compound	NF54 IC_{50} (μM)	β-haematin IC_{50} (μM)	Unsequestered haem (fmol/cell)
1	0.019 ± 0.004	32 ± 0.5	0.15 ± 0.02
2	0.020 ± 0.007	17 ± 2	0.14 ± 0.02
3	5.0 ± 1	13 ± 1	0.86 ± 0.08
4	0.26 ± 0.07	5.4 ± 0.03	0.22 ± 0.01
5	1.7 ± 0.4	14 ± 0.4	0.26 ± 0.09
6	0.41 ± 0.03	32 ± 1	0.23 ± 0.03
7	1.3 ± 0.01	30 ± 2	0.25 ± 0.03
8	7.5 ± 0.07	22 ± 1	1.1 ± 0.06

The parasiticidal effects of each tested compound at the different incubation times at the IC_{50} concentration were investigated. Since the IC_{50} value is defined as the minimum inhibitory concentration to clear at least 50% of the parasite population, it was expected that this parameter could be used to measure the effectiveness of the compounds over the various incubation periods. This is because it was believed that during the specific incubation time (or period) at which a specific compound was efficacious, the parasite clearance should be at least half or less (≤ 50%) in comparison to the control parasites – thus resulting in a close estimation of the actual IC_{50} value as reported in Table 7.1. Accordingly, this would then indicate the estimated time taken for the compound to exert its parasiticidal effects in the parasite. As mentioned in the data analysis section above, histogram plots of the events in the FL1 channel were plotted to visualise the parasiticidal effects (represented by counts on the y-axis and loosely referred to as clearance) of the compounds at each washout time. Figure 7.4 (a-h) shows all the parasiticidal effects of the compounds from times 4 h to 72 h.

For conceptual purposes, compound **1** (Figure 7.4a) is used as an example to explain these observed effects as illustrated in the histogram plots. The representative plots of **1** at the washout times of 4 (blue line) and 8 (orange line) h, show that there are no observed differences in the parasiticidal effects in comparison to the control parasites (red line). This indicates that these incubation periods were insufficient to bring about any parasiticidal effects. However, subsequent incubation periods at 12 (lime green), 24 (green line), 48 (pink line) and 72 (violet line) hours before washing out of **1**, resulted in differences in the observed parasiticidal effects in comparison to the control parasites (red line). Consequently, such observations indicate that **1** certainly exerts its parasiticidal effects between the 8 and 12 h incubation periods. Similar procedural visual deductions were performed for compounds **2**–**8** as illustrated in Figures 7.4b-h, respectively. In general, compounds that produce lower levels of unsequestered haem were observed to exert their parasiticidal effects earlier in the incubation periods as opposed to those that produce very high haem levels. Compound **2**

showed parasiticidal effects as early as 8 h, followed by compounds **1**, **4**, and **5** at 12 h. Compounds **3**, **6**, **7** and **8** had slowed or delayed effects on the parasite, albeit at varying time points. Surprisingly, compounds **6** and **7,** which had intermediately high unsequestered haem levels, displayed delayed toxic effects on the parasite, similar to compound **8** with high unsequestered haem levels.

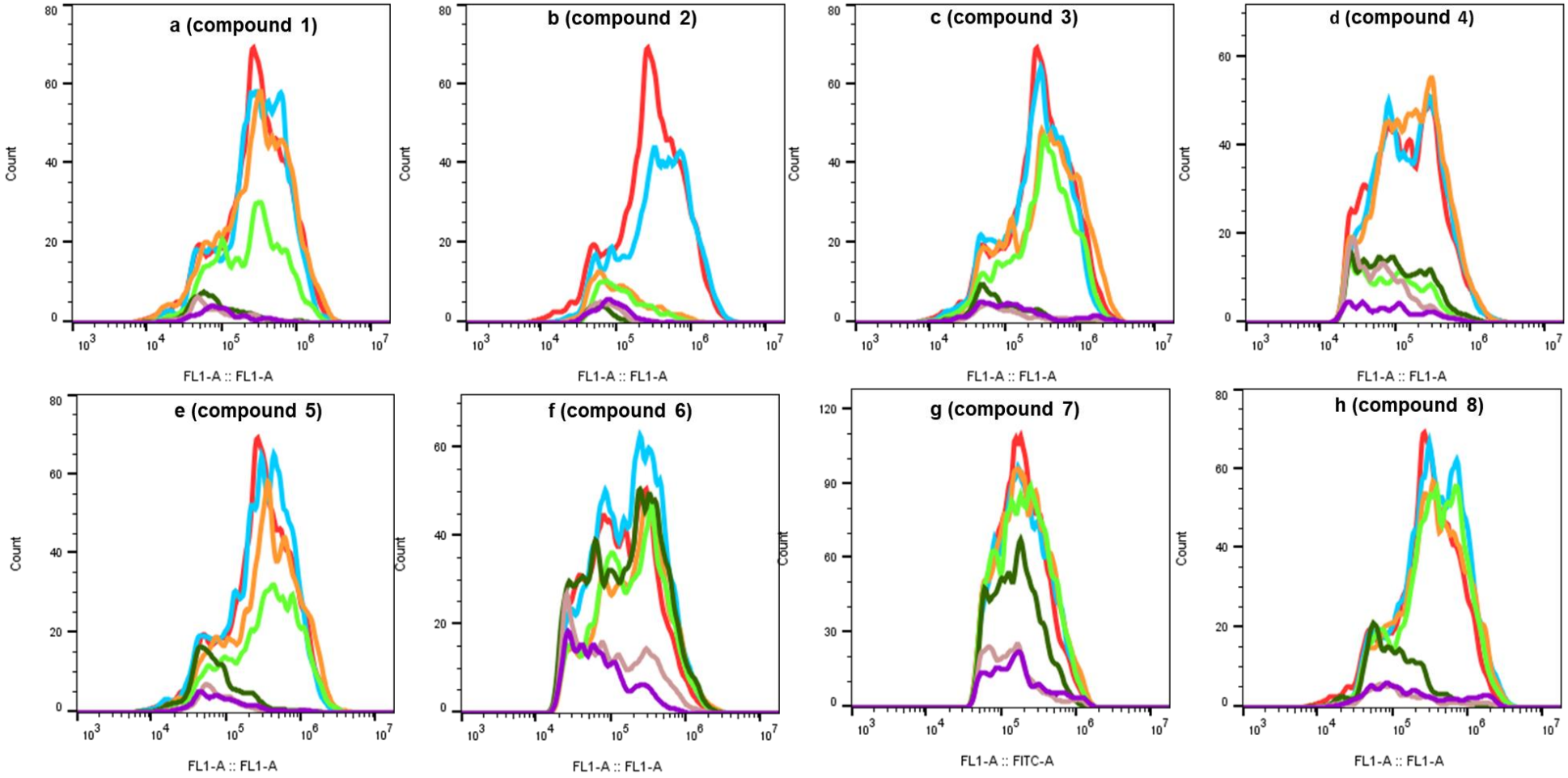

Figure 7.4: Comparing the parasiticidal effects of the eight test compounds: 1 (a), 2 (b), 3 (c), 4 (d), 5 (e), 6 (f), 7 (g), 8 (h). These graphs represent testing at 1x IC_{50} value for each compound over the 72 h period. Each colour plot indicates the specific washout time: 4 h = blue, 8 h = orange, 12 h = lime green, 24 h = green, 48 h = pink, 72 h = violet, and the red plot (line/histogram) represents the untreated control parasite population. All the compounds presented had variable levels of unsequestered haem at the 1x IC_{50} value. Here, each specific histogram plot (or coloured line) visualises the parasiticidal effects of each compound at the indicated washout times. Observed changes in the count (y-axis) for each compound at the washout time (represented by a histogram plot/colour line) characterises the parasiticidal effects (reduction in y-axis count), which can be compared to the untreated parasites (red line).

To quantify the observed effects, the IC_{50}s of each compound were determined at the incubation periods of 4, 8, 12, 24, 48 and 72 h. The observation at a single concentration provides only a partial observation of the presented effects. Therefore, using relative IC_{50} ratios ($IC_{50}^{t}/IC_{50}^{72h}$) as shown in Figure 7.5, it was determined that compound **2** was the fastest acting, followed by **1** with required inoculation times of 8 and 12 h, respectively, to reach their activities. Compounds **4**, **5**, **6** and **7** were intermediately active and attained their effectiveness within 24 h. Compounds **3** and **8** were the slowest, with their activities requiring an incubation period of over 24 h.

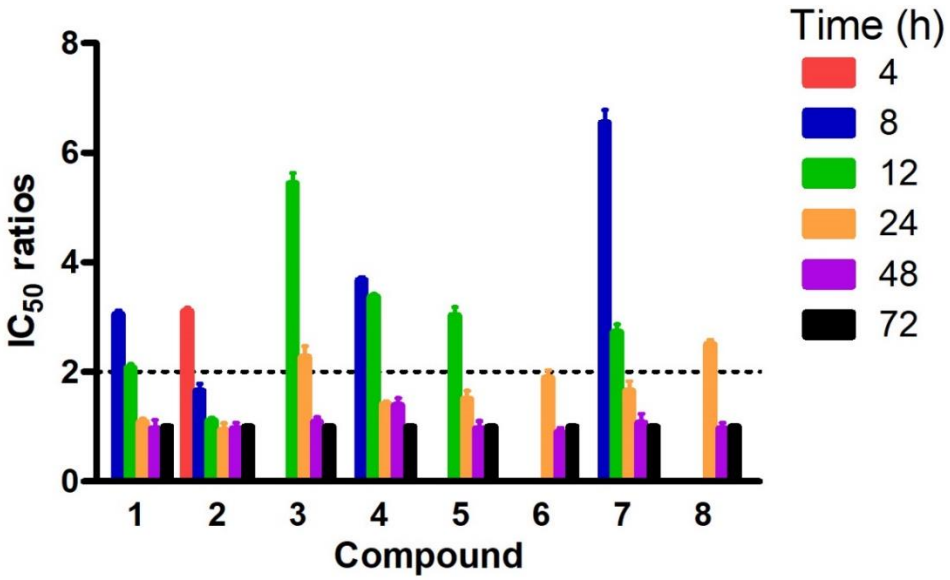

Figure 7.5: Comparisons of the IC_{50} ratio values ($IC_{50}^{t}/IC_{50}^{72h}$) for all compounds at the different washouts (IC_{50}^{t}) against that at no washout (IC_{50}^{72h}). Where no IC_{50} bar is shown at a specific washout time, an IC_{50} value could not be established after the exposure period. The dotted line represents the two-fold differences in IC_{50} concentrations.

During the analysis, an interesting phenomenon was observed. Compounds that produced lower levels of unsequestered haem resulted in lower median fluorescence intensity (MFI) values compared to those with higher levels. This was indicative of the presence of distinct parasite population groups which showed that fast-acting compounds inhibit the maturation of the parasite cells as opposed to slow-acting compounds that allow for maturation into later stages of the life cycle. This is especially meaningful considering that an MFI value is obtained from the fluorescent properties of the parasite's DNA bound to the SYBR green I dye. It is known that mature populations (e.g., trophozoites) contain more DNA content than less mature populations (e.g., rings), which subsequently leads to higher MFI values. To investigate this phenomenon, compounds **2** (fast acting) and **3** (slow acting) were selected to demonstrate these observed effects over the 72 h timeline using the $3xIC_{50}$ for each compound (Figure 7.6). The histogram plots at the various washout times in Figure 7.6a (**2**) show there

is a discernible population shift from the right (higher MFI) to the left (lower MFI) in the curves over time – compared to the untreated control population. This pattern is not observed in Figure 7.6b (**3**), where there appears to be a similar distribution of populations at the various washouts to the untreated control population, albeit with less parasite survival (as seen with the decrease in the count on the y-axis).

To further visualise these observations, a plot of the MFI results of both **2** and **3** was produced over the various incubation periods, as illustrated in Figure 7.6c. These graphs show the distinct discrimination in populations between the fast- and slow-acting haem–inhibitor complexes. This was further confirmed by viewing Giemsa-stained slides of a sample of the treated and untreated cell culture, as shown in Figures 7.6d-f. As predicted, the morphological appearance of the cells from the untreated control trophozoites (Figure 7.6d) were different from the immature ring-stage population observed in parasites treated with compound **2** (Figure 7.6e), and the more mature trophozoites observed in parasites treated with compound **3** (Figure 7.6f). This provides further evidence to support the observed distribution of the MFI values determined in Figure 7.6c. Altogether, these data suggest distinct toxic effects on the parasite by the various haemozoin-inhibiting compounds.

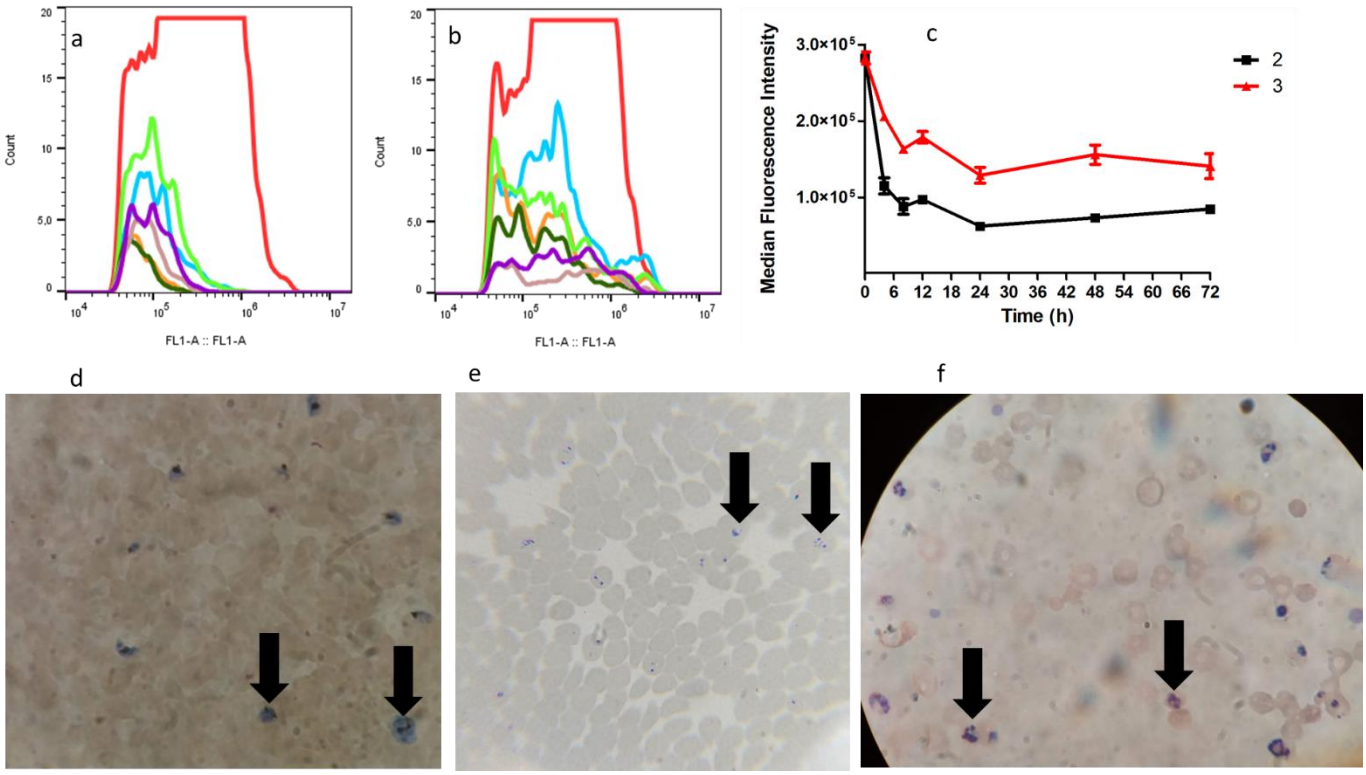

Figure 7.6: The parasiticidal effects of compounds **2** and **3** at 3x IC_{50} value. (a) The observed effects on parasite survival of compound **2** at 3x IC_{50} compared to (b) those of compound **3** over the 72 h period. Each colour plot in a and b indicates a specific washout time: 4 h = blue, 8 h = orange, 12 h = lime green, 24 h = green, 48 h = pink, 72 h = violet, and the red plot = untreated control parasites. (c) The MFI plots of the expected parasite populations as a function of incubation time with the compounds **2** or **3**. The MFI at 0 h is taken from untreated control parasites and serves only as an illustration. (d) Untreated trophozoite-staged parasites to serve as an illustration control at 72 h. (e) Compound **2** treated parasites at 72 h show mostly immature ring-stage parasites. (f) Compound **3** treated parasites at 72 h showed trophozoite-stage parasites, albeit distinct from the untreated trophozoite cells. All 10% Giemsa-stained slides were viewed at 100x magnification on a light microscope.

From the collated data, it was found that the levels of unsequestered haem obtained with each compound could be correlated to the stage-specific speed of killing, given that fast-killing compounds were associated with lower levels of unsequestered haem, and slow killing compounds expressed higher levels of unsequestered haem. To visualise all these three parameters – IC_{50}, unsequestered haem, and speed of killing – we used a three-dimensional scatter plot (bubble chart). In the plot, the IC_{50} value of each compound serves as a function of the size of the individual bubble. As Figure 7.7 shows, the tested compounds can be classified under three related groupings: fast acting, intermediately fast acting, and slow acting. Interestingly, we observed a correlation between all the three parameters as per the initial propositions, that slow-acting compounds present with higher unsequestered haem levels because they have more time to build up haem–inhibitor complexes. It was observed (Figure 7.7) that compounds which produce lower levels of unsequestered haem (**1** and **2**) exerted their parasiticidal effects faster in comparison to those that produce intermediate (**4**, **5**, **6**, and **7**) and higher levels (**3** and **8**) of

unsequestered haem, which were intermediately and slow acting, respectively. This suggests that toxicity to the parasite is haem–inhibitor specific, so providing evidence supporting the previous hypothesis that haem–inhibitor complexes were responsible for parasite death *via* a stage-specific speed of killing mechanism.

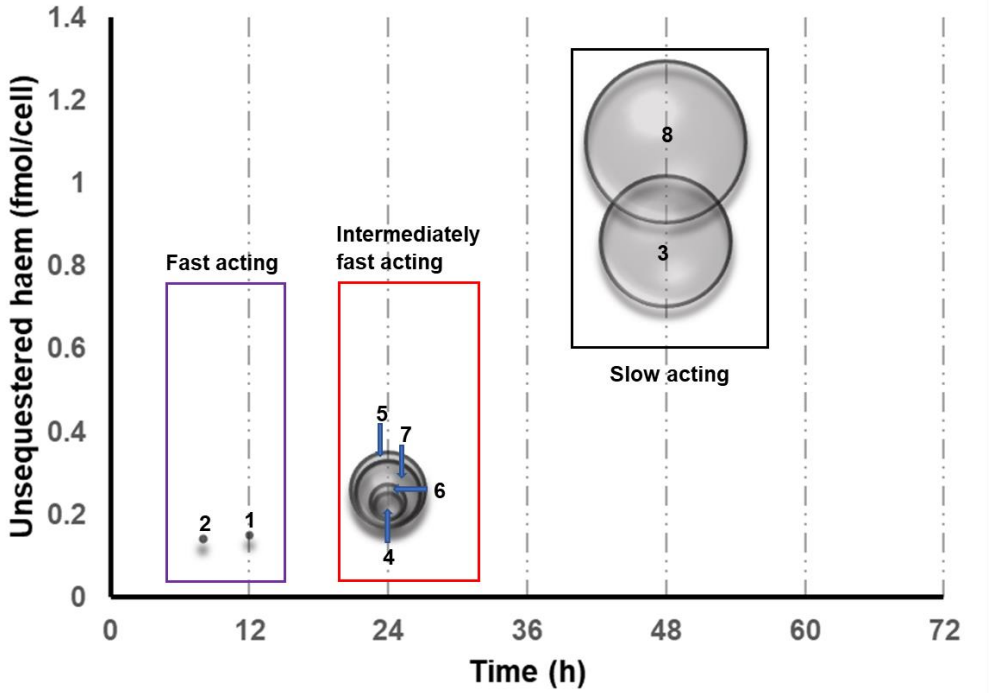

Figure 7.7: A three-dimensional bubble chart of the levels of unexchangeable haem at the 1x IC_{50} concentration as a function of each compound's parasiticidal effects timing. The time shown is that at which the compound was washed out and subsequently reaches 2x IC_{50} activity. The size of the circle is a function of the IC_{50} value for each test compound. A gated rectangular shape provides for grouping the different compounds based on their stage-specific killing speed.

7.4. Discussion

It is clear that the inhibition of haemozoin formation results in a build-up of unsequestered haem, which coincides with parasite death. However, from the data collated in this chapter, it is evident that the toxicity of unsequestered haem appears to be compound-specific. This observation substantiates the research of Chou *et al.* and Kapishnikov *et al*. that haem–inhibitor complexes exist, as observed in the cases with chloroquine and bromoquine, respectively.[139,155] Openshaw *et al*. also demonstrated using electron spectroscopic imaging and Raman microscopy that indeed a haem–inhibitor complex exists in treated parasites.[187] This theory is probable since evidence against the simplest explanation that the build-up of unsequestered haem caused by haemozoin inhibitors kills the parasite directly is continually evolving. Recent findings by the Bioinorganic Research Group at UCT show that the levels of unsequestered haem at the 1x IC_{50} are variable and compound-specific. Therefore, if only

unsequestered haem were responsible for parasite toxicity, it would be expected that haem levels at the IC_{50} values should be the same for each compound, but this is not the case. Instead, the data suggest that the variabilities observed for both unsequestered haem levels and parasiticidal activity for each haem-compound formed complex may be better understood in relation to their stage specificity and speed of killing.

As this chapter showed, the above hypothesis is firstly supported by the observed effects at the various incubation times for each compound at the respective IC_{50}. This data set illustrates a tendency for compounds producing lower unsequestered haem to exert their toxic effects earlier, whereas intermediately high producing haem compounds tend to show ambiguity in the timing of their parasiticidal effects. In the case of CQ (**1**) and AQ (**2**), which present lower unsequestered haem levels, the observed parasiticidal effects were not as surprising since studies by Le Manach *et al.* and Linares *et al.* also found them to be fast acting.[242,243] In contrast, the high producing unsequestered haem complexes effected their parasiticidal toxicities more slowly, as expected. However, the observations of the parasiticidal effects alone remained inconclusive on the exact timing or rate of killing for the compounds. To investigate this phenomenon, a more quantitative approach to the observed effects was applied by determining the IC_{50} values of each compound at the different incubation periods, since the partial observations at a single compound concentration could significantly distort the overall effects. These studies showed that compounds with lower IC_{50} values kill the parasites earlier in the life cycle compared to those with intermediate and higher IC_{50} values. Therefore, fundamentally, this supports the idea of haemozoin inhibitors having distinct antiplasmodium toxicities as a result of the pre-formed haem–inhibitor complexes.

One possible explanation for these phenomena could be that slow-acting complexes allow for more Hb digestion compared to fast-acting complexes. This would not be surprising since these slow-acting complexes' killing rate coincides with the trophozoite stage responsible for the rapid growth and digestion of Hb.[233] This further raised questions about the basis of the inhibitor toxicity in the parasite. This is because there are suggestions that haemozoin inhibitors are responsible for the increase in reactive oxygen species in the parasite, as a direct consequence of the pro-oxidant properties of the increased accumulation of unsequestered haem.[85,241,244] Accordingly, the redox oxidative abilities of compounds **1** and **6** were explored in Openshaw *et al.* to determine their pro-oxidant effects on the parasite.[187] The findings established that these previous redox observations do not hold for all haemozoin-inhibiting compounds for the following two reasons: (1) compound **1**'s parasiticidal activity was significantly reduced with the reductant glutathione precursor N-acetylcysteine (NAC), while enhanced by the introduction of the pro-oxidant Luperox, thus suggesting a pro-oxidative reliant mechanism of parasite toxicity. (2) On the other hand, neither NAC nor Luperox

influenced the activity of **6**, demonstrating the unique toxicity and specificity posed by each haem–compound complex.

Another possibility for the observed unique toxicities could be that these haem–inhibitor complexes make the parasite DV more vulnerable, so allowing for the permeabilisation of these complexes into the cytoplasm or elsewhere in the parasite, which then exert secondary effects. This scenario is probable since micro-molar CQ (**1**) levels were previously shown to permeabilise the DV, leading to calcium efflux, mitochondrial depolarisation, and DNA degradation.[245] Furthermore, studies using transmission electron microscopy (TEM) by Combrinck *et al.* demonstrated the redistribution of haem outside of the DV when parasites were treated with CQ.[159] Recently, it was shown with compound **6** that this redistributed haem colocalises with the inhibitor, which further supports the proposition that cytotoxic specificity exists among haem–inhibitor complexes.[187] In addition, the observed population groups from both the light microscope images and the MFI data above suggest Hb-dependent catabolism mechanisms for these compounds. These images show that for fast-acting compounds the cell growth is arrested in the immature stages of the parasite life cycle, whereas for the slow-acting compounds the cells were allowed to mature. This is even though a clear morphological distinction between these treated mature trophozoite cells and the untreated trophozoites cells still existed. This suggests that slow-acting compounds' mechanism may involve enabling the parasite to grow further into the trophozoite stages (allow for more Hb catabolism), thus resulting in more haem being available for binding with the test compound – while the opposite would occur with fast-acting compounds. Lastly, it was unequivocally shown that the quantification of this data using MFI histogram plots supported the morphological parasite maturation differences observed. This was unsurprising as Feng *et al.*[246] showed a regress in development to mature stages in CQ-treated parasites, and in cases where development had occurred there was an apparent enlargement of the DV which differed morphologically from that of untreated parasites. However, whether these mature treated trophozoites still allow for Hb catabolism remains unclear. This morphological information alone is insufficient to allow understanding of the intricacies of the biochemical processes induced by these compounds, therefore necessitating further investigations that will provide more insights into these processes.

Correlating the stage-specific speed of killing for each compound with their unsequestered haem and IC_{50} values perpetuated the distinct separation and groupings of the complexes. These were effectively divided into a group of three: fast acting (within 12 h), intermediately fast acting (at 24 h), and slow acting (at 48 h). Notably, no discernible morphological differences of parasites were observed between the intermediately fast acting and slow acting inhibitor complexes. Nonetheless, this reinforced the hypothesis that the activities and levels

of unsequestered haem for these complexes could be better explained in relation to the maturation of the parasite, as shown by their consistent groupings based on their exchangeable haem levels. The first set of compounds (**1** and **2**) effect their parasiticidal activities earlier in the immature stage of the life cycle where haem catabolism is still relatively lower. For the second set (**4**, **5**, **6** and **7**), these parasiticidal effects occur during the steady increase in growth and Hb catabolism, while for set three (**3** and **8**), such effects were observed at the peak of haem catabolism. This clearly indicates that future studies may need to be developed based on the proposed Hb-catabolism hypothesis, in order to investigate the parasiticidal effects observed with the different haem–inhibitor complexes.

7.5. Conclusions

A series of eight diverse haemozoin-inhibiting compounds presenting varying unsequestered haem levels in *P. falciparum* parasites were investigated for their stage-specific speed of killing in this chapter. This was explored because these compounds exhibited varying degrees of haem toxicity. Compounds with weaker activity presented higher levels of unsequestered haem, while highly active compounds exhibited lower levels of unsequestered haem. It was initially believed and later proven that the activities of these haemozoin-inhibiting compounds resulted from their respective haem–inhibitor complexes and not specifically because of the sole effects of haem. Thus, it was hypothesised that the disparities in activities and unsequestered haem levels resulted from the speed of killing from these inhibitor complexes.

As reported above, with increasing levels of unsequestered haem there was a tendency for a decreased speed of killing for each compound. This suggests that the observed differences in haem levels for slower-acting compounds could be attributed to parasites incubated with these compounds having more time to build up unsequestered haem complexes. These findings are supported by the observed morphological differences in parasite populations that are evident between fast- and slow-acting compounds. This is because there was an evident tendency of fast-acting compounds to result immature parasites after incubation, which potentially suffered regress in Hb catabolism. In contrast, slow-acting complexes were generally associated with more mature parasites, which is a comparative indication of pronounced Hb catabolism. It is clear from these findings that there is a compound-specific toxicity related to the toxic effects of unsequestered haem. These observations present more questions about the actual biochemical processes affected by haemozoin-inhibiting compounds. This drives the need for more insights into the haem detoxification pathway, specifically in relation to haemozoin inhibition.

Chapter 8: Conclusions and Future Work

8.1. Summaries and conclusions

Plasmodium falciparum's haemozoin formation process detoxifies at least 90% of toxic haem (Fe(III)PPIX) released during Hb degradation.[62] This is because when left unsequestered, haem causes several detrimental physiological changes such as cell lyses, lipid peroxidation, and possibly membrane destabilisation through a colloid osmotic mechanism.[50,51,55] As a result, haemozoin remains an insightful research theme for malaria research, especially since it is unique to the parasite, and despite the widespread resistance to antimalarials like CQ which are associated with this crystalline target. The persistent interest in the haemozoin formation pathway prevails primarily because, as previously mentioned, resistance, like parasiticidal activity, is compound-specific. Notably, resistance to these drugs arises from parasite mutations that encode for *pfcrt* and *pfmdr1* genes and does not relate to any proteins or molecular agents involved in the haemozoin crystal formation pathway.[43] Therefore, the haemozoin crystal remains a viable target for developing future antimalarial drugs. However, our understanding of haemozoin formation and its inhibition has to be improved, and progression on some fronts is necessary. Firstly, having tools that can easily predict β-haematin inhibition for drug discovery and development campaigns would help greatly when selecting potential lead molecules, owing to the fact that some of the most active and successful antimalarial drugs are haemozoin inhibitors. The tools can also be applicable when other targets in the parasite are needed since they can exclude any molecules that show active inhibition of the pathway.

Interestingly, in a comprehensive study to find parasite targets with the highest probability of delivering successful novel drugs, Chaparro *et al.* quantitatively classified the Hb degradation pathway as being among the top-ranked to produce candidates.[203] However, to achieve this, discovering new scaffolds is essential to help avoid issues associated with cross-resistance. An important technique that has often contributed to the discovery of identifying new leads with diverse scaffolds is high-throughput screening (HTS) *via* a virtually computer-aided approach (virtual screening).[210] This method allows large chemical libraries to be screened *in silico* against specific drug targets. Specifically, this requires knowledge of a fully characterised structure of the target to perform the directed molecular docking.[181] Therefore, since the haemozoin structure has been successfully identified and characterised, this allows for coordinated virtual screening (ligand- or structure-based) to discover new molecules. Subsequently, these discovered compounds must be tested using *in vitro* and whole-cell assays to confirm their predicted activity and MoA.

In this study, we first investigated the biological activity and cellular MoA of virtually screened compounds, indicated *in silico* by de Sousa *et al*.. These were to inhibit β-haematin formation and were subsequently found to be active against β-haematin *in vitro* using the NP-40 assay.[182,190,212] Second, we developed and validated improved throughput bioanalytical techniques to help determine the MoA and effects exerted by these compounds on *P. falciparum* – specifically, as related to haemozoin inhibition.

In the first instance, 39 *in silico* predicted and β-haematin active compounds were evaluated for their activity against the pLDH assay, with the most active compounds being evaluated for their haemozoin-inhibiting capabilities using the pyridine-based haem fractionation assay. As previously mentioned in Chapter 3, these compounds were discovered using SBVS of the ZINC15 database and USFDA database libraries to find new β-haematin inhibitors. All the details of these techniques and their methodologies appear in three publications by de Sousa *et al.*[182,190,212] Nonetheless, of the 39 compounds biologically evaluated, only 16 potential novel compounds with antiplasmodium activities below 10 μM were discovered. This was a desirable hit rate (~41%), proving that SBVS is a valuable, cost-effective tool in the search for novel scaffolds that inhibit haemozoin formation and which have potential biological activity. Of the biologically active compounds (Chapter 3), six (**6**, **11**, **16**, **17**, **19** and **26**) were selected for MoA investigations using the pyridine-based assay by Combrinck *et al.*[143] It was found that four of the chosen novel compounds (**11**, **16**, **17**, and **19**) inhibited HZ formation with the observed signature increase in unsequestered haem – a behaviour similar to that of CQ and AQ. However, a conclusive MoA for the other two compounds (**6** and **26**) could not be reached, although it was certain that these were not haemozoin inhibitors since they led to no significant increase in unsequestered haem.

These results demonstrated the importance of utilising HTS to discover novel scaffolds that have good biological activity against the parasite and which exert this activity *via* haemozoin inhibition. Moreover, none of the discovered compounds displayed any significant cross-resistance issues with CQ. Even more intriguing was the discovery of FDA-approved drugs (**16**, **17**, **19** and **26**) that showed good parasite activity (<1 μM) and acted by inhibiting haemozoin formation, except in the case of **26**. Although the compounds discovered were inferior in parasiticidal activity to CQ, they present an opportunity for further studies in other parasite stages, since here they were only evaluated for asexual erythrocytic stage activity. Furthermore, given that these are already FDA-approved, they offer an ideal opportunity for drug repurposing, which is less costly than conventional drug development. Notably, these newly discovered haemozoin-inhibiting scaffolds can be used for QSAR studies to improve activity, hence improving the feasibility of rational drug design to source new haemozoin inhibitors with activity against the parasite for a specifically identified target.

In conclusion, it is vital to mention that the purpose of the current study was different from medicinal chemistry campaigns designed to discover drug candidates that are subsequently optimised via structure-activity or structure-property relationship analysis. This study was aimed at investigating the feasibility of developing a workflow for *in silico* techniques developed in the Bioinorganic Chemistry and Pharmacokinetic Labs at UCT for finding newly predicted haemozoin-inhibiting compounds. Nonetheless, the above investigation highlighted some challenges when searching for and confirming haemozoin-inhibiting compounds. First, to show the inhibition of haemozoin formation in the parasite proved cumbersome, because the available method presented with low throughput, required large amounts of parasite material, and used toxic reagents to complex haem for colourimetric detection. Therefore, this necessitated an improved assay that would improve throughput, use less parasite material, and use non-volatile toxic reagents to complex haem. We aimed to develop HPLC methods that use smaller sample sizes, and that can be carried out in 96-well plates and improve throughput. Furthermore, we prioritised employing detection techniques that would make the assay readily accessible to many medicinal chemistry laboratories.

The second part of this work aimed to develop and validate a bioanalytical technique which would accommodate a 96-well plate-based haem fractionation assay to test for haemozoin inhibition of four compounds simultaneously. The development work explored the possibility of haem species' detection with mass spectrometry (LC-MS/MS) and diode array for UV (DAD). Both detection methods were found to be effective and reproducible. However, the HPLC-DAD assay was prioritised over the LC-MS/MS because of technicalities discussed in Chapter 4. Moreover, it was my belief that HPLC systems with UV detections are more commonly available than mass spectrometry systems. Hence, it was even more advantageous to have DAD (easily transferrable to a UV-Vis detector) to enable more accessibility. Nevertheless, the four-compound 96-well HPLC-DAD assay was successfully validated using four known inhibitors (CQ, AQ, LPT and LOM) and four non-inhibitors (Lum, MQ, THC and PYR). More importantly, the assay substantially increased the throughput by four-fold, so decreasing the required sample size by an identical magnitude. Furthermore, accuracy and precision experiments demonstrated that the method was robust and reproducible.

Subsequently, we adapted the assay to the high-throughput 96-well plate to simultaneously evaluate 33 compounds. This assay was applied at a single concentration (2x IC_{50}) for each compound to determine their effects on haemozoin inhibition. The investigation was performed using selected inhibitors, non-inhibitors, and experimental compounds. Using these, we demonstrated in Chapter 6 that the predictive capability of the single-point assay for determining inhibitors and non-inhibitors was accurate and reliable. To further substantiate

this, we applied the four-compound 96-well plate method on four selected experimental compounds (Chapter 6: compounds **26**, **27**, **31** and **32**). The qualitative intracellular medium high-throughput approach was specifically developed to complement the use of the extracellular NP-40 β-hematin assay for performing definitive haemozoin MoA predictions. This is because, unlike the β-hematin assay, this qualitative assay will allow for haemozoin MoA predictions intracellularly. Furthermore, the assay presents with improved throughput, turnaround time and is readily accessible as a standardised form of predicting haemozoin inhibition directly in the parasite. The decision to develop the assay was informed by the fact that extracellular predictions for inhibition with the β-hematin assay have previously proven inadequate, as many inhibitions by compounds have turned out to be false positives (e.g., compounds **6** and **26**, as reported in Chapter 3). These predictions give no information on whether the compound will even enter the parasite DV to exert these effects. Hence, this intracellular predictive assay will be crucial in conjunction with the β-haematin method in validating whether haemozoin formation is the MoA. The full-dose response assay should therefore be performed for definitive determination of the actual MoA – for reasons specified in Chapter 6.

Inevitably, haemozoin-inhibiting molecules interfere with the detoxification of haem by binding to either one of the well-defined faces (e.g., 010, 101) of the growing haemozoin crystal.[79] These interactions are thought to primarily occur via pi-pi interaction, thus leading to interference in haemozoin formation.[152] Although initially believed to cause the accumulation of toxic unsequestered haem, various studies have now demonstrated that these inhibitors coordinate with haem resulting in haem–inhibitor complexes instead.[155,187] As shown by Chou *et al.* with CQ, the complexes, like unsequestered haem, are toxic.[139] Thus, the cytotoxic effects observed in treated parasites of haemozoin-inhibiting compounds are believed to be a result of the haem–inhibitor complexes and not necessarily unsequestered haem alone. This further implies that the demonstrated cases of morphological changes, vacuolar swelling, pigment clumping, and accumulation of Hb-containing vesicles that lead to parasite death may be an effect of these complexes and not only haem.[247–251] These may explain the characterised cytotoxic specificity in the observed morphology for each compound. Furthermore, Openshaw *et al*. showed that a diverse range of haemozoin-inhibiting scaffolds acted as complexes and that each complex exhibited unique activity, so substantiating the proposal that these haem–inhibitor complexes do exist in treated parasites.[187] Consequently, this necessitated a better understanding of the haemozoin formation pathway – especially its inhibition by the various compounds. We believe that the haemozoin inhibition MoA has proven to be compound-specific. Evidence of this proposition is that a diverse range of

haemozoin-inhibiting scaffolds produce varying intracellular haem concentrations and diverse parasiticidal activities.[143,144,160,161,176,180,192]

Therefore, we sought to investigate these differences of unsequestered haem levels at the IC_{50} caused by the diverse haemozoin-inhibiting scaffolds using a flow-cytometry speed of killing assay. This assay established that these compounds were stage-specific and exerted their parasiticidal activity at various times during the parasite life cycle. The results showed that compounds which produce lower levels of unsequestered haem tend to kill the parasites earlier in the life cycle. In contrast, those compounds that produce higher levels of unsequestered haem tend to kill later in the life cycle. As explained in Openshaw *et al.*, these observations suggest that slower-acting compounds get an opportunity to build up haem–inhibitor complexes over time, while fast-acting compounds have less time to do so.[187] More intriguingly, not all anti-parasitic activity of these haemozoin-inhibiting compounds is associated with the pro-oxidant effects of unsequestered haem, a further corroboration that each haem–inhibitor complex exerts unique parasiticidal activity. Accordingly, the ordinarily simplistic explanation that haemozoin-inhibiting compounds cause a build-up of unsequestered haem, which directly causes cytotoxic effects, is not supported by the evidence that is shared in Chapter 7.

It was shown in this work that the cellular haem fractionation assay can be used in the target deconvolution of new candidate antimalarial compounds and that a high-throughput approach for cellular predictions is desirable. Furthermore, flow cytometry can be implemented to understand better the effects caused by the observed varying unsequestered haem levels in the parasite. However, several things remain unresolved and will require improvement:

- The observed differences in the Hb fraction for the 96-well four compound method in comparison to the pyridine-based method need further investigation. Also, the incubation period (30 hours) used in this assay will need to be re-evaluated, mainly because it is believed that it could be associated with sample losses (through cell death caused by the compounds) that may ultimately be reduced during shorter incubation periods (e.g., 24 hours). This is a huge concern because the sample volume is already minimal and is thus believed to be associated with the variances observed in the Hb fraction.
- The medium- to high-throughput capacity of the 33-compound method will need to be reduced. Instead, the method should be used to test 22 compounds in triplicate, so possibly reducing the number of experimental repeats in cases of inter-experimental variations.

- The observations of haem–inhibitor complexes being responsible for the parasiticidal activities of haemozoin-inhibiting compounds will need to be further explored in detail. This is especially in terms of determining the structures of these complexes and evaluating their cytotoxic effects on various biological cell lines once they have been successfully synthesised or recovered from intracellular cell lysates.

Future efforts must therefore ascertain that advancements are made to address these critical issues, which were not resolved by the current project. Suggestions are offered below on some of the interventions that could be taken to offer solutions to problems resulting from the limitations of the reported methodologies.

8.2. Future Work

This study reported in Chapter 3 that the four compounds (**16**, **17**, **19** and **26**) found to have activity below 1 µM were FDA-approved and used in the therapeutic alleviation of other diseases. Therefore, further investigations are required to determine the future prospects of these compounds, especially pertaining to repurposing. In this regard, the following studies are suggested for each of the four compounds:

- Compounds **16** and **17** are approved drugs used for different cancer treatments: lapatinib and nilotinib, respectively. Given their promising parasiticidal activities, these should be evaluated: (1) for gametocytocidal activity, (2) for hypnozoitocidal activity, and (3) using *in vivo* models.
- Compound **19** (lomitapide) should be considered for hypnozoitocidal activity studies because of its use to treat familial hypercholesterolaemia (in the human liver). Expertise and tools to perform these assays (gametocytocidal and hypnozoitocidal) are not available in our labs, and thus studies will require collaborations with other laboratories.
- Compound **26** (THC) should also be considered for the above studies. However, given its psychoactive properties, only analogues of THC should be purchased and evaluated for activity in *P. falciparum*.

All these active compounds were evaluated for their activity with the pyridine-based and 96-well four-compound methods for quantifying haem. These results were discussed in detail and are different from the subject of this section. However, we seek to highlight the findings on the limitations of the newly developed four-compound method (Chapter 5) used to quantify the haem species in treated *P. falciparum* for all these compounds. In this regard, the following studies are suggested to remedy these limitations further:

- The Hb fraction determinations were found to be different between the pyridine-based and 96-well four-compound methods. Thus, the causes of these variations need to be

established. We suggest that a suitable internal standard be incorporated into the 96-well method, specifically for the Hb fraction. The internal standard, however, needs to be carefully chosen, as it must not interfere with the experimental techniques validated. Furthermore, this should not interfere with the parasite's haem levels or have any sign of exerting parasiticidal activity if it is decided that incubation with the internal standard is required. Thus, compounds like Zinc(II) protoporphyrin IX may be problematic as a result of their observed inhibition of parasite growth.[187] However, this would be applicable only when investigating for possible cell loss during harvesting. Nonetheless, it is suggested that protoporphyrin IX be investigated as a possible internal standard instead, following the determination of its solubility in the solvents used to solubilise the Hb fraction. This should be achieved in water at the selected concentration. Titration experiments akin to those with imidazole and HEPES in Chapter 4 will also need to be performed to determine the effects of the experimental conditions on protoporphyrin IX.

- The incubation period of the assay needs to be changed from 30 to 24 hours. This is to help avoid reductions in sample size caused by the parasiticidal effects of the investigated compounds.

Crucially, the theme of haem–inhibitor complexes will need to be expanded since there is enough evidence to support that they are responsible for the parasiticidal activities of haemozoin-inhibiting compounds. As highlighted in De Villiers *et al*., the key areas to address are:[145]

- The recovery of the precipitates (haem–inhibitor complex) from the parasite and subsequent deconvolution of the structures will need to be achieved. However, as highlighted in an earlier review, this is rather difficult given that previous efforts to obtain a solid state of the haem-CQ complex were unsuccessful.[252] Nonetheless, given the recent studies of dihydroartemisinin−ferriprotoporphyrin IX adducts by Heller *et al.,* we believe that an attempt at a similar approach to recover a precipitant should be emulated, albeit with different novel analytical techniques for structure elucidations.[53,163]
- Once successful, the strengths of association in different physiological environments, solubilities, and lipophilicities need to be investigated. I do appreciate that these are complex problems that will be very difficult to resolve. However, this is necessary to improve our understanding of haemozoin inhibitors and their actual parasite activity.

For investigating the disconnect between the variable levels of unsequestered haem and the unique parasite toxicity by the haem-inhibitor complexes, the following potential experiments are suggested:

- Fluorescence microscopic imaging experiments with fluorescently tagged haemozoin-inhibiting compounds should be performed to discern the fate and possible localisation of these complexes once they are formed. Notably, this may assist in characterising if whether slow-acting and fast-acting haem-inhibitor complexes have different localisations in the parasite — which may assist in explaining the discrepancies in their toxic effects and parasite morphology. Furthermore, these experiments may also reveal the potential interactions of these haem-inhibitor complexes with lipid membranes or other organelles.
- A possible explanation for the disconnect between parasite killing and unsequestered haem levels may lie in the solubilities of the different haem-inhibitor complexes in DV conditions. Perhaps the increased concentrations of unsequestered haem and weaker parasite activity observed for slow-acting compounds is as a result of decreased solubility of the formed haem-inhibitor complexes, which may have precipitated at the DV pH (Openshaw et al.).[187] Accordingly, this may then imply that the observed unsequestered haem for all complexes is a combination of mainly a precipitated and a dissolved haem-inhibitor complex. Consequently, if that is the case, it can be expected that only the dissolved complex is then responsible for parasiticidal activity — as it may diffuse across compartments to inhibit enzymes or membrane transporters. Therefore, it is important that once the complexes have been recovered, different solubility experiments (e.g., turbidity assays) be performed to test this hypothesis.
- Lastly, time-dependent LC-MS/MS-based proteomics experiments with test compounds from both the slow-acting and fast-acting sets should be performed to establish the variations in basal concentrations of parasite proteins expressed during the life cycle. This may prove important in helping to elucidate the potential enzymatic or protein interactions (or inhibition) of these haem-inhibitor complexes. Furthermore, this may lead to analysing if whether fast-acting and slow-acting complexes may be down-regulating or up-regulating the production of similar or different parasite proteins. This is important because as discussed in Chapter 7, not all haem-inhibitor complexes lead to redox activity. Hence, this may infer different target interactions of the complexes and as a consequence unique killing mechanisms.

This work has enabled significant progress in improving techniques for quantifying haemozoin inhibition. However, the exact mechanisms with which haemozoin-inhibiting compounds kill

the parasite remain elusive because these compounds form complexes with haem which exert unique time-dependent parasiticidal effects. Further studies are required to advance our understanding of haemozoin-inhibiting molecules. These would provide crucial insights for resolving the future rational drug design of compounds that act through this MoA, specifically on resolving their association with haem and the physico-chemical properties of the formed inhibitor complexes. It is believed that such an improved understanding of the fate of these haem–inhibitor complexes may help resolve whether their actual antiplasmodium effects occur either directly by inhibiting enzyme targets or via other indirect biological processes. This may also elucidate the compound-specific resistance mechanisms of haemozoin inhibitors. However, these are all challenging problems that will require innovative approaches to resolve them. But they do present as an opportunity that should be embraced by African scientists: To contribute to and align with the global efforts in developing health innovations and in malaria drug development. This is critical because Africa carries the greatest global disease burden of malaria and thus requires local capacity-building in innovative infectious disease research.

References:

(1) World Health Organization (WHO). *World Malaria Report 2021*; Geneva, 2022.

(2) World Health Organization (WHO). *World Health Statistics 2022*; Geneva, 2022.

(3) World Health Organization (WHO). *Global Technical Strategy for Malaria 2016–2030*; Geneva, 2016.

(4) World Health Organization (WHO). *Health in 2015 from Millenium Development Goals to Sustainable Development Goals*; Geneva, 2015. https://doi.org/10.1007/BF01918387.

(5) Murray, C. J. L.; Rosenfeld, L. C.; Lim, S. S.; Andrews, K. G.; Foreman, K. J.; Haring, D.; Fullman, N.; Naghavi, M.; Lozano, R.; Lopez, A. D. Global Malaria Mortality between 1980 and 2010: A Systematic Analysis. *Lancet* **2012**, *379* (9814), 413–431. https://doi.org/10.1016/S0140-6736(12)60034-8.

(6) *Malaria - Our World in Data*. https://ourworldindata.org/malaria#citation (accessed 2022-12-01).

(7) World Health Organization (WHO). *Global Malaria Programme: The Use of DDT in Malaria Vector Control*; Geneva, 2011.

(8) Pasvol, G. The Treatment of Complicated and Severe Malaria. *Br. Med. Bull.* **2005**, *75*, 29–47. https://doi.org/10.1093/bmb/ldh059.

(9) Carter, R.; Mendis, K. N. Evolutionary and Historical Aspects of the Burden of Malaria. *Clin. Microbiol. Rev.* **2002**, *15* (4), 564–594. https://doi.org/10.1128/CMR.15.4.564-594.2002.

(10) Salas, P. F.; Herrmann, C.; Orvig, C. Metalloantimalarials. *Chem. Rev.* **2013**, 3450–3492. https://doi.org/10.1021/cr3001252.

(11) Institute of Medicine Committee on the Economics of Antimalarial Drugs. *Saving Lives, Buying Time: Economics of Malaria Drugs in an Age of Resistance*; Arrow, K. J., Panosian, C., Gelband, H., Eds.; National Academies Press: Washington, DC, 2004.

(12) Carter, R.; Mendis, K. N. Evolutionary and Historical Aspects of the Burden of Malaria. *Clin. Microbiol. Rev* **2002**, *15* (4), 564–594. https://doi.org/10.1128/CMR.15.4.564.

(13) Cox, E. F. History of the Discovery of the Malaria Parasites and Their Vectors. *Parasit. Vectors* **2010**, *3* (5). https://doi.org/10.1186/1756-3305-3-5.

(14) Van Leewenhoeck, A. Observations, Communicated to the Publisher by Mr. Antony van Leewenhoeck, in a Dutch Letter of the 9th Octob. 1676. Here English'd Concerning Little Animals by Him Observed in Rain-Well-Sea- and Snow Water; as Also in Water Wherein Pepper Had Lain Infuse. *Philos. Trans. R. Soc. London* **1677**, *12* (133).

(15) Smeele, W. Grounding Miasma, or Anticipating the Germ Theory of Disease in Victorian Cholera Satire. *J. Midwest Mod. Lang. Assoc.* **2016**, *49* (2), 15–27. https://doi.org/10.1353/mml.2016.0046.

(16) Center for Disease Control and Prevention (CDC). *Malaria - About Malaria - History - Ross and the Discovery that Mosquitoes Transmit Malaria Parasites*. https://www.cdc.gov/malaria/about/history/ross.html (accessed 2022-12-06).

(17) Majori, G. Short History of Malaria and Its Eradication in Italy With Short Notes on the Fight Against the Infection in the Mediterranean Basin. *Mediterr. J. Hematol. Infect. Dis.* **2012**, *4* (1), e2012016. https://doi.org/10.4084/MJHID.2012.016.

(18) Center for Disease Control and Prevention (CDC). *Malaria - About Malaria - Biology*. https://www.cdc.gov/malaria/about/biology/index.html#tabs-1-5 (accessed 2022-12-08).

(19) Hang, J. W.; Tukijan, F.; Lee, E. Q. H.; Abdeen, S. R.; Aniweh, Y.; Malleret, B. Zoonotic Malaria: Non-Laverania Plasmodium Biology and Invasion Mechanisms. *Pathogens* **2021**, *10* (7), 889. https://doi.org/10.3390/PATHOGENS10070889/S1.

(20) *Malaria Atlas Project | Data*. https://data.malariaatlas.org/maps?layers=Malaria:202206_Global_Pv_Incidence_Rate,Malaria:202206_Global_Pf_Incidence_Rate&extent=-18778765.75181205,-7156586.723441234,21296250.93376644,9723970.435132517 (accessed 2023-01-16).

(21) Garrido-Cardenas, J. A.; González-Cerón, L.; Manzano-Agugliaro, F.; Mesa-Valle, C. Plasmodium Genomics: An Approach for Learning about and Ending Human Malaria. *Parasitol. Res.* **2018**, *118* (1), 1–27. https://doi.org/10.1007/S00436-018-6127-9.

(22) Bartoloni, A.; Zammarchi, L. Clinical Aspects of Uncomplicated and Severe Malaria. *Mediterr. J. Hematol. Infect. Dis.* **2012**, *4* (1), 201. https://doi.org/10.4084/MJHID.2012.026.

(23) Greenwood, B. M.; Fidock, D. A.; Kyle, D. E.; Kappe, S. H. I.; Alonso, P. L.; Collins, F. H.; Duffy, P. E. Malaria: Progress, Perils, and Prospects for Eradication. *J. Clin.*

Invest. **2008**, *118* (4), 1266. https://doi.org/10.1172/JCI33996.

(24) *DDT - A Brief History and Status* | *US EPA*. https://www.epa.gov/ingredients-used-pesticide-products/ddt-brief-history-and-status (accessed 2022-12-05).

(25) World Health Organization (WHO). *WHO Guidelines for Malaria Treatment 2021*; Geneva, 2021.

(26) Maier, A. G.; Cooke, B. M.; Cowman, A. F.; Tilley, L. Malaria Parasite Proteins That Remodel the Host Erythrocyte. *Nat. Rev. Microbiol.* **2009**, *7* (5), 341–354. https://doi.org/10.1038/nrmicro2110.

(27) Bannister, L.; Mitchell, G. The Ins, Outs and Roundabouts of Malaria. *Trends Parasitol.* **2003**, *19* (5), 209–213. https://doi.org/10.1016/S1471-4922(03)00086-2.

(28) Bannister, L. H.; Hopkins, J. M.; Fowler, R. E.; Krishna, S.; Mitchell, G. H. A Brief Illustrated Guide to the Ultrastructure of Plasmodium Falciparum Asexual Blood Stages. *Parasitol. Today* **2000**, *16* (10), 427–433. https://doi.org/10.1016/S0169-4758(00)01755-5.

(29) Marti, M.; Baum, J.; Rug, M.; Tilley, L.; Cowman, A. F. Signal-Mediated Export of Proteins from the Malaria Parasite to the Host Erythrocyte. *J. Cell Biol.* **2005**, *171* (4), 587–592. https://doi.org/10.1083/jcb.200508051.

(30) Bhattacharjee, S.; Van Ooij, C.; Balu, B.; Adams, J. H.; Haldar, K. Maurer's Clefts of Plasmodium Falciparum Are Secretory Organelles That Concentrate Virulence Protein Reporters for Delivery to the Host Erythrocyte. *Blood* **2008**, *111* (4), 2418–2425. https://doi.org/10.1182/blood-2007-09-115279.

(31) Hanssen, E.; Goldie, K. N.; Tilley, L. Ultrastructure of the Asexual Blood Stages of Plasmodium Falciparum. *Methods Cell Biol.* **2010**, *96*, 93–116. https://doi.org/10.1016/S0091-679X(10)96005-6.

(32) Bakar, N. A.; Klonis, N.; Hanssen, E.; Chan, C.; Tilley, L. Digestive-Vacuole Genesis and Endocytic Processes in the Early Intraerythrocytic Stages of Plasmodium Falciparum. *J. Cell Sci.* **2010**, *123* (3), 441–450. https://doi.org/10.1242/jcs.061499.

(33) Pagola, S.; Stephens, P. W.; Bohle, D. S.; Kosar, A. D.; Madsen, S. K. The Structure of Malaria Pigment β-Haematin. *Int. J. Parasitol.* **2000**, *32* (13), 307–310. https://doi.org/10.1038/35005132.

(34) Tilley, L.; Dixon, M. W. A.; Kirk, K. The Plasmodium Falciparum-Infected Red Blood Cell. *Int. J. Biochem. Cell Biol.* **2011**, *43* (6), 839–842.

https://doi.org/10.1016/j.biocel.2011.03.012.

(35) Moore, L. R.; Fujioka, H.; Williams, P. S.; Chalmers, J. J.; Grimberg, B.; Zimmerman, P. A.; Zborowski, M. Hemoglobin Degradation in Malaria-Infected Erythrocytes Determined from Live Cell Magnetophoresis. *FASEB J.* **2006**, *20* (6), 747–749. https://doi.org/10.1096/FJ.05-5122FJE.

(36) Salmon, B. L.; Oksman, A.; Goldberg, D. E. Malaria Parasite Exit from the Host Erythrocyte: A Two-Step Process Requiring Extraerythrocytic Proteolysis. *Proc. Natl. Acad. Sci. U. S. A.* **2001**, *98* (1), 271–276. https://doi.org/10.1073/pnas.98.1.271.

(37) Matz, J. M. Plasmodium's Bottomless Pit: Properties and Functions of the Malaria Parasite's Digestive Vacuole. *Trends Parasitol.* **2022**, *38* (7), 525–543. https://doi.org/10.1016/j.pt.2022.02.010.

(38) Grüring, C.; Heiber, A.; Kruse, F.; Ungefehr, J.; Gilberger, T. W.; Spielmann, T. Development and Host Cell Modifications of Plasmodium Falciparum Blood Stages in Four Dimensions. *Nat. Commun.* **2011**, *2* (1). https://doi.org/10.1038/ncomms1169.

(39) Francis, S. E.; Sullivan, D. J.; Goldberg, D. E. Hemoglobin Metabolism in the Malaria Parasite Plasmodium Falciparum. *Annu. Rev. Microbiol.* **1997**, *51*, 97–123.

(40) Goldberg, D. E. Complex Nature of Malaria Parasite Hemoglobin Degradation. *Proc. Natl. Acad. Sci. U. S. A.* **2013**, *110* (14), 5283–5284. https://doi.org/10.1073/PNAS.1303299110.

(41) Coronado, L. M.; Nadovich, C. T.; Spadafora, C. Malarial Hemozoin: From Target to Tool. *Biochim. Biophys. Acta - Gen. Subj.* **2014**, *1840* (6), 2032–2041. https://doi.org/10.1016/j.bbagen.2014.02.009.

(42) Rosenthal, M. R.; Ng, C. L. Plasmodium Falciparum Artemisinin Resistance: The Effect of Heme, Protein Damage, and Parasite Cell Stress Response. *ACS Infect. Dis.* **2020**, *6*, 1599–1614. https://doi.org/10.1021/acsinfecdis.9b00527.

(43) Wicht, K. J.; Mok, S.; Fidock, D. A. Molecular Mechanisms of Drug Resistance in Plasmodium Falciparum Malaria. *Annu. Rev. Microbiol.* **2020**, *74*, 431–454. https://doi.org/10.1146/annurev-micro-020518-115546.

(44) Mishra, M.; Singh, V.; Singh, S. Structural Insights into Key Plasmodium Proteases as Therapeutic Drug Targets. *Front. Microbiol.* **2019**, *10* (394). https://doi.org/10.3389/FMICB.2019.00394/BIBTEX.

(45) Harbut, M. B.; Velmourougane, G.; Dalal, S.; Reiss, G.; Whisstock, J. C.; Onder, O.;

Brisson, D.; McGowan, S.; Klemba, M.; Greenbaum, D. C. Bestatin-Based Chemical Biology Strategy Reveals Distinct Roles for Malaria M1- and M17-Family Aminopeptidases. *Proc. Natl. Acad. Sci. U. S. A.* **2011**, *108* (34). https://doi.org/10.1073/PNAS.1105601108/-/DCSUPPLEMENTAL/APPENDIX.PDF.

(46) Mathew, R.; Wunderlich, J.; Thivierge, K.; Cwiklinski, K.; Dumont, C.; Tilley, L.; Rohrbach, P.; Dalton, J. P. Biochemical and Cellular Characterisation of the Plasmodium Falciparum M1 Alanyl Aminopeptidase (PfM1AAP) and M17 Leucyl Aminopeptidase (PfM17LAP). *Sci. Rep.* **2021**, *11* (1), 1–17. https://doi.org/10.1038/s41598-021-82499-4.

(47) Drinkwater, N.; Lee, J.; Yang, W.; Malcolm, T. R.; McGowan, S. M1 Aminopeptidases as Drug Targets: Broad Applications or Therapeutic Niche? *FEBS J.* **2017**, *284* (10), 1473–1488. https://doi.org/10.1111/febs.14009.

(48) Egan, T. J. Haemozoin Formation. *Mol. Biochem. Parasitol.* **2008**, *157* (2), 127–136. https://doi.org/10.1016/j.molbiopara.2007.11.005.

(49) Atamna, H.; Ginsburg, H. Origin of Reactive Oxygen Species in Erythrocytes Infected with Plasmodium Falciparum. *Mol. Biochem. Parasitol.* **1993**, *61* (2), 231–241. https://doi.org/10.1016/0166-6851(93)90069-A.

(50) Chou, A. C.; Fitch, C. D. Mechanism of Hemolysis Induced by Ferriprotoporphyrin IX. *J. Clin. Invest.* **1981**, *68* (3), 672–677. https://doi.org/10.1172/JCI110302.

(51) Oliveira, M. F.; Timm, B. L.; Machado, E. A.; Miranda, K.; Attias, M.; Silva, J. R.; Dansa-Petretski, M.; De Oliveira, M. A.; De Souza, W.; Pinhal, N. M.; Sousa, J. J. F.; Vugman, N. V.; Oliveira, P. L. On the Pro-Oxidant Effects of Haemozoin. *FEBS Lett.* **2002**, *512* (1–3), 139–144. https://doi.org/10.1016/S0014-5793(02)02243-3.

(52) Grenoble, D. C.; Drickamer, H. G. The Effect of Pressure on the Oxidation State of Iron, III. Hemin and Hematin*. *Proc. Natl. Acad. Sci.* **1968**, *61*.

(53) Heller, L. E.; Roepe, P. D. Quantification of Free Ferriprotoporphyrin IX Heme and Hemozoin for Artemisinin Sensitive versus Delayed Clearance Phenotype Plasmodium Falciparum Malarial Parasites. *Biochemistry* **2018**, *57* (51), 6927–6934. https://doi.org/10.1021/acs.biochem.8b00959.

(54) Müller, S. Redox and Antioxidant Systems of the Malaria Parasite Plasmodium Falciparum. *Mol. Microbiol.* **2004**, *53* (5), 1291–1305. https://doi.org/10.1111/j.1365-2958.2004.04257.x.

(55) Schmitt, T. H.; Frezzatti, W. A.; Schreier, S. Hemin-Induced Lipid Membrane Disorder and Increased Permeability: A Molecular Model for the Mechanism of Cell Lysis. *Arch. Biochem. Biophys.* **1993**, *307* (1), 96–103. https://doi.org/10.1006/abbi.1993.1566.

(56) Hempelmann, E.; Krafts, K. Bad Air, Amulets and Mosquitoes: 2,000 Years of Changing Perspectives on Malaria. *Malar. J.* **2013**, *12* (1), 1–14. https://doi.org/10.1186/1475-2875-12-232/FIGURES/9.

(57) Brown, W. H. Malarial Pigment (So-Called Melanin): Its Nature and Mode of Production. *J. Exp. Med.* **1911**, *13* (2), 290–299.

(58) Fitch, C. D.; Kanjananggulpan, P. The State of Ferriprotoporphyrin IX in Malaria Pigment. *J. Biol. Chem.* **1987**, *262* (32). https://doi.org/10.1016/S0021-9258(18)47761-7.

(59) Slater, A. F.; Swiggard, W. J.; Orton, B. R.; Flitter, W. D.; Goldberg, D. E.; Cerami, A.; Henderson, G. B. An Iron-Carboxylate Bond Links the Heme Units of Malaria Pigment. *Proc. Natl. Acad. Sci.* **1991**, *88* (2), 325–329. https://doi.org/10.1073/pnas.88.2.325.

(60) Scott Bohle, D.; Dinnebier, R. E.; Madsen, S. K.; Stephens, P. W. Characterization of the Products of the Heme Detoxification Pathway in Malarial Late Trophozoites by X-Ray Diffraction. *J. Biol. Chem.* **1997**, *272* (2), 713–716. https://doi.org/10.1074/jbc.272.2.713.

(61) Egan, T. J. Haemozoin (Malaria Pigment): A Unique Crystaline Drug Target. *Targets* **2003**, *2* (3), 115–124.

(62) Egan, T. J.; Combrinck, J. M.; Egan, J.; Hearne, G. R.; Marques, H. M.; Ntenteni, S.; Sewell, B. T.; Smith, P. J.; Taylor, D.; Van Schalkwyk, D. A.; Walden, J. C. Fate of Haem Iron in the Malaria Parasite Plasmodium Falciparum. *Biochem. J.* **2002**, *365* (2), 343–347. https://doi.org/10.1042/bj20020793.

(63) Slater, A. F. G.; Cerami, A. Inhibition by Chloroquine of a Novel Haem Polymerase Enzyme Activity in Malaria Trophozoites. *Nature* **1992**, *359*, 710–713.

(64) Sullivan Jr, D. J.; Gluzman, I. Y.; Goldberg, D. E. Plasmodium Hemozoin Formation Mediated by Histidine-Rich Proteins. *Science (80-.).* **1996**, *271*, 219–222.

(65) Papalexis, V.; Siomos, M. A.; Campanale, N.; Guo, X.; Kocak, G.; Foley, M.; Tilley, L. Histidine-Rich Protein 2 of the Malaria Parasite, Plasmodium Falciparum, Is Involved in Detoxification of the by-Products of Haemoglobin Degradation. *Mol. Biochem.*

Parasitol. **2001**, *115* (1), 77–86. https://doi.org/10.1016/S0166-6851(01)00271-7.

(66) Sullivan, D. J. Invited Review Theories on Malarial Pigment Formation and Quinoline Action. *Int. J. Parasitol.* **2002**, *32* (13), 1645–1653.

(67) Jani, D.; Nagarkatti, R.; Beatty, W.; Angel, R.; Slebodnick, C.; Andersen, J.; Kumar, S.; Rathore, D. HDP - A Novel Heme Detoxification Protein from the Malaria Parasite. *PLoS Pathog.* **2008**, *4* (4), e1000053. https://doi.org/10.1371/journal.ppat.1000053.

(68) Matz, J. M.; Drepper, B.; Blum, T. B.; Van Genderen, E.; Burrell, A.; Martin, P.; Stach, T.; Collinson, L. M.; Abrahams, J. P.; Matuschewski, K.; Blackman, M. J. A Lipocalin Mediates Unidirectional Heme Biomineralization in Malaria Parasites. *Proc. Natl. Acad. Sci. U. S. A.* **2020**, *117* (28), 16546–16556. https://doi.org/10.1073/PNAS.2001153117/-/DCSUPPLEMENTAL.

(69) Bendrat, K.; Berger, B. J.; Cerami, A. Haem Polymerization in Malaria. *Nature* **1995**, *378* (6553), 138. https://doi.org/10.1038/378138A0.

(70) Egan, T. J.; Mavuso, W. W.; Ncokazi, K. K. The Mechanism of β-Hematin Formation in Acetate Solution. Parallels between Hemozoin Formation and Biomineralization Processes. *Biochemistry* **2001**, *40* (1), 204–213. https://doi.org/10.1021/bi0013501.

(71) Egan, T. J.; Chen, J. Y. J.; De Villiers, K. A.; Mabotha, T. E.; Naidoo, K. J.; Ncokazi, K. K.; Langford, S. J.; McNaughton, D.; Pandiancherri, S.; Wood, B. R. Haemozoin (β-Haematin) Biomineralization Occurs by Self-Assembly near the Lipid/Water Interface. *FEBS Lett.* **2006**, *580* (21), 5105–5110. https://doi.org/10.1016/j.febslet.2006.08.043.

(72) Huy, N. T.; Maeda, A.; Uyen, D. T.; Trang, D. T. X.; Sasai, M.; Shiono, T.; Oida, T.; Harada, S.; Kamei, K. Alcohols Induce Beta-Hematin Formation via the Dissociation of Aggregated Heme and Reduction in Interfacial Tension of the Solution. *Acta Trop.* **2007**, *101* (2), 130–138. https://doi.org/10.1016/J.ACTATROPICA.2007.01.001.

(73) Sandlin, R. D.; Carter, M. D.; Lee, P. J.; Auschwitz, J. M.; Leed, S. E.; Johnson, J. D.; Wright, D. W. Use of the NP-40 Detergent-Mediated Assay in Discovery of Inhibitors of β-Hematin Crystallization. *Antimicrob. Agents Chemother.* **2011**, *55* (7), 3363–3369. https://doi.org/10.1128/AAC.00121-11.

(74) Pisciotta, J. M.; Coppens, I.; Tripathi, A. K.; Scholl, P. F.; Shuman, J.; Bajad, S.; Shulaev, V.; Sullivan, D. J. The Role of Eutral Lipid Nanospheres in Plasmodium Falciparum Haem Crystallization. *Biochem. J.* **2007**, *402* (1), 197–204. https://doi.org/10.1042/BJ20060986.

(75) Ambele, M. A.; Sewell, B. T.; Cummings, F. R.; Smith, P. J.; Egan, T. J. Synthetic Hemozoin (β-Hematin) Crystals Nucleate at the Surface of Neutral Lipid Droplets That Control Their Sizes. *Cryst. Growth Des.* **2013**, *13*, 4442–4452. https://doi.org/10.1021/cg4009416.

(76) Kapishnikov, S.; Berthing, T.; Hviid, L.; Dierolf, M.; Menzel, A.; Pfeiffer, F.; Als-Nielsen, J.; Leiserowitz, L. Aligned Hemozoin Crystals in Curved Clusters in Malarial Red Blood Cells Revealed by Nanoprobe X-Ray Fe Fluorescence and Diffraction. *Proc. Natl. Acad. Sci. U. S. A.* **2012**, *109* (28), 11184–11187. https://doi.org/10.1073/PNAS.1118134109/-/DCSUPPLEMENTAL/PNAS.1118134109_SI.PDF.

(77) Buller, R.; Peterson, M. L.; Almarsson, O.; Leiserowitz, L. Quinoline Binding Site on Malaria Pigment Crystal: A Rational Pathway for Antimalaria Drug Design. *Cryst. Growth Des.* **2002**, *2* (6), 553–562. https://doi.org/10.1021/cg025550i.

(78) Gildenhuys, J.; Le Roex, T.; Egan, T. J.; De Villiers, K. A. The Single Crystal X-Ray Structure of β-Hematin DMSO Solvate Grown in the Presence of Chloroquine, a β-Hematin Growth-Rate Inhibitor. *J. Am. Chem. Soc.* **2013**, *135* (3), 1037–1047. https://doi.org/10.1021/ja308741e.

(79) Olafson, K. N.; Ketchum, M. A.; Rimer, J. D.; Vekilov, P. G. Mechanisms of Hematin Crystallization and Inhibition by the Antimalarial Drug Chloroquine. *Proc. Natl. Acad. Sci. U. S. A.* **2015**, *112* (16), 4946–4951. https://doi.org/10.1073/PNAS.1501023112/-/DCSUPPLEMENTAL/PNAS.201501023SI.PDF.

(80) World Health Organization (WHO). *The Role of Mass Drug Administration, Mass Screening and Treatment, and Focal Screening and Treatment for Malaria*; Geneva, 2015.

(81) Cortese, J. F.; Caraballo, A.; Contreras, C. E.; Plowe, C. V. Origin and Dissemination of Plasmodium Falciparum Drug-Resistance Mutations in South America. *J. Infect. Dis.* **2002**, *186* (7), 999–1006.

(82) Stepniewska, K.; Allen, E. N.; Humphreys, G. S.; Poirot, E.; Craig, E.; Kennon, K.; Yilma, D.; Bousema, T.; Guerin, P. J.; White, N. J.; Price, R. N.; Raman, J.; Martensson, A.; Mwaiswelo, R. O.; Bancone, G.; Bastiaens, G. J. H.; Bjorkman, A.; Brown, J. M.; D'Alessandro, U.; Dicko, A. A.; El-Sayed, B.; Elzaki, S. E.; Eziefula, A. C.; Gonçalves, B. P.; Hamid, M. M. A.; Kaneko, A.; Kariuki, S.; Khan, W.; Kwambai, T. K.; Ley, B.; Ngasala, B. E.; Nosten, F.; Okebe, J.; Samuels, A. M.; Smit, M. R.; Stone, W. J. R.; Sutanto, I.; Ter Kuile, F.; Tine, R. C.; Tiono, A. B.; Drakeley, C. J.; Gosling,

R.; Stergachis, A.; Barnes, K. I.; Chen, I. Safety of Single-Dose Primaquine as a Plasmodium Falciparum Gametocytocide: A Systematic Review and Meta-Analysis of Individual Patient Data. *BMC Med.* **2022**, *20* (1), 1–19. https://doi.org/10.1186/S12916-022-02504-Z/FIGURES/4.

(83) White, N. J. Primaquine to Prevent Transmission of Falciparum Malaria. *Lancet Infect. Dis.* **2013**, *13* (2), 175–181. https://doi.org/10.1016/S1473-3099(12)70198-6.

(84) Hill, D. R.; Kevin Baird, J.; Parise, M. E.; Lewis, L. S.; Ryan, E. T.; Kevin, J. Primaquine: Report from CDC Expert Meeting on Malaria Chemoprophylaxis I. *Am. J. Trop. Med. Hyg.* **2006**, *75* (3), 402–415.

(85) Sugioka, Y.; Suzuki, M. The Chemical Basis for the Ferriprotoporphyrin IX-Chloroquine Complex Induced Lipid Peroxidation. *BBA - Gen. Subj.* **1991**, *1074* (1), 19–24. https://doi.org/10.1016/0304-4165(91)90032-C.

(86) Parapini, S.; Basilico, N.; Pasini, E.; Egan, T. J.; Olliaro, P.; Taramelli, D.; Monti, D. Standardization of the Physicochemical Parameters to Assess in Vitro the β-Hematin Inhibitory Activity of Antimalarial Drugs. *Exp. Parasitol.* **2000**, *96* (4), 249–256. https://doi.org/10.1006/expr.2000.4583.

(87) Nana, R. R. D.; Hawadak, J.; Foko, L. P. K.; Kumar, A.; Chaudhry, S.; Arya, A.; Singh, V. Intermittent Preventive Treatment with Sulfadoxine Pyrimethamine for Malaria: A Global Overview and Challenges Affecting Optimal Drug Uptake in Pregnant Women. *Pathog. Glob. Health* **2022**, 1–14. https://doi.org/10.1080/20477724.2022.2128563.

(88) Roh, M. E.; Kuile, F. O. T.; Rerolle, F.; Glymour, M. M.; Shiboski, S.; Gosling, R.; Gutman, J.; Kakuru, A.; Desai, M.; Kajubi, R.; L'Ianziva, A.; Kamya, M. R.; Dorsey, G.; Chico, R. M. Overall, Anti-Malarial, and Non-Malarial Effect of Intermittent Preventive Treatment during Pregnancy with Sulfadoxine-Pyrimethamine on Birthweight: A Mediation Analysis. *Lancet Glob. Heal.* **2020**, *8* (7), e942–e953. https://doi.org/10.1016/S2214-109X(20)30119-4.

(89) Olliaro, P. Mode of Action and Mechanisms of Resistance for Antimalarial Drugs. *Pharmacol. Ther.* **2001**, *89* (2), 207–219. https://doi.org/10.1016/S0163-7258(00)00115-7.

(90) Kajubi, R.; Ochieng, T.; Kakuru, A.; Jagannathan, P.; Nakalembe, M.; Ruel, T.; Opira, B.; Ochokoru, H.; Ategeka, J.; Nayebare, P.; Clark, T. D.; Havlir, D. V.; Kamya, M. R.; Dorsey, G. Monthly Sulfadoxine–Pyrimethamine versus Dihydroartemisinin–Piperaquine for Intermittent Preventive Treatment of Malaria in Pregnancy: A Double-

Blind, Randomised, Controlled, Superiority Trial. *Lancet* **2019**, *393* (10179), 1428–1439. https://doi.org/10.1016/S0140-6736(18)32224-4.

(91) Takala-Harrison, S.; Laufer, M. K. Antimalarial Drug Resistance in Africa: Key Lessons for the Future. *Ann. N. Y. Acad. Sci.* **2015**, *1342* (1), 62–67. https://doi.org/10.1111/NYAS.12766.

(92) Beshir, K. B.; Muwanguzi, J.; Nader, J.; Mansukhani, R.; Traore, A.; Gamougam, K.; Ceesay, S.; Bazie, T.; Kolie, F.; Lamine, M. M.; Cairns, M.; Snell, P.; Scott, S.; Diallo, A.; Merle, C. S.; NDiaye, J. L.; Razafindralambo, L.; Moroso, D.; Ouedraogo, J.-B.; Zongo, I.; Kessely, H.; Doumagoum, D.; Bojang, K.; Ceesay, S.; Loua, K.; Maiga, H.; Dicko, A.; Sagara, I.; Laminou, I. M.; Ogboi, S. J.; Eloike, T.; Milligan, P.; Sutherland, C. J. Prevalence of Plasmodium Falciparum Haplotypes Associated with Resistance to Sulfadoxine–Pyrimethamine and Amodiaquine before and after Upscaling of Seasonal Malaria Chemoprevention in Seven African Countries: A Genomic Surveillance Study. *Lancet Infect. Dis.* **2022**, *23* (3), 361–370. https://doi.org/10.1016/S1473-3099(22)00593-X.

(93) Boateng, R. A.; Myers-Hansen, J. L.; Dolling, N. N. O.; Mensah, B. A.; Brodsky, E.; Mazumder, M.; Ghansah, A. Global Analysis of Plasmodium Falciparum Dihydropteroate Synthase Variants Associated with Sulfadoxine Resistance Reveals Variant Distribution and Mechanisms of Resistance: A Computational-Based Study. *Molecules* **2022**, *28* (1), 145. https://doi.org/10.3390/MOLECULES28010145.

(94) Peterson, D. S.; Walliker, D.; Wellems, T. E. Evidence That a Point Mutation in Dihydrofolate Reductase-Thymidylate Synthase Confers Resistance to Pyrimethamine in Falciparum Malaria. *Proc. Natl. Acad. Sci.* **1988**, *85* (23), 9114–9118. https://doi.org/10.1073/PNAS.85.23.9114.

(95) Baggish, A. L.; Hill, D. R. Antiparasitic Agent Atovaquone. *Antimicrob. Agents Chemother.* **2002**, *46* (5), 1163–1173. https://doi.org/10.1128/AAC.46.5.1163-1173.2002.

(96) Srivastava, I. K.; Morrlsey, J. M.; Darrouzet, E.; Daldal, F.; Vaidya, A. B. Resistance Mutations Reveal the Atovaquone-Binding Domain of Cytochrome b in Malaria Parasites. *Mol. Microbiol.* **1999**, *33* (4), 704–711. https://doi.org/10.1046/J.1365-2958.1999.01515.X.

(97) Kessl, J. J.; Lange, B. B.; Merbitz-Zahradnik, T.; Zwicker, K.; Hill, P.; Meunier, B.; Pálsdóttir, H.; Hunte, C.; Meshnick, S.; Trumpower, B. L. Molecular Basis for Atovaquone Binding to the Cytochrome Bc1 Complex. *J. Biol. Chem.* **2003**, *278* (33),

31312–31318. https://doi.org/10.1074/jbc.M304042200.

(98) Srivastava, I. K.; Rottenberg, H.; Vaidya, A. B. Atovaquone, a Broad Spectrum Antiparasitic Drug, Collapses Mitochondrial Membrane Potential in a Malarial Parasite. *J. Biol. Chem.* **1997**, *272* (7), 3961–3966. https://doi.org/10.1074/jbc.272.7.3961.

(99) Staines, H. M.; Burrow, R.; Teo, B. H. Y.; Ster, I. C.; Kremsner, P. G.; Krishna, S. Clinical Implications of Plasmodium Resistance to Atovaquone/Proguanil: A Systematic Review and Meta-Analysis. *J. Antimicrob. Chemother.* **2018**, *73* (3), 581–595. https://doi.org/10.1093/JAC/DKX431.

(100) Lell, B.; Mordmüller, B.; Mordmüller, M.; Agobe, J.-C. D.; Honkpehedji, J.; Zinsou, J.; Mengue, J. B.; Loembe, M. M.; Adegnika, A. A.; Held, J.; Lalremruata, A.; Nguyen, T. T.; Esen, M.; Kc, N.; Ruben, A. J.; Chakravarty, S.; Kim, B.; Sim, L.; Billingsley, P. F.; James, E. R.; Richie, T. L.; Hoffman, S. L.; Kremsner, P. G. Impact of Sickle Cell Trait and Naturally Acquired Immunity on Uncomplicated Malaria after Controlled Human Malaria Infection in Adults in Gabon. *Am. J. Trop. Med. Hyg* **2018**, *98* (2), 508–515. https://doi.org/10.4269/ajtmh.17-0343.

(101) Langhorne, J.; Ndungu, F. M.; Sponaas, A. M.; Marsh, K. Immunity to Malaria: More Questions than Answers. *Nat. Immunol.* **2008**, *9* (7), 725–732. https://doi.org/10.1038/ni.f.205.

(102) Duffy, P. E. Making a Good Malaria Vaccine Better. *Trends Parasitol.* **2022**, *38* (1), 9–10. https://doi.org/10.1016/j.pt.2021.11.006.

(103) Sissoko, M. S.; Healy, S. A.; Katile, A.; Zaidi, I.; Hu, Z.; Kamate, B.; Samake, Y.; Sissoko, K.; Mwakingwe-Omari, A.; Lane, J.; Imeru, A.; Mohan, R.; Thera, I.; Guindo, C. O.; Dolo, A.; Niare, K.; Koïta, F.; Niangaly, A.; Rausch, K. M.; Zeguime, A.; Guindo, M. A.; Bah, A.; Abebe, Y.; James, E. R.; Manoj, A.; Murshedkar, T.; KC, N.; Sim, B. K. L.; Billingsley, P. F.; Richie, T. L.; Hoffman, S. L.; Doumbo, O.; Duffy, P. E. Safety and Efficacy of a Three-Dose Regimen of Plasmodium Falciparum Sporozoite Vaccine in Adults during an Intense Malaria Transmission Season in Mali: A Randomised, Controlled Phase 1 Trial. *Lancet Infect. Dis.* **2022**, *22* (3), 377–389. https://doi.org/10.1016/S1473-3099(21)00332-7.

(104) World Health Organization (WHO). *World Malaria Report 2017*; Geneva, 2017.

(105) Okell, L. C.; Reiter, L. M.; Ebbe, L. S.; Baraka, V.; Bisanzio, D.; Watson, O. J.; Bennett, A.; Verity, R.; Gething, P.; Roper, C.; Alifrangis, M. Emerging Implications of

Policies on Malaria Treatment: Genetic Changes in the Pfmdr-1 Gene Affecting Susceptibility to Artemether–Lumefantrine and Artesunate–Amodiaquine in Africa. *BMJ Glob. Heal.* **2018**, *3*, 1–12. https://doi.org/10.1136/bmjgh-2018-000999.

(106) Venkatesan, M.; Gadalla, N. B.; Stepniewska, K.; Dahal, P.; Nsanzabana, C.; Moriera, C.; Price, R. N.; Mårtensson, A.; Rosenthal, P. J.; Dorsey, G.; Sutherland, C. J.; Guérin, P.; Davis, T. M. E.; Ménard, D.; Adam, I.; Ademowo, G.; Arze, C.; Baliraine, F. N.; Berens-Riha, N.; Björkman, A.; Borrmann, S.; Checchi, F.; Desai, M.; Dhorda, M.; Djimdé, A. A.; El-Sayed, B. B.; Eshetu, T.; Eyase, F.; Falade, C.; Faucher, J. F.; Fröberg, G.; Grivoyannis, A.; Hamour, S.; Houzé, S.; Johnson, J.; Kamugisha, E.; Kariuki, S.; Kiechel, J. R.; Kironde, F.; Kofoed, P. E.; LeBras, J.; Malmberg, M.; Mwai, L.; Ngasala, B.; Nosten, F.; Nsobya, S. L.; Nzila, A.; Oguike, M.; Otienoburu, S. D.; Ogutu, B.; Ouédraogo, J. B.; Piola, P.; Rombo, L.; Schramm, B.; Somé, A. F.; Thwing, J.; Ursing, J.; Wong, R. P. M.; Zeynudin, A.; Zongo, I.; Plowe, C. V.; Sibley, C. H. Polymorphisms in Plasmodium Falciparum Chloroquine Resistance Transporter and Multidrug Resistance 1 Genes: Parasite Risk Factors That Affect Treatment Outcomes for P. Falciparum Malaria after Artemether-Lumefantrine and Artesunate-Amodiaquine. *Am. J. Trop. Med. Hyg.* **2014**, *91* (4), 833–843. https://doi.org/10.4269/AJTMH.14-0031/-/DC3/SD3.PDF.

(107) Renschler, J. P.; Walters, K. M.; Newton, P. N.; Laxminarayan, R. Estimated Under-Five Deaths Associated with Poor-Quality Antimalarials in Sub-Saharan Africa. *Am. J. Trop. Med. Hyg* **2015**, *92* (Suppl 6), 119–126. https://doi.org/10.4269/ajtmh.14-0725.

(108) Moss, S.; Mańko, E.; Krishna, S.; Campino, S.; Clark, T. G.; Last, A. How Has Mass Drug Administration with Dihydroartemisinin - Piperaquine Impacted Molecular Markers of Drug Resistance? A Systematic Review. *Malar. J.* **2022**, *21* (186), 1–23. https://doi.org/10.1186/s12936-022-04181-y.

(109) Leang, R.; Barrette, A.; Bouth, D. M.; Menard, D.; Abdur, R.; Duong, S.; Ringwald, P. Efficacy of Dihydroartemisinin-Piperaquine for Treatment of Uncomplicated Plasmodium Falciparum and Plasmodium Vivax in Cambodia, 2008 to 2010. *Antimicrob. Agents Chemother.* **2013**, *57* (2), 818–826. https://doi.org/10.1128/AAC.00686-12/FORMAT/EPUB.

(110) Wootton, J. C.; Feng, X.; Ferdig, M. T.; Cooper, R. A.; Mu, J.; Baruch, D. I.; Magill, A. J.; Su, X. Z. Genetic Diversity and Chloroquine Selective Sweeps in Plasmodium Falciparum. *Nature* **2002**, *418* (6895), 320–323. https://doi.org/10.1038/nature00813.

(111) Balikagala, B.; Fukuda, N.; Ikeda, M.; Katuro, O. T.; Tachibana, S.-I.; Yamauchi, M.;

Opio, W.; Emoto, S.; Anywar, D. A.; Kimura, E.; Palacpac, N. M. Q.; Odongo-Aginya, E. I.; Ogwang, M.; Horii, T.; Mita, T. Evidence of Artemisinin-Resistant Malaria in Africa. *N. Engl. J. Med.* **2021**, *385* (13), 1163–1171. https://doi.org/10.1056/NEJMOA2101746/SUPPL_FILE/NEJMOA2101746_DISCLOSURES.PDF.

(112) Thanh, N. V.; Nhien, N. T.; Thi, N.; Tuyen, K.; Tong, N. T.; Thuy, N.; Ca, N.; Dong, L. T.; Quang, H. H.; Farrar, J.; Thwaites, G.; White, N. J.; Wolbers, M.; Hien, T. T. Rapid Decline in the Susceptibility of Plasmodium Falciparum to Dihydroartemisinin–Piperaquine in the South of Vietnam. *Malar. J.* **2017**, *16* (27), 1–10. https://doi.org/10.1186/s12936-017-1680-8.

(113) Ariey, F.; Witkowski, B.; Amaratunga, C.; Beghain, J.; Langlois, A. C.; Khim, N.; Kim, S.; Duru, V.; Bouchier, C.; Ma, L.; Lim, P.; Leang, R.; Duong, S.; Sreng, S.; Suon, S.; Chuor, C. M.; Bout, D. M.; Ménard, S.; Rogers, W. O.; Genton, B.; Fandeur, T.; Miotto, O.; Ringwald, P.; Le Bras, J.; Berry, A.; Barale, J. C.; Fairhurst, R. M.; Benoit-Vical, F.; Mercereau-Puijalon, O.; Ménard, D. A Molecular Marker of Artemisinin-Resistant Plasmodium Falciparum Malaria. *Nature* **2013**, *505* (7481), 50–55. https://doi.org/10.1038/nature12876.

(114) Pelleau, S.; Moss, E. L.; Dhingra, S. K.; Volney, B.; Casteras, J.; Gabryszewski, S. J.; Volkman, S. K.; Wirth, D. F.; Legrand, E.; Fidock, D. A.; Neafsey, D. E.; Musset, L. Adaptive Evolution of Malaria Parasites in French Guiana: Reversal of Chloroquine Resistance by Acquisition of a Mutation in Pfcrt. *Proc. Natl. Acad. Sci. U. S. A.* **2015**, *112* (37), 11672–11677. https://doi.org/10.1073/PNAS.1507142112/SUPPL_FILE/PNAS.201507142SI.PDF.

(115) Lehane, A. M.; Hayward, R.; Saliba, K. J.; Kirk, K. A Verapamil-Sensitive Chloroquine-Associated H+ Leak from the Digestive Vacuole in Chloroquine-Resistant Malaria Parasites. *J. Cell Sci.* **2008**, *121* (10), 1624–1632. https://doi.org/10.1242/JCS.016758.

(116) Summers, R. L.; Nash, M. N.; Martin, R. E. Know Your Enemy : Understanding the Role of PfCRT in Drug Resistance Could Lead to New Antimalarial Tactics. *Cell. Mol. Life Sci.* **2012**, *69*, 1967–1995. https://doi.org/10.1007/s00018-011-0906-0.

(117) Birnbaum, J.; Scharf, S.; Schmidt, S.; Jonscher, E.; Sabitzki, R.; Bergmann, B.; Fröhlke, U.; Mesén-ramírez, P. A Kelch13-Defined Endocytosis Pathway Mediates Artemisinin Resistance in Malaria Parasites. *Science (80-.).* **2020**, *59* (January), 51–59.

(118) Ashley, E. A.; Dhorda, M.; Fairhurst, R. M.; Amaratunga, C.; Lim, P.; Suon, S.; Sreng, S.; Anderson, J. M.; Mao, S.; Sam, B.; Sopha, C.; Chuor, C. M.; Nguon, C.; Sovannaroth, S.; Pukrittayakamee, S.; Jittamala, P.; Chotivanich, K.; Chutasmit, K.; Suchatsoonthorn, C.; Runcharoen, R.; Hien, T. T.; Thuy-Nhien, N. T.; Thanh, N. V.; Phu, N. H.; Htut, Y.; Han, K.-T.; Aye, K. H.; Mokuolu, O. A.; Olaosebikan, R. R.; Folaranmi, O. O.; Mayxay, M.; Khanthavong, M.; Hongvanthong, B.; Newton, P. N.; Onyamboko, M. A.; Fanello, C. I.; Tshefu, A. K.; Mishra, N.; Valecha, N.; Phyo, A. P.; Nosten, F.; Yi, P.; Tripura, R.; Borrmann, S.; Bashraheil, M.; Peshu, J.; Faiz, M. A.; Ghose, A.; Hossain, M. A.; Samad, R.; Rahman, M. R.; Hasan, M. M.; Islam, A.; Miotto, O.; Amato, R.; MacInnis, B.; Stalker, J.; Kwiatkowski, D. P.; Bozdech, Z.; Jeeyapant, A.; Cheah, P. Y.; Sakulthaew, T.; Chalk, J.; Intharabut, B.; Silamut, K.; Lee, S. J.; Vihokhern, B.; Kunasol, C.; Imwong, M.; Tarning, J.; Taylor, W. J.; Yeung, S.; Woodrow, C. J.; Flegg, J. A.; Das, D.; Smith, J.; Venkatesan, M.; Plowe, C. V.; Stepniewska, K.; Guerin, P. J.; Dondorp, A. M.; Day, N. P.; White, N. J. Spread of Artemisinin Resistance in Plasmodium Falciparum Malaria . *N. Engl. J. Med.* **2014**, *371* (5), 411–423. https://doi.org/10.1056/NEJMOA1314981/SUPPL_FILE/NEJMOA1314981_DISCLOSURES.PDF.

(119) Yang, T.; Yeoh, L. M.; Tutor, M. V.; Dixon, M. W.; McMillan, P. J.; Xie, S. C.; Bridgford, J. L.; Gillett, D. L.; Duffy, M. F.; Ralph, S. A.; McConville, M. J.; Tilley, L.; Cobbold, S. A. Decreased K13 Abundance Reduces Hemoglobin Catabolism and Proteotoxic Stress, Underpinning Artemisinin Resistance. *Cell Rep.* **2019**, *29* (9), 2917-2928.e5. https://doi.org/10.1016/J.CELREP.2019.10.095.

(120) Wang, J.; Zhang, C. J.; Chia, W. N.; Loh, C. C. Y.; Li, Z.; Lee, Y. M.; He, Y.; Yuan, L. X.; Lim, T. K.; Liu, M.; Liew, C. X.; Lee, Y. Q.; Zhang, J.; Lu, N.; Lim, C. T.; Hua, Z. C.; Liu, B.; Shen, H. M.; Tan, K. S. W.; Lin, Q. Haem-Activated Promiscuous Targeting of Artemisinin in Plasmodium Falciparum. *Nat. Commun.* **2015**, *6* (1), 1–11. https://doi.org/10.1038/ncomms10111.

(121) Fidock, D. A.; Nomura, T.; Talley, A. K.; Cooper, R. A.; Dzekunov, S. M.; Ferdig, M. T.; Ursos, L. M. B.; Sidhu, A. B.; Naudé, B.; Deitsch, K. W.; Su, X.; Wootton, J. C.; Roepe, P. D.; Wellems, T. E. Mutations in the P. Falciparum Digestive Vacuole Transmembrane Protein PfCRT and Evidence for Their Role in Chloroquine Resistance. *Mol. Cell* **2000**, *6* (4), 861–871. https://doi.org/10.1016/S1097-2765(05)00077-8.

(122) Cooper, R. A.; Ferdig, M. T.; Su, X. Z.; Ursos, L. M. B.; Mu, J.; Nomura, T.; Fujioka,

H.; Fidock, D. A.; Roepe, P. D.; Wellems, T. E. Alternative Mutations at Position 76 of the Vacuolar Transmembrane Protein PfCRT Are Associated with Chloroquine Resistance and Unique Stereospecific Quinine and Quinidine Responses in Plasmodium Falciparum. *Mol. Pharmacol.* **2002**, *61* (1), 35–42. https://doi.org/10.1124/mol.61.1.35.

(123) Martin, R. E.; Marchetti, R. V; Cowan, A. I.; Howitt, S. M.; Bröer, S.; Kirk, K. Chloroquine Transport via the Malaria Parasite's Resistance Transporter. *Science (80-.).* **2009**, *325* (5948), 1680–1683. https://doi.org/10.1126/science.1175667 Malaria.

(124) Kim, J.; Tan, Y. Z.; Wicht, K. J.; Erramilli, S. K.; Dhingra, S. K.; Okombo, J.; Vendome, J.; Hagenah, L. M.; Giacometti, S. I.; Warren, A. L.; Nosol, K.; Roepe, P. D.; Potter, C. S.; Carragher, B.; Kossiakoff, A. A.; Quick, M.; Fidock, D. A.; Mancia, F. Structure and Drug Resistance of the Plasmodium Falciparum Transporter PfCRT. *Nature* **2019**, *576* (7786), 315–320. https://doi.org/10.1038/s41586-019-1795-x.

(125) Lakshmanan, V.; Bray, P. G.; Verdier-Pinard, D.; Johnson, D. J.; Horrocks, P.; Muhle, R. A.; Alakpa, G. E.; Hughes, R. H.; Ward, S. A.; Krogstad, D. J.; Sidhu, A. B. S.; Fidock, D. A. A Critical Role for PfCRT K76T in Plasmodium Falciparum Verapamil-Reversible Chloroquine Resistance. *EMBO J.* **2005**, *24* (13), 2294–2305. https://doi.org/10.1038/SJ.EMBOJ.7600681.

(126) Callaghan, P. S.; Hassett, M. R.; Roepe, P. D. Functional Comparison of 45 Naturally Occurring Isoforms of the Plasmodium Falciparum Chloroquine Resistance Transporter (PfCRT). *Biochemistry* **2015**, *54* (32), 5083–5094. https://doi.org/10.1021/acs.biochem.5b00412.

(127) Valderramos, S. G.; Valderramos, J. C.; Musset, L.; Purcell, L. A.; Mercereau-Puijalon, O.; Legrand, E.; Fidock, D. A. Identification of a Mutant PfCRT-Mediated Chloroquine Tolerance Phenotype in Plasmodium Falciparum. *PLoS Pathog.* **2010**, *6* (5), 1–14. https://doi.org/10.1371/JOURNAL.PPAT.1000887.

(128) Rohrbach, P.; Sanchez, C. P.; Hayton, K.; Friedrich, O.; Patel, J.; Sidhu, A. B. S.; Ferdig, M. T.; Fidock, D. A.; Lanzer, M. Genetic Linkage of Pfmdr1 with Food Vacuolar Solute Import in Plasmodium Falciparum. *EMBO J.* **2006**, *25* (13), 3000–3011. https://doi.org/10.1038/SJ.EMBOJ.7601203.

(129) Sidhu, A. B. S.; Valderramos, S. G.; Fidock, D. A. Pfmdr1 Mutations Contribute to Quinine Resistance and Enhance Mefloquine and Artemisinin Sensitivity in Plasmodium Falciparum. *Mol. Microbiol.* **2005**, *57* (4), 913–926.

https://doi.org/10.1111/J.1365-2958.2005.04729.X.

(130) Amaratunga, C.; Lim, P.; Suon, S.; Sreng, S.; Mao, S.; Sopha, C.; Sam, B.; Dek, D.; Try, V.; Amato, R.; Blessborn, D.; Song, L.; Tullo, G. S.; Fay, M. P.; Anderson, J. M.; Tarning, J.; Fairhurst, R. M. Dihydroartemisinin–Piperaquine Resistance in Plasmodium Falciparum Malaria in Cambodia: A Multisite Prospective. *Lancet Infect. Dis.* **2016**, *3099* (15), 1–9. https://doi.org/10.1016/S1473-3099(15)00487-9.

(131) Amato, R.; Lim, P.; Miotto, O.; Amaratunga, C.; Dek, D.; Pearson, R. D.; Almagro-Garcia, J.; Neal, A. T.; Sreng, S.; Suon, S.; Drury, E.; Jyothi, D.; Stalker, J.; Kwiatkowski, D. P.; Fairhurst, R. M. Genetic Markers Associated with Dihydroartemisinin–Piperaquine Failure in Plasmodium Falciparum Malaria in Cambodia: A Genotype–Phenotype Association Study. *Lancet Infect. Dis.* **2017**, *17* (2), 164–173. https://doi.org/10.1016/S1473-3099(16)30409-1.

(132) Witkowski, B.; Duru, V.; Khim, N.; Ross, L. S.; Saintpierre, B.; Beghain, J.; Chy, S.; Kim, S.; Ke, S.; Kloeung, N.; Eam, R.; Khean, C.; Ken, M.; Loch, K.; Bouillon, A.; Domergue, A.; Ma, L.; Bouchier, C.; Leang, R.; Huy, R.; Nuel, G.; Barale, J. C.; Legrand, E.; Ringwald, P.; Fidock, D. A.; Mercereau-Puijalon, O.; Ariey, F.; Ménard, D. A Surrogate Marker of Piperaquine-Resistant Plasmodium Falciparum Malaria: A Phenotype–Genotype Association Study. *Lancet Infect. Dis.* **2017**, *17* (2), 174–183. https://doi.org/10.1016/S1473-3099(16)30415-7.

(133) Mukherjee, A.; Gagnon, D.; Wirth, D. F.; Richard, D. Inactivation of Plasmepsins 2 and 3 Sensitizes Plasmodium Falciparum to the Antimalarial Drug Piperaquine. *Antimicrob. Agents Chemother.* **2018**, *62* (4). https://doi.org/10.1128/AAC.02309-17.

(134) Boonyalai, N.; Kirativanich, K.; Thamnurak, C.; Praditpol, C.; Vesely, B. A.; Wojnarski, M.; Griesenbeck, J. S.; Waters, N. C. A Single Point Mutation in the Plasmodium Falciparum 3′–5′ Exonuclease Does Not Alter Piperaquine Susceptibility. *Malar. J.* **2022**, *21* (1), 1–14. https://doi.org/10.1186/S12936-022-04148-Z/FIGURES/3.

(135) *World Health Organization (WHO), World Malaria Report 2019*; 2019.

(136) Burrows, J. N.; Van Huijsduijnen, R. H.; Möhrle, J. J.; Oeuvray, C.; Wells, T. N. Designing the next Generation of Medicines for Malaria Control and Eradication. *Malar. J.* **2013**, *12* (187), 1–20. https://doi.org/10.1186/1475-2875-12-187.

(137) Burrows, J. N.; Leroy, D.; Lotharius, J.; Waterson, D. Challenges in Antimalarial Drug Discovery. *Future Med. Chem.* **2011**, *3* (11), 1401–1412. https://doi.org/10.4155/fmc.11.91.

(138) Chou, A. C.; Chevli, R.; Fitch, C. D. Ferriprotoporphyrin IX Fulfills the Criteria for Identification as the Chloroquine Receptor of Malaria Parasites. *Biochemistry* **1980**, *19*, 1543–1549.

(139) Chou, A. C.; Fitch, C. D. Hemolysis of Mouse Erythrocytes by Ferriprotoporphyrin IX and Chloroquine. *J. Clin. Invest.* **1980**, *66* (4), 856–858. https://doi.org/10.1172/JCI109925.

(140) Ismail, H. M.; Barton, V.; Phanchana, M.; Charoensutthivarakul, S.; Wong, M. H. L.; Hemingway, J.; Biagini, G. A.; O'neill, P. M.; Ward, S. A. Artemisinin Activity-Based Probes Identify Multiple Molecular Targets within the Asexual Stage of the Malaria Parasites Plasmodium Falciparum 3D7. *Proc. Natl. Acad. Sci.* **2016**, *113* (8), 2080–2085. https://doi.org/10.1073/pnas.1600459113.

(141) Greenwood, D. The Quinine Connection. *J. Antimicrob. Chemother.* **1992**, *30* (4), 417–427. https://doi.org/10.1093/jac/30.4.417.

(142) Egan, T. J. Quinoline Antimalarials. *Expert Opin. Ther. Pat.* **2001**, *11* (2), 185–209. https://doi.org/10.1517/13543776.2010.518674.

(143) Combrinck, J. M.; Fong, K. Y.; Gibhard, L.; Smith, P. J.; Wright, D. W.; Egan, T. J. Optimization of a Multi-Well Colorimetric Assay to Determine Haem Species in Plasmodium Falciparum in the Presence of Anti-Malarials. *Malar. J.* **2015**, *14* (1), 1–14. https://doi.org/10.1186/s12936-015-0729-9.

(144) Vanaerschot, M.; Lucantoni, L.; Li, T.; Combrinck, J. M.; Ruecker, A.; Kumar, T. R. S.; Rubiano, K.; Ferreira, P. E.; Siciliano, G.; Gulati, S.; Henrich, P. P.; Ng, C. L.; Murithi, J. M.; Corey, V. C.; Duffy, S.; Lieberman, O. J.; Veiga, M. I.; Sinden, R. E.; Alano, P.; Delves, M. J.; Sim, K. L.; Winzeler, E. A.; Egan, T. J.; Hoffman, S. L.; Avery, V. M.; Fidock, D. A. Hexahydroquinolines Are Antimalarial Candidates with Potent Blood-Stage and Transmission-Blocking Activity. *Nat. Microbiol.* **2017**, *2*, 1403–1414. https://doi.org/10.1038/s41564-017-0007-4.

(145) De Villiers, K. A.; Egan, T. J. Heme Detoxification in the Malaria Parasite: A Target for Antimalarial Drug Development. *Acc. Chem. Res.* **2021**, *54* (11), 2649–2659. https://doi.org/10.1021/acs.accounts.1c00154.

(146) Saliba, K. J.; W Allen, R. J.; Zissis, S.; Bray, P. G.; Ward, S. A.; Kirk, K. Acidification of the Malaria Parasite's Digestive Vacuole by a H+-ATPase and a H+-Pyrophosphatase. *J. Biol. Chem.* **2002**, *278* (8), 5605–5612. https://doi.org/10.1074/jbc.M208648200.

(147) Sullivan, D. J.; Gluzman, I. Y.; Russell, D. G.; Goldberg, D. E. On the Molecular Mechanism of Chloroquine's Antimalarial Action. *Proc. Natl. Acad. Sci. U. S. A.* **1996**, *93* (21), 11865–11870. https://doi.org/10.1073/PNAS.93.21.11865.

(148) Yayon, A.; Cabantchik, Z. I.; Ginsburg, H. Susceptibility of Human Malaria Parasites to Chloroquine Is PH Dependent. *Proc. Natl. Acad. Sci. U. S. A.* **1985**, *82* (9), 2784–2788. https://doi.org/10.1073/PNAS.82.9.2784.

(149) Dzekunov, S. M.; Ursos, L. M. B.; Roepe, P. D. Digestive Vacuolar PH of Intact Intraerythrocytic P. Falciparum Either Sensitive or Resistant to Chloroquine. *Mol. Biochem. Parasitol.* **2000**, *110* (1), 107–124. https://doi.org/10.1016/S0166-6851(00)00261-9.

(150) Bennett, T. N.; Kosar, A. D.; Ursos, L. M. B.; Dzekunov, S.; Sidhu, A. B. S.; Fidock, D. A.; Roepe, P. D. Drug Resistance-Associated PfCRT Mutations Confer Decreased Plasmodium Falciparum Digestive Vacuolar PH. *Mol. Biochem. Parasitol.* **2004**, *133* (1), 99–114. https://doi.org/10.1016/J.MOLBIOPARA.2003.09.008.

(151) Klonis, N.; Tan, O.; Jackson, K.; Goldberg, D.; Klemba, M.; Tilley, L. Evaluation of PH during Cytostomal Endocytosis and Vacuolar Catabolism of Haemoglobin in Plasmodium Falciparum. *Biochem. J.* **2007**, *407* (3), 343–354. https://doi.org/10.1042/BJ20070934.

(152) Egan, T. J.; Ross, D. C.; Adams, P. A. Quinoline Anti-Malarial Drugs Inhibit Spontaneous Formation of β-Haematin (Malaria Pigment). *FEBS Lett.* **1994**, *352* (1), 54–57. https://doi.org/10.1016/0014-5793(94)00921-X.

(153) Solomonov, I.; Osipova, M.; Feldman, Y.; Baehtz, C.; Kjaer, K.; Robinson, I. K.; Webster, G. T.; McNaughton, D.; Wood, B. R.; Weissbuch, I.; Leiserowitz, L. Crystal Nucleation, Growth, and Morphology of the Synthetic Malaria Pigment β-Hematin and the Effect Thereon by Quinoline Additives: The Malaria Pigment as a Target of Various Antimalarial Drugs. *J. Am. Chem. Soc.* **2007**, *129* (9), 2615–2627. https://doi.org/10.1021/JA0674183/SUPPL_FILE/JA0674183SI20061217_050145.PDF.

(154) Olafson, K. N.; Nguyen, T. Q.; Rimer, J. D.; Vekilov, P. G. Antimalarials Inhibit Hematin Crystallization by Unique Drug–Surface Site Interactions. *Proc. Natl. Acad. Sci. U. S. A.* **2017**, *114* (29), 7531–7536. https://doi.org/10.1073/PNAS.1700125114/-/DCSUPPLEMENTAL/PNAS.1700125114.SAPP.PDF.

(155) Kapishnikov, S.; Staalsø, T.; Yang, Y.; Lee, J.; Pérez-Berná, A. J.; Pereiro, E.; Yang,

Y.; Werner, S.; Guttmann, P.; Leiserowitz, L.; Als-Nielsen, J. Mode of Action of Quinoline Antimalarial Drugs in Red Blood Cells Infected by Plasmodium Falciparum Revealed in Vivo. *Proc. Natl. Acad. Sci. U. S. A.* **2019**, *116* (46), 22946–22952. https://doi.org/10.1073/pnas.1910123116.

(156) Dorn, A.; Stoffel, R.; Matile, H.; Bubendorf, A.; Ridley, R. G. Malarial Haemozoin/β-Haematin Supports Haem Polymerization in the Absence of Protein. *Lett. to Nat.* **1995**, *374*, 269–271.

(157) Fitch, C. D.; Cai, G. Z.; Chen, Y. F.; Shoemaker, J. D. Involvement of Lipids in Ferriprotoporphyrin IX Polymerization in Malaria. *Biochim. Biophys. Acta - Mol. Basis Dis.* **1999**, *1454* (1), 31–37. https://doi.org/10.1016/S0925-4439(99)00017-4.

(158) Ncokazi, K. K.; Egan, T. J. A Colorimetric High-Throughput b -Hematin Inhibition Screening Assay for Use in the Search for Antimalarial Compounds. *Anal. Biochem.* **2005**, *338*, 306–319. https://doi.org/10.1016/j.ab.2004.11.022.

(159) Combrinck, J. M.; Mabotha, T. E.; Ncokazi, K. K.; Ambele, M. A.; Taylor, D.; Smith, P. J.; Hoppe, H. C.; Egan, T. J. Insights into the Role of Heme in the Mechanism of Action of Antimalarials. *ACS Chem. Biol.* **2013**, *8* (1), 133–137. https://doi.org/10.1021/cb300454t.

(160) L'abbate, F. P.; Müller, R.; Openshaw, R.; Combrinck, J. M.; De Villiers, K. A.; Hunter, R.; Egan, T. J. Hemozoin Inhibiting 2-Phenylbenzimidazoles Active against Malaria Parasites. *Eur. J. Med. Chem.* **2018**, *159*, 243–254. https://doi.org/10.1016/j.ejmech.2018.09.060.

(161) Wicht, K. J.; Combrinck, J. M.; Smith, P. J.; Hunter, R.; Egan, T. J. Identification and Mechanistic Evaluation of Hemozoin-Inhibiting Triarylimidazoles Active against Plasmodium Falciparum. *ACS Med. Chem. Lett.* **2017**, *8* (2), 201–205. https://doi.org/10.1021/acsmedchemlett.6b00416.

(162) Pashynska, V. A.; Van Den Heuvel, H.; Claeys, M.; Kosevich, M. V. Characterization of Noncovalent Complexes of Antimalarial Agents of the Artemisinin-Type and Fe(III)-Heme by Electrospray Mass Spectrometry and Collisional Activation Tandem Mass Spectrometry. *J. Am. Soc. Mass Spectrom.* **2004**, *15* (8), 1181–1190. https://doi.org/10.1016/j.jasms.2004.04.030.

(163) Heller, L. E.; Goggins, E.; Roepe, P. D. Dihydroartemisinin-Ferriprotoporphyrin IX Adduct Abundance in Plasmodium Falciparum Malarial Parasites and the Relationship to Emerging Artemisinin Resistance. *Biochemistry* **2018**, *57* (51), 6935–

6945. https://doi.org/10.1021/acs.biochem.8b00960.

(164) Swartz, M. HPLC Detectors: A Brief Review. *J. Liq. Chromatogr. Relat. Technol.* **2010**, *33* (9–12), 1130–1150. https://doi.org/10.1080/10826076.2010.484356.

(165) Orjih, A. U.; Banyal, H. S.; Foster, R. C.; Fitch, C. D. Hemin Lyses Malaria Parasites. *Science (80-.).* **1981**, *214*, 667–669. https://doi.org/10.1126/science.7027441.

(166) Chatterjee, A. K.; Yeung, B. K. S. Back to the Future: Lessons Learned in Modern Target-Based and Whole-Cell Lead Optimization of Antimalarials. *Curr. Top. Med. Chem.* **2012**, *12* (5), 473–483. https://doi.org/10.2174/156802612799362977.

(167) Winstanley, P. A.; Breckenridge, A. M. Currently Important Antimalarial Drugs. *Ann. Trop. Med. Parasitol.* **1987**, *81* (5), 619–627. https://doi.org/10.1080/00034983.1987.11812163.

(168) Sanchez, C. P.; Dave, A.; Stein, W. D.; Lanzer, M. Transporters as Mediators of Drug Resistance in Plasmodium Falciparum. *Int. J. Parasitol.* **2010**, *40*, 1109–1118. https://doi.org/10.1016/j.ijpara.2010.04.001.

(169) Kaschula, C. H.; Egan, T. J.; Hunter, R.; Basilico, N.; Parapini, S.; Taramelli, D.; Pasini, E.; Monti, D. Structure-Activity Relationships in 4-Aminoquinoline Antiplasmodials. The Role of the Group at the 7-Position. *J. Med. Chem.* **2002**, *45* (16), 3531–3539. https://doi.org/10.1021/JM020858U/ASSET/IMAGES/LARGE/JM020858UF00005.JPEG.

(170) Stringer, T.; De Kock, C.; Guzgay, H.; Okombo, J.; Liu, J.; Kanetake, S.; Kim, J.; Tam, C.; Cheng, L. W.; Smith, P. J.; Hendricks, D. T.; Land, K. M.; Egan, T. J.; Smith, G. S. Mono- and Multimeric Ferrocene Congeners of Quinoline-Based Polyamines as Potential Antiparasitics. *Dalt. Trans.* **2016**, *45* (34), 13415–13426. https://doi.org/10.1039/C6DT02685K.

(171) Wani, W. A.; Jameel, E.; Baig, U.; Mumtazuddin, S.; Hun, L. T. Ferroquine and Its Derivatives: New Generation of Antimalarial Agents. *Eur. J. Med. Chem.* **2015**, *101* (2015), 534–551. https://doi.org/10.1016/j.ejmech.2015.07.009.

(172) Vippagunta, S. R.; Dorn, A.; Matile, H.; Bhattacharjee, A. K.; Karle, J. M.; Ellis, W. Y.; Ridley, R. G.; Vennerstrom, J. L. Structural Specificity of Chloroquine-Hematin Binding Related to Inhibition of Hematin Polymerization and Parasite Growth. *J. Med. Chem.* **1999**, *42* (22), 4630–4639. https://doi.org/10.1021/JM9902180/ASSET/IMAGES/LARGE/JM9902180F00003.JPE

G.

(173) Egan, T. J.; Hunter, R.; Kaschula, C. H.; Marques, H. M.; Misplon, A.; Walden, J. Structure-Function Relationships in Aminoquinolines: Effect of Amino and Chloro Groups on Quinoline-Hematin Complex Formation, Inhibition of β- Hematin Formation, and Antiplasmodial Activity. *J. Med. Chem.* **2000**, *43* (2), 283–291. https://doi.org/10.1021/JM990437L/ASSET/IMAGES/LARGE/JM990437LF00005.JPEG.

(174) Nantasenamat, C.; Isarankura-Na-Ayudhya, C.; Naenna, T.; Prachayasittikul, V. Review Article: A Practical Overview of Quantitative Structure-Activity Relationship. *EXCLI J.* **2009**, *8*, 74–88.

(175) Zishiri, V. K.; Hunter, R.; Smith, P. J.; Taylor, D.; Summers, R.; Kirk, K.; Martin, R. E.; Egan, T. J. A Series of Structurally Simple Chloroquine Chemosensitizing Dibemethin Derivatives That Inhibit Chloroquine Transport by PfCRT. *Eur. J. Med. Chem.* **2011**, *46* (5), 1729–1742. https://doi.org/10.1016/J.EJMECH.2011.02.026.

(176) Joshi, M. C.; Okombo, J.; Nsumiwa, S.; Ndove, J.; Taylor, D.; Wiesner, L.; Hunter, R.; Chibale, K.; Egan, T. J. 4-Aminoquinoline Antimalarials Containing a Benzylmethylpyridylmethylamine Group Are Active against Drug Resistant Plasmodium Falciparum and Exhibit Oral Activity in Mice. *J. Med. Chem.* **2017**, *60* (24), 10245–10256. https://doi.org/10.1021/ACS.JMEDCHEM.7B01537/SUPPL_FILE/JM7B01537_SI_002.CSV.

(177) Nsumiwa, S.; Kuter, D.; Wittlin, S.; Chibale, K.; Egan, T. J. Structure-Activity Relationships for Ferriprotoporphyrin IX Association and β-Hematin Inhibition by 4-Aminoquinolines Using Experimental and Ab Initio Methods. *Bioorganic Med. Chem.* **2013**, *21* (13), 3738–3748. https://doi.org/10.1016/J.BMC.2013.04.040.

(178) Joshi, M. C.; Wicht, K. J.; Taylor, D.; Hunter, R.; Smith, P. J.; Egan, T. J. In Vitro Antimalarial Activity, β-Haematin Inhibition and Structure-Activity Relationships in a Series of Quinoline Triazoles. *Eur. J. Med. Chem.* **2013**, *69*, 338–347. https://doi.org/10.1016/J.EJMECH.2013.08.046.

(179) Wang, N.; Wicht, K. J.; Imai, K.; Wang, M. Q.; Anh Ngoc, T.; Kiguchi, R.; Kaiser, M.; Egan, T. J.; Inokuchi, T. Synthesis, β-Haematin Inhibition, and in Vitro Antimalarial Testing of Isocryptolepine Analogues: SAR Study of Indolo[3,2-c]Quinolines with Various Substituents at C2, C6, and N11. *Bioorg. Med. Chem.* **2014**, *22* (9), 2629–2642. https://doi.org/10.1016/J.BMC.2014.03.030.

(180) Wicht, K. J.; Combrinck, J. M.; Smith, P. J.; Hunter, R.; Egan, T. J. Identification and SAR Evaluation of Hemozoin-Inhibiting Benzamides Active against Plasmodium Falciparum. *Am. Chem. Soc.* **2016**, *59* (13), 6512–6530. https://doi.org/10.1021/acs.jmedchem.6b00719.

(181) Lionta, E.; Spyrou, G.; Vassilatis, D. K.; Cournia, Z. Structure-Based Virtual Screening for Drug Discovery: Principles, Applications and Recent Advances. *Curr. Top. Med. Chem.* **2014**, *14* (16), 1923–1938.

(182) De Sousa, A. C. C.; Combrinck, J. M.; Maepa, K.; Egan, T. J. Virtual Screening as a Tool to Discover New β-Haematin Inhibitors with Activity against Malaria Parasites. *Sci. Rep.* **2020**, *10* (1), 3374. https://doi.org/10.1038/s41598-020-60221-0.

(183) Amod, L.; Mohunlal, R.; Teixeira, N.; Egan, T. J.; Wicht, K. J. Identifying Inhibitors of β-Haematin Formation with Activity against Chloroquine-Resistant Plasmodium Falciparum Malaria Parasites via Virtual Screening Approaches. *Sci. Reports 2023 131* **2023**, *13* (1), 1–10. https://doi.org/10.1038/s41598-023-29273-w.

(184) Dziekan, J. M.; Wirjanata, G.; Dai, L.; Go, K. D.; Yu, H.; Lim, Y. T.; Chen, L.; Wang, L. C.; Puspita, B.; Prabhu, N.; Sobota, R. M.; Nordlund, P.; Bozdech, Z. Cellular Thermal Shift Assay for the Identification of Drug–Target Interactions in the Plasmodium Falciparum Proteome. *Nat. Protoc.* **2020**, *15* (6), 1881–1921. https://doi.org/10.1038/s41596-020-0310-z.

(185) Hoelz, L. V.; Calil, F. A.; Nonato, M. C.; Pinheiro, L. C.; Boechat, N. Plasmodium Falciparum Dihydroorotate Dehydrogenase: A Drug Target against Malaria. *Future Med. Chem.* **2018**, *10* (15), 1853–1874. https://doi.org/10.4155/fmc-2017-0250.

(186) Hasan, A. M.; Mazumder, H. M. H.; Chowdhury, S. A.; Datta, A.; Khan, A. M. Molecular-Docking Study of Malaria Drug Target Enzyme Transketolase in Plasmodium Falciparum 3D7 Portends the Novel Approach to Its Treatment. *Source Code Biol. Med.* **2015**, *10* (1), 1–14. https://doi.org/10.1186/s13029-015-0037-3.

(187) Openshaw, R.; Maepa, K.; Benjamin, S. J.; Wainwright, L.; Combrinck, J. M.; Hunter, R.; Egan, T. J. A Diverse Range of Hemozoin Inhibiting Scaffolds Act on Plasmodium Falciparum as Heme Complexes. *ACS Infect. Dis.* **2021**, *7* (2), 362–376. https://doi.org/10.1021/acsinfecdis.0c00680.

(188) Birkholtz, L. M.; Coetzer, T. L.; Mancama, D.; Leroy, D.; Alano, P. Discovering New Transmission-Blocking Antimalarial Compounds: Challenges and Opportunities. *Trends Parasitol.* **2016**, *32* (9), 669–681. https://doi.org/10.1016/j.pt.2016.04.017.

(189) Sandlin, R. D.; Fong, K. Y.; Wicht, K. J.; Carrell, H. M.; Egan, T. J.; Wright, D. W. Identification of β-Hematin Inhibitors in a High-Throughput Screening Effort Reveals Scaffolds with in Vitro Antimalarial Activity. *Int. J. Parasitol. Drugs Drug Resist.* **2014**, *4* (3), 316–325. https://doi.org/10.1016/j.ijpddr.2014.08.002.

(190) De Sousa, A. C. C.; Maepa, K.; Combrinck, J. M.; Egan, T. J. Lapatinib, Nilotinib and Lomitapide Inhibit Haemozoin Formation in Malaria Parasites. *Molecules* **2020**, *25* (7), 1–15. https://doi.org/10.3390/molecules25071571.

(191) Antony, H. A.; Parija, S. C. Antimalarial Drug Resistance: An Overview. *Trop. Parasitol.* **2016**, *6* (1), 30–41. https://doi.org/10.4103/2229-5070.175081.

(192) Dhingra, S. K.; Redhi, D.; Combrinck, J. M.; Yeo, T.; Winzeler, E.; Mok, S.; Egan, T. J.; Fidock, A. A Variant PfCRT Isoform Can Contribute to Plasmodium Falciparum Resistance to the First-Line Partner Drug Piperaquine. *Am. Soc. Microbiol.* **2017**, *8* (3), e00303-17. https://doi.org/10.1128/mBio.00303-17.

(193) Trager, W.; Jensen, J. B. Human Malaria Parasites in Continuous Culture. *Science (80-.).* **1976**, *193* (4254), 673–675.

(194) Lambros, C.; Vandenberg, J. P. Synchronization of Plasmodium Falciparum Erythrocytic Stages in Culture. *J. Parasitol.* **1979**, *65* (3), 418–420.

(195) Kutner, S., Breuer, W.V., Ginsburg, H,. Aley, S.B., Cabantchik, Z. I. Characterization of Permeation Pathways in the Plasma Membrane of Human Erythrocytes Infected with Early Stages of Plasmodium Falciparum: Association With Parasite Development. *J. Cell. Physiol.* **1985**, *125*, 521–527.

(196) Makler, M. T.; Hinrichs, D. J. Measurement of the Lactate Dehydrogenase Activity of Plasmodium Falciparum as an Assessment of Parasitemia. *Am. J. Trop. Med. Hyg.* **1993**, *48* (2), 205–210.

(197) Sherman, I. W. Molecular Heterogeneity of Lactic Dehydrogenase In Avian Malaria (Plasmodium Lophurae). *J. Exp. Med.* **1961**, *114* (6), 1049–1062. https://doi.org/10.1084/jem.114.6.1049.

(198) Markwalter, C. F.; Davis, K. M.; Wright, D. W. Immunomagnetic Capture and Colorimetric Detection of Malarial Biomarker Plasmodium Falciparum Lactate Dehydrogenase. *Anal. Biochem.* **2016**, *493*, 30–34. https://doi.org/10.1016/j.ab.2015.10.003.

(199) Zeman, E. M.; Brown, J. M.; Lemmon, M. J.; Hirst, V. K.; Lee, W. W. SR-4233: A New

Bioreductive Agent with High Selective Toxicity for Hypoxic Mammalian Cells. *Int. J. Radiat. Oncol. Biol. Phys.* **1986**, *12* (7), 1239–1242. https://doi.org/10.1016/0360-3016(86)90267-1.

(200) Noh, S. M.; Sathyamurthy, M.; Lee, G. M. Development of Recombinant Chinese Hamster Ovary Cell Lines for Therapeutic Protein Production. *Curr. Opin. Chem. Eng.* **2013**, *2* (4), 391–397. https://doi.org/10.1016/j.coche.2013.08.002.

(201) Wurm, F. M. Production of Recombinant Protein Therapeutics in Cultivated Mammalian Cells. *Nat. Biotechnol.* **2004**, *22* (11), 1393–1399. https://doi.org/10.1038/nbt1026.

(202) Mosmann, T. Rapid Colorimetric Assay for Cellular Growth and Survival: Application to Proliferation and Cytotoxicity Assays. *J. Immunol. Methods* **1983**, *65* (1–2), 55–63. https://doi.org/10.1016/0022-1759(83)90303-4.

(203) Chaparro, M. J.; Calderon, F.; Castaneda, P.; Fernandez-Alvaro, E.; Gabarro, R.; Gamo, F. J.; Gomez-Lorenzo, M. G.; Martin, J.; Fernandez, E. Efforts Aimed To Reduce Attrition in Antimalarial Drug Discovery: A Systematic Evaluation of the Current Antimalarial Targets Portfolio. *ACS Infect. Dis.* **2018**, *4*, 568–576. https://doi.org/10.1021/acsinfecdis.7b00211.

(204) Carter, M.; Phelan, V.; Sandlin, R.; Bachmann, B.; Wright, D. Lipophilic Mediated Assays for β-Hematin Inhibitors. *Comb. Chem. High Throughput Screen.* **2010**, *13* (3), 285–292. https://doi.org/10.2174/138620710790980496.

(205) Bennett, T. N.; Paguio, M.; Gligorijevic, B.; Seudieu, C.; Kosar, A. D.; Davidson, E.; Roepe, P. D. Novel, Rapid, and Inexpensive Cell-Based Quantification of Antimalarial Drug Efficacy. *Antimicrob. Agents Chemother.* **2004**, *48* (5), 1807–1810. https://doi.org/10.1128/AAC.48.5.1807-1810.2004.

(206) Johnson, J. D.; Dennull, R. A.; Gerena, L.; Lopez-Sanchez, M.; Roncal, N. E.; Waters, N. C. Assessment and Continued Validation of the Malaria SYBR Green I-Based Fluorescence Assay for Use in Malaria Drug Screening. *Antimicrob. Agents Chemother.* **2007**, *51* (6), 1926–1933. https://doi.org/10.1128/AAC.01607-06.

(207) Macey, M. G. *Flow Cytometry: Principles and Applications*; Macey, M. G., Ed.; Humana Press: Totowa, NJ, 2007. https://doi.org/10.1007/978-1-59745-451-3.

(208) Phyo, A. P.; Ashley, E. A.; Anderson, T. J. C.; Bozdech, Z.; Carrara, V. I.; Sriprawat, K.; Nair, S.; White, M. M. D.; Dziekan, J.; Ling, C.; Proux, S.; Konghahong, K.; Jeeyapant, A.; Woodrow, C. J.; Imwong, M.; McGready, R.; Lwin, K. M.; Day, N. P. J.;

White, N. J.; Nosten, F. Declining Efficacy of Artemisinin Combination Therapy Against P. Falciparum Malaria on the Thai-Myanmar Border (2003-2013): The Role of Parasite Genetic Factors. *Clin. Infect. Dis.* **2016**, *63* (6), 784–791. https://doi.org/10.1093/cid/ciw388.

(209) Sams-Dodd, F. Target-Based Drug Discovery: Is Something Wrong? *Drug Discov. Today* **2005**, *10* (2), 139–147. https://doi.org/10.1016/S1359-6446(04)03316-1.

(210) Shoichet, B. K. Virtual Screening of Chemical Libraries. *Nature* **2004**, *432*, 862–865. https://doi.org/10.1038/nature03197.

(211) De Villiers, K. A.; Gildenhuys, J.; le Roex, T. Iron(III) Protoporphyrin IX Complexes of the Antimalarial Cinchona Alkaloids Quinine and Quinidine. *ACS Chem. Biol.* **2012**, *7* (4), 666–671. https://doi.org/10.1021/cb200528z.

(212) De Sousa, A. C. C.; Combrinck, J. M.; Maepa, K.; Egan, T. J. THC Shows Activity against Cultured Plasmodium Falciparum. *Bioorg. Med. Chem. Lett.* **2021**, *54*, 128442. https://doi.org/10.1016/J.BMCL.2021.128442.

(213) *DrugBank Online | Database for Drug and Drug Target Info*. https://go.drugbank.com/ (accessed 2023-06-12).

(214) *Chemdiv Inc - Fully Integrated Target-to-Clinic Contract Research Organization (CRO).* https://www.chemdiv.com/?campaignid=16700518486&adgroupid=140238572532&keyword=chemdiv&device=c&gclid=CjwKCAjwhJukBhBPEiwAniIcNWWRZX-tS7Vkon2yjW6dV9cAv97sJOKq8d6BqKaBr0Ouj6sXkBqNVBoCYCQQAvD_BwE (accessed 2023-06-12).

(215) Gaisey, J.; Narouze, S. N. Dronabinol (Marinol®). In *Cannabinoids and Pain*; Narouze, S. . N., Ed.; Springer International Publishing: Cham, 2021; pp 105–107. https://doi.org/10.1007/978-3-030-69186-8_14.

(216) Yang, J.; He, Y.; Li, Y.; Zhang, X.; Wong, Y.; Shen, S.; Zhong, T.; Zhang, J.; Liu, Q.; Wang, J. Advances in the Research on the Targets of Anti-Malaria Actions of Artemisinin. *Pharmacol. Ther.* **2020**, *216* (107697). https://doi.org/10.1016/j.pharmthera.2020.107697.

(217) Medina, P. J.; Goodin, S. Lapatinib: A Dual Inhibitor of Human Epidermal Growth Factor Receptor Tyrosine Kinases. *Clin. Ther.* **2008**, *30* (8), 1426–1447. https://doi.org/10.1016/j.clinthera.2008.08.008.

(218) Deininger, M. W. Nilotinib. *Clin. Cancer Res.* **2008**, *14* (13), 4027–4031. https://doi.org/10.1158/1078-0432.CCR-07-5015.

(219) Goulooze, S. C.; Cohen, A. F.; Rissmann, R. Lomitapide. *Br. J. Clin. Pharmacol.* **2015**, *80* (2), 179–181. https://doi.org/10.1111/bcp.12612.

(220) Laifenfeld, C. D.; Industries, T. P.; Papapetropoulos, S.; Grossman, I.; Laifenfeld, D. Drug Repurposing from the Perspective of Pharmaceutical Companies. *Br. J. Pharmacol.* **2018**, *175* (2), 168–180. https://doi.org/10.1111/bph.13798.

(221) Pushpakom, S.; Iorio, F.; Eyers, P. A.; Escott, K. J.; Hopper, S.; Wells, A.; Doig, A.; Guilliams, T.; Latimer, J.; Mcnamee, C.; Norris, A.; Sanseau, P.; Cavalla, D.; Pirmohamed, M. Drug Repurposing: Progress, Challenges and Recommendations. *Nat. Rev. drug Discov.* **2018**, *18*, 41–58. https://doi.org/10.1038/nrd.2018.168.

(222) Ashburn, T. T.; Thor, K. B. Drug Repositioning : Identifying and Developing New Uses for Existing Drugs. *Nat. Rev. drug Discov.* **2004**, *3*, 673–683. https://doi.org/10.1038/nrd1468.

(223) Ward, P.; Equinet, L.; Packer, J.; Doerig, C. Protein Kinases of the Human Malaria Parasite Plasmodium Falciparum : The Kinome of a Divergent Eukaryote. *BMC Genomics* **2004**, *5* (19), 1–19. https://doi.org/10.1186/1471-2164-5-79.

(224) Homewood, C. A.; Warhurst, D. C.; Peters, W.; Baggaley, V. C. Lysosomes, PH and the Anti-Malarial Action of Chloroquine. *Nature* **1972**, *235*, 50–52. https://doi.org/10.1038/235050a0.

(225) Egan, T. J. Structure-Function Relationships in Chloroquine and Related 4-Aminoquinoline Antimalarials. *Mini-Reviews Med. Chem.* **2001**, *1* (1), 113–123. https://doi.org/10.2174/1389557013407188.

(226) Alder, A.; Sanchez, C. P.; Russell, M. R. G.; Collinson, L. M.; Lanzer, M.; Blackman, M. J.; Gilberger, T. W.; Matz, J. M. The Role of Plasmodium V-ATPase in Vacuolar Physiology and Antimalarial Drug Uptake. *Proc. Natl. Acad. Sci. U. S. A.* **2023**, *120* (30). https://doi.org/10.1073/PNAS.2306420120/SUPPL_FILE/PNAS.2306420120.SM01.AVI.

(227) Aweeka, F. T.; German, P. I. Clinical Pharmacology of Artemisinin-Based Combination Therapies. *Clin. Pharmacokinet.* **2008**, *47* (2), 91–102.

(228) Kuter, D.; Chibale, K.; Egan, T. J. Linear Free Energy Relationships Predict

Coordination and π-Stacking Interactions of Small Molecules with Ferriprotoporphyrin IX. *J. Inorg. Biochem.* **2011**, *105* (5), 684–692. https://doi.org/10.1016/j.jinorgbio.2011.02.008.

(229) Asakura, T.; Minakata, K.; Adachi, K. Denatured Hemoglobulin in Sickle Erythrocytes. *J. Clin. Invest.* **1977**, *59* (4), 633–640. https://doi.org/10.1172/JCI108681.

(230) Erman, J. E.; Chinchilla, D.; Studer, J.; Vitello, L. B. Binding of Imidazole, 1-Methylimidazole and 4-Nitroimidazole to Yeast Cytochrome c Peroxidase (CcP) and the Distal Histidine Mutant, CcP(H52L). *Physiol. Behav.* **2016**, *176* (3), 139–148. https://doi.org/10.1016/j.bbapap.2015.04.013.Binding.

(231) Streiner, D. L.; Norman, G. R. '"Precision"' and '"Accuracy"': Two Terms That Are Neither. *J. Clin. Epidemiol.* **2006**, *59* (4), 327–330. https://doi.org/10.1016/j.jclinepi.2005.09.005.

(232) *Process Validation: General Principles and Practices | FDA*. https://www.fda.gov/regulatory-information/search-fda-guidance-documents/process-validation-general-principles-and-practices (accessed 2022-12-23).

(233) Rosenthal, P. J.; Meshnick, S. R. Hemoglobin Catabolism and Iron Utilization by Malaria Parasites. *Mol. Biochem. Parasitol.* **1996**, *83* (2), 131–139. https://doi.org/10.1016/S0166-6851(96)02763-6.

(234) Altman, D. G.; Bland, J. M. Measurement in Medicine : The Analysis of Method Comparison Studies. *Stat.* **1983**, *32* (3), 307–317. https://doi.org/10.2307/2987937.

(235) Turrigiano, G. Homeostatic Signaling: The Positive Side of Negative Feedback. *Curr. Opin. Neurobiol.* **2007**, *17* (3), 318–324. https://doi.org/10.1016/j.conb.2007.04.004.

(236) Giavarina, D. Understanding Bland Altman Analysis. *Biochem. Medica* **2015**, *25* (2), 141–151. https://doi.org/10.11613/BM.2015.015.

(237) Landeta, C.; Mejia-Santana, A. Union Is Strength: Target-Based and Whole-Cell High-Throughput Screens in Antibacterial Discovery. *J. Bacteriol.* **2022**, *204* (4). https://doi.org/10.1128/jb.00477-21.

(238) Macarró, R.; Hertzberg, R. P. Design and Implementation of High Throughput Screening Assays. *Mol. Biotechnol.* **2011**, *47* (3), 270–285. https://doi.org/10.1007/s12033-010-9335-9.

(239) Cheng, T.; Li, Q.; Zhou, Z.; Wang, Y.; Bryant, S. H. Structure-Based Virtual Screening for Drug Discovery: A Problem-Centric Review. *AAPS J.* **2012**, *14* (1), 133–141.

https://doi.org/10.1208/s12248-012-9322-0.

(240) Attene-Ramos, M. S.; Austin, C. P.; Xia, M. High Throughput Screening. In *Encyclopedia of Toxicology: Third Edition*; Elsevier, 2014; pp 916–917. https://doi.org/10.1016/B978-0-12-386454-3.00209-8.

(241) Sugioka, Y.; Suzuki, M.; Sugioka, K.; Nakano, M. A Ferriprotoporphyrin IX-Chloroquine Complex Promotes Membrane Phospholipid Peroxidation. A Possible Mechanism for Antimalarial. *FEBS Lett.* **1987**, *223* (2), 251–254. https://doi.org/10.1016/0014-5793(87)80299-5.

(242) Le Manach, C.; Scheurer, C.; Sax, S.; Schleiferböck, S.; Cabrera, D. G.; Younis, Y.; Paquet, T.; Street, L.; Smith, P.; Ding, X. C.; Waterson, D.; Witty, M. J.; Leroy, D.; Chibale, K.; Wittlin, S. Fast in Vitro Methods to Determine the Speed of Action and the Stage-Specificity of Anti-Malarials in Plasmodium Falciparum. *Malar. J.* **2013**, *12* (424).

(243) Linares, M.; Viera, S.; Crespo, B.; Franco, V.; Gómez-Lorenzo, M. G.; Jiménez-Diáz, M. B.; Angulo-Barturen, Í.; Sanz, L. M.; Gamo, F. J. Identifying Rapidly Parasiticidal Anti-Malarial Drugs Using a Simple and Reliable in Vitro Parasite Viability Fast Assay. *Malar. J.* **2015**, *14* (1), 1–8. https://doi.org/10.1186/s12936-015-0962-2.

(244) Becker, K.; Tilley, L.; Vennerstrom, J. L.; Roberts, D.; Rogerson, S.; Ginsburg, H. Oxidative Stress in Malaria Parasite-Infected Erythrocytes: Host-Parasite Interactions. *Int. J. Parasitol.* **2004**, *34* (2), 163–189. https://doi.org/10.1016/j.ijpara.2003.09.011.

(245) Ch'ng, J. H.; Liew, K.; Goh, A. S. P.; Sidhartha, E.; Tan, K. S. W. Drug-Induced Permeabilization of Parasite's Digestive Vacuole Is a Key Trigger of Programmed Cell Death in Plasmodium Falciparum. *Cell Death Dis.* **2011**, *2* (10). https://doi.org/10.1038/cddis.2011.97.

(246) Feng, T. S.; Guantai, E. M.; Nell, M.; Van Rensburg, C. E. J.; Ncokazi, K.; Egan, T. J.; Hoppe, H. C.; Chibale, K. Effects of Highly Active Novel Artemisinin-Chloroquinoline Hybrid Compounds on β-Hematin Formation, Parasite Morphology and Endocytosis in Plasmodium Falciparum. *Biochem. Pharmacol.* **2011**, *82* (3), 236–247. https://doi.org/10.1016/j.bcp.2011.04.018.

(247) Jacobs, G. H.; Oduola, A. M. J.; Kyle, D. E.; Milhous, W. K.; Martin, S. K.; Aikawa, M. Ultrastructural Study of the Effects of Chloroquine and Verapamil on Plasmodium Falciparum. *Am. J. Trop. Med. Hyg.* **1988**, *39* (1), 15–20. https://doi.org/10.4269/AJTMH.1988.39.15.

(248) Warhurst, D. C.; Gould, S. The Chemotherapy of Rodent Malaria XXXIII. *Ann. Trop. Med. Parasitol.* **1982**, *76* (3), 257–264. https://doi.org/10.1080/00034983.1982.11687540.

(249) Hoppe, H. C.; Van Schalkwyk, D. A.; Wiehart, U. I. M.; Meredith, S. A.; Egan, J.; Weber, B. W. Antimalarial Quinolines and Artemisinin Inhibit Endocytosis in Plasmodium Falciparum. *Antimicrob. Agents Chemother.* **2004**, *48* (7), 2370–2378. https://doi.org/10.1128/AAC.48.7.2370-2378.2004/ASSET/38D60527-0984-4379-AB52-5A1CAB50C355/ASSETS/GRAPHIC/ZAC0070441590006.JPEG.

(250) Yayon, A.; Timberg, R.; Friedman, S.; Ginsburg, H. Effects of Chloroquine on the Feeding Mechanism of the Intraerythrocytic Human Malarial Parasite Plasmodium Falciparum. *J. Protozool.* **1984**, *31* (3), 367–372. https://doi.org/10.1111/J.1550-7408.1984.TB02981.X.

(251) Olliaro, P.; Castelli, F.; Caligaris, S.; Druilhe, P.; Carosi, G. Ultrastructure of Plasmodium Falciparum “in Vitro”. II. Morphological Patterns of Different Quinolines Effects. *Microbiologica* **1989**, *12* (1), 15–28.

(252) Egan, T. J. Interactions of Quinoline Antimalarials with Hematin in Solution. *J. Inorg. Biochem.* **2006**, *100* (5–6), 916–926. https://doi.org/10.1016/J.JINORGBIO.2005.11.005.